Departamento de Teoría de la Materia Condensada
Instituto de Ciencia de Materiales de Madrid
Consejo Superior de Investigaciones Científicas

Spin and Charge Transport through Driven Quantum Dot Systems and their Fluctuations

Rafael Sánchez Rodrigo

Departamento de Física Teórica de la Materia Condensada
Facultad de Ciencias
Universidad Autónoma de Madrid

Departamento de Teoría de la Materia Condensada
Instituto de Ciencia de Materiales de Madrid
Consejo Superior de Investigaciones Científicas

Spin and Charge Transport through Driven Quantum Dot Systems and their Fluctuations

Rafael Sánchez Rodrigo

Director: Prof. Gloria Platero Coello
Tutor: Prof. Carlos Tejedor

Memoria presentada para acceder al grado de Doctor
Departamento de Física Teórica de la Materia Condensada
Facultad de Ciencias
Universidad Autónoma de Madrid

Madrid, 2007

Resumen

La presente tesis estudia fenmenos de transporte tanto de la carga como del espín electrónicos en sistemas de puntos cuánticos bajo la acción de campos electromagnéticos alternos. Para ello, se ha hecho necesario, en algunos casos, analizar no sólo el flujo de corriente sino también las fluctuaciones de la misma.

Se han derivado las ecuaciones de evolución de la matriz de densidad para el caso en que el sistema se haya bajo el efecto de potenciales externos dependietes del tiempo. En presencia de campos alternos, que actúan como una oscilación en los niveles de energía de cada punto cuántico, los procesos de transferencia electrónica a través de las barreras que delimitan el sistema se ven afectados por la eventual absorción o emisión de fotones del campo. De esta forma, procesos que, sin la presencia del campo, no estarían energéticamente permitidos, pueden ahora ocurrir gracias a la energía suministrada por el campo (proporcional a su frecuencia). Estos procesos no estaban incorporados en previos estudios de este tipo de sistemas mediante la matriz de densidad.

Se ha estudiado un sistema de dos puntos cuánticos, conectados a dos contactos (que actúan como reservorios electrónicos) sin diferencia de potencial alguna aplicada a ellos como sistema de bombeo electrónico cuando se aplica un potencial alterno cuya frecuencia coincide con la diferencia de energía entre los estados de simple ocupación de cada punto cuántico. Para ello, es necesaria cierta inhomogeneidad espacial o bien que no se mantenga la reversibilidad temporal del sistema. En este caso, le inhomogeneidad viene dada por la distribución de los niveles energéticos de cada punto cuántico: en uno de ellos, por debajo del potencial químico de los contactos y, en el otro, por encima. Entonces, los electrones que entran en el sistema son coherentemente deslocalizados entre los dos puntos cuánticos y finalmente transferidos al colector. De esta forma, se genera una corriente finita en una situación de equilibrio electrostático.

Esta idea puede ser aplicada a sistemas de dos puntos cuánticos en una configuración que permita la presencia simultánea de hasta cuatro electrones. En ese caso, si la frecuencia del campo pone en resonancia los estados de doble ocupación de cada punto cuántico, se ha mostrado cómo se puede seleccionar la polarización de la corriente bombeada, actuando entonces como *filtro de espín*. La corriente estará completamente polarizada en cada uno de los dos casos, a no ser que los procesos asistidos por fotones en las barreras de los contactos tengan una contribución apreciable. Como se ha demostrado, esto sólo ocurre cuando la intesidad del campo es pequeña en comparación con su frecuencia. Por otra parte, es necesario tener en cuenta la influencia de los procesos de relajación de espín debidos a la interacción con el medio nuclear (interacción hiperfina) o por effecto espín órbita. El estudio de la forma de los picos de resonancia permiten extraer información sobre la magnitud de estos procesos.

Por otra parte, se ha demostrado cómo los procesos de transferencia asistidos por fotones entre los reservorios y el doble punto cuántico son capaces de deshacer la situación de bloqueo de espín. Esto sucede cuando ambos puntos cuánticos están ocupados por un electrón con el mismo espín, de forma que el principio de exclusión de Pauli impide la formación de estados de doble ocupación que contribuyan al transporte. La importancia de este efecto reside en la reciente utilización de situaciones de bloqueo de

espin para la manipulación coherente del espín del electrón mediante campor electromagéticos.

La rotación de espines en dobles puntos cuánticos mediante campos magnéticos oscilantes en resonancia con el desdoblamiento provocado por otro campo magnético estático es analizada en sistemas abiertos donde los procesos de transporte coherente pueden eventualmente mezclarse con las oscilaciones producidas por el campo alterno. En concreto, cuando el desplazamiento de Zeeman es similar para los electrones de ambos puntos cuánticos, ambas dinámicas son independientes. En ese caso, el sistema se queda atrapado en el subespacio triplete (que no contribuye al transporte electrónico) y la corriente se cancela, mientras que los dos electrones permanecen rotando coherentemente. Esta situación es muy sensible a las inhomogeneidades en el desplazamiento Zeeman, debidas a campos magnéticos de distinta intensidad, puntos cuánticos con distinto factor giromagnético o la interacción hiperfina con los espines nucleares del medio. En ambos casos, aparece una corriente finita que oscila con una frecuendia que depende de manera no trivial tanto de la intensidad del campo magnético oscilante como de la anchura de la barrera que separa los dos puntos cuánticos.

El formalismo de la matriz de densidad también permite el análisis de las fluctuaciones de la corriente. Mediante la derivación de la ecuación de movimiento para el operador que describe el número de electrones acumulados en un contacto, se puede obtener tanto la corriente como el ruido de baja frecuencia para sistemas que incluyan potenciales dependientes del tiempo.

Este nuevo formalismo se ha aplicado a casos relevantes de transporte coherente como los sitemas de bombeo de carga y espín analizados en capítulos anteriores o sistemas con bloqueo de espín. Los primeros muestran ruido sub-poissoniano, como es de esperar en sistemas de transferencia electrónica resonante. Por contra, los segundos se rigen por un mecanismo más complejo que provoca que los electrones se transfieran en grupos, en aparente contradicción de su naturaleza fermiónica, provocando que el ruido sea super-poissoniano.

También se ha analizado el ruido super-poissoniano observado en muestras de puntos cuánticos dobles alrededor de ciertos picos de corriente resonante. El comportamiento con la temperatura es achacado a la decoherencia inducida por efecto de los fonones de la red, mientras que los valores del ruido alcanzados se explican mediante el acoplo capacitivo de dos canales con resonancia en voltages cercanos.

La alteración de las propiedades estadísticas se da también en bosones. En concreto, la relajación electrónica en átomos de dos niveles puestos en resonancia mediante una iluminación coherente (resonancia fluorescente) provoca la emisión de fotones *desperdigados*, esto es, mostrando ruido sub-Poissoniano, pese a su naturaleza bosónica. Este tipo de sistemas puede ser considerado también en puntos cuánticos de dos niveles en el régimen de transporte donde los procesos de relajación se deben a la emisión de fonones (provinientes de la interacción con las vibraciones del sólido) en lugar de fotones. Se demuestra en esta tesis cómo estas propiedades pueden ser alteradas mediante la variación de los parámetros del sistema (la, intensidad del campo, el potencial químico de los contactos y el grosor de las barreras de los contactos).

Para la obtención simultánea de las correlaciones entre eventos electrónicos y fonónicos a cualquier orden, se ha desarrollado una técnica que permite la obtención de términos de correlación cruzada entre distintas cuasipartćulas (en este caso, electrones y fonones) que no han sido consideradas con anterioridad.

Agradecimientos

Ante todo, tengo que agradecer la posibilidad que se me brindó no sólo de hacer esta tesis sino de dedicarme a la física. Esa responsabilidad debería repartirse, no sé en qué proporción, entre Helena, que encontró el anuncio de la beca, Gloria y Ramón, que me la concedieron, y mis padres, que siempre me animaron a trabajar en lo que me gustara. Parece que el que menos tiene que ver con el asunto soy yo.

A Gloria le quiero agradecer profundamente su confianza, cercanía y dedicación. Y su disponibilidad y trato personal más allá del profesional. También debo acordarme del Prof. Ernesto Cota, a quien primero se le *apareció* esta tesis, aunque tal vez no se pareciera entonces a la que ha acabado siendo. Y a Ramón por su ayuda en los primeros meses de beca, psicodelias varias aparte.

Agradezco a The University of Manchester, Technische Universität Berlin y Augsburg Universität, donde una parte muy importante de esta tesis se ha realizado, por su hospitalidad durante las estancias allí realizadas. En concreto, a la colaboración con los grupos del Prof. Tobias Brandes y del Prof. Peter Hänggi. Especialmente, a Tobias y a Sigmund les quiero agradecer su confianza y su ayuda sin reservas, además de todo lo aprendido y a Franz por el trabajo en colaboración y compañía. No puedo olvidarme, hablando de hospitalidad, de Miguel, la semana que pasé en su casa y su complicidad.

Estos cinco años, más que por esta tesis quedarán por lo vivido dentro y fuera y la gran amistad de Nacho, Miguel, Carlos y Samuel, Manolo, siempre dispuesto a todo, Eduardo, Ramón, Jángel, Ricardo, Ivan, Jesús, María y Ricardo, Fernando y Javi. Y al resto de los compañeros: Rafa, Berni, César, Alberto, Juan Luis, Débora, Fernando, David, Geli, Ana y Pablo.

Gracias a las incontables horas de trabajo porque al menos han dado fruto. Y a Sandra, Virginia, Jaime, el Nose y el Pitu porque hay vida más allá de la física, aunque a veces no lo parezca.

Gracias a mis padres (sin ellos sí que esto no hubiera sido posible) porque nunca me ha faltado su apoyo, a Laura y la abuela.

Y, por último, a Helena por su amor.

Rafa
Madrid, 2007

Table of contents

Resumen . . . 1
Agradecimientos . . . 3
Table of contents . . . 5

1 Introduction **7**
1.1 Quantum dots . . . 7
1.2 Coherent transport. Double quantum dots . . . 9
1.3 Coherent manipulation by external time dependent fields . . . 10
1.4 Current fluctuations . . . 12

2 Density matrix formalism **15**
2.1 Time evolution . . . 16
2.2 Relaxation to the stationary regime. Master equation . . . 17
2.3 Transition rates . . . 21
2.4 Current . . . 23
2.5 Single resonant level in a quantum dot–Sequencial tunneling . . . 24
2.6 Spatial Rabi oscillations in a double quantum dot . . . 25

3 Time-dependent potentials. Photon-assited tunneling **31**
3.1 Master equation in the presence of AC potentials . . . 31
3.2 Photon-assisted tunneling . . . 33
3.3 A simple case: AC driven single level quantum dot . . . 34
3.4 AC driven double quantum dot. Photon-assisted delocalization . . . 36

4 Spin pumping in double quantum dots **45**
4.1 Spin pumping . . . 45
4.2 Spin filtering . . . 48
4.3 Spin relaxation effects . . . 52
4.4 Photon-assisted tunneling effects . . . 56
4.5 Conclusions . . . 62

5 Coherent spin rotations in double quantum dots **63**
5.1 Electron spin resonance in an open double quantum dot . . . 64
5.2 Closed system. Coherent dynamics . . . 65
5.3 Transport regime . . . 71
5.4 Conclusions . . . 74

6 Shot noise **77**
6.1 Master equation . . . 78
6.2 Single resonant level in a quantum dot–Sub-Poissonian shot noise . . . 81
6.3 Shot noise in double quantum dots . . . 81
6.4 Double quantum dot pumps . . . 84
6.5 Shot noise in spin pumps . . . 86
6.6 Spin blockade in AC driven double quantum dots . . . 88
6.7 Conclusions . . . 91

7 Electron Bunching in Stacks of Coupled Quantum Dots **93**
7.1 Transport through a single channel . . . 95
7.2 Transport through two coupled channels . . . 96
7.3 Conclusions . . . 100

8 Electron and Phonon Counting Statistics. **101**
8.1 Low bias regime. Resonance Fluorescent Phonon Emission . . . 105
8.2 Dynamical Channel Blockade regime. . . . 107
8.3 High Bias regime. . . . 110
8.4 High Bias–Step Configuration. . . . 113
8.5 High Bias–Level-dependent tunneling . . . 117
8.6 Conclusions . . . 122

A Moments of the electron-phonon counting statistics **123**
A.1 Low Bias Regime . . . 123
A.2 Dynamical Channel Blockade regime. . . . 124
A.3 High Bias regime. . . . 125
A.4 High Bias-Step Configuration . . . 126

B Single resonant level shot noise **127**

C Bessel functions **129**

Bibliography **133**

Chapter 1

Introduction

The access to the quantum nature of matter has been for years restricted to quantum optics experiments where the study of the spectra resulting from the illumination of atomic and molecular systems provides information on their energy distribution and gives the opportunity to coherently excite internal transitions. This changed drastically when in 1980 the first measurements of the quantum Hall effect in two dimensional electron gases in semiconductor structures was reported[1]. There, for the first time, quantized magnitudes were reached in *mesoscopic* artificial devices of hundreds of μm.

From that moment, the size of fabricated solid state structures has rapidly decreased by the impulse of technologic and industrial development, with the aim of being able to buid as much electronic circuits is the less space. However, basic investigation has benefited from this advances, having the opportunity to design systems where to explore quantum properties of electrons raising from their low dimensionality and including, for example, chaotic cavities, carbon nanotubes–serving as one dimensional conductors–, single atomic or molecular junctions. Among them, quantum dots deserve special importance for being a realization of zero dimensional systems with a discrete energy distribution. For this reason, they are also know as *artificial atoms*[2, 3, 4, 5], with the particularity that, in quantum dots, one can explore regimes that are not accesible for atoms[6, 7], manipulate their properties by extrenal voltages[8] or investigate a wide range of effects coming from interactions which are a small perturbation in atoms, as hyperfine or spin-orbit interactions[9].

The analogy can be taken further, since coherent phenomena typical for quantum optics have usually an electron transport counterpart[10]. Therefore, the introduction of time-dependent electromagnetic fields was soon considered as a powerful tool to extract information about the internal dynamics of a quantum dot system and even to control and operate electronic states.

Also, quantum dots have become a physical realization of two level systems. In particular, spin states or single occupation states in coupled quantum dots, where the interdot tunneling barrer acts as a coherent interaction[11], allow quantum dots to be considered for as building blocks for spintronic circuits or qubits in the search of quantum information procesors, apart from the original intention to use them as single electron transistors.

1.1 Quantum dots

Depending on their fabrication, one can distinguish several types of quantum dots. Lateral quantum dots consist in a two dimensional electron gas in the interface between two semiconductor

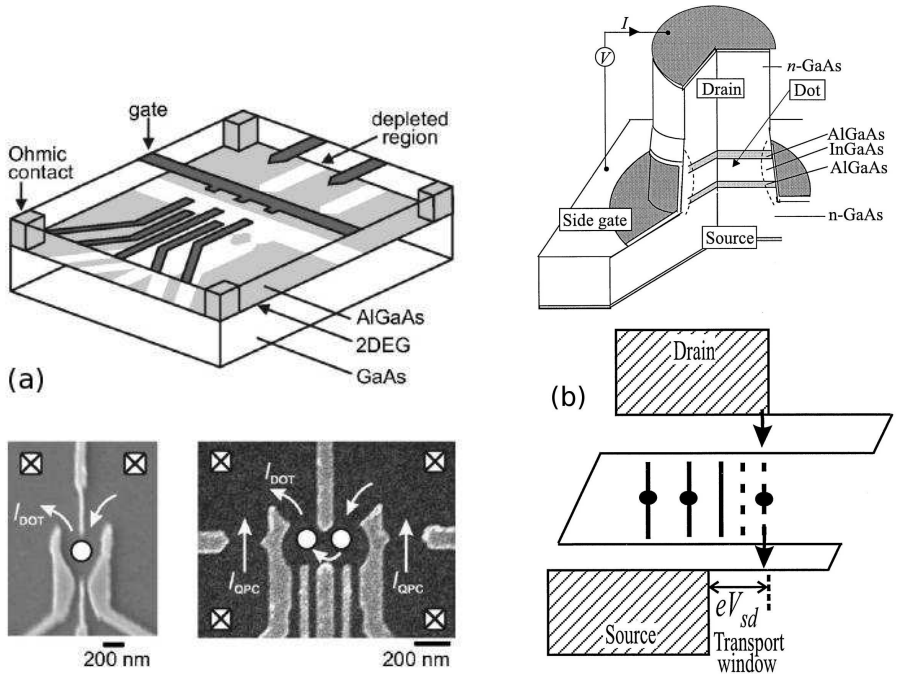

Fig. 1.1: (a) Lateral and (b) vertical quantum dots (taken from Ref. [9] and [7], respectively), including an energy diagram of a quantum dot where the three electrons state is in the bias window, allowing electron transport to the collector.

layers with different band gap (for example, AlGaAs and GaAs) and confined by quantum point contacts nanolitographied on top of one of them, cf. Fig. 1.1a. Vertical quantum dots are grown nanostructures confined between isolating barriers, cf. Fig. 1.1b. Lateral quantum dots have the advantage to be completely tunable by external voltages. Concretely, the voltages applied to the two quantum point contacts modify the tunneling strength while by the central gate voltage one can tune up and down the quantum dot level energies.

As learned from basic quantum mechanics, an electron confined in a region of space show a discrete energy distribution. The energy separation with the excited states is proportional to L^{-2}, where L is the size of the region. As can be seen in Fig. 1.2, for ultrasmall quantum dots, this energies can be resolved by transport spectroscopy measurements.

Transport is also conditioned by Coulomb interaction wich is assumed to be high for electrons inside the quantum dot. Thus, the transference of an electron to the collector needs the presence of the state with an extra electron in the bias window, defined by the difference of Fermi energies of the source and drain leads. In the experiment shown in Fig. 1.2, this is the case when the gate voltage is increased (then, the energy levels decrease) until the ground state with an additional electron enters the bias window, defining the bounds of the Coulomb blockade region. The theory of this processes is described classicaly by Kulik and Shekhter[12] and, considering discrete levels, in the works by Beenakker[13] and Averin, Korotkov and Likharev[14].

These approaches have in common a description of transport in terms of rate equations that evaluate the evolution of the quantum dot occupation states by the tunneling rates of outgoing and incom-

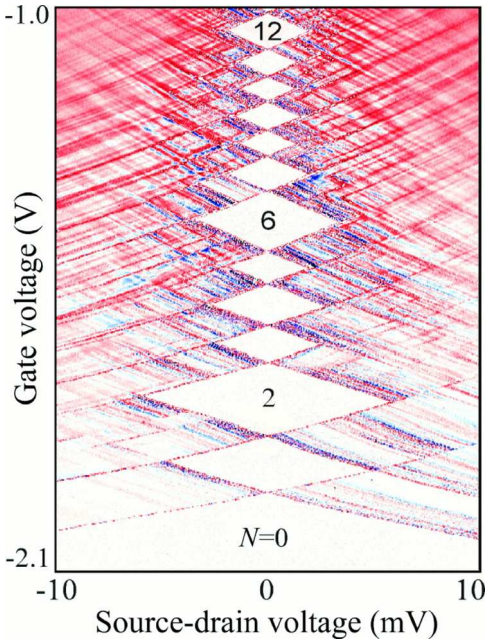

Fig. 1.2: Coulomb blockade diamonds in the differential conductance, $\partial I/\partial V_{\rm sd}$, through a single quantum dot. In the white regions, transport is blocked due to intradot Coulomb repulsion, where tunneling is only possible involving virtual states–*cotunneling*[16, 17, 18]. The entering of excited states in the bias window is fingerprinted by the paralel to the Coulomb diamond lines (taken from Ref. [6]). The numbers inside the Coulomb diamonds denote the number of electrons inside the quantum dot for each configuration.

ing electrons to/from the leads. The theory was definitely stablished by considering intradot correlations by Gurvitz, Lipkin and Prager[15].

1.2 Coherent transport. Double quantum dots

One can also consider systems of two or more quantum dots separated by a tunneling barrier– then, the analogy with atoms can be brought to call them *artificial molecules*. If the interdot coupling is strong, the electrons will ocuppy *molecular orbitals* extended all over the dots. On the other hand, if it is weak, orbitals in each dot can be considered individually. Charge displacements within the quantum dot system are then considered as coherent processes leading to a superposition of states localized in the different dots.

In Fig. 1.1a, a double quantum dot is represented, where the energies of each dot can be tuned separately by different gate voltages. Then, if the single occupation states of each dot are not aligned, interdot tunneling will be highly supressed and an electron entering the system remains in the quantum dot that is directly coupled to the emitter. On the other hand, when the levels are resonant, the electron will be delocalized performing coherent oscillations between the two sites, in a spatial version of Rabi oscillations. Then, it has a finite probability to be extracted to the collector.

This transport dependence on the detuning of the levels in different dots makes this systems highly manipulable and precise control of their bonds have been achived[19]. They can also be considered

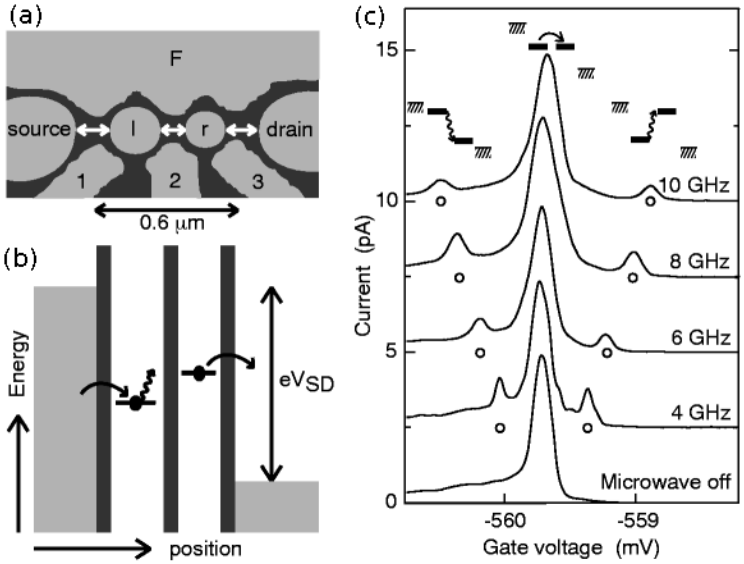

Fig. 1.3: AC driven transport in a double quantum dot. (a) Sketch of the double quantum dot system coupled to the source and drain leads. Gate 2 modulates the interdot barrier while gates 1 and 3 act on the energy levels of each dot. (b) Energy diagram of the device, showing the high source-drain voltage regime where transport is unidirectional. (c) Current as a function of the gate voltage for different AC frequencies. When the AC frequency match the energy difference between the levels of each dot, resonant tunneling through the absorption/emission of one photon appears in the form of satellite peaks (taken from Ref. [78]).

as two level systems where to test the spin boson model[184] through the coupling to the phononic vibrations of the host material[185], which are the main dissipative sources in these systems.

To consider these effects, the *classical* rate equations used to describe transport through single quantum dots needed to be be reformulated to include non-diagonal terms of the density matrix, accounting for the coherent dynamics[20, 21, 22, 23].

1.3 Coherent manipulation by external time dependent fields

Quantum coherence can be exploited by means of time dependent AC fields, as has been done for years in atomic physics and quantum optics. In this sence, electric AC fields have been applied to double quantum dots in order to drive internal charge transitions. For instance, electron delocalization can be achieved even when the detuning of the states in each dot is high if the frequency of the AC field matches that energy separation[78], cf. Fig. 1.3.

This photon-assisted tunneling involves the renormalization of the interdot coupling which now depends on both the intensity and the frequency of the AC field through a series of Bessel functions. Then, one can exploit the properties of these functions to find interesting regimes as, for example, dynamical charge localization[51]. In that case, the AC intensitity is such that the Bessel function of order correnponding to the number of photons involved in the interdot transition reaches its zero, and so it is the renormalized tunneling coupling. Then, the two quantum dots are effectively uncoupled and no charge flows through the system. This case is discussed in chapter 3.

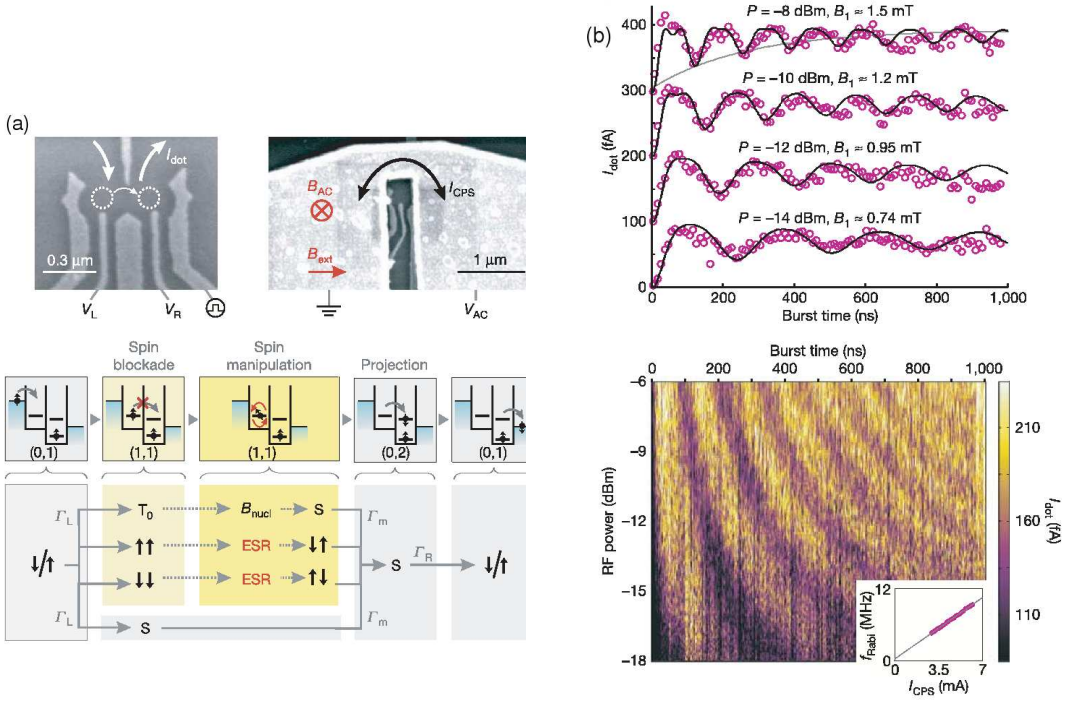

Fig. 1.4: Experimental setup for the detection of spin rotations in double quantum dots (a) where a coplanar gold stripline is situated near by the device in order to induce an oscillating magnetic field perpendicular a the external DC magnetic field. (b) When transport is cancelled by spin blockade, a pulsed magnetic field rotates one of the spins so that current can be restablished, reflecting coherent oscillations due to the spin dynamics inside the double quantum dot (taken from Ref. [95]).

This effect leads to the pumping effect, when finite current flows through an unbiased double quantum dot provided that time reversability is lifted or the system is spatially inhomogeneous[48]. As will be shown in chapter 4, the frequency of the AC field can be tuned to select processes involving electrons with different spin polarization, leading to spin pumping and spin filter devices.

However, photon-assisted tunneling also affects to the contact barriers, introducing in the dynamics processes that would be energetically forbidden in the absence of driving[36, 68]. This effect can lead to a limitation of the operativeness of the electronic device and are an additional source of decoherence which must be taken into account.

1.3.1 Spin degree of freedom. AC magnetic fields

The electron spin also plays a important role. In fact, a whole new field has raised consisting in the spin transport properties, *spintronics*, as an alternative to charge based electronics[24]. Also, spin is essential in the search of qubits for quantum information processing.

Electronic transport through quantum dot systems is not fully described in terms of Coulomb

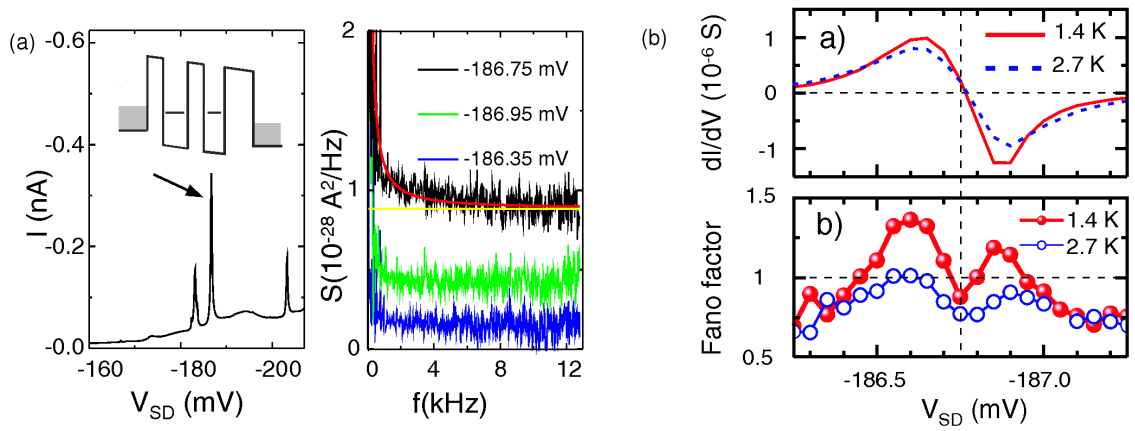

Fig. 1.5: Transport through stacks of self-grown double quantu dots. (a) Current voltage charateristics and shot noise spectra for different voltages with the fit to $A/f + S_0$ that allows to extract the cero frequency noise. (b) Differential conductance and shot noise around a current peak for different temperatures (taken from Ref. [188]).

blockade but also by considering Pauli exclusion[92]. It leads to spin blockade when an electron cannot tunnel from one quantum dot to an orbital in an adjacent quantum dot which is already occupied by an electron with opposite spin. Then, the two electrons are trapped in the double quantum dot. This effect has opened the way to manipulate electronic spins in double quantum dots by the introduction of magnetic fields: a DC magnetic field in the Z direction breaks spin degeneracy by a Zeeman splitting while an AC magnetic field in the perpendicular plane, whose frequency is resonant with the Zeeman splitting, rotates the Z component of the electron spins. Once one of the electrons is rotated, spin blockade is removed (under certain conditions that will be discussed in chapter 5) and transport can flow through the system[95]. The current thus produced shows oscillations reflecting the coherent rotation of the spins, as seen in Fig. 1.4. This spin rotation, combined with recently achieved control of exchange interaction between two spins[82]–also in the spin blockade regime–, permit the operation of two electron double quantum dots as qubits.

Photon-assisted tunneling effects, as those discussed above have to be considered since they can lift spin blockade and introduce additional decoherence. This effect will be treated in the pumping configuration in chapter 4.

1.4 Current fluctuations

Far from being an incovenient for transport measurements, the fluctuations of the electronic current contain information not provided by measurements on the electronic averaged current. In concrete, those originated in the discreteness of the charge carriers–shot noise–are strongly influenced by the internal dynamics of the quantum system[25, 26] and electronic correlations. The concrete transport mechanism can modify the statistical properties of the transferred particles. From Pauli exclusion principle, one expects the probability of detecting two close in time electronic events to be low (contrary to what is expected for bosons), involving a supression of the fluctuations with respect to those shown by classical stochastic processes. In that case, the noise is said to be sub-Poissonian.

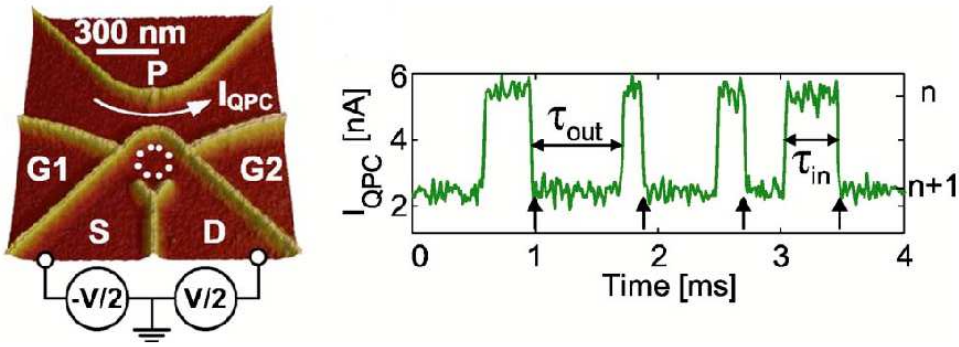

Fig. 1.6: Time resolved detection of electronic tunneling through a quantum dot. The changes in the occupation of the quantum dot affects the current through a quantum point contact situated close to it. By analyzing the statistical distribution of the lapses of time between events, one can obtain the full counting statistics of transport (taken from Ref. [162]).

Recent experiments have found how transport through quantum dot systems can affect the shot noise by turning it super-Poissonian, meaning that electrons are detected in bunches, imitating the bosonic behaviour. The measurements of Barthold *et al.* in self-grown double quantm dots samples[188] show sub-Poissonian noise at resonant peaks, that goes super-Poissonian in its vicinity, evidenced by the regions with Fano factor greater than one in Fig. 1.5b. The origin of this behaviour will be the subject of chapter 7.

Also, time-resolved tunneling measurements in multilevel single quantum dots (see Fig. 1.6) have demonstrated super-Poissonian shot noise when Coulomb interaction avoids the tunneling through a conducting level if another level–below the bias window–is occupied[162]. This method allows the calculation of higher order correlations, giving the full counting statistics of the electronic transport[150].

Opposite to fermions, bosons tend to be detected in bunches. However, antibunched photons are emitted from resonantly illuminated two level atoms–*resonance fluorescence*[154]. This phenomena, which originated the development of full counting statistics, can be brought to AC driven quantum dots where phonon mediated relaxation plays the role of spontaneously emitted photons. In chapter 8, the electronic and phononic counting statistics of such a system are analyzed, together with their mutual correlation.

Chapter 2

Density matrix formalism

A comprenhensive description of a quantum system, its statistical properties and internal dynamics is provided by its density matrix. For instance, wave functions are only able to describe *pure* states, i.e., when the state of the system can be determined by a series of measurements. However, having a reduced system coupled to an environment–which is the case for the measurement problem as well as for transport, it may form *mixed* superpositions of states which cannot be determined by any measurement. A mixed state can be represented by a statistical mixture of pure states described by the density operator[83]

$$\hat{\rho} = \sum_n p_n |\psi_n\rangle\langle\psi_n| \tag{2.1}$$

which, for this reason, is also known as *statistical operator*. Chosing an appropriate basis, $|\phi_i\rangle$, these states one can write in matricial form:

$$\hat{\rho} = \sum_{nij} p_n a^*_{n,i} a_{n,j} |\phi_i\rangle\langle\phi_j| \tag{2.2}$$

where the diagonal elements, $\rho_{ii} = \sum_n p_n |a_{n,i}|^2$, represent the probability of finding the system in a given state, $|\phi_i\rangle$. This involves a *normalization condition* for the diagonal elements of the density matrix

$$tr\rho = \sum_i \rho_{ii} = 1 \tag{2.3}$$

and[27]

$$\rho_{ii} \geq 0 \tag{2.4}$$

$$\rho_{ii}\rho_{jj} \geq |\rho_{ij}|^2. \tag{2.5}$$

The off-diagonal elements, $\rho_{i,j}$, account for the coherent superpositions between states, and their time evolution will describe the coherent dynamics and interference effects.

The expectation value of any observable, $\hat{\mathcal{O}}$, can be expressed in terms of the density matrix:

$$\langle\hat{\mathcal{O}}\rangle = \sum_{nij} p_n a^*_{n,i} a_{n,j} \langle\phi_i|\hat{\mathcal{O}}|\phi_j\rangle = \sum_{ij} \rho_{ij} \langle\phi_i|\hat{\mathcal{O}}|\phi_j\rangle = tr(\hat{\rho}\hat{\mathcal{O}}). \tag{2.6}$$

2.1 Time evolution

The time dependence of a wave function is given by the Schödinger equation

$$i\hbar\partial_t|\psi(t)\rangle = \hat{H}(t)|\psi(t)\rangle, \tag{2.7}$$

where $\hat{H}$ is the Hamiltonian of the system. In general, a time evolution operator can be defined such that

$$|\psi(t)\rangle = \hat{\mathcal{U}}(t)|\psi(0)\rangle, \tag{2.8}$$

where $\hat{\mathcal{U}}(t)$ is unitary and, by substituying in (2.7), satisfies

$$i\hbar\partial_t\hat{\mathcal{U}}(t) = \hat{H}(t)\hat{\mathcal{U}}(t). \tag{2.9}$$

If the Hamiltonian is time independent, $\hat{\mathcal{U}}(t) = e^{-i\hat{H}t/\hbar}$.

From (2.1), one can get the time evolution of the density operator:

$$\hat{\rho}(t) = \sum_n p_n|\psi_n(t)\rangle\langle\psi_n(t)| = \sum_n p_n\hat{\mathcal{U}}(t)|\psi_n(0)\rangle\langle\psi_n(0)|\hat{\mathcal{U}}^\dagger(t) = \hat{\mathcal{U}}(t)\hat{\rho}(0)\hat{\mathcal{U}}^\dagger(t). \tag{2.10}$$

Derivating with respect to time:

$$i\hbar\partial_t\hat{\rho}(t) = i\hbar\partial_t\hat{\mathcal{U}}(t)\hat{\rho}(0)\hat{\mathcal{U}}^\dagger(t) + i\hbar\hat{\mathcal{U}}(t)\hat{\rho}(0)\partial_t\hat{\mathcal{U}}^\dagger(t) = \hat{H}(t)\hat{\mathcal{U}}(t)\hat{\rho}(0)\hat{\mathcal{U}}^\dagger(t) - \hat{\mathcal{U}}(t)\hat{\rho}(0)\hat{\mathcal{U}}^\dagger(t)\hat{H}(t) \tag{2.11}$$

thus satisfying the equation of motion:

$$i\hbar\partial_t\hat{\rho}(t) = [\hat{H}(t), \hat{\rho}(t)] \tag{2.12}$$

analogue to the Liouville equation for a classical phase space probability distribution.

2.1.1 Interaction picture. Perturbative expansion

If the time dependence of the Hamiltonian is due to an external potencial, $\hat{H}(t) = \hat{H}_0 + \hat{V}(t)$, it is much more convenient to consider the Heisenberg interaction picture, where the term $\hat{H}_0$ *re-defines* the wave function so $|\psi_{\mathrm{I}}(t)\rangle = e^{i\hat{H}_0t/\hbar}|\psi(t)\rangle$ and the Schrödinger equation depends only on the external potencial:

$$i\hbar\partial_t|\psi_{\mathrm{I}}(t)\rangle = \hat{V}_{\mathrm{I}}(t)|\psi_{\mathrm{I}}(t)\rangle, \tag{2.13}$$

where $\hat{V}_{\mathrm{I}}(t) = e^{i\hat{H}_0t/\hbar}\hat{V}(t)e^{-i\hat{H}_0t/\hbar}$. Therefore, the time evolution operator, in the interaction picture, $\hat{\mathcal{U}}_{\mathrm{I}}(t) = e^{i\hat{H}_0t/\hbar}\hat{\mathcal{U}}$, satisfies the differential equation

$$i\hbar\partial_t\hat{\mathcal{U}}_{\mathrm{I}}(t) = \hat{V}_{\mathrm{I}}(t)\hat{\mathcal{U}}_{\mathrm{I}}(t) \tag{2.14}$$

with the initial condition $\hat{\mathcal{U}}_{\mathrm{I}}(0) = \mathbb{I}$. The exact solution

$$\hat{\mathcal{U}}_{\mathrm{I}}(t) = \mathbb{I} - \frac{i}{\hbar}\int_0^t d\tau\hat{V}_{\mathrm{I}}(\tau)\hat{\mathcal{U}}_{\mathrm{I}}(\tau) \tag{2.15}$$

can be solved iteratively, if the external potential is considered as a small perturbation. Up to second order:

$$\hat{\mathcal{U}}_{\mathrm{I}}^{(2)}(t) \approx \mathbb{I} - \frac{i}{\hbar}\int_0^t d\tau\hat{V}_{\mathrm{I}}(\tau) - \frac{1}{\hbar^2}\int_0^t d\tau\int_0^\tau d\tau\hat{V}_{\mathrm{I}}(\tau)\hat{V}_{\mathrm{I}}(\tau'). \tag{2.16}$$

In the same way, the Liouville equation for the density matrix in the interaction picture

$$i\hbar\partial_t\hat{\rho}_{\rm I}(t) = [\hat{V}_{\rm I}(t), \hat{\rho}_{\rm I}(t)] \tag{2.17}$$

can be written into an integral form

$$\hat{\rho}_{\rm I}(t) = \hat{\rho}_{\rm I}(0) - \frac{i}{\hbar}\int_0^t d\tau[\hat{V}_{\rm I}(\tau), \hat{\rho}_{\rm I}(\tau)] \tag{2.18}$$

which can be solved iteratively:

$$\hat{\rho}_{\rm I}^{(0)}(t) = \hat{\rho}_{\rm I}(0) \tag{2.19}$$

$$\hat{\rho}_{\rm I}^{(1)}(t) = \hat{\rho}_{\rm I}^{(0)} - \frac{i}{\hbar}\int_0^t d\tau[\hat{V}_{\rm I}(\tau), \hat{\rho}_{\rm I}(0)] \tag{2.20}$$

$$\hat{\rho}_{\rm I}^{(2)}(t) = \hat{\rho}_{\rm I}^{(1)} - \frac{1}{\hbar^2}\int_0^t d\tau\int_0^\tau d\tau'[\hat{V}_{\rm I}(\tau), [\hat{V}_{\rm I}(\tau'), \hat{\rho}_{\rm I}(0)]], \tag{2.21}$$

and so on, to obtain the small deviations caused by the external perturbation in the system.

2.2 Relaxation to the stationary regime. Master equation

On contrary, the problems considered in this thesis all consist a small system (one or more quantum dots) that is taken out of equilibrium by its interaction with a bigger environment (two fermionic reservoirs) in which it is embeded. The theory for these irreversible problems was developed in the 50's by Wangsness, Bloch[28, 43], Fano[30] and Redfield[31] for a quantum system interacting with a thermal bath. The system can be modeled by the Hamiltonian

$$\hat{H} = \hat{H}_{\mathcal{S}} + \hat{H}_{\mathcal{R}} + \hat{V}, \tag{2.22}$$

where the first two terms represent the quantum system and the reservoir, respectively and the last one, the interaction between them, which will be treated perturbatively. As explained in the previous section, one would rather work in the interaction picture which is obtained by writting $\hat{H}_0 = \hat{H}_{\mathcal{S}} + \hat{H}_{\mathcal{R}}$.

Then, one can write a differential equation for the density matrix of the whole system in the interaction picture, $\hat{\chi}_{\rm I}$, by introducing (2.18) into the Liouville equation (2.17), to obtain

$$\dot{\hat{\chi}}_{\rm I}(t) = -\frac{i}{\hbar}[\hat{V}_{\rm I}(t), \hat{\chi}_{\rm I}(0)] - \frac{1}{\hbar^2}\int_0^t dt'[\hat{V}_{\rm I}(t), [\hat{V}_{\rm I}(t'), \hat{\chi}_{\rm I}(t')]]. \tag{2.23}$$

By tracing out the contribution of the reservoirs, one can write the dynamical equations for the reduced density matrix, $\rho = tr_{\mathcal{R}}\chi$. If we consider $t = 0$ as the time when the interaction *begins*, the initial state can be written as a product: $\hat{\chi}(0) = \hat{\chi}_{\mathcal{S}}(0)\hat{\chi}_{\mathcal{R}}(0) = \hat{\chi}_{\rm I}(0)$, where $\hat{\chi}_{\mathcal{S}}(0) = \hat{\rho}(0)$. Considering that the environment remains in equilibrium and only the small system is affected by the interaction, one can write

$$\hat{\chi}(t) = \hat{\rho}(t)\hat{\chi}_{\mathcal{R}}(0), \tag{2.24}$$

involving that the processes related with the interaction between $\mathcal{S}$ and $\mathcal{R}$ will be irreversible. This approximation is equivalent to the first order–*Born* approximation in perturbation theory, when the initial uncorrelation between $\mathcal{S}$ and $\mathcal{R}$ is only slightly modified by the external potential. Then, one obtains

$$\dot{\hat{\rho}}_{\rm I}(t) = -\frac{i}{\hbar}tr_{\mathcal{R}}[\hat{V}_{\rm I}(t), \hat{\rho}(0)\hat{\chi}_{\mathcal{R}}(0)] - \frac{1}{\hbar^2}\int_0^t dt' tr_{\mathcal{R}}[\hat{V}_{\rm I}(t), [\hat{V}_{\rm I}(t'), \hat{\rho}_{\rm I}(t')\hat{\chi}_{\mathcal{R}}(0)]]. \tag{2.25}$$

Asuming that the time when the reservoir mantains its correlation is much shorter than the time when $\mathcal{S}$ is significantly damped, the influence of the past times on the evolution of the system is lost. Then, the system is said to not preserve memory and one can substitute $\hat{\rho}_{\rm I}(t') \approx \hat{\rho}_{\rm I}(t)$ in (2.25)–*Markov approximation*:

$$\dot{\hat{\rho}}_{\rm I}(t) = -\frac{i}{\hbar} tr_{\mathcal{R}}[\hat{V}_{\rm I}(t), \hat{\rho}(0)\hat{\chi}_{\mathcal{R}}(0)] - \frac{1}{\hbar^2}\int_0^t dt' tr_{\mathcal{R}}[\hat{V}_{\rm I}(t), [\hat{V}_{\rm I}(t'), \hat{\rho}_{\rm I}(t)\hat{\chi}_{\mathcal{R}}(0)]]. \tag{2.26}$$

The interaction potential can in general be written as products

$$\hat{V} = \sum_i \hat{s}_i \hat{r}_i, \tag{2.27}$$

where $\hat{s}_i$ and $\hat{r}_i$ are operators from the small system and the reservoirs, respectively. They commute, so that in the interaction picture, one finds

$$\hat{V}_{\rm I}(t) = \sum_i \hat{s}_i(t)\hat{r}_i(t), \tag{2.28}$$

where $\hat{s}_i(t) = e^{-i\hat{H}_{\mathcal{S}}t/\hbar}\hat{s}_i e^{-i\hat{H}_{\mathcal{S}}t/\hbar}$ and $\hat{r}_i(t) = e^{-i\hat{H}_{\mathcal{R}}t/\hbar}\hat{r}_i e^{-i\hat{H}_{\mathcal{R}}t/\hbar}$. Inserting it into (2.26):

$$\dot{\hat{\rho}}_{\rm I}(t) = -\frac{i}{\hbar}\sum_i tr_{\mathcal{R}}[\hat{s}_i(t)\hat{r}_i(t), \hat{\rho}_{\rm I}(0)\chi_{\mathcal{R}}(0)] - \frac{1}{\hbar^2}\sum_{ij}\int_0^t dt' tr_{\mathcal{R}}[\hat{s}_i(t)\hat{r}_i(t), [\hat{s}_j(t')\hat{r}_j(t'), \hat{\rho}_{\rm I}(t)\hat{\chi}_{\mathcal{R}}(0)]]. \tag{2.29}$$

After writing the commutation relations and extracting the operators of $\mathcal{S}$ out of the trace, if one considers the cyclic property of the trace, $tr(\hat{A}\hat{B}\hat{C}) = tr(\hat{C}\hat{A}\hat{B}) = tr(\hat{B}\hat{C}\hat{A})$:

$$\dot{\hat{\rho}}_{\rm I}(t) = -\frac{i}{\hbar}\sum_i (\hat{s}_i(t)\hat{\rho}_{\rm I}(0) - \hat{\rho}_{\rm I}(0)\hat{s}_i(t))\langle \hat{r}_i(t)\rangle \tag{2.30}$$

$$-\frac{1}{\hbar^2}\sum_{ij}\int_0^t dt'\{(\hat{s}_i(t)\hat{s}_j(t')\hat{\rho}_{\rm I}(t) - \hat{s}_j(t')\hat{\rho}_{\rm I}(t)\hat{s}_i(t))\langle \hat{r}_i(t)\hat{r}_j(t')\rangle \tag{2.31}$$

$$+ (\hat{\rho}_{\rm I}(t)\hat{s}_j(t')\hat{s}_i(t) - \hat{s}_i(t')\hat{\rho}_{\rm I}(t)\hat{s}_j(t))\langle \hat{r}_j(t')\hat{r}_i(t)\rangle\}, \tag{2.32}$$

where $\langle ...\rangle = tr(...\rho)$. While $\hat{\chi}_{\mathcal{R}}(0) = \frac{1}{Z}e^{-\beta\hat{H}_{\mathcal{R}}}$ is diagonal, all the elements $\langle N|\hat{r}|N'\rangle$ (where $|N\rangle$ are the eigenstates of $\hat{H}_{\mathcal{R}}$) are non-diagonal or they would be absorbed by $\hat{H}_{\mathcal{R}}$. Then, the expectation values

$$\langle \hat{r}_i(t)\rangle = \sum_{NN'}\langle N|\hat{r}_i(t)|N'\rangle\langle N'|\hat{\chi}_{\mathcal{R}}(0)|N\rangle = \sum_N \langle N|\hat{r}_i(t)|N\rangle\langle N|\hat{\chi}_{\mathcal{R}}(0)|N\rangle = 0. \tag{2.33}$$

As asumed by the Markov approximation, the correlations $\langle \hat{r}_i(t)\hat{r}_j(t')\rangle$ only survive for short lapses of time, τ, so

$$\langle \hat{r}_i(t)\hat{r}_j(t')\rangle \approx \langle \hat{r}_i(t)\rangle\langle \hat{r}_j(t')\rangle = 0 \tag{2.34}$$

if $t - t' \gg \tau$. On the other hand, for $t - t' \lesssim \tau$, it is convenient to rewrite the reservoirs correlations as a function of the difference of times:

$$\langle \hat{r}_i(t)\hat{r}_j(t')\rangle = tr_{\mathcal{R}}\left(e^{-i\hat{H}_{\mathcal{R}}t/\hbar}\hat{r}_i e^{-i\hat{H}_{\mathcal{R}}t/\hbar}e^{-i\hat{H}_{\mathcal{R}}t'/\hbar}\hat{r}_i e^{-i\hat{H}_{\mathcal{R}}t'/\hbar}\hat{\chi}_{\mathcal{R}}(0)\right) = \langle \hat{r}_i(t-t')\hat{r}_j\rangle \tag{2.35}$$

again by using the cyclic property of the trace and $[\hat{H}_{\mathcal{R}}, \hat{\chi}_{\mathcal{R}}(0)] = 0$. Introducing $t'' = t - t'$ and extending the integration limit to infinite, which is allowed by (2.34) and by the Markov approximation (one considers times t large compared to τ):

$$\dot{\hat{\rho}}_{\rm I}(t) = -\frac{1}{\hbar^2}\sum_{ij}\int_0^\infty dt''\{[\hat{s}_i(t), \hat{s}_j(t-t'')\hat{\rho}_{\rm I}(t)]\langle \hat{r}_i(t'')\hat{r}_j\rangle - [\hat{s}_i(t), \hat{\rho}_{\rm I}(t)\hat{s}_j(t-t'')]\langle \hat{r}_j\hat{r}_i(t'')\rangle\}. \tag{2.36}$$

In the basis of eigenstates of $\hat{H}_{\mathcal{S}}$, $\langle m|\hat{s}_i(t)|n\rangle = e^{i\omega_{mn}t}\langle m|\hat{s}_i|n\rangle$, where $\hbar\omega_{mn} = E_m - E_n$:

$$\begin{aligned}\langle m'|[\hat{s}_i(t), \hat{s}_j(t-t'')\hat{\rho}_{\rm I}(t)]|m\rangle &= \sum_{kk'}\Big(e^{i\omega_{m'k'}t}e^{i\omega_{kk'}(t-t'')}\langle m'|\hat{s}_i|k\rangle\langle k|\hat{s}_j|k'\rangle\langle k'|\hat{\rho}_{\rm I}(t)|m\rangle \\ &\quad -e^{i\omega_{m'k'}(t-t'')}e^{i\omega_{km}t}\langle m'|\hat{s}_j|k'\rangle\langle k'|\hat{\rho}_{\rm I}(t)|k\rangle\langle k|\hat{s}_j|m\rangle\Big) \qquad (2.37)\\ \langle m'|[\hat{s}_i(t), \hat{\rho}_{\rm I}(t)\hat{s}_j(t-t'')]|m\rangle &= \sum_{kk'}\Big(e^{i\omega_{m'k}t}e^{i\omega_{k'm}(t-t'')}\langle m'|\hat{s}_i|k\rangle\langle k|\hat{\rho}_{\rm I}(t)|k'\rangle\langle k'|\hat{s}_j|m\rangle \\ &\quad -e^{i\omega_{km}t}e^{-i\omega_{kk'}t''}\langle m'|\hat{\rho}_{\rm I}(t)|k\rangle\langle k|\hat{s}_j|k'\rangle\langle k'|\hat{s}_i|m\rangle\Big). \qquad (2.38)\end{aligned}$$

Then, by rewritting $\sum_k f_{kk'mm'} = \sum_{k\alpha} f_{\alpha k'km'}\delta_{km}$ where necessary

$$\begin{aligned}\langle m'|\dot{\hat{\rho}}_{\rm I}(t)|m\rangle = -\frac{1}{\hbar^2}\sum_{ijkk'}\langle k'|\hat{\rho}_{\rm I}(t)|k\rangle\Bigg\{&e^{i\omega_{m'k'}t}\sum_\alpha\langle m'|\hat{s}_i|k\rangle\langle k|\hat{s}_j|k'\rangle\int_0^\infty dt''e^{-i\omega_{\alpha k'}t''}\langle\hat{r}_i(t'')\hat{r}_j\rangle\delta_{mk} \\ &-e^{i(\omega_{m'k'}+\omega_{km})t}\langle m'|\hat{s}_j|k'\rangle\langle k|\hat{s}_i|m\rangle\int_0^\infty dt''e^{-i\omega_{m'k'}t''}\langle\hat{r}_i(t'')\hat{r}_j\rangle \qquad (2.39)\\ &-e^{i(\omega_{m'k'}+\omega_{km})t}\langle m'|\hat{s}_i|k'\rangle\langle k|\hat{s}_j|m\rangle\int_0^\infty dt''e^{-i\omega_{km}t''}\langle\hat{r}_j\hat{r}_i(t'')\rangle \\ &+e^{i\omega_{km}t}\sum_\alpha\langle k|\hat{s}_j|\alpha\rangle\langle\alpha|\hat{s}_i|m\rangle\int_0^\infty dt''e^{-i\omega_{k\alpha}t''}\langle\hat{r}_j\hat{r}_i(t'')\rangle\delta_{m'k'}\Bigg\}.\end{aligned}$$

Defining

$$\lambda^+_{mkln} = \frac{1}{\hbar^2}\sum_{ij}\langle m|\hat{s}_i|k\rangle\langle l|\hat{s}_j|n\rangle\int_0^\infty dt''e^{-i\omega_{ln}t''}\langle\hat{r}_i(t'')\hat{r}_j\rangle \qquad (2.40)$$

$$\lambda^-_{mkln} = \frac{1}{\hbar^2}\sum_{ij}\langle m|\hat{s}_j|k\rangle\langle l|\hat{s}_i|n\rangle\int_0^\infty dt''e^{-i\omega_{mk}t''}\langle\hat{r}_j\hat{r}_i(t'')\rangle, \qquad (2.41)$$

one obtains the differential equation for the density matrix elements

$$\langle m'|\dot{\hat{\rho}}_{\rm I}(t)|m\rangle = \sum_{kk'}\langle k'|\hat{\rho}_{\rm I}(t)|k\rangle R_{m'mk'k}e^{t(\omega_{m'k'}+\omega_{km})t}, \qquad (2.42)$$

where the *Redfield relaxation coefficients* are defined as

$$R_{m'mk'k} = -\delta_{mk}\sum_\alpha\lambda^+_{m'\alpha\alpha k'} + \lambda^+_{kmm'k'} + \lambda^-_{kmm'k'} - \delta_{m'k'}\sum_\alpha\lambda^-_{k\alpha\alpha m}. \qquad (2.43)$$

Note, that the coefficients (2.40) and (2.41) satisfy

$$\lambda^{-*}_{mnkl} = \lambda^+_{lknm} \qquad (2.44)$$

$$\lambda^\pm_{mmln} = \lambda^\pm_{lkmm} = 0. \qquad (2.45)$$

Considering that the typical period of variation of the system, ω^{-1}_{mn}, is much shorter than the time integration step (which also must be long enough to satisfy the Markov approximation), one can keep only the (*secular*) terms satisfying

$$E_{m'} - E_{k'} + E_k - E_m = 0. \qquad (2.46)$$

All the rest only contribute to fast oscillating terms and can be neglected[31]. Then, if the states are non-degenerate, so each energy defines only one state, and the separation between energies is not-regular, only three cases satisfy (2.46):

1. $m' = k'$, $m = k$, $m' \neq m$
2. $m' = m$, $k' = k$, $m' \neq k'$
3. $m' = m = k' = k$.

Then, (2.42) is written in terms of time-independent terms:

$$\begin{aligned}\langle m'|\dot{\hat{\rho}}_{\rm I}(t)|m\rangle &= (1-\delta_{m'm})\langle m'|\hat{\rho}_{\rm I}(t)|m\rangle R_{m'mm'm} + \delta_{mm'}\sum_{k\neq m}\langle k|\hat{\rho}_{\rm I}(t)|k\rangle R_{mmkk} \\ &\quad +\delta_{mm'}\langle m'|\hat{\rho}_{\rm I}(t)|m'\rangle R_{m'm'm'm'}. \end{aligned} \tag{2.47}$$

The first and third terms can be grouped by dropping the condition $m \neq m'$ and using (2.45):

$$R_{m'mm'm} = -\sum_{\alpha\neq m'}\lambda^{+}_{m'\alpha\alpha m'} - \sum_{\alpha\neq m}\lambda^{-}_{m\alpha\alpha m} \tag{2.48}$$

while the second one is

$$R_{mmkk} = \lambda^{+}_{kmmk} + \lambda^{-}_{kmmk} = 2{\rm Re}\lambda^{+}_{kmmk}. \tag{2.49}$$

These two terms will contribute in a very different way, so it is convenient to rename them, $\Lambda_{m'm} = -R_{m'mm'm}$ and $\Gamma_{mk} = R_{mmkk}$. Then, the equation of motion–*master equation* for the reduced density matrix elements is finally:

$$\langle m'|\dot{\hat{\rho}}_{\rm I}(t)|m\rangle = \delta_{mm'}\sum_{k\neq m}\langle k|\hat{\rho}_{\rm I}(t)|k\rangle\Gamma_{mk} - \langle m'|\hat{\rho}_{\rm I}(t)|m'\rangle\Lambda_{m'm}. \tag{2.50}$$

It is interesting to distinguish the diagonal ($m = m'$) and off-diagonal ($m \neq m'$) terms. For the first ones,

$$\Lambda_{mm} = \sum_{\alpha\neq m}\left(\lambda^{+}_{m\alpha\alpha m} + \lambda^{-}_{m\alpha\alpha m}\right) = \sum_{\alpha\neq m}\Gamma_{\alpha m} \tag{2.51}$$

so they coincide with the classical rate equations for the populations

$$\langle m|\dot{\hat{\rho}}_{\rm I}(t)|m\rangle = \sum_{k\neq m}\left(\langle k|\hat{\rho}_{\rm I}(t)|k\rangle\Gamma_{mk} - \langle m|\hat{\rho}_{\rm I}(t)|m\rangle\Gamma_{km}\right). \tag{2.52}$$

These kind of equations are also called *loss and gain equations* since they relate the de-population of some states with the population of others. Then, the coeficients Γ_{km} can be interpreted as the transition rates from state $|m\rangle$ to $|k\rangle$ due to the perturbative interaction.

The off diagonal terms–called *coherences*– describe the decoherence, i.e. how the coherence is damped:

$$\langle m'|\dot{\hat{\rho}}_{\rm I}(t)|m\rangle = -\langle m'|\hat{\rho}_{\rm I}(t)|m'\rangle\Lambda_{m'm}, \qquad \text{for} \quad m \neq m' \tag{2.53}$$

with the hermiticity condition fulfilled by $\Lambda_{m'm} = \Lambda^{*}_{mm'}$.

The real part of $\Lambda_{m'm}$ is related to the transition rates:

$$\begin{aligned}{\rm Re}\Lambda_{m'm} &= {\rm Re}\left(\sum_{\alpha\neq m'}\lambda^{+}_{m'\alpha\alpha m'} + \sum_{\alpha\neq m}\lambda^{-}_{m\alpha\alpha m}\right) = {\rm Re}\left(\sum_{\alpha\neq m'}\lambda^{+}_{m'\alpha\alpha m'} + \sum_{\alpha\neq m}\lambda^{+}_{m\alpha\alpha m}\right) \\ &= \frac{1}{2}\left(\sum_{\alpha\neq m'}\Gamma_{\alpha m'} + \sum_{\alpha\neq m}\Gamma_{\alpha m}\right) \end{aligned} \tag{2.54}$$

by taking into account (2.44) and (2.49). The imaginary part can be disregarded when going back into the Schödinger picture as they only introduce a small shift in the energies:

$$\langle m|\dot{\hat{\rho}}(t)|m\rangle = \sum_{k\neq m}\left(\Gamma_{mk}\langle k|\hat{\rho}(t)|k\rangle - \Gamma_{km}\langle m|\hat{\rho}(t)|m\rangle\right) \tag{2.55}$$

$$\langle m'|\dot{\hat{\rho}}(t)|m\rangle = -\frac{i}{\hbar}\langle m'|[\hat{H}_{\mathcal{S}},\hat{\rho}(t)]|m\rangle - \frac{1}{2}\left(\sum_{\alpha\neq m'}\Gamma_{\alpha m'} + \sum_{\alpha\neq m}\Gamma_{\alpha m}\right)\langle m'|\hat{\rho}(t)|m'\rangle \quad (m\neq m') \tag{2.56}$$

These equations of motion describe the transition from the initial state, $\rho(0)$, to the asymptotic limit, ρ_∞, when the system reaches its stationary solution, so $\dot{\rho}_\infty(t)=0$.

2.3 Transition rates

As discussed above, the coefficients Γ_{mn} give the probability by unit time that the interaction with the reservoir induced a transition $|n\rangle\to|m\rangle$ in $\mathcal{S}$. By writing explicitely

$$\begin{aligned}\langle\hat{r}_i(t'')\hat{r}_j\rangle &= \sum_{NN'N''}\langle N|\hat{r}_i(t'')|N'\rangle\langle N'|\hat{r}_j|N''\rangle\langle N''|\hat{\chi}_{\mathcal{R}}(0)|N\rangle \\ &= \sum_{NN'} e^{i(E_N-E_{N'})t''/\hbar}\langle N|\hat{r}_i|N'\rangle\langle N'|\hat{r}_j|N\rangle\langle N|\hat{\chi}_{\mathcal{R}}(0)|N\rangle,\end{aligned} \tag{2.57}$$

where it has been considered that the density matrix of the reservoir is diagonal and, in the same way,

$$\langle\hat{r}_j\hat{r}_i(t'')\rangle = \sum_{NN'} e^{i(E_{N'}-E_N)t''/\hbar}\langle N|\hat{r}_j|N'\rangle\langle N'|\hat{r}_i|N\rangle\langle N|\hat{\chi}_{\mathcal{R}}(0)|N\rangle, \tag{2.58}$$

(2.49) becomes

$$\begin{aligned}\Gamma_{mn} = \frac{1}{\hbar^2}\sum_{ijNN'}\langle N|\hat{\chi}_{\mathcal{R}}(0)|N\rangle\Bigg(&\langle n|\hat{s}_i|m\rangle\langle m|\hat{s}_j|n\rangle\int_0^\infty dt'' e^{i(E_N-E_{N'}-\hbar\omega_{mn})t''/\hbar}\langle N|\hat{r}_i|N'\rangle\langle N'|\hat{r}_j|N\rangle \\ &+\langle n|\hat{s}_j|m\rangle\langle m|\hat{s}_i|n\rangle\int_0^\infty dt'' e^{i(E_{N'}-E_N-\hbar\omega_{nm})t''/\hbar}\langle N|\hat{r}_j|N'\rangle\langle N'|\hat{r}_i|N\rangle\Bigg).\end{aligned} \tag{2.59}$$

By changing $t''\to -t''$ in the last integral:

$$\begin{aligned}\Gamma_{mn} = \frac{1}{\hbar^2}\sum_{ijNN'}\langle N|\hat{\chi}_{\mathcal{R}}(0)|N\rangle\Bigg(&\langle nN|\hat{s}_i\hat{r}_i|mN'\rangle\langle mN'|\hat{s}_j\hat{r}_j|nN\rangle\int_0^\infty dt'' e^{i(E_N-E_{N'}-\hbar\omega_{mn})t''/\hbar} \\ &+\langle nN|\hat{s}_j\hat{r}_j|mN'\rangle\langle mN'|\hat{s}_i\hat{r}_i|nN\rangle\int_{-\infty}^0 dt'' e^{i(E_{N'}-E_N-\hbar\omega_{nm})t''/\hbar}\Bigg).\end{aligned} \tag{2.60}$$

Using the definition of the Dirac delta, $\int_{-\infty}^{\infty} dk e^{\pm ik(x-a)} = 2\pi\delta(x-a)$, the transition rates

$$\Gamma_{mn} = \frac{2\pi}{\hbar}\sum_{NN'}\langle N|\hat{\chi}_{\mathcal{R}}(0)|N\rangle\left|\langle nN|\hat{V}|mN'\rangle\right|^2\delta(E_N-E_{N'}-\hbar\omega_{mn}) \tag{2.61}$$

adopt the well known Fermi Golden Rule for the first order time dependent perturbation theory. The Dirac delta ensures energy conservation during the process.

2.3.1 Tunneling rates

In the case of electronic transport, the perturbation $\hat{V}$ consists in the coupling to electronic leads, which is modeled by the tunneling Hamiltonian

$$\hat{H}_T = \sum_{lk\sigma} \gamma_l \hat{d}^\dagger_{lk\sigma} \hat{c}_\sigma + \text{h.c.}, \tag{2.62}$$

where the operators $\hat{d}^\dagger_{lk\sigma}$ creates an electron with spin σ in the lead $l = \{\text{L}, \text{R}\}$ while $\hat{c}_\sigma$ annihilates an electron with spin σ in the quantum system. The strength of the coupling, γ_l is asumed to be small.

If $|m\rangle$ and $|n\rangle$ in (2.61) represent occupation states of $\mathcal{S}$ that differ in one electron, two different rates can be considered: Γ^+_{mn} and Γ^-_{mn} if an electron tunnels out or into the system in the transition from $|n\rangle$ to $|m\rangle$, respectively. Denoting $\chi_{lN} = \langle N|\hat{\chi}_l(0)|N\rangle$ to the probability of finding the lead l in the state N, one have

$$\Gamma_{mn} = \frac{2\pi}{\hbar} \sum_{NN'} \chi_{lN} \left|\langle nN|\hat{H}_T|mN'\rangle\right|^2 \delta(E_N - E_{N'} - \hbar\omega_{mn}). \tag{2.63}$$

In the case when an electron is extracted to the collector, only the terms in $\hat{H}_T$ containing $\hat{c}_\sigma$ contribute:

$$\begin{aligned}
\sum_{NN'k} \chi_{lN} \left|\langle nN|\hat{H}_T|mN'\rangle\right|^2 &= \sum_{NN'k} \chi_{lN}|\gamma_l|^2 \langle nN|\hat{c}^\dagger \hat{d}_{lk}|mN'\rangle\langle mN'|\hat{d}^\dagger_{lk}\hat{c}|nN\rangle \\
&= \sum_{NN'k} \chi_{lN}|\gamma_l|^2 \langle N|\hat{d}_{lk}|N'\rangle\langle N'|\hat{d}^\dagger_{lk}|N\rangle \\
&= \sum_{Nk} \chi_{lN}|\gamma_l|^2 \langle N|\hat{d}_{lk}\hat{d}^\dagger_{lk}|N\rangle = \sum_{Nk} \chi_{lN}|\gamma_l|^2 \left(1 - \langle N|\hat{d}^\dagger_{lk}\hat{d}_{lk}|N\rangle\right).
\end{aligned} \tag{2.64}$$

The terms depending on N satisfy the definition of the Fermi distribution function

$$f_l(\varepsilon_k) = \sum_N \chi_{lN} \langle N|\hat{d}^\dagger_{lk}\hat{d}_{lk}|N\rangle \tag{2.65}$$

and

$$\sum_N \chi_{lN} = 1. \tag{2.66}$$

The electronic states in the leads conform a continuum, so $\sum_k$ can be replaced by an integral $\int d\varepsilon$, so the rate becomes:

$$\Gamma^+_{mn} = \frac{2\pi}{\hbar} \sum_l |\gamma_l|^2 \int d\varepsilon \, (1 - f_l(\varepsilon_k)) \, \delta(\varepsilon - \hbar\omega_{mn}) = \frac{2\pi}{\hbar} \sum_l |\gamma_l|^2 \, (1 - f_l(\hbar\omega_{mn})), \tag{2.67}$$

with

$$f_l(\varepsilon) = \frac{1}{1 + e^{(\varepsilon-\mu)\beta}}. \tag{2.68}$$

$\beta = \frac{1}{k_B T}$ and μ is the chemical potential of the lead. In the same way:

$$\Gamma^-_{mn} = \frac{2\pi}{\hbar} \sum_l |\gamma_l|^2 f_l(\hbar\omega_{mn}). \tag{2.69}$$

The $\pm$ sign in the superindex of the tunneling rates indicates whether they contribute to the increasing or decreasing of the number of electrons transferred to the lead. This will define the sign of the electronic current.

2.4 Current

As seen in (2.6), every observable can be expressed in terms of the density matrix. The current can be defined as the time derivative of the number of electrons accumulated in the collector, $\hat{\mathcal{N}}_{\rm R}$[12]:

$$I = -e\langle\dot{\hat{\mathcal{N}}}_{\rm R}\rangle = -e\langle[\hat{H},\hat{\mathcal{N}}_{\rm R}]\rangle = -tr\left(e[\hat{H},\hat{\mathcal{N}}_{\rm R}]\hat{\rho}\right). \tag{2.70}$$

The cyclic property of the trace allows to rewrite the previous expression

$$-tr\left([\hat{H},\hat{\mathcal{N}}_{\rm R}]\hat{\rho}\right) = -tr\left(\hat{H}\hat{\mathcal{N}}_{\rm R}\hat{\rho} - \hat{\mathcal{N}}_{\rm R}\hat{H}\hat{\rho}\right) = -tr\left(\hat{\mathcal{N}}_{\rm R}\hat{\rho}\hat{H} - \hat{\mathcal{N}}_{\rm R}\hat{H}\hat{\rho}\right) = tr\left(\hat{\mathcal{N}}_{\rm R}[\hat{H},\hat{\rho}]\right) \tag{2.71}$$

and, therefore,

$$I = tr\left(e\hat{\mathcal{N}}_{\rm R}\dot{\hat{\rho}}\right). \tag{2.72}$$

Then, it is convenient to decompose the reduced density matrix in terms with different number of electrons in the collector[21]

$$\rho(t) = \sum_N \rho^{(N)}(t). \tag{2.73}$$

The master equations for these elements is

$$\langle mN|\dot{\hat{\rho}}(t)|mN\rangle = \sum_{k\neq m}\sum_{N'}\left(\Gamma_{mk}^{NN'}\langle kN'|\hat{\rho}(t)|kN'\rangle - \Gamma_{km}^{N'N}\langle mN|\hat{\rho}(t)|mN\rangle\right) \tag{2.74}$$

with

$$\Gamma_{mn}^{N'N} = \frac{2\pi}{\hbar}\chi_{lN}\left|\langle nN|\hat{H}_T|mN'\rangle\right|^2\delta(E_N - E_{N'} - \hbar\omega_{mn}). \tag{2.75}$$

$\hat{\mathcal{N}}_{\rm R}$ is diagonal in this basis, so the off-diagonal elements (2.53) of the density matrix do not contribute to the current. Then,

$$\begin{aligned} tr\left(\hat{\mathcal{N}}_{\rm R}\dot{\hat{\rho}}\right) &= \sum_{mN} N\langle mN|\dot{\hat{\rho}}(t)|mN\rangle \\ &= \sum_{mNN'} N\sum_{k\neq m}\left(\Gamma_{mk}^{NN'}\langle kN'|\hat{\rho}(t)|kN'\rangle - \Gamma_{km}^{N'N}\langle mN|\hat{\rho}(t)|mN\rangle\right). \end{aligned} \tag{2.76}$$

If only sequencial transport is considered, electrons will be transferred one by one and $N = N' \pm 1$. The condition $k \neq m$ can be removed since all the transitions change the state of the system and $\Gamma_{mm} = 0$. Then,

$$\begin{aligned} tr\left(\hat{\mathcal{N}}_{\rm R}\dot{\hat{\rho}}\right) &= \sum_{kmN} N\left(\Gamma_{mk}^{NN+1}\langle kN+1|\hat{\rho}(t)|kN+1\rangle + \Gamma_{mk}^{NN-1}\langle kN-1|\hat{\rho}(t)|kN-1\rangle\right. \\ &\quad \left. -\Gamma_{km}^{N+1N}\langle mN|\hat{\rho}(t)|mN\rangle - \Gamma_{km}^{N-1N}\langle mN|\hat{\rho}(t)|mN\rangle\right). \end{aligned} \tag{2.77}$$

By considering new variables, $N' = N+1$ and $N' = N-1$ in the third and fourth terms in the right side of (2.77), respectively and then rewriting again $N' \to N$ and changing $k \leftrightarrow m$:

$$\begin{aligned} tr\left(\hat{\mathcal{N}}_{\rm R}\dot{\hat{\rho}}\right) &= \sum_{kmN}\left(N\Gamma_{mk}^{NN+1}\langle kN+1|\hat{\rho}(t)|kN+1\rangle + N\Gamma_{mk}^{NN-1}\langle kN-1|\hat{\rho}(t)|kN-1\rangle\right. \\ &\quad \left. -(N-1)\Gamma_{mk}^{NN-1}\langle kN-1|\hat{\rho}(t)|kN-1\rangle - (N+1)\Gamma_{mk}^{NN+1}\langle kN+1|\hat{\rho}(t)|kN+1\rangle\right) \end{aligned} \tag{2.78}$$

can be simplified

$$tr\left(\hat{\mathcal{N}}_{\rm R}\dot{\hat{\rho}}\right) = \sum_{kmN}\left(\Gamma_{mk}^{NN-1}\langle kN-1|\hat{\rho}(t)|kN-1\rangle - \Gamma_{mk}^{NN+1}\langle kN+1|\hat{\rho}(t)|kN+1\rangle\right). \tag{2.79}$$

As shown in the previous section, one can write $\Gamma_{nm}^{NN'}$ depends only on the change of particles in the collector in the transition from $|m\rangle$ to $|n\rangle$ so, writting it as $\Gamma_{nm}^{N-N'}$, they can be extracted from the sum:

$$\begin{aligned} tr\left(\hat{\mathcal{N}}_{\rm R}\dot{\hat{\rho}}\right) &= \sum_{km}\left(\Gamma_{mk}^{+1}\sum_{N}\langle kN-1|\hat{\rho}(t)|kN-1\rangle - \Gamma_{mk}^{-1}\sum_{N}\langle kN+1|\hat{\rho}(t)|kN+1\rangle\right) \\ &= \sum_{km}\left(\Gamma_{mk}^{+1}-\Gamma_{mk}^{-1}\right)\langle k|\hat{\rho}(t)|k\rangle. \end{aligned} \tag{2.80}$$

Thus, the final expression for the current is

$$I(t) = e\sum_{km}\left(\Gamma_{mk}^{+}-\Gamma_{mk}^{-}\right)\langle k|\hat{\rho}(t)|k\rangle, \tag{2.81}$$

where Γ_{mk}^{+} and Γ_{mk}^{-} are the rates for processes that involve an electron tunneling to and from the collector, respectively. Their expressions is analogue to those shown in (2.67) and (2.69), considering only the terms involving the collector.

2.5 Single resonant level in a quantum dot–Sequencial tunneling

A quantum dot (QD) with a single level (which will serve us as the small system $\mathcal{S}$) is coupled to two fermionic leads, L and R in the Coulomb blockade regime. That is, double occupancy is forbidden in the QD due to a high Coulomb repulsion and an electron cannot enter the system before it is empty. The model Hamiltonian is, considering *spinless* electrons

$$\hat{H} = \hat{H}_{\rm QD} + \hat{H}_{\rm leads} + \hat{H}_{\rm T} = \varepsilon\hat{c}^{\dagger}\hat{c} + \sum_{lk}\varepsilon_{lk}d_{lk}^{\dagger}\hat{d}_{lk} + \sum_{lk}\left(\gamma_l\hat{d}_{lk}^{\dagger}c + \text{H.c.}\right). \tag{2.82}$$

The basis consists in two states: $|0\rangle$ and $|1\rangle$ labeling the cases when the level in the QD is empty or it contains one electron, respectively.

In the high bias regime, the energy of the level falls in the transport window:

$$\mu_{\rm L} \gg \varepsilon \gg \mu_{\rm R} \tag{2.83}$$

so the tunneling rates are $\Gamma_{10} = \frac{2\pi}{\hbar}|\gamma_{\rm L}|^2 = \Gamma_{\rm L}$ and $\Gamma_{01} = \Gamma_{01}^{+} = \frac{2\pi}{\hbar}|\gamma_{\rm R}|^2 = \Gamma_{\rm R}$. Then, transport is uni-directional with electrons flowing through the system from the left to the right lead.

The basis consist on two states: $|0\rangle$, when the QD is empty, and $|1\rangle$, when there is an electron inside the QD. Then, one can write the master equations:

$$\dot{\rho}_{00} = -\Gamma_{\rm L}\rho_{00} + \Gamma_{\rm R}\rho_{11} \tag{2.84}$$

$$\dot{\rho}_{11} = \Gamma_{\rm L}\rho_{00} - \Gamma_{\rm R}\rho_{11} \tag{2.85}$$

with the normalization condition $\rho_{00}+\rho_{00}=1$. Note that there is no coherent processes inside the QD, so the off-diagonal terms do not contribute to the dynamics. The stationary solution is obtained by making $\dot{\rho}_{ij}=0$. This makes (2.84) equal to (2.85), giving:

$$\Gamma_{\rm L}\rho_{00} = \Gamma_{\rm R}\rho_{11} = \Gamma_{\rm R}(1-\rho_{00}). \tag{2.86}$$

Then,

$$\frac{1}{\Gamma_{\rm R}}\rho_{00} = \frac{1}{\Gamma_{\rm L}}\rho_{11} = \frac{1}{\Gamma_{\rm L}+\Gamma_{\rm R}}. \tag{2.87}$$

The stationary current is, then:

$$I = e\Gamma_{\rm R}\rho_{11} = \frac{e\Gamma_{\rm L}\Gamma_{\rm R}}{\Gamma_{\rm L}+\Gamma_{\rm R}}. \tag{2.88}$$

2.6 Spatial Rabi oscillations in a double quantum dot

Density matrix formalism allows to describe the reversible dynamics of the system, contained in the off diagonal terms. Ine example of that is Rabi oscillations in two level systems. If the states are in two differents sites, connected by a tunnel barrier, electrons would oscillate becoming spatially delocalized between them.

Considering now two quantum dots weakly coupled in series where one of them is coupled to the emitter and the other to the collector, again in the Coulomb blockade regime (only one electron is allowed in the DQD), the Hamiltonian is

$$\hat{H} = \hat{H}_{\rm DQD} + \hat{H}_{\rm leads} + \hat{H}_{\rm T} = \sum_l \varepsilon_l \hat{c}_l^\dagger \hat{c}_l + t_{\rm LR}\left(\hat{c}_{\rm L}^\dagger \hat{c}_{\rm R} + {\rm H.c.}\right) + \sum_{lk} \varepsilon_{lk} d_{lk}^\dagger \hat{d}_{lk} + \sum_{lk}\left(\gamma_l \hat{d}_{lk}^\dagger c + {\rm H.c.}\right). \tag{2.89}$$

The unperturbed Hamiltonian of the DQD can be represented in matricial form by

$$H_{\rm DQD} = \begin{pmatrix} \varepsilon_{\rm R} & t_{\rm LR} \\ t_{\rm LR}^* & \varepsilon_{\rm L} \end{pmatrix}, \tag{2.90}$$

which can be diagonalized yielding the eigenenergies

$$E_\pm = \frac{1}{2}\left(\varepsilon_{\rm R}+\varepsilon_{\rm L} \pm \sqrt{(\varepsilon_{\rm R}-\varepsilon_{\rm L})^2 + 4|t_{\rm LR}|^2}\right) \tag{2.91}$$

and eigenvectors[32]

$$|+\rangle = \cos\frac{\theta}{2}e^{-i\frac{\phi}{2}}|{\rm R}\rangle + \sin\frac{\theta}{2}e^{i\frac{\phi}{2}}|{\rm L}\rangle \tag{2.92}$$

$$|-\rangle = -\sin\frac{\theta}{2}e^{-i\frac{\phi}{2}}|{\rm R}\rangle + \cos\frac{\theta}{2}e^{i\frac{\phi}{2}}|{\rm L}\rangle, \tag{2.93}$$

with $\tan\theta = \frac{2|t_{\rm LR}|^2}{\varepsilon_{\rm R}-\varepsilon_{\rm L}}$ and $t_{\rm LR}^* = |t_{\rm LR}|e^{i\phi}$. $|{\rm R}\rangle$ and $|{\rm L}\rangle$ represent the states with one electron in the right and left QD, respectively. $|\pm\rangle$ then describe states where the charge is delocalized all over the DQD, usually referred as *bonding* and *antibonding* states, in analogy with the H_2^+ molecule.

In this basis, the tunneling rates are $\Gamma_{0+} = \cos^2\frac{\theta}{2}\Gamma_{\rm R}$, $\Gamma_{0-} = \sin^2\frac{\theta}{2}\Gamma_{\rm R}$, for the electrons tunneling to the collector and $\Gamma_{+0} = \sin^2\frac{\theta}{2}\Gamma_{\rm L}$ and $\Gamma_{-0} = \cos^2\frac{\theta}{2}\Gamma_{\rm L}$ for the electrons entering the DQD from the emitter and the master equation results

$$\begin{aligned}
\dot{\rho}_{00} &= \cos^2\frac{\theta}{2}\Gamma_{\rm R}\rho_{++} + \sin^2\frac{\theta}{2}\Gamma_{\rm R}\rho_{--} - \Gamma_{\rm L}\rho_{00} \\
\dot{\rho}_{++} &= \sin^2\frac{\theta}{2}\Gamma_{\rm L}\rho_{00} - \cos^2\frac{\theta}{2}\Gamma_{\rm R}\rho_{++} \\
\dot{\rho}_{--} &= \cos^2\frac{\theta}{2}\Gamma_{\rm L}\rho_{00} - \sin^2\frac{\theta}{2}\Gamma_{\rm R}\rho_{--}.
\end{aligned} \tag{2.94}$$

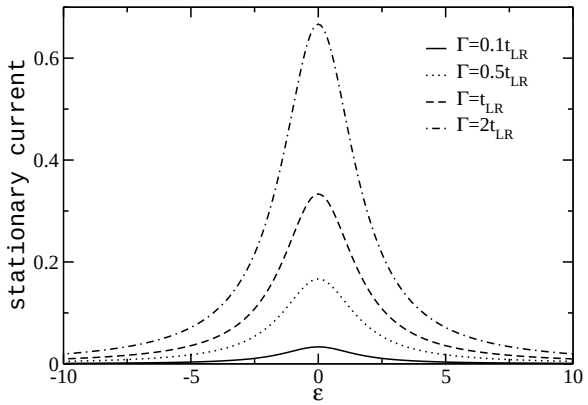

Fig. 2.1: Current as a function of the detuning for $t_{\rm LR} = 1$ and different couplings to the leads, $\Gamma_{\rm L} = \Gamma_{\rm R} = \Gamma$.

The stationary solution gives the occupation probabilities

$$\frac{\rho_0}{\Gamma_{\rm R}\tan^2\frac{\theta}{2}} = \frac{\rho_-}{\Gamma} = \frac{\rho_+}{\Gamma_{\rm L}\tan^4\frac{\theta}{2}} = \frac{1}{\Gamma_{\rm R}\tan^2\frac{\theta}{2} + \Gamma_{\rm L}(1+\tan^4\frac{\theta}{2})} \tag{2.95}$$

and a current

$$I = e\Gamma_{\rm R}(\cos^2\frac{\theta}{2}\rho_+ + \sin^2\frac{\theta}{2}\rho_-) = e\Gamma_{\rm L}\Gamma_{\rm R}\frac{\tan^2\frac{\theta}{2}}{\Gamma_{\rm R}\tan^2\frac{\theta}{2} + \Gamma_{\rm L}(1+\tan^4\frac{\theta}{2})} \tag{2.96}$$

which is maximal at resonance: $\varepsilon_{\rm L} = \varepsilon_{\rm R}$, see Fig. 2.1.

The master equation was derived considering the elements of the density matrix in the eigenbasis of $\mathcal{S}$, in this case, (2.92) and (2.93). However, this molecular basis does not provide any information on the coherent dynamics within the system. In order to describe it, it is convenient to consider the localized basis $|lr\rangle$, with $l, r = 0, 1$, which coincides with the *molecular* one $|\pm\rangle$ if $|t|^2 \ll (\varepsilon_{\rm R} = \varepsilon_{\rm L})^2$ i.e., for weak interdot coupling and finite detuning.

2.6.1 Coherent dynamics. Closed system

It is interesting to consider first the *closed* system, where the DQD is uncoupled to the leads and there is always an electron into the DQD. Then, the equation of motion can be written simply as $\dot{\hat{\rho}}(t) = [\hat{H}_{\rm DQD}, \hat{\rho}(t)]$. Note that, in this case, there is no relaxation in the system and the equations holds for any basis. Writing it in matricial form, $\dot{\rho}(t) = \mathcal{M}\rho(t)$, one obtains:

$$\begin{pmatrix} \dot{\rho}_{\rm LL} \\ \dot{\rho}_{\rm LR} \\ \dot{\rho}_{\rm RL} \\ \dot{\rho}_{\rm RR} \end{pmatrix} = \begin{pmatrix} 0 & it_{\rm LR} & -it_{\rm LR} & 0 \\ it_{\rm LR} & i\varepsilon & 0 & -it_{\rm LR} \\ -it_{\rm LR} & 0 & -i\varepsilon & it_{\rm LR} \\ 0 & -it_{\rm LR} & it_{\rm LR} & 0 \end{pmatrix} \begin{pmatrix} \rho_{\rm LL} \\ \rho_{\rm LR} \\ \rho_{\rm RL} \\ \rho_{\rm RR} \end{pmatrix}. \tag{2.97}$$

and taking the Laplace transform, $\mathcal{L}(\dot{\rho}(t)) = z\tilde{\rho}(z) = \mathcal{M}\tilde{\rho}(z) + \rho(0)$. Then, the time dependence of the density matrix elements is obtained by the inverse transform

$$\rho(t) = \mathcal{L}^{-1}\left\{(z - \mathcal{M})^{-1}\rho(0)\right\}. \tag{2.98}$$

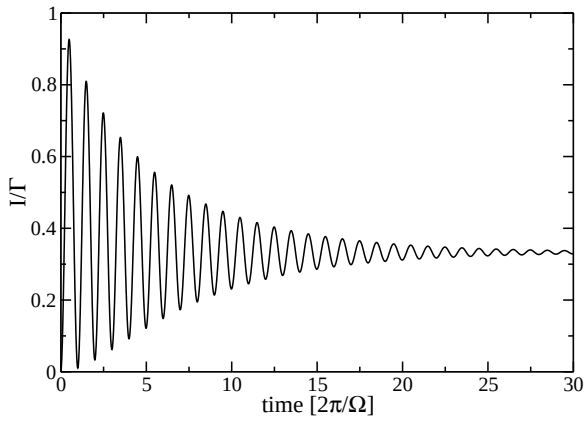

Fig. 2.2: Time dependence of the resonant current ($\varepsilon = 0$) for $t_{\rm LR} = 1$ and $\Gamma = 0.1$. The current shows periodic oscillations of frequency $\Omega = 2t_{\rm LR}$ due to the coherent charge delocalization inside the DQD.

When both levels are in resonance, the electron is coherently delocalized by the interdot coupling performing spacial Rabi oscillations with a frequency $\Omega = 2t_{\rm LR}$[32]:

$$\rho_{\rm RR}(t) = 1 - \rho_{\rm LL}(t) = \frac{4t_{\rm LR}^2}{4t_{\rm LR}^2 + \varepsilon^2} \sin^2\left(\frac{1}{2}\sqrt{\varepsilon^2 + 4t_{\rm LR}^2}\, t\right). \tag{2.99}$$

2.6.2 Decoherence

The coupling to the contacts produces incoherence and the oscillations are damped to a stationary solution, cf. Fig. 2.2, given by $\dot\rho_{ij} = 0$. The only finite transition rates for the high bias regime are: $\Gamma_{\rm L0} = \frac{2\pi}{\hbar}|\gamma_{\rm L}|^2 = \Gamma_{\rm L}$, $\Gamma_{\rm 0R} = \Gamma_{\rm 0R}^{+} = \frac{2\pi}{\hbar}|\gamma_{\rm R}|^2 = \Gamma_{\rm R}$. The master equation is[33]

$$\begin{aligned}
\dot\rho_{00} &= -\Gamma_{\rm L0}\rho_{00} + \Gamma_{\rm 0R}\rho_{\rm RR} \\
\dot\rho_{\rm LL} &= \Gamma_{\rm L0}\rho_{00} - it_{\rm LR}(\rho_{\rm RL} - \rho_{\rm LR}) \\
\dot\rho_{\rm LR} &= \left(i\varepsilon - \frac{1}{2}\Gamma_{\rm 0R}\right)\rho_{\rm LR} - it_{\rm LR}(\rho_{\rm RR} - \rho_{\rm LL}) \\
\dot\rho_{\rm RR} &= -\Gamma_{\rm 0R}\rho_{\rm RR} - it_{\rm LR}(\rho_{\rm LR} - \rho_{\rm RL}),
\end{aligned} \tag{2.100}$$

where $\varepsilon = \varepsilon_{\rm R} - \varepsilon_{\rm L}$ is the detuning. The stationary state is then

$$\rho_{00} = \frac{4t_{\rm LR}^2}{4t_{\rm LR}^2\Gamma_{\rm R} + \Gamma_{\rm L}(8t_{\rm LR}^2 + \Gamma_{\rm R}^2 + 4\varepsilon^2)} \tag{2.101}$$

$$\rho_{\rm LL} = \frac{\Gamma_{\rm L}(8t_{\rm LR}^2 + \Gamma_{\rm R}^2 + 4\varepsilon^2)}{4t_{\rm LR}^2\Gamma_{\rm R} + \Gamma_{\rm L}(8t_{\rm LR}^2 + \Gamma_{\rm R}^2 + 4\varepsilon^2)} \tag{2.102}$$

$$\rho_{\rm RR} = \frac{4t_{\rm LR}^2\Gamma_{\rm L}}{4t_{\rm LR}^2\Gamma_{\rm R} + \Gamma_{\rm L}(8t_{\rm LR}^2 + \Gamma_{\rm R}^2 + 4\varepsilon^2)} \tag{2.103}$$

$$\tag{2.104}$$

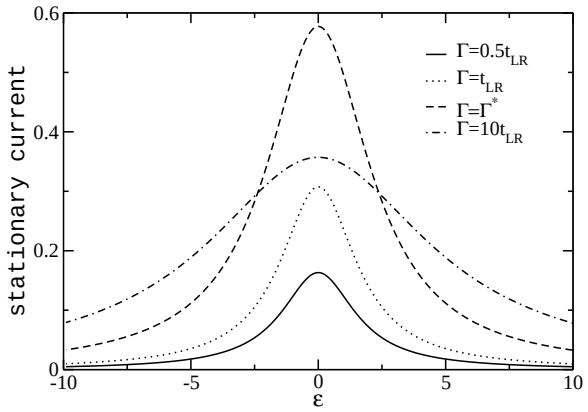

Fig. 2.3: Current as a function of the detuning for $t_{\rm LR} = 1$ and different couplings to the leads as calculated in the localized basis. For $\Gamma = \Gamma^* = \sqrt{12}t_{\rm LR}$ the current is maximal at resonance.

giving a stationary current which shows a Lorentzian peak $I = e\Gamma_{\rm R}\rho_{\rm RR} = \frac{I_0 W^2}{W^2+\varepsilon^2}$ with height I_0 and half width at half maximum W^2:

$$W^2 = \frac{4t_{\rm LR}^2(\Gamma_{\rm R}+2\Gamma_{\rm L})+\Gamma_{\rm L}\Gamma_{\rm R}^2}{4\Gamma_{\rm L}} \tag{2.105}$$

$$I_0 = e\Gamma_{\rm L}\Gamma_{\rm R}\frac{4t_{\rm LR}^2}{4t_{\rm LR}^2(\Gamma_{\rm R}+2\Gamma_{\rm L})+\Gamma_{\rm L}\Gamma_{\rm R}^2} \tag{2.106}$$

around the resonance condition, cf. Fig. 2.3. In the simpler case $\Gamma_{\rm L} = \Gamma_{\rm R} = \Gamma$, it is easy to see how the width of the peak increases with the coupling to the leads:

$$W^2 = 3t_{\rm LR}^2 + \frac{1}{4}\Gamma^2 \tag{2.107}$$

$$I_0 = e\Gamma\frac{4t_{\rm LR}^2}{12t_{\rm LR}^2+\Gamma^2}. \tag{2.108}$$

This result holds if the coupling to the leads is weak. If $\Gamma > t_{\rm LR}$, the processes through the contacts become more important and it is needed to consider the eigenbasis for which the master equation was derived. It can be seen by comparing Fig. 2.1 and 2.3, were the current calculated in the localized basis decreases for tunneling rates larger than $\Gamma = \sqrt{12}t_{\rm LR}$.

Another limitation of the formulation in the localized basis is that it may lead to results that violate thermodinamic properties of equilibrium[34]. For instance, if the DQD is coupled to un-biased leads with chemical potential μ, no current flows through the system. Having a configuration such that $\varepsilon_{\rm L} < \mu < \varepsilon_{\rm R}$, the only finite tunneling rates are $\Gamma_{0+} = \cos^2\frac{\theta}{2}\Gamma_{\rm R}$ and $\Gamma_{-0} = \sin^2\frac{\theta}{2}\Gamma_{\rm L}$, so the master equation obtained for the molecular basis becomes:

$$\begin{aligned}
\dot\rho_{00} &= \cos^2\frac{\theta}{2}\Gamma_{\rm R}\rho_{++} - \cos^2\frac{\theta}{2}\Gamma_{\rm L}\rho_{00} \\
\dot\rho_{++} &= -\cos^2\frac{\theta}{2}\Gamma_{\rm R}\rho_{++} \\
\dot\rho_{--} &= \cos^2\frac{\theta}{2}\Gamma_{\rm L}\rho_{00},
\end{aligned} \tag{2.109}$$

giving the stationary solution $\rho_{00} = \rho_{++} = 0$ and $\rho_{--} = 1$ and $I = 0$.

However, in the localized basis, (2.100) still hold. Though now the detuning can be arbitrarily high, the solution always provide an eventually residual but finite current *in equilibrium*, $I \sim \frac{|t_{\mathrm{LR}}|^2}{\varepsilon^2}$.

Chapter 3

Time-dependent potentials. Photon-assited tunneling

Electric fields –via laser illumination– have been largely applied to excite and explore the spectrum of multilevel atoms in the field of quantum optics. Similar methods can be used considering quantum dots, where the electric fields are usually applied by time-dependent gate voltages that introduce an oscillatory component in the energy levels. This affects the quantum dots by adding photo-sidebands in their energy spectrum which may open new conduction channels.

In the previous chapter, it was shown how the interaction of a small system, $\mathcal{S}$, with an out of equilibrium environment, $\mathcal{R}$, perturbed its equilibrium state (section 2.1.1), or took it out of equilibrium obliging it to relax to a stationary state (section 2.2). As a particular case, the electrostatic coupling of a quantum dot system to a biased environment (two electronic leads) produces a finite stationary current which can be described by means of tunneling-mediated relaxation processes. A similar description, however, can be made for cases where the small system is not brought out of equilibrium by the interaction with the environment(as, for instance, if no bias voltage is applied to the contacts of the quantum dot) but for an external potential.

The introduction of an external time dependent potencial may induce internal transitions and populate states involved in the incoherent transport, so the system will relax to a new stationary state in consonance with the new dynamics. Then, a finite current appears, under certain conditions (discussed below), in an unbiased system by the effect of the time dependent driving, which is known as *pumping*.

An important difference between the transport induced by a driving field and a bias voltage is the possibility of accessing internal processes of the quantum system by tuning the properties of the field (intensity and frequency). New properties appear as, for instance, the rotation of the electron spin by magnetic fields, spin filtering in double quantum dots or the coherent quenching of the current by electric fields[68]. These effects will be analyzed below.

3.1 Master equation in the presence of AC potentials

The effect of a sinusoidal time dependent potential gives a oscillatory component in the energies of $\mathcal{S}$: $\varepsilon_l \to \varepsilon_l + \tilde{\varepsilon}_l \cos\omega t$. In general, it will affect the interaction with the environment and one should take it into account in the derivation of the master equation.

The Hamiltonian is now

$$\hat{H}(t) = \hat{H}_{\mathcal{S}}(t) + \hat{H}_{\mathcal{R}} + \hat{V}, \tag{3.1}$$

where $\hat{H}_{\mathcal{S}}(t) = \hat{H}_{\mathcal{S}} + \hat{H}_{\rm AC}(t)$ and $[\hat{H}_{\mathcal{S}}, \hat{H}_{\rm AC}(t)] = 0$. A unitary transformation

$$\hat{U}(t) = e^{-i\int dt' \hat{H}_{\rm AC}(t')/\hbar} \tag{3.2}$$

removes the explicit time dependence from the Hamiltonian of the isolated system, $\hat{H}_{\mathcal{S}}$ according to

$$\hat{\tilde{H}}(t) = \hat{U}^{\dagger}(t)\left(\hat{H}(t) - i\hbar\partial_t\right)\hat{U}(t) = \hat{H}_{\mathcal{S}} + \hat{H}_{\mathcal{R}} + \hat{\tilde{V}}(t) \tag{3.3}$$

Then, the time dependence has been transferred to the interaction term which in the iteraction picture reads

$$\hat{\tilde{V}}_{\rm I}(t) = \sum_i \left(e^{i\int dt' \hat{H}_{\mathcal{S}}(t')/\hbar}\hat{s}_i e^{-i\int dt' \hat{H}_{\mathcal{S}}(t')/\hbar}\right)\left(e^{i\hat{H}_{\mathcal{R}}t/\hbar}\hat{r}_i e^{-i\hat{H}_{\mathcal{R}}t/\hbar}\right) = \sum_i \hat{s}_i(t)\hat{r}_i(t). \tag{3.4}$$

By comparing with (2.28), one sees that the same procedure as in the previous chapter can be followed here. Asuming that the same properties for the environment still hold, i.e., Markovian dynamics and irreversible interactions, one can write the same equation for the reduced density operator:

$$\dot{\hat{\rho}}_{\rm I}(t) = -\frac{1}{\hbar^2}\sum_{ij}\int_0^{\infty} dt''\{[\hat{s}_i(t), \hat{s}_j(t-t'')\hat{\rho}_{\rm I}(t)]\langle\hat{r}_i(t'')\hat{r}_j\rangle - [\hat{s}_i(t), \hat{\rho}_{\rm I}(t)\hat{s}_j(t-t'')]\langle\hat{r}_j\hat{r}_i(t'')\rangle\}. \tag{3.5}$$

Now, the time dependence is explicitely different:

$$\begin{aligned}\langle m'|[\hat{s}_i(t), \hat{s}_j(t-t'')\hat{\rho}_{\rm I}(t)]|m\rangle &= \sum_{kk'}(\mathcal{A}_{m'k'}(t)\mathcal{A}_{kk'}(t-t'')\langle m'|\hat{s}_i|k\rangle\langle k|\hat{s}_j|k'\rangle\langle k'|\hat{\rho}_{\rm I}(t)|m\rangle \\ &\quad -\mathcal{A}_{m'k'}(t-t'')\mathcal{A}_{km}(t)\langle m'|\hat{s}_j|k'\rangle\langle k'|\hat{\rho}_{\rm I}(t)|k\rangle\langle k|\hat{s}_j|m\rangle) \end{aligned} \tag{3.6}$$

$$\begin{aligned}\langle m'|[\hat{s}_i(t), \hat{\rho}_{\rm I}(t)\hat{s}_j(t-t'')]|m\rangle &= \sum_{kk'}(\mathcal{A}_{m'k}(t)\mathcal{A}_{k'm}(t-t'')\langle m'|\hat{s}_i|k\rangle\langle k|\hat{\rho}_{\rm I}(t)|k'\rangle\langle k'|\hat{s}_j|m\rangle \\ &\quad -\mathcal{A}_{km}(t)\mathcal{A}_{kk'}(t'')\langle m'|\hat{\rho}_{\rm I}(t)|k\rangle\langle k|\hat{s}_j|k'\rangle\langle k'|\hat{s}_i|m\rangle)\,, \end{aligned} \tag{3.7}$$

where $\mathcal{A}_{km}(t) = e^{i(\omega_{km}t + \frac{\zeta_{km}}{\hbar\omega}\sin\omega t)}$ and $\zeta_{km} = \tilde{\varepsilon}_k - \tilde{\varepsilon}_m$. Note that if the effect of the AC potential is the same in all the states connected by the relaxation it will not affect the interaction. Expressions (3.6) and (3.7) can be rewritten by using the relation

$$e^{i\alpha\sin\omega t} = \sum_{\nu} J_{\nu}(\alpha)e^{i\nu\omega t}, \tag{3.8}$$

where $J_\nu(\alpha)$ is the ν-th order Bessel function of the first kind obtaining the coefficients $\mathcal{A}_{km}(t) = \sum_\nu J_\nu\left(\frac{\zeta_{km}}{\hbar\omega}\right)e^{i(\omega_{km}+\nu\hbar\omega)t}$ and ν can be intrepreted as the number of photons involved or the sideband, with a spectral density $J_\nu(\alpha)$, that participates in the transition[68].

By defining

$$\lambda^{+}_{mkln,\nu\nu'} = \frac{1}{\hbar^2}\sum_{ij} J_\nu\left(\frac{\zeta_{mk}}{\hbar\omega}\right)J_{\nu'}\left(\frac{\zeta_{ln}}{\hbar\omega}\right)\langle m|\hat{s}_i|k\rangle\langle l|\hat{s}_j|n\rangle\int_0^{\infty} dt'' e^{-i\left(\omega_{ln}+\nu'\hbar\omega\right)t''}\langle\hat{r}_i\left(t''\right)\hat{r}_j\rangle \tag{3.9}$$

$$\lambda^{-}_{mkln,\nu\nu'} = \frac{1}{\hbar^2}\sum_{ij} J_\nu\left(\frac{\zeta_{ln}}{\hbar\omega}\right)J_{\nu'}\left(\frac{\zeta_{mk}}{\hbar\omega}\right)\langle m|\hat{s}_j|k\rangle\langle l|\hat{s}_i|n\rangle\int_0^{\infty} dt'' e^{-i\left(\omega_{mk}+\nu'\hbar\omega\right)t''}\langle\hat{r}_j\hat{r}_i(t'')\rangle, \tag{3.10}$$

one gets a *Redfield-like* equation

$$\langle m'|\dot{\hat{\rho}}_{\rm I}(t)|m\rangle = \sum_{kk'}\langle k'|\hat{\rho}_{\rm I}(t)|k\rangle R_{m'mk'k,\nu\nu'}e^{t(\omega_{m'k'}+\omega_{km}+(\nu+\nu')\hbar\omega)t}, \tag{3.11}$$

with coefficients

$$R_{m'mk'k,\nu\nu'} = -\delta_{mk}\sum_{\alpha}\lambda^{+}_{m'\alpha\alpha k'\nu\nu'} + \lambda^{+}_{kmm'k'\nu\nu'} + \lambda^{-}_{kmm'k'\nu\nu'} - \delta_{m'k'}\sum_{\alpha}\lambda^{-}_{k\alpha\alpha m\nu\nu'}. \tag{3.12}$$

modified by the photonic terms. If the frequency of the AC potential does not match the energy difference of the states of $\mathcal{S}$ involved in the relaxation transitions, the same secular terms as in the non-driven case (see previous chapter) can be kept by just considering $\nu' = -\nu$.

Then, defining $\Lambda_{m'm} = -\sum_{\nu} R_{m'mm'm,\nu-\nu}$ and $\Gamma_{mk} = \sum_{\nu} R_{mmkk,\nu-\nu}$, one obtains a master equation that is formally equal to (2.52) and (2.53) or, going back to the Schrödiger picture,

$$\langle m|\dot{\hat{\rho}}(t)|m\rangle = \sum_{k\neq m}\left(\Gamma_{mk}\langle k|\hat{\rho}(t)|k\rangle - \Gamma_{km}\langle m|\hat{\rho}(t)|m\rangle\right) \tag{3.13}$$

$$\langle m'|\dot{\hat{\rho}}(t)|m\rangle = -\frac{i}{\hbar}\langle m'|[\hat{H}_{\mathcal{S}},\hat{\rho}(t)]|m\rangle - \frac{1}{2}\left(\sum_{\alpha\neq m'}\Gamma_{\alpha m'} + \sum_{\alpha\neq m}\Gamma_{\alpha m}\right)\langle m'|\hat{\rho}(t)|m'\rangle \quad (m\neq m') \tag{3.14}$$

with coefficients that depend on the parameters of the AC potential. In the same way as done in section 2.3, and considering the property $J_{-\nu}(\alpha) = (-1)^{\nu}J_{\nu}(\alpha)$, one obtains the *photo-assisted* transition rates:

$$\Gamma_{mn} = \frac{2\pi}{\hbar}\sum_{\nu}\sum_{NN'}J^2_{\nu}\left(\frac{\zeta_{mn}}{\hbar\omega}\right)\langle N|\hat{\chi}_{\mathcal{R}}(0)|N\rangle\left|\langle nN|\hat{V}|mN'\rangle\right|^2\delta\left(E_N - E_{N'} - \hbar\omega_{mn} - \nu\hbar\omega\right). \tag{3.15}$$

3.2 Photon-assisted tunneling

If the interaction between $\mathcal{S}$ being a quantum dot and $\mathcal{R}$ electronic leads consists in a tunnel barrier, then:

$$\hat{H}_T = \sum_{lk\sigma}\gamma_l\hat{d}^{\dagger}_{lk\sigma}\hat{c}_{\sigma} + \text{h.c.}, \tag{3.16}$$

where the operators $\hat{d}^{\dagger}_{lk\sigma}$ creates an electron with spin σ in the lead $l = \{\text{L},\text{R}\}$ while $\hat{c}_{\sigma}$ annihilates an electron with spin σ in the quantum dot, the rates (3.15) describe tunneling processes mediated by the absorption or the emission of photons coming from the AC potential.

Following the steps sketched in section 2.3.1, it is straightforward to obtain the photo-assisted tunneling rates for electrons being transferred to the collector

$$\Gamma^{+}_{mn} = \frac{2\pi}{\hbar}\sum_{l\nu}J^2_{\nu}\left(\frac{\zeta_{mn}}{\hbar\omega}\right)|\gamma_l|^2\left(1 - f_l(\hbar\omega_{mn} + \nu\hbar\omega)\right) \tag{3.17}$$

and the ones entering the quantum dot

$$\Gamma^{-}_{mn} = \frac{2\pi}{\hbar}\sum_{l\nu}J^2_{\nu}\left(\frac{\zeta_{mn}}{\hbar\omega}\right)|\gamma_l|^2 f_l(\hbar\omega_{mn} + \nu\hbar\omega). \tag{3.18}$$

Here, as will be shown bellow, the coefficients ζ_{mn} depend only on the intensity of the AC potential and the number of transferred charges in each tunneling event (one, in this case).

Thus, electrons that, in the absence of a driving potential, will be confined in the quantum dot because the chemical potential of the transition is smaller than the Fermi level of the lead, $\mu_l > \hbar\omega_{out,in}$, can be extracted by the absorption of ν photons that provide the energy needed to satisfy the condition $\mu_l < \hbar\omega_{out,in} + \nu\hbar\omega$. In the same way, an electron from the collector can absorb photons to enter the quantum dot by a transition that requires an energy greater than μ_l. Then, states which are energetically non available have a finite occupation probability.

This effect limits the operativeness of devices based in electrically driven transitions, as will be further discussed.

3.3 A simple case: AC driven single level quantum dot

Let consider a quantum dot with spinless elcetrons where the Coulomb repulsion is high enough to avoid double occupancy of its single level. Then, only the states $|0\rangle$ and $|1\rangle$, representing the empty and occupied quantum dot, respectively, participate in the dynamics. An AC potential is introduced as a sinusoidal signal in the gate voltage which manifests as an oscillation in the energy of the occupied state. The Hamiltonian is then:

$$\hat{H}(t) = \left(\varepsilon + \frac{V_{\rm AC}}{2}\cos\omega t\right) c^\dagger c + \sum_{lk} \varepsilon_k d_{lk}^\dagger d_{lk} + \sum_{lk} \left(\gamma_l c^\dagger d_{lk} + \text{H.c.}\right). \tag{3.19}$$

By the unitary transformation $U(t) = e^{-i\frac{V_{\rm AC}}{2\hbar\omega}c^\dagger c}$, and the conmutation realation

$$[d_{lk}^\dagger c, c^\dagger c] = d_{lk}^\dagger c, \tag{3.20}$$

the time dependence is removed from the energy and appears in the tunneling terms which become

$$\sum_{lk\nu} (-1)^\nu J_\nu \left(\frac{V_{\rm AC}}{2\hbar\omega}\right) \left(\gamma_l e^{i\nu\hbar\omega t} c^\dagger d_{lk} + \text{H.c.}\right). \tag{3.21}$$

Then, the tunneling rates are

$$\Gamma_{01} = \frac{2\pi}{\hbar}\sum_{l\nu} J_\nu^2\left(\frac{V_{\rm AC}}{2\hbar\omega}\right)|\gamma_l|^2\left(1 - f_l(\hbar\omega_{01} + \nu\hbar\omega)\right) \tag{3.22}$$

$$\Gamma_{10} = \frac{2\pi}{\hbar}\sum_{l\nu} J_\nu^2\left(\frac{V_{\rm AC}}{2\hbar\omega}\right)|\gamma_l|^2 f_l(\hbar\omega_{10} + \nu\hbar\omega). \tag{3.23}$$

Assuming that the Fermi level of the left lead is high enough, i.e., that the electron in the quantum dot would need a large number of photons to tunnel to it, $\mu_{\rm L} \gg \hbar\omega$, all the terms proportional to $1 - f_{\rm L}(\hbar\omega_{01} + \nu\hbar\omega)$ will vanish. In the same way, tunneling from the left lead to the empty quantum dot is always allowed and $f_{\rm L}(\hbar\omega_{10} + \nu\hbar\omega) = 1$ for all ν. This is equivalent to say that tunneling through the left barrier is not affected by the AC potential. On contrary, if $\varepsilon < \mu_{\rm R} < \varepsilon + \hbar\omega$ the absorption of a single photon will be enough to extract the confined electron to the right lead, cf. Fig. 3.1. Then, the contribution of each barrier can be considered separately

$$\Gamma_{01,\rm L} = 0 \tag{3.24}$$

$$\Gamma_{10,\rm L} = \frac{2\pi}{\hbar}\sum_{\nu} J_\nu^2\left(\frac{V_{\rm AC}}{2\hbar\omega}\right)|\gamma_{\rm L}|^2 = \frac{2\pi}{\hbar}|\gamma_{\rm L}|^2 = \Gamma_{\rm L}, \tag{3.25}$$

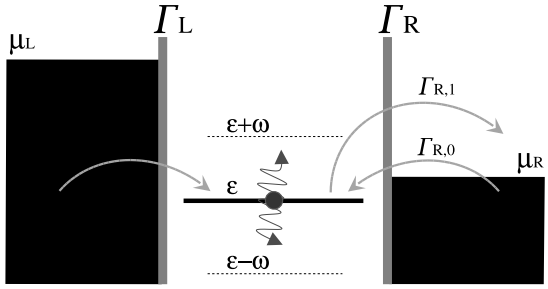

Fig. 3.1: Schematic diagram of an AC-driven quantum dot where transport requires photo-assisted tunneling.

for the left barrier and

$$\Gamma_{01,\mathrm{R}} = \frac{2\pi}{\hbar}\sum_{\nu=1}^{\infty} J_\nu^2\left(\frac{V_{\mathrm{AC}}}{2\hbar\omega}\right)|\gamma_{\mathrm{R}}|^2 = \frac{\pi}{\hbar}\left(1-J_0^2\left(\frac{V_{\mathrm{AC}}}{2\hbar\omega}\right)\right)|\gamma_{\mathrm{R}}|^2 = \Gamma_{\mathrm{R},1} \tag{3.26}$$

$$\Gamma_{10,\mathrm{R}} = \frac{2\pi}{\hbar}\sum_{\nu=-\infty}^{0} J_\nu^2\left(\frac{V_{\mathrm{AC}}}{2\hbar\omega}\right)|\gamma_{\mathrm{R}}|^2 = \frac{\pi}{\hbar}\left(1+J_0^2\left(\frac{V_{\mathrm{AC}}}{2\hbar\omega}\right)\right)|\gamma_{\mathrm{R}}|^2 = \Gamma_{\mathrm{R},0}, \tag{3.27}$$

for the right one, where it was used the normalization condition for the Bessel functions:

$$\sum_{\nu} J_\nu^2(\alpha) = J_0^2(\alpha) + 2\sum_{\nu>0} J_\nu^2(\alpha) = 1. \tag{3.28}$$

Note that $\Gamma_{\mathrm{R},0}+\Gamma_{\mathrm{R},1} = \frac{2\pi}{\hbar}|\gamma_{\mathrm{R}}|^2 = \Gamma_{\mathrm{R}}$.

The master equation has a balanced rate equations form

$$\dot{\rho}_0 = \Gamma_{\mathrm{R},1}\rho_1 - (\Gamma_{\mathrm{L}}+\Gamma_{\mathrm{R},0})\,\rho_0 \tag{3.29}$$

$$\dot{\rho}_1 = (\Gamma_{\mathrm{L}}+\Gamma_{\mathrm{R},0})\,\rho_0 - \Gamma_{\mathrm{R},1}\rho_1 \tag{3.30}$$

with $\rho_0+\rho_1 = 1$. The stationary solution is, then:

$$\rho_0 = \frac{\Gamma_{\mathrm{R},1}}{\Gamma_{\mathrm{L}}+\Gamma_{\mathrm{R}}} \tag{3.31}$$

$$\rho_1 = \frac{\Gamma_{\mathrm{L}}+\Gamma_{\mathrm{R},0}}{\Gamma_{\mathrm{L}}+\Gamma_{\mathrm{R}}} \tag{3.32}$$

which gives a finite current

$$I = e\,(\Gamma_{\mathrm{R},1}\rho_1 - \Gamma_{\mathrm{R},0}\rho_0) = \frac{e\Gamma_{\mathrm{L}}\Gamma_{\mathrm{R},1}}{\Gamma_{\mathrm{L}}+\Gamma_{\mathrm{R}}} = \frac{e}{2}\frac{\Gamma_{\mathrm{L}}\Gamma_{\mathrm{R}}}{\Gamma_{\mathrm{L}}+\Gamma_{\mathrm{R}}}\left(1-J_0^2\left(\frac{V_{\mathrm{AC}}}{2\hbar\omega}\right)\right) \tag{3.33}$$

that can be manipulated externally by tuning the intensity and frequency of the driving. In the low intensity limit, $V_{\mathrm{AC}} \to 0$,

$$I \sim \frac{e\Gamma_{\mathrm{L}}\Gamma_{\mathrm{R}}}{\Gamma_{\mathrm{L}}+\Gamma_{\mathrm{R}}}\frac{V_{\mathrm{AC}}^2}{16} \tag{3.34}$$

since $J_\nu(\alpha) \sim \frac{\alpha^\nu}{2^\nu \nu!}$ when $\alpha \to 0$[35]. On the other hand, $J_0(\alpha) \to 0$, when $\alpha \to \infty$ so in the high intensity limit, the current is:

$$I \to \frac{e}{2}\frac{\Gamma_{\mathrm{L}}\Gamma_{\mathrm{R}}}{\Gamma_{\mathrm{L}}+\Gamma_{\mathrm{R}}}. \tag{3.35}$$

3.3.1 Photo-sidebands

This result can be interpreted also in terms of the spectral decomposition of the wave function into sidebands corresponding to different numbers of photons. Considering an electron confined in an infinite well and under the effect of a time-dependent potential $V\cos\omega t$, the Schrödinger equation can be written

$$i\hbar\partial_t\psi(\mathbf{r},t)=\hat{H}(t)\psi(\mathbf{r},t)=(\varepsilon+V\cos\hbar\omega t)\psi(\mathbf{r},t), \tag{3.36}$$

where ε depends on the spatial coordinates. Solving (3.36) gives a wave function

$$\psi(\mathbf{r},t)=\psi(\mathbf{r},0)e^{-i(\varepsilon t+\frac{V}{\hbar\omega}\sin\hbar\omega t)/\hbar}=\psi(\mathbf{r},0)\sum_\nu J_\nu\left(\frac{V}{\hbar\omega}\right)e^{-i(\varepsilon+\nu\hbar\omega)t/\hbar}, \tag{3.37}$$

formally equivalent to the static one and indicating that the electron have a probability proportional to $J_\nu^2\left(\frac{V}{\hbar\omega}\right)$ to have an energy $\varepsilon\pm\nu\hbar\omega$[36].

It is interesting to note that, considering an open quantum dot in the weak coupling–high frequency limit[37], $\Gamma_i\ll\omega$, one obtains the photo-assisted tunneling rates (3.17) and (3.18) and the master equations (3.29) and (3.30), when considering tunneling through the photo-sidebands in the non-driven tunneling rates (2.67) and (2.69)[38].

The effect of sidebands has been detected in quantum dots by varying the gate voltage which shifts the energy levels in the quantum dot. When a side band enters the bias window, $\mu_{\rm R}>\varepsilon\pm\nu\hbar\omega>\mu_{\rm L}$, the current shows a resonant peak added to the undriven resonance described in section 2.5[39, 40] whose height is now proportional to $J_0^2\left(\frac{V}{\hbar\omega}\right)$. In the same way, the contribution of every ν-th satellite peak can be tuned by the intensity of the field through $J_\nu^2\left(\frac{V}{\hbar\omega}\right)$[39].

3.4 AC driven double quantum dot. Photon-assisted delocalization

Transport through a double quantum dot is supressed if the levels of the dots are not resonant, i.e., they do not have the same energy $\varepsilon_{\rm L}\neq\varepsilon_{\rm R}$, as seen in section 2.6. The electron is not able to tunnel through the interdot barrier and then remains localized in the left quantum dot. However, the introduction of time dependent potentials may induce photon-assisted tunneling when the frequency of the oscillation matches the energy separation between the discrete energy levels of the two quantum dots[41, 78]. It can be interpreted as resonances of the sidebands with different number of photons.

Considering two quantum dots coupled to two electronic leads modeled by the Hamiltonian

$$\hat{H}=\hat{H}_{\rm DQD}+\hat{H}_{\rm LR}+\hat{H}_{\rm leads}+\hat{H}_{\rm T} \tag{3.38}$$

where $\hat{H}_{\rm DQD}=\sum_l\left(\sum_\sigma\varepsilon_l\hat{c}_{l\sigma}^\dagger\hat{c}_{l\sigma}+U_i\hat{n}_{i\uparrow}\hat{n}_{i\downarrow}\right)+U_{\rm LR}\hat{n}_{\rm L}\hat{n}_{\rm R}$ represents the two isolated quantum dots with intra and inter-dot Coulomb repulsion, U_i and $U_{\rm LR}$, respectively, $\hat{H}_{\rm LR}=\sum_\sigma\left(t_{\rm LR}\hat{c}_{{\rm L}\sigma}^\dagger\hat{c}_{{\rm R}\sigma}+{\rm H.c.}\right)$, the interdot coupling, $\hat{H}_{\rm leads}=\sum_{lk\sigma}\varepsilon_{lk\sigma}\hat{d}_{lk\sigma}^\dagger\hat{d}_{lk\sigma}$, the leads and $\hat{H}_{\rm T}=\sum_{lk\sigma}\gamma_l\hat{c}_{l\sigma}^\dagger\hat{d}_{lk\sigma}$ the contacts to the leads. When applying an oscillatory potential with opposite phase to the gate voltages of the two dots, a term

$$\hat{H}_{\rm AC}(t)=\frac{V_{\rm AC}}{2\hbar\omega}\cos\omega t\sum_\sigma\left(\hat{c}_{{\rm L}\sigma}^\dagger\hat{c}_{{\rm L}\sigma}-\hat{c}_{{\rm R}\sigma}^\dagger\hat{c}_{{\rm R}\sigma}\right)=\frac{V_{\rm AC}}{2\hbar\omega}\cos\omega t\left(\hat{n}_{\rm L}-\hat{n}_{\rm R}\right) \tag{3.39}$$

must be added to the total Hamiltonian. A difference of phase–for simplicity and a higher experimental feasability, π– between the oscillations of gate voltages of each dot is essential or the internal dynamics

will not be affected. Also, spatial inhomogeneity or time reversal symmetry breaking is needed in order to obtain finite current. in our cse, it is provided by being le level in the left dot below the Fermi level of the leads, while the one in the right dot is above them.

As in previous sections, a unitary transformation

$$\hat{U}(t) = e^{i\int_{t_0}^{t} dt' \hat{H}_{\rm AC}(t')/\hbar} = e^{i\frac{V_{ac}}{2\hbar\omega}\sin\omega t(\hat{n}_{\rm L}-\hat{n}_{\rm R})} \tag{3.40}$$

is applied to the Hamiltonian

$$\hat{\tilde{H}}(t) = \hat{U}(t)\left(\hat{H} - i\hbar\partial_t\right)\hat{U}^{\dagger}(t) = \hat{H}_{\rm DQD} + \hat{\tilde{H}}_{LR}(t) + \hat{\tilde{H}}_{T}(t). \tag{3.41}$$

All the explicit time dependence enters the coupling terms since $\hat{H}_{\rm DQD}$ and $\hat{H}_{\rm leads}$ both commute with $\hat{U}(t)$. One have the relationships

$$[\hat{c}^{\dagger}_{{\rm R}\sigma}\hat{c}_{{\rm L}\sigma}, \hat{n}_{\rm L}] = \hat{c}^{\dagger}_{{\rm R}\sigma}\hat{c}_{{\rm L}\sigma} \tag{3.42}$$

$$[\hat{c}^{\dagger}_{{\rm R}\sigma}\hat{c}_{{\rm L}\sigma}, \hat{n}_{\rm R}] = -\hat{c}^{\dagger}_{{\rm R}\sigma}\hat{c}_{{\rm L}\sigma}, \tag{3.43}$$

for the interdot transitions and

$$[\hat{d}^{\dagger}_{lk\sigma}\hat{c}_{l\sigma}, \hat{n}_{l'}] = \hat{d}^{\dagger}_{kl\sigma}\hat{c}_{l\sigma}\delta_{ll'}, \tag{3.44}$$

for the coupling to the leads, obtaining the expressions for the transformed terms

$$\hat{\tilde{H}}_{\rm LR}(t) = \sum_{\nu=-\infty}^{\infty}(-1)^{\nu}J_{\nu}\left(\frac{V_{\rm AC}}{\hbar\omega}\right)\sum_{\sigma}\left(t_{\rm LR}e^{i\nu\hbar\omega t}\hat{c}^{\dagger}_{{\rm L}\sigma}\hat{c}_{{\rm R}\sigma} + {\rm H.c.}\right) \tag{3.45}$$

and

$$\hat{\tilde{H}}_{T}(t) = \sum_{\nu=-\infty}^{\infty}(-1)^{\nu}J_{\nu}\left(\frac{V_{\rm AC}}{2\hbar\omega}\right)\sum_{lk\sigma}\left(\gamma_l e^{i\nu\hbar\omega t}\hat{d}^{\dagger}_{lk\sigma}\hat{c}_{l\sigma} + {\rm H.c.}\right). \tag{3.46}$$

after using the property

$$\hat{\tilde{\mathcal{O}}} = \hat{\mathcal{O}} + [\hat{\mathcal{T}}, \hat{\mathcal{O}}] + \frac{1}{2!}[\hat{\mathcal{T}}, [\hat{\mathcal{T}}, \hat{\mathcal{O}}]] + ... \tag{3.47}$$

Note that the argument of the Bessel function in the interdot term is twice the one in the couplig to the leads. This is because the expected value of $\hat{n}_{\rm L} - \hat{n}_{\rm R}$ changes in ± 2 when an electron tunnels from one QD to the other and in ± 1 when it tunnels through the contact barriers. As discussed above, if the two dots were oscillating in phase so $\hat{H}_{\rm AC}(t) \propto \hat{n}_{\rm L} + \hat{n}_{\rm R}$, it is easy to see from (3.42), (3.43) and (3.47) that the interdot hopping term would not be transformed by the AC[42].

The AC field produces *coherent delocalization* between the two quantum dots via the interaction with ν photons when the energies of the states of each dot satify $\varepsilon_{\rm R} - \varepsilon_{\rm L} \sim \nu\hbar\omega$. Then, one can keep only the terms of (3.46) that put the states of the DQD in resonance by say n photons, which is analogue to consider the rotating wave approximation (RWA) in Quantum Optics[43, 44, 45, 46, 47] and disregard non-resonant oscillating terms:

$$\hat{\tilde{H}}^{\rm RWA}_{\rm LR} = (-1)^n J_n\left(\frac{V_{\rm AC}}{\hbar\omega}\right)\sum_{\sigma}\left(t_{\rm LR}e^{in\omega t}\hat{c}^{\dagger}_{{\rm L}\sigma}\hat{c}_{{\rm R}\sigma} + {\rm H.c.}\right). \tag{3.48}$$

It allows to define a Rabi frequency for the electronic oscillations between the two dots[48]

$$\Omega_n = 2J_{-n}\left(\frac{V_{\rm AC}}{\hbar\omega}\right)t_{\rm LR}, \tag{3.49}$$

renormalized in comparison with the undriven case studied in section 2.6.

3.4.1 Closed system

Let consider the closed system with a single electron and $\varepsilon = \varepsilon_{\rm R} - \varepsilon_{\rm L} = n\hbar\omega$, the dynamics is described by the coherent terms, $\dot{\hat{\rho}}(t) = [\hat{H}_{\rm DQD} + \hat{\tilde{H}}^{\rm RWA}_{\rm LR}, \hat{\rho}(t)]$. In matricial form $\dot{\rho} = \mathcal{M}\rho$

$$\begin{pmatrix} \dot{\rho}_{\rm LL} \\ \dot{\rho}_{\rm LR} \\ \dot{\rho}_{\rm RL} \\ \dot{\rho}_{\rm RR} \end{pmatrix} = \begin{pmatrix} 0 & i\frac{\Omega_n}{2}e^{in\hbar\omega t} & -i\frac{\Omega_n}{2}e^{-in\hbar\omega t} & 0 \\ i\frac{\Omega_n}{2}e^{in\hbar\omega t} & i\varepsilon & 0 & i\frac{\Omega_n}{2}e^{in\hbar\omega t} \\ -i\frac{\Omega_n}{2}e^{-in\hbar\omega t} & 0 & -i\varepsilon & -i\frac{\Omega_n}{2}e^{-in\hbar\omega t} \\ 0 & -i\frac{\Omega_n}{2}e^{-in\hbar\omega t} & i\frac{\Omega_n}{2}e^{in\hbar\omega t} & 0 \end{pmatrix} \begin{pmatrix} \rho_{\rm LL} \\ \rho_{\rm LR} \\ \rho_{\rm RL} \\ \rho_{\rm RR} \end{pmatrix}. \tag{3.50}$$

Changing the off-diagonal variables

$$\rho'_{\rm LR}(t) = e^{-in\hbar\omega t}\rho_{\rm LR}(t) \tag{3.51}$$

so $\dot{\rho}'_{\rm LR} = -in\hbar\omega\rho'_{\rm LR} + e^{-in\hbar\omega t}\dot{\rho}_{\rm LR}$, one obtains a differential equation with time-independent coefficients

$$\begin{pmatrix} \dot{\rho}_{\rm LL} \\ \dot{\rho}'_{\rm LR} \\ \dot{\rho}'_{\rm RL} \\ \dot{\rho}_{\rm RR} \end{pmatrix} = \begin{pmatrix} 0 & i\frac{\Omega_n}{2} & -i\frac{\Omega_n}{2} & 0 \\ i\frac{\Omega_n}{2} & i(\varepsilon - n\hbar\omega) & 0 & i\frac{\Omega_n}{2} \\ -i\frac{\Omega_n}{2} & 0 & -i(\varepsilon - n\hbar\omega) & -i\frac{\Omega_n}{2} \\ 0 & -i\frac{\Omega_n}{2} & i\frac{\Omega_n}{2} & 0 \end{pmatrix} \begin{pmatrix} \rho_{\rm LL} \\ \rho'_{\rm LR} \\ \rho'_{\rm RL} \\ \rho_{\rm RR} \end{pmatrix} \tag{3.52}$$

which is formally equivalent to the undriven (2.97), yielding a stationary solution

$$\rho_{\rm RR}(t) = 1 - \rho_{\rm LL}(t) = \frac{\Omega_n^2}{\Omega_n^2 + (\varepsilon - n\hbar\omega)^2}\sin^2\left(\frac{1}{2}\sqrt{(\varepsilon - n\hbar\omega)^2 + \Omega_n^2}t\right). \tag{3.53}$$

Comparing to (2.99), the AC potential allows resonant delocalization dynamics in systems with a large energy levels separation.

Additionally, the interdot tunneling dependence on the Bessel functions introduces the possibility of manipulating the internal dynamics by means of the intensity and frequency of the AC potential. A particularly interesting case appears when the argument of the Bessel function of the order n, so is the renormalized Rabi frequency $\Omega_n = 2J_{-n}\left(\frac{V_{\rm AC}}{\hbar\omega}\right)t_{\rm LR}$ and interdot tunneling is supressed, leading to *dynamical charge localization*[49, 50, 51, 52, 53]. This effect has been recently measured in double quantum well systems[54]. When considering the open system, this property allows the switching on and off of the electronic current by tuning $V_{\rm AC}$.

3.4.2 Up to one electron in the system

Considering that the Coulomb repulsion is high enough that only one electron is allowed in the DQD, that is, $U_{\rm L}, U_{\rm R}, U_{\rm LR} \to \infty$, if the DQD is coupled to highly biased contacts, as considered in section 2.6, so an electron in the left QD would need the absorption of a high number of photons to tunnel to the emitter (*idem* an electron in the collector to enter the right dot), one can disregard photon-assisted tunneling, cf. Fig. 3.2. Then, the only tunneling rates that contribute to transport are $\Gamma_{\rm L0} = \frac{2\pi}{\hbar}|\gamma_{\rm L}|^2 = \Gamma_{\rm L}$, $\Gamma_{\rm 0R} = \Gamma^+_{\rm 0R} = \frac{2\pi}{\hbar}|\gamma_{\rm R}|^2 = \Gamma_{\rm R}$ and the master equation reads

$$\begin{aligned} \dot{\rho}_{00} &= -\Gamma_{\rm L}\rho_{00} + \Gamma_{\rm R}\rho_{\rm RR} \\ \dot{\rho}_{\rm LL} &= \Gamma_{\rm L}\rho_{00} - i\frac{\Omega_1}{2}(\rho_{\rm RL} - \rho_{\rm LR}) \\ \dot{\rho}_{\rm LR} &= \left(i(\varepsilon - \hbar\omega) - \frac{1}{2}\Gamma_{\rm R}\right)\rho_{\rm LR} - i\frac{\Omega_1}{2}(\rho_{\rm RR} - \rho_{\rm LL}) \\ \dot{\rho}_{\rm RR} &= -\Gamma_{\rm R}\rho_{\rm RR} - i\frac{\Omega_1}{2}(\rho_{\rm LR} - \rho_{\rm RL}), \end{aligned} \tag{3.54}$$

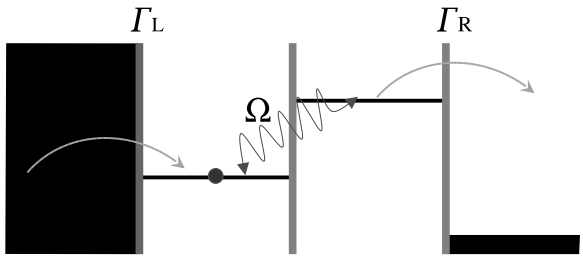

Fig. 3.2: Double quantum dot in the high bias regime, where photon-assisted tunneling is considered to not affect tunneling processes through the contact barriers.

if $\varepsilon_{\mathrm{R}} - \varepsilon_{\mathrm{L}} = \hbar\omega$, after similar steps as those made to obtain (3.52). The stationary current is

$$I = \frac{\Omega_1^2 \Gamma_{\mathrm{L}} \Gamma_{\mathrm{R}}}{\Gamma_{\mathrm{R}} \Omega_1^2 + \Gamma_{\mathrm{L}} \left(2\Omega_1^2 + \Gamma_{\mathrm{R}}^2 + 4(\varepsilon - \hbar\omega)^2\right)}. \tag{3.55}$$

giving a Lorentzian shaped peak, cf. Fig. 3.4, similar to the undriven case (2.106) and (2.105) with the difference that the Rabi frequency of the oscillations is now tunable by means of the AC intensity and leads to dynamical charge localization when the Bessel function of first order goes to zero.

Photon-assisted tunneling through the contact barriers become important as the applied bias is reduced. In particular, one can consider the *pumping* configuration where $\mu_{\mathrm{L}} = \mu_{\mathrm{R}} = \mu$, i.e., no external bias is applied to the leads. For pumping to be efficient, a spatial asymmetry is required which is this case is the finite detuning $\varepsilon = \varepsilon_{\mathrm{R}} - \varepsilon_{\mathrm{L}} = \varepsilon$ such that $\varepsilon_{\mathrm{L}} < \mu \varepsilon_{\mathrm{R}}$. Then, the photon-assisted delocalization of the electron–which would remain in the left quantum dot in the absence of driving– gives a finite occupation probability to the right quantum dot and the subsequent extraction to the collector. Then, finite electronic current from left to right appears through the pumping cycle $|\mathrm{L}\rangle \leftrightsquigarrow |\mathrm{R}\rangle \to |0\rangle \to |\mathrm{L}\rangle$–as in the high bias regime. However, electrons in the left quantum dot or in the right lead can absorb a photon and tunnel to the emitter or the right quantum dot, respectively, thus contributing to electronic current from right to left, opposite to the previously considered, cf. Fig. 3.3.

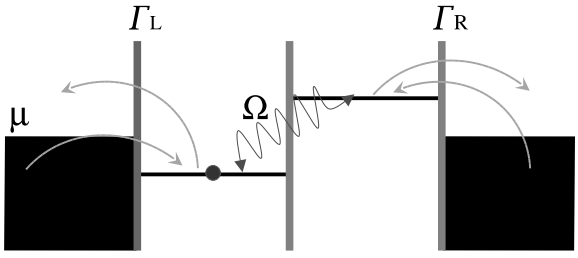

Fig. 3.3: Double quantum dot in the pumping configuration.

The photon-assisted tunneling rates are

$$\Gamma_{0\mathrm{L}} = \frac{2\pi}{\hbar}\sum_{\nu=-\infty}^{0} J_\nu^2\left(\frac{V_{\mathrm{AC}}}{2\hbar\omega}\right)|\gamma_{\mathrm{L}}|^2 = \frac{\pi}{\hbar}\left(1+J_0^2\left(\frac{V_{\mathrm{AC}}}{2\hbar\omega}\right)\right)|\gamma_{\mathrm{L}}|^2 \tag{3.56}$$

$$\Gamma_{\mathrm{L}0} = \frac{2\pi}{\hbar}\sum_{\nu=1}^{\infty} J_\nu^2\left(\frac{V_{\mathrm{AC}}}{2\hbar\omega}\right)|\gamma_{\mathrm{L}}|^2 = \frac{\pi}{\hbar}\left(1-J_0^2\left(\frac{V_{\mathrm{AC}}}{2\hbar\omega}\right)\right)|\gamma_{\mathrm{L}}|^2 \tag{3.57}$$

$$\Gamma_{0\mathrm{R}} = \frac{2\pi}{\hbar}\sum_{\nu=1}^{\infty} J_\nu^2\left(\frac{V_{\mathrm{AC}}}{2\hbar\omega}\right)|\gamma_{\mathrm{R}}|^2 = \frac{\pi}{\hbar}\left(1-J_0^2\left(\frac{V_{\mathrm{AC}}}{2\hbar\omega}\right)\right)|\gamma_{\mathrm{R}}|^2 \tag{3.58}$$

$$\Gamma_{\mathrm{R}0} = \frac{2\pi}{\hbar}\sum_{\nu=-\infty}^{0} J_\nu^2\left(\frac{V_{\mathrm{AC}}}{2\hbar\omega}\right)|\gamma_{\mathrm{R}}|^2 = \frac{\pi}{\hbar}\left(1+J_0^2\left(\frac{V_{\mathrm{AC}}}{2\hbar\omega}\right)\right)|\gamma_{\mathrm{R}}|^2, \tag{3.59}$$

so the master equation, for $\omega \approx \varepsilon$, is

$$\begin{aligned}
\dot\rho_{00} &= -(\Gamma_{\mathrm{L}0}+\Gamma_{\mathrm{R}0})\rho_{00} + \Gamma_{0\mathrm{L}}\rho_{\mathrm{LL}} + \Gamma_{0\mathrm{R}}\rho_{\mathrm{RR}} \\
\dot\rho_{\mathrm{LL}} &= \Gamma_{\mathrm{L}0}\rho_{00} - \Gamma_{0\mathrm{L}}\rho_{\mathrm{LL}} - i\frac{\Omega_1}{2}(\rho_{\mathrm{RL}}-\rho_{\mathrm{LR}}) \\
\dot\rho_{\mathrm{LR}} &= \left(i(\varepsilon-\hbar\omega)-\frac{1}{2}(\Gamma_{0\mathrm{L}}+\Gamma_{0\mathrm{R}})\right)\rho_{\mathrm{LR}} - i\frac{\Omega_1}{2}(\rho_{\mathrm{RR}}-\rho_{\mathrm{LL}}) \\
\dot\rho_{\mathrm{RR}} &= \Gamma_{\mathrm{R}0}\rho_{00} - \Gamma_{0\mathrm{R}}\rho_{\mathrm{RR}} - i\frac{\Omega_1}{2}(\rho_{\mathrm{LR}}-\rho_{\mathrm{RL}}).
\end{aligned} \tag{3.60}$$

The stationary current

$$I = \Gamma_{0\mathrm{R}}\rho_{\mathrm{RR}} - \Gamma_{\mathrm{R}0}\rho_{00} \tag{3.61}$$

in resonance results, after taking into account $\Gamma_{0i}+\Gamma_{i0} = \frac{2\pi}{\hbar}|\gamma_{\mathrm{L}}|^2 = \Gamma_i$,

$$I = \frac{\Omega_1^2\left(\Gamma_{\mathrm{L}0}\Gamma_{0\mathrm{R}} - \Gamma_{0\mathrm{L}}\Gamma_{\mathrm{R}0}\right)}{\left(\Gamma_{\mathrm{L}0}+\Gamma_{\mathrm{R}0}+\Gamma_{\mathrm{L}}+\Gamma_{\mathrm{R}}\right)\Omega_1^2 + \left(\Gamma_{0\mathrm{L}}+\Gamma_{0\mathrm{R}}\right)\left(\Gamma_{0\mathrm{L}}\Gamma_{\mathrm{R}}+\Gamma_{\mathrm{L}0}\Gamma_{0\mathrm{R}}\right)}. \tag{3.62}$$

In the simpler case $\Gamma_{\mathrm{L}0} = \Gamma_{0\mathrm{R}} = \Gamma_+$ and $\Gamma_{0\mathrm{L}} = \Gamma_{\mathrm{R}0} = \Gamma_-$, it is clear the contribution of photon-assisted processes to the *negative* current

$$I = \frac{\Omega_1^2\left(\Gamma_+-\Gamma_-\right)\left(\Gamma_++\Gamma_-\right)^2}{3\Omega_1^2\left(\Gamma_+^2+\Gamma_-^2\right)+\left(\Gamma_+^2+\Gamma_-^2+\Gamma_+\Gamma_-\right)\left(\left(\Gamma_++\Gamma_-\right)^2+4(\varepsilon-\omega)^2\right)}. \tag{3.63}$$

Note that, if photon-assisted processes are not considered in the tunneling through the contact barriers, the same expression (3.55) as in the high bias regime is obtained. As seen in Fig. 3.4, this is a good approximation for low driving intensities, $V_{\mathrm{AC}} < \hbar\omega$.

3.4.3 Up to two electrons

If the Coulomb repulsion between the spinless electrons in different dots is small, $U_{\mathrm{LR}} \to 0$, two electrons can be simultaneously in the DQD, one in each dot. Still, $U_{\mathrm{L}}, U_{\mathrm{R}} \to \infty$, so only one electron is allowed in each quantum dot. Then, the spatial Rabi oscillations of an electron between $|\mathrm{L}\rangle$ and $|\mathrm{R}\rangle$ are damped not only by the extraction of the electron through one of the contact barriers but also by an additional electron entering the DQD to the state $|2\rangle$.

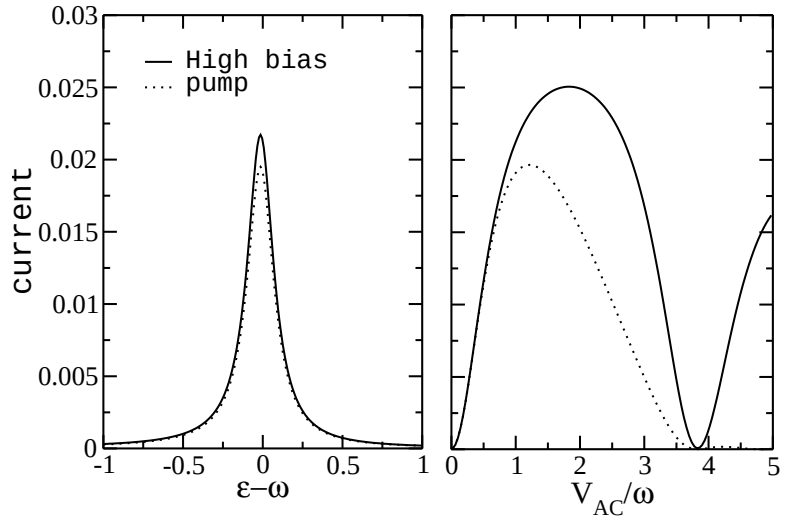

Fig. 3.4: Current as a function of the detuning when $V_{\rm AC} = \omega$ (left) and as a function of the AC intensity for $\omega = \varepsilon$ (right) for the high bias and pump regimes. It was considered $t_{\rm LR} = \Gamma_{\rm L} = \Gamma_{\rm R} = 0.1$, $e = \hbar = 1$ and $U_{\rm L}, U_{\rm R}, U_{\rm LR} \to \infty$, so only one electron is allowed at a time in the system. The influence of photon-assisted tunneling through the contact barriers is clear in the decreasing of the current in the pumping regime, following the behaviour of $J_0\left(\frac{V_{\rm AC}}{2\omega}\right)$. By comparing both regimes follows that the effect of photon-assisted tunneling in the contacts is negligible for low AC intensities. The dynamical charge localization is manifested in the current quenching (for both regimes) at $\frac{V_{\rm AC}}{\omega} = 3.8317$, when the Bessel function of first order is zero.

Following the same proccedure as before, the master equation for the high bias regime $\mu_{\rm L} \gg \varepsilon_{\rm L} + U_{\rm LR}$ and $\mu_{\rm R} \ll \varepsilon_{\rm R} + U_{\rm LR}$

$$\begin{aligned}
\dot{\rho}_{00} &= -\Gamma_{\rm L}\rho_{00} + \Gamma_{\rm R}\rho_{\rm RR} \\
\dot{\rho}_{\rm LL} &= \Gamma_{\rm L}\rho_{00} - \Gamma_{\rm L}\rho_{RR} - i\frac{\Omega_1}{2}(\rho_{\rm RL} - \rho_{\rm LR}) \\
\dot{\rho}_{\rm LR} &= \left(i(\varepsilon - \hbar\omega) - \frac{1}{2}(\Gamma_{\rm L} + \Gamma_{\rm R})\right)\rho_{\rm LR} - i\frac{\Omega_1}{2}(\rho_{\rm RR} - \rho_{\rm LL}) \qquad (3.64) \\
\dot{\rho}_{\rm RR} &= -(\Gamma_{\rm L} + \Gamma_{\rm R})\rho_{\rm RR} - i\frac{\Omega_1}{2}(\rho_{\rm LR} - \rho_{\rm RL}) \\
\dot{\rho}_{22} &= \Gamma_{\rm L}\rho_{RR} - \Gamma_{\rm R}\rho_{22}
\end{aligned} \qquad (3.65)$$

gives a stationary current[42]

$$I = \frac{\Omega_1^2\Gamma_{\rm L}\Gamma_{\rm R}\left(\Gamma_{\rm L} + \Gamma_{\rm R}\right)}{\left(\Gamma_{\rm L}^2 + \Gamma_{\rm R}^2\right)\Omega_1^2 + \left(2\Omega_1^2 + \left(\Gamma_{\rm L} + \Gamma_{\rm R}\right)^2 + 4(\varepsilon - \hbar\omega)^2\right)\Gamma_{\rm L}\Gamma_{\rm R}}. \qquad (3.66)$$

Comparing the latest expression to the strong repulsion case (3.55), the current increases when a second electron is allowed to enter the system. The entrance of a second electron *interrupts* the coherent delocalization and *pushes* the first electron to the right quantum dot, increasing its probability of being transferred to the collector. In effect, if $\Gamma_{\rm L} = \Gamma_{\rm R} = \Gamma \ll \Omega$, the resonant current is $\frac{\Gamma}{3}$, if $U_{\rm LR} \to \infty$, and $\frac{\Gamma}{2}$, if $U_{\rm LR} \to 0$.

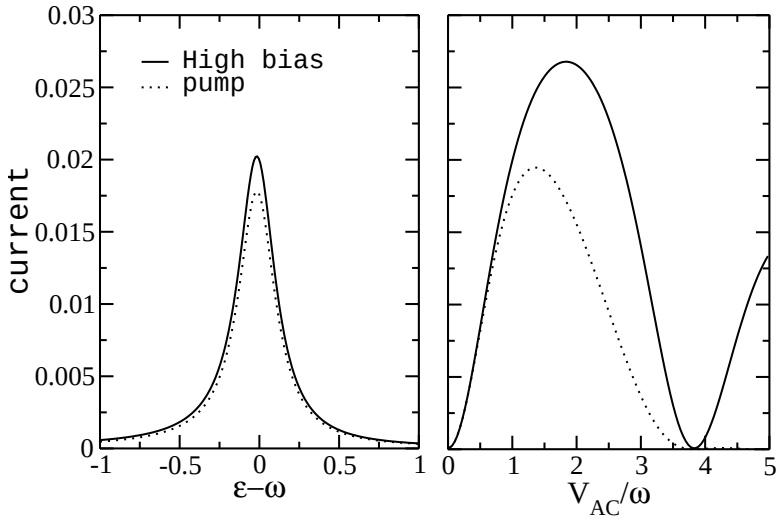

Fig. 3.5: Current as a function of the detuning when $V_{\rm AC}=\omega$ (left) and as a function of the AC intensity for $\omega=\varepsilon$ (right) for the high bias and pump regimes. It was considered $t_{\rm LR}=\Gamma_{\rm L}=\Gamma_{\rm R}=0.1$, $e=\hbar=1$, $U_{\rm L},U_{\rm R}\to\infty$ and $U_{\rm LR}\to 0$, so towo electrons can be simultaneously (on in each dot) in the system. The decreasing of the current in the pump regime is proportional to $J_0^2\left(\frac{V_{\rm AC}}{2\omega}\right)$, as described in (3.70). The dynamical charge localization is manifested in the current quenching (for both regimes) at $\frac{V_{\rm AC}}{\omega}=3.8317$, when the Bessel function of first order is zero. At $\frac{V_{\rm AC}}{\omega}=4.8096$ (two times the first zero of the Bessel function of zeroth order), the current from left to right is compensated by the photon-assisted current from right to left and the net current is zero. In comparison with Fig. 3.4, the current is higher for non interacting electrons, as expected.

In the pumping configuration, the master equation becomes

$$\begin{aligned}
\dot\rho_{00} &= -(\Gamma_{\rm L0}+\Gamma_{\rm R0})\rho_{00}+\Gamma_{\rm 0L}\rho_{\rm LL}+\Gamma_{\rm 0R}\rho_{\rm RR}\\
\dot\rho_{\rm LL} &= \Gamma_{\rm L0}\rho_{00}-(\Gamma_{\rm 0L}+\Gamma_{\rm 2L})\rho_{\rm LL}-i\frac{\Omega_1}{2}(\rho_{\rm RL}-\rho_{\rm LR})\\
\dot\rho_{\rm LR} &= \left(i(\varepsilon-\hbar\omega)-\frac{1}{2}(\Gamma_{\rm 0L}+\Gamma_{\rm 2L}+\Gamma_{\rm 0R}+\Gamma_{\rm 2R})\right)\rho_{\rm LR}-i\frac{\Omega_1}{2}(\rho_{\rm RR}-\rho_{\rm LL})\\
\dot\rho_{\rm RR} &= \Gamma_{\rm R0}\rho_{00}-(\Gamma_{\rm 0R}+\Gamma_{\rm 2R})\rho_{\rm RR}-i\frac{\Omega_1}{2}(\rho_{\rm LR}-\rho_{\rm RL})\\
\dot\rho_{22} &= \Gamma_{\rm 2L}\rho_{\rm LL}+\Gamma_{\rm 2R}\rho_{\rm RR}-(\Gamma_{\rm L2}+\Gamma_{\rm R2})\rho_{22}.
\end{aligned}\tag{3.67}$$

Considering $\Gamma_{\rm 0R}=\Gamma_{\rm L0}=\Gamma_{\rm L2}=\Gamma_{\rm 2R}=\Gamma_+$ and $\Gamma_{\rm R0}=\Gamma_{\rm 0L}=\Gamma_{\rm 2L}=\Gamma_{\rm R2}=\Gamma_-$, where

$$\Gamma_+=\frac{\Gamma}{2}\left(1+J_0^2\left(\frac{V_{\rm AC}}{2\hbar\omega}\right)\right)\tag{3.68}$$

$$\Gamma_-=\frac{\Gamma}{2}\left(1-J_0^2\left(\frac{V_{\rm AC}}{2\hbar\omega}\right)\right)\tag{3.69}$$

are the tunneling rates for processes contributing to positive (from left to right) or negative (from right to left) current, respectively. Since $\Gamma_++\Gamma_-=\Gamma$, one obtains a stationary current

$$I=\frac{\frac{1}{2}\Omega_1^2\,(\Gamma_+-\Gamma_-)}{\Omega_1^2+\Gamma^2+(\varepsilon-\hbar\omega)^2}=\frac{\Omega_1^2\Gamma}{\Omega_1^2+\Gamma^2+(\varepsilon-\hbar\omega)^2}J_0^2\left(\frac{V_{\rm AC}}{2\hbar\omega}\right).\tag{3.70}$$

The dependence on the Bessel function of zeroth order makes the current vanish not only when the AC intensity satisfies the dynamical charge localization condition, $J_1\left(\frac{V_{\mathrm{AC}}}{\hbar\omega}\right) = 0$, but also when $J_0\left(\frac{V_{\mathrm{AC}}}{2\hbar\omega}\right) = 0$. In this case, the probability for an electron in the right lead to be transferred to the left is the same as for the reverse process. Also $J_0(\alpha) \to 0$ when $\alpha \to \infty$, so the net current vanishes for high AC intensities, as can be seen in Fig. 3.5.

Chapter 4

Spin pumping in double quantum dots

In the previous chapter, some examples of charge pumping through systems of two single-level quantum dots in series were exposed. Spatial coherence in an asymmetric system was exploited in order to produce a finite current in unbiased configuration. In that case, the asymmetry came by the detuning between the level of the right dot (which has an energy larger than the chemical potential of the right lead and thus contributes to the extraction of electrons to the collector) and the level in the left dot (whose energy is smaller than the chemical potential of the left lead, so electrons can tunnel directly from the emitter). The pumping mechanism comes from an AC potential applied to the gate voltages of each dot such that the frequency of the sinusoidal signal matched the static detuning of the double quantum dot (DQD). There, only single occupied states were considered, so the spin degree of freedom was not important.

However, in the last few years a new field has rised by exploiting the electronic spin in the search of new devices with properties that differ from those based on electronic charge–*spintronics* as an alternative to electronics[24]. This is mostly due to the long coherence times of spins, as compared to charge, giving rise to possible applications in quantum information processing. In this sence, *adiabatic*[59, 60, 61, 62] and non-adiabatic quantum dot spin pumps[63, 75, 76] has been proposed as an alternative to previous proposals for generating spin-polarized currents by using ferromagnetic metals[55, 56] or magnetic semiconductors[57, 58]. Indeed, the spin of an isolated electron in a QD has been proposed as a quantum bit for transport of quantum information. For QD spin filters, dc transport through few electron states is used to obtain spin-polarized currents which are almost 100% spin-polarized as demonstrated experimentally by Hanson *et al.* [64] following the proposal of Recher *et al.* [65].

4.1 Spin pumping

The basic principle of spin pumps is closely related to that of charge pumps where a DC current is generated by combining AC driving with either absence of inversion symmetry in the device, or lack of time-reversal symmetry in the AC signal (ratchets). The range of possible pumps includes turnstiles [66], adiabatic pumps[67] or non-adiabatic pumps based on photon-assisted tunneling (PAT) [68, 69] which are treated here. In the last few years, the application of AC electric fields in quantum dots has shown to be very accurate both to control and to modify their transport and electronic properties[68]. For

instance, Sun *et al.*[70] have proposed a spin cell based on a double quantum dot driven by microwave radiation in the presence of an external *non-uniform* magnetic field. An AC potential modifies as well the electron dynamics within single and double quantum dots and, as seen in the previous chapter, under certain conditions it induces charge localization and destroys the tunneling, allowing, by tuning the parameters of the AC field, to control the time evolution of the state occupation, and therefore the entanglement character of the electronic wave function[52, 53, 68]. Regarding detection of single spin states in semiconductor quantum dots, this has been achieved[73, 74] using quantum point contacts and spin to charge conversion allowing the determination of spin relaxation times on the order of milliseconds.

The separation of spin and charge dynamics is made by the introduction of an in-plane magnetic field that breaks the spin degeneracy producing Zeeman splitting in the energy levels of the DQD. Then, by chosing an appropriate chemical potential distribution (by tuning the gate voltages of the QDs), electrons will be transmitted to the collector depending on their spin polarization[63]. In order to do that, up to four electrons must be allowed in the DQD. The single occupation configuration discussed in the previous chapter will be blocked as soon as an electron with the spin polarization that is not allowed to tunnel to the collector enters the system. Then, one must consider doubly occupied states in both the right QD–in order to be able to extract one of the electrons– and in the left one–to circumvent the spin blockade effect, consisting in the avoiding of interdot tunneling by Pauli exclusion principle when both QDs have only one electron with the same spin polarization[94]. Spin blockade effect will be consider in following chapters.

The AC potential can be also used to select which electron is being to be transmitted by considering a second level in the right QD so each level serves as a channel for resonant transmision of a different spin polarization[75]. Then, for the right dot, we can have the following singlet and triplet states, in order of increasing energy:

$$|S_0\rangle = \frac{1}{\sqrt{2}}\left(|\downarrow\uparrow\rangle - |\uparrow\downarrow\rangle\right) \tag{4.1}$$

$$|T_+\rangle = |\uparrow\uparrow^*\rangle \tag{4.2}$$

$$|T_0\rangle = \frac{1}{\sqrt{2}}\left(|\downarrow\uparrow^*\rangle + |\uparrow\downarrow^*\rangle\right) \tag{4.3}$$

$$|T_-\rangle = |\downarrow\downarrow^*\rangle \tag{4.4}$$

$$|S_1\rangle = \frac{1}{\sqrt{2}}\left(|\downarrow\uparrow^*\rangle - |\uparrow\downarrow^*\rangle\right), \tag{4.5}$$

where the electrons in the upper level are marked with an asterisk (*). In such a configuration, the system acts as a *bipolar* spin filter just by tuning the ac frequency to be resonant with one of these channels.

Consider an asymmetric DQD connected to two Fermi-liquid leads which are in equilibrium with reservoirs kept at the chemical potentials μ_α, $\alpha = L, R$. Using a standard tunneling Hamiltonian approach, we write for the full Hamiltonian

$$\hat{H} = \hat{H}_{\rm DQD} + \hat{H}_{\rm Z} + \hat{H}_{\rm leads} + \hat{H}_{\rm T}, \tag{4.6}$$

where $\hat{H}_{\rm DQD} = \hat{H}_{\rm L} + \hat{H}_{\rm R} + \hat{H}_{\rm LR}$ describes the DQD and $\hat{H}_{\rm leads} = \sum_\alpha \sum_{k_\alpha,\sigma} \epsilon_{k_\alpha} \hat{d}^\dagger_{k_\alpha\sigma} \hat{d}_{k_\alpha\sigma}$ describes the leads. The presence of an external magnetic field is taken into account through the term $\hat{H}_{\rm Z} = \frac{1}{2}\sum_{\alpha,\sigma,\sigma'} \Delta_\alpha c^\dagger_{\alpha,\sigma}(\sigma_z)_{\sigma\sigma'} c_{\alpha,\sigma'}$, where $\Delta_\alpha \equiv g\mu_B B_\alpha$ is the Zeeman splitting of the energy levels of each QD in the presence of an external magnetic field $\vec{B}_\alpha = (0, 0, B_\alpha)$. It is assumed that only one orbital in the left dot participates in the spin-polarized pumping process whereas *two* orbitals in the right dot (energy separation $\Delta\epsilon$) are considered. The isolated left dot is thus modelled as a one–level Anderson

impurity: $\hat{H}_{\rm L} = \sum_\sigma E_{{\rm L}\sigma}\hat{c}^\dagger_{{\rm L}\sigma}\hat{c}_{{\rm L}\sigma} + U_L\hat{n}_{{\rm L}\uparrow}\hat{n}_{{\rm L}\downarrow}$, whereas the isolated right dot is modelled as: $\hat{H}_{\rm R} = \sum_{i\sigma} E_{{\rm R}i\sigma}\hat{c}^\dagger_{{\rm R}i\sigma}\hat{c}_{{\rm R}i\sigma} + U_{\rm R}(\sum_i \hat{n}_{{\rm R}i\uparrow}\hat{n}_{{\rm R}i\downarrow} + \sum_{\sigma,\sigma'}\hat{n}_{{\rm R}0\sigma}\hat{n}_{{\rm R}1\sigma'}) + J\hat{\mathbf{S}}_0\hat{\mathbf{S}}_1$ including the exchange interaction term. The index $i = 0, 1$ denotes the two levels. The effect of the magnetic field is asummed by the gate voltages so it increases the energy of the electrons with spin down polarization, while the ones with spin up remain the same

$$\begin{aligned} E_{{\rm L}\uparrow} &= E_{R0\uparrow} \\ E_{{\rm L}\downarrow} &= E_{{\rm L}\uparrow} + \Delta_{\rm L} \\ E_{{\rm R}i\downarrow} &= E_{{\rm R}i\uparrow} + \Delta_{\rm R}. \end{aligned} \tag{4.7}$$

with charging energies $U_{\rm R} > U_{\rm L}$. $\mathbf{S}_i = (1/2)\sum_{\sigma\sigma'}\hat{c}^\dagger_{{\rm R}i\sigma}\sigma_{\sigma\sigma'}\hat{c}_{{\rm R}i\sigma'}$ are the spin operators of the two levels. $\hat{H}_{\rm LR} = \sum_{i,\sigma} t_{\rm LR}(\hat{c}^\dagger_{{\rm L}\sigma}\hat{c}_{{\rm R}i\sigma} + H.c.)$ describes interdot tunneling. The tunneling between leads and each QD is described by the perturbation $\hat{H}_{\rm T} = \sum_{k_{\rm L},\sigma} V_{\rm L}(\hat{d}^\dagger_{k_{\rm L}\sigma}\hat{c}_{{\rm L}\sigma} + {\rm H.c.}) + \sum_{i,k_{\rm R},\sigma} V_{\rm R}(\hat{d}^\dagger_{k_{\rm R}\sigma}\hat{c}_{{\rm R}i\sigma} + {\rm H.c.})$.

As a consequence of Hund's rule, the intra-dot exchange, J, is ferromagnetic ($J < 0$) such that the energy of the singlet $|S_1\rangle = (1/\sqrt{2})(\hat{c}^\dagger_{{\rm R}0\uparrow}\hat{c}^\dagger_{{\rm R}1\downarrow} - \hat{c}^\dagger_{{\rm R}0\downarrow}\hat{c}^\dagger_{{\rm R}1\uparrow})|0\rangle$ ($E_{S_1,{\rm R}} = U_{\rm R} + \Delta_{\rm R} + \Delta\varepsilon - \frac{3J}{4}$) is higher than the energy of the triplets $|T_+\rangle = \hat{c}^\dagger_{{\rm R}0\uparrow}\hat{c}^\dagger_{{\rm R}1\uparrow}|0\rangle$, ($E_{T_+,{\rm R}} = U_{\rm R} + \Delta\varepsilon + \frac{J}{4}$), $|T_0\rangle = (1/\sqrt{2})(\hat{c}^\dagger_{{\rm R}0\uparrow}\hat{c}^\dagger_{{\rm R}1\downarrow} + \hat{c}^\dagger_{{\rm R}0\downarrow}\hat{c}^\dagger_{{\rm R}1\uparrow})|0\rangle$ ($E_{T_0,{\rm R}} = U_{\rm R} + \Delta_{\rm R} + \Delta\varepsilon + \frac{J}{4}$), and $|T_-\rangle = \hat{c}^\dagger_{R0\downarrow}\hat{c}^\dagger_{{\rm R}1\downarrow}|0\rangle$ ($E_{T_-1,{\rm R}} = U_{\rm R} + 2\Delta_{\rm R} + \Delta\varepsilon + \frac{J}{4}$). As can be seen, due to the Zeeman splitting, $E_{T_-} > E_{T_0} > E_{T_+}$. Finally, we consider the case where $\Delta\epsilon > \Delta_{\rm R} - J/4$ such that the triplet $|T_+\rangle$ is higher in energy than the singlet $|S_0\rangle = (1/\sqrt{2})(\hat{c}^\dagger_{{\rm R}0\uparrow}\hat{c}^\dagger_{{\rm R}0\downarrow} - \hat{c}^\dagger_{{\rm R}0\downarrow}\hat{c}^\dagger_{{\rm R}0\uparrow})|0\rangle$ ($E_{S_0,{\rm L(R)}} = U_{\rm L(R)} + \Delta_{\rm L(R)}$).

The pumping force is included as an external AC field acting on the dots, such that the single particle energy levels become time dependent:

$$E_{{\rm L(R)}\sigma} \to E_{{\rm L(R)}\sigma}(t) = E_{{\rm L(R)}\sigma} \pm \frac{V_{\rm AC}}{2}\cos\omega t \tag{4.8}$$

where $V_{\rm AC}$ and ω are the amplitude and frequency, respectively, of the applied field. We have considered a basis of 40 states in the particle number representation which are obtained under these conditions, considering up to two electrons in each QD.

To study the dynamics of a system connected to reservoirs one can consider the reduced density matrix operator, $\hat{\rho} = tr_{\rm leads}\hat{\chi}$, where one traces all the reservoir states in the complete density operator of the system, $\hat{\chi}$. The evolution of the system will be given by the Liouville equation: $\dot{\hat{\rho}}(t) = -i[\hat{H}(t), \hat{\rho}(t)]$. Assuming the Markov approximation[83], the master equation reads:

$$\begin{aligned} \dot{\rho}(t)_{m'm} &= -i\omega_{m'm}(t)\rho_{m'm}(t) - i[\hat{H}_{L\Leftrightarrow R}, \hat{\rho}(t)]_{m'm} \\ &\quad + \left(\sum_{k\neq m}\Gamma_{mk}\rho_{kk}(t) - \sum_{k\neq m}\Gamma_{km}\rho_{mm}(t)\right)\delta_{m'm} \\ &\quad -\Lambda_{m'm}\rho_{m'm}(t)(1-\delta_{m'm}) \end{aligned} \tag{4.9}$$

where $\omega_{m'm}(t) = E_{m'}(t) - E_m(t)$ is the energy difference between the states $|m\rangle$ and $|m'\rangle$ of the isolated DQD, Γ_{mk} are the transition rates for electrons tunneling through the leads, from state $|k\rangle$ to state $|m\rangle$ and $\Lambda_{m'm}$ describes the decoherence of the DQD states due to the interaction with the reservoir. This decoherence rate is related with the transition rates by: $\Re\gamma_{m'm} = \frac{1}{2}\left(\sum_{k\neq m'}\Gamma_{km'} + \sum_{k\neq m}\Gamma_{km}\right)$.

Let first neglect for simplicity the influence of the AC field on tunneling processes through the leads which, as discussed in the previous chapter, is a good approximation for low AC intensities, so the rates

$$\Gamma_{mn} = \sum_l \Gamma_l(f(\omega_{mn} - \mu_l)\delta_{N_m,N_n+1} + (1 - f(\omega_{nm} - \mu_l))\delta_{N_m,N_n-1}), \tag{4.10}$$

where $\Gamma_l = 2\pi\mathcal{D}_l|V_l|^2$, $l = \mathrm{L,R}$, determine the tunneling events for each lead. It is assumed that the density of states in both leads $\mathcal{D}_{L,R}$ and the tunneling couplings $V_{L,R}$ are energy-independent. N_k is the number of electrons in the system when it is in state $|k\rangle$.

Spin relaxation and decoherence are included phenomenologically in the corresponding elements of the equation for the RDM. Relaxation processes are described by the spin relaxation time $T_1 = (W_{\uparrow\downarrow} + W_{\downarrow\uparrow})^{-1}$, where $W_{\uparrow\downarrow}$ and $W_{\downarrow\uparrow}$ are spin-flip relaxation rates fulfilling a detailed balance: $W_{\downarrow\uparrow} = \exp(-\Delta_z/k_\mathrm{B}T)W_{\uparrow\downarrow}$, where k_B is the Boltzman constant and T the temperature. A lower bound for the spin relaxation time T_1 on the order of μs at $B \approx 0 - 2T$ was obtained by Fujisawa *et al.*[84]. Recently a value of $T_1 = 2.58$ ms with a field $B = 0.02$ T was measured [74] for a single QD using a tunnel-rate-selective readout method. In the following, we focus on low temperature limit such that $W_{\downarrow\uparrow} \approx 0$ and thus $T_1 \approx W_{\uparrow\downarrow}^{-1}$. T_2 is the spin decoherence time, i.e., the time over which a superposition of opposite spin states of a single electron remains coherent. Recently, Loss *et al.*[85] obtained that $T_2 = 2T_1$ for spin decoherence induced by spin-orbit interaction. This time can be affected by spin relaxation and by spin dephasing time ${T_2}^*$, i.e., the spin decoherence time for an ensemble of spins. For processes involving hyperfine interaction between electron and nuclear spins, Petta *et al.*[82] have obtained ${T_2}^* \approx 10\,\mathrm{ns}$ from singlet-triplet spin relaxation studies in a DQD. Here we consider two cases: ${T_2}^* = 0.1T_1$ and ${T_2}^* = 0.001T_1$.
In practice, the dynamics of the reduced density matrix is integrated numerically the in the chosen basis. In particular, all the results shown in the next paragraphs are obtained by letting the system evolve from the initial state $|\downarrow\uparrow,\uparrow\rangle$ until a stationary state is reached. The dynamical behavior of the system is governed by rates which depend on the electrochemical potentials of the corresponding transitions.

Second order processes as co-tunneling are not included. The current from the right dot to the right contact is given by:

$$I(t) = \sum_{ss'}{}' \left(\Gamma_{s's}\rho_{ss}(t) - \Gamma_{ss'}\rho_{s's'}\right), \tag{4.11}$$

where the sum consider only states such that the right dot has one electron more when the system is in state $|s\rangle$ than in state $|s'\rangle$. These transitions ocur through the right contact, so $\Gamma_{s's} = \Gamma_\mathrm{R}$.

4.2 Spin filtering

The current through an AC-driven double quantum dot is analyzed, with V_AC and ω the amplitude and frequency of the AC-field, weakly coupled to the external leads, in the presence of a magnetic field which induces a spin splitting Δ_z in the discrete states of each dot. The ground state in each dot is assumed to be the one with spin-up. The proposed model is of general application, i.e., it is valid for both small or large inter-dot coupling. The presented results correspond to a particular configuration such that the coupling of the dots with the leads is weak and symmetric: $\Gamma_{L,R} = 0.001$, the hopping between the dots is $t_\mathrm{LR} = 0.005$ and the charging energy for the left and right dots are $U_\mathrm{L} = 1.0$ and $U_\mathrm{R} = 1.3$ respectively. All energy units are in meV. The Zeeman splitting produced by an external homogeneous magnetic field is: $\Delta_\mathrm{L} = \Delta_\mathrm{R} = 0.026$, corresponding to a magnetic field $B \approx 1T$; the exchange constant for the right dot is $J = -0.2$ and the chemical potentials in the left and right leads are $\mu_\mathrm{L} = \mu_\mathrm{R} = 1.31$, respectively. Two levels are considered in the right dot with energy separation $\Delta\epsilon = 0.45$. Inter-dot Coulomb and exchange interactions are neglected.

In order to configure the system in a way that electrons can only be extracted from the state $|S_0\rangle$ to the right lead through the transitions: $|\uparrow\downarrow\rangle_\mathrm{R} \rightarrow |\uparrow\rangle_\mathrm{R}$ the energy parameters must satisfy $U_\mathrm{R} < \mu_\mathrm{R} < U_\mathrm{R} + \Delta_\mathrm{R}$. The energy cost of introducing a second electron with either spin-up or spin-

down polarization in the left dot has to be smaller than the chemical potential of the left lead. This is always satisfied if $\mu_{\rm L} > U_{\rm L} + \Delta_{\rm L}$. The system is considered to be in the pumping configuration $\mu_L = \mu_R$ throughout.

Then, if the DQD is initially in the state $|\uparrow\downarrow,\uparrow\rangle$, no current will flow through the system unless the AC frequency fits the energy difference between the different doubly occupied states for the left and right dots and one of the electrons is delocalized within the DQD. For instance: $|\uparrow\downarrow,\uparrow\rangle \leftrightsquigarrow |\uparrow,\uparrow\downarrow\rangle$ (at $\omega = \omega_{S_0\downarrow} = U_R - U_L + \Delta_R - \Delta_L$), $|\uparrow\downarrow,\uparrow\rangle \leftrightsquigarrow |\uparrow,T_0\rangle$ (at $\omega = \omega_{T_0\downarrow} = U_R - U_L + \Delta_R - \Delta_L + \Delta\epsilon + J/4$), $|\uparrow\downarrow,\uparrow\rangle \leftrightsquigarrow |\uparrow,S_1\rangle$ (at $\omega = \omega_{S_1\downarrow} = U_R - U_L + \Delta_R - \Delta_L + \Delta\epsilon - 3J/4$) or $|\uparrow\downarrow,\uparrow\rangle \leftrightsquigarrow |\downarrow,T_+\rangle$ (at $\omega = \omega_{T_+\uparrow} = U_R - U_L + \Delta\epsilon + J/4$). The suffix $\uparrow$ ($\downarrow$) is used to remark that the inter-dot tunneling electron has spin-up (down) polarization. At these frequencies, one electron becomes delocalized undergoing Rabi oscillations with frequency[68]

$$\Omega_R = 2t_{LR} J_\nu \left(\frac{V_{ac}}{\omega}\right), \tag{4.12}$$

where J_ν is the νth-order Bessel function of the first kind and ν is the number of photons required for bringing the two states into resonance. It is important to note that the frequencies for transitions involving spin down depend on the difference $\Delta_R - \Delta_L$ while the one involving spin up does not, see (4.7). As will be shown below, this is the main reason for requiring an inhomogeneous magnetic field to obtain spin-up polarized current. One should remark also that the resonance achieved between $|\uparrow\downarrow,\downarrow\rangle \Leftrightarrow |\uparrow,T_-\rangle$ occurs at a photon frequency: $\omega_{T_-\downarrow} = \omega_{T_0\downarrow}$. Similarly, the resonance $|\uparrow\downarrow,\downarrow\rangle \Leftrightarrow |\downarrow,T_0\rangle$ occurs at $\omega_{T_0\uparrow} = \omega_{T_+\uparrow}$.

4.2.1 Homogeneous magnetic field. $\Delta_R = \Delta_L$

If the frequency of the AC field is tuned to the resonance between the doubly occupied states with lower energy, i.e., $\omega = \omega_{S_0\downarrow}$, the electron with spin down polarization becomes delocalized between them. The energy configuration does not allow the extraction of the spin up electron in the right dot to the collector. On the other and, since the left dot has only one level, Pauli exclusion principle avoids the entrance of spin-up electrons to the left QD. Thus, the system follow the cycle

$$|\uparrow\downarrow,\uparrow\rangle \leftrightsquigarrow |\uparrow,\uparrow\downarrow\rangle \rightarrow \{|\uparrow,\uparrow\rangle \quad \text{or} \quad |\uparrow\downarrow,\uparrow\downarrow\rangle\} \rightarrow |\uparrow\downarrow,\uparrow\rangle \tag{4.13}$$

and the pumped current will be fully polarized with spin down electrons[63]. Then, the device acts as a filter and pump of electrons with spin down polarization, see the peak at $\omega = 0.3$ Fig. 4.1a. Note that the electrons with spin up polarization do not participate in the dynamics, so the system behaves roughly as the up to two particles case shown in section 3.4.

By increasing the frequency of the AC field, the single state of the left QD is put in resonance with the triplet states of the right QD. Since the Zeeman splitting is the same in both dots, inter-dot tunneling processes involving electrons with different spins, as for instance: $|\uparrow\downarrow,\uparrow\rangle \leftrightsquigarrow |\uparrow,T_0\rangle$ (at $\omega = \omega_{T_0\downarrow}$) and $|\uparrow\downarrow,\uparrow\rangle \leftrightsquigarrow |\downarrow,T_+\rangle$ (at $\omega = \omega_{T_+\uparrow}$) occur at the same frequency, i.e., $\omega_{T_0\downarrow} = \omega_{T_+\uparrow} \approx 0.65$ and we find two overlapping peaks (see Fig.4.1b. The current is created through several processes. The dominant ones are

$$|\uparrow\downarrow,\uparrow\rangle \leftrightsquigarrow |\uparrow,T_0\rangle \rightarrow \{|\uparrow,\uparrow\rangle \quad \text{or} \quad |\uparrow\downarrow,T_0\rangle\} \rightarrow |\uparrow\downarrow,\uparrow\rangle, \tag{4.14}$$

which contributes to spin-down current, and

$$|\uparrow\downarrow,\uparrow\rangle \leftrightsquigarrow |\downarrow,T_+\rangle \rightarrow \{|\downarrow,\uparrow\rangle \quad \text{or} \quad |\uparrow\downarrow,T_+\rangle\} \rightarrow |\uparrow\downarrow,\uparrow\rangle, \tag{4.15}$$

or

$$|\uparrow\downarrow,\uparrow\rangle \leftrightsquigarrow |\uparrow,T_0\rangle \rightarrow |\uparrow,\downarrow\rangle \rightarrow |\uparrow\downarrow,\downarrow\rangle, \tag{4.16}$$

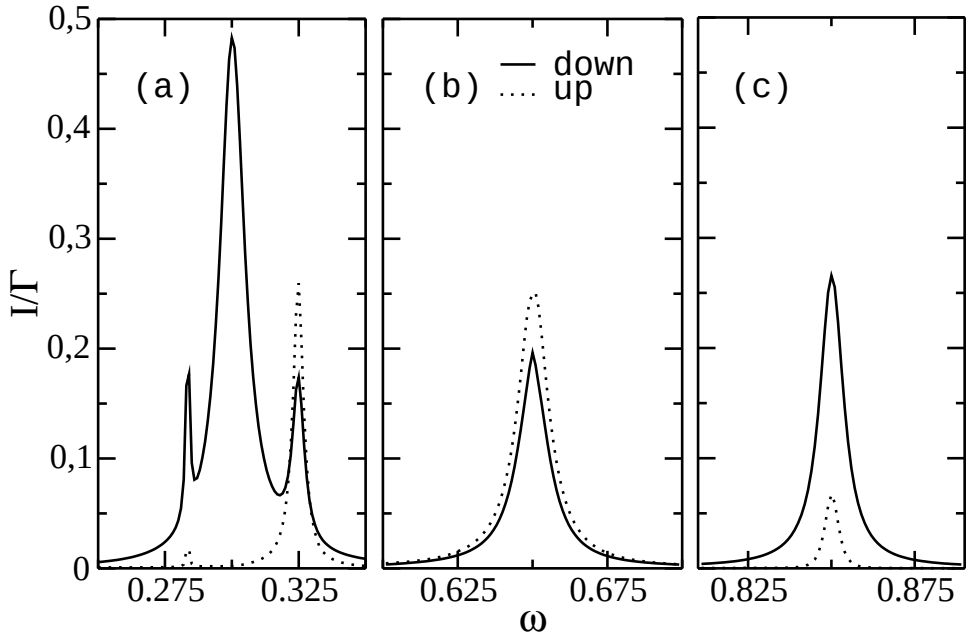

Fig. 4.1: Pumped current as a function of the ac frequency ($\Delta_L = \Delta_R$), for the resonances (a) $\omega_{T_0\downarrow} = \omega_{T_+\uparrow} \approx 0.65$ and (b) $\omega_{S_0\downarrow} \approx 0.3$. At this frequency, the current is fully spin down polarized. The smaller peaks in (b) are multi-photon satellites of other processes: at $\omega \approx 0.283$, the three-photon process corresponding to the resonance between the singlet S_0 in the left dot and the singlet S_1 in the right dot occurs. The two overlapping peaks at $\omega \approx 0.325$ correspond to two-photon satellites of the resonance in (a). Parameters: $t_{LR} = 0.005$, $\Gamma = 0.001$, $U_L = 1.0$, $U_R = 1.3$, $\Delta_L = \Delta_R = 0.026$ (corresponding to a magnetic field of $1T$), $\Delta\varepsilon = 0.4$, $J = -0.2$, $\mu_L = \mu_R = 1.31$, $V_{ac} = \omega_{T_+\uparrow}$[89].

which contribute to spin-up current. So, in this case, the current is partially spin-up polarized.

At higher frequencies, the resonance with the excited singlet $|S_1\rangle$ appears (at $\omega = \omega_{S_1\uparrow} = \omega_{S_1\downarrow}$), cf. Fig. 4.1c. The processes are similar then to the ones through $|T_0\rangle$

$$|\uparrow\downarrow,\uparrow\rangle \leftrightsquigarrow |\uparrow, S_1\rangle \rightarrow \{|\uparrow,\uparrow\rangle \quad \text{or} \quad |\uparrow\downarrow, S_1\rangle\} \rightarrow |\uparrow\downarrow,\uparrow\rangle, \tag{4.17}$$

for spin-down transport and

$$|\uparrow\downarrow,\downarrow\rangle \leftrightsquigarrow |\downarrow, S_1\rangle \rightarrow \{|\downarrow,\downarrow\rangle \quad \text{or} \quad |\uparrow\downarrow, S_1\rangle\} \rightarrow |\uparrow\downarrow,\downarrow\rangle, \tag{4.18}$$

for spin-up. So this resonance also shows a mixed polarization.

Two peaks appear in the vicinity of $\omega_{S_0\downarrow}$, one at $\omega = \omega_{S_1\downarrow}/3 \approx 0.283$ (which corresponds to the three-photon satellite of resonance $\omega_{S_1\downarrow}$) and two overlapping peaks at $\omega \approx 0.325$ (corresponding to the two-photon satellites at $\omega_{T_0\downarrow}/2 = \omega_{T_+\uparrow}/2$, see Fig.4.1a). The positions of these peaks are completely independent of each other and are determined by the energetics of the system.

4.2.2 Inhomogeneous magnetic field. $\Delta_R \neq \Delta_L$

In order to get a fully spin-up polarized current peak, we consider different Zeeman splittings between both dots which can be due to an inhomogeneous magnetic field, with different intensity in

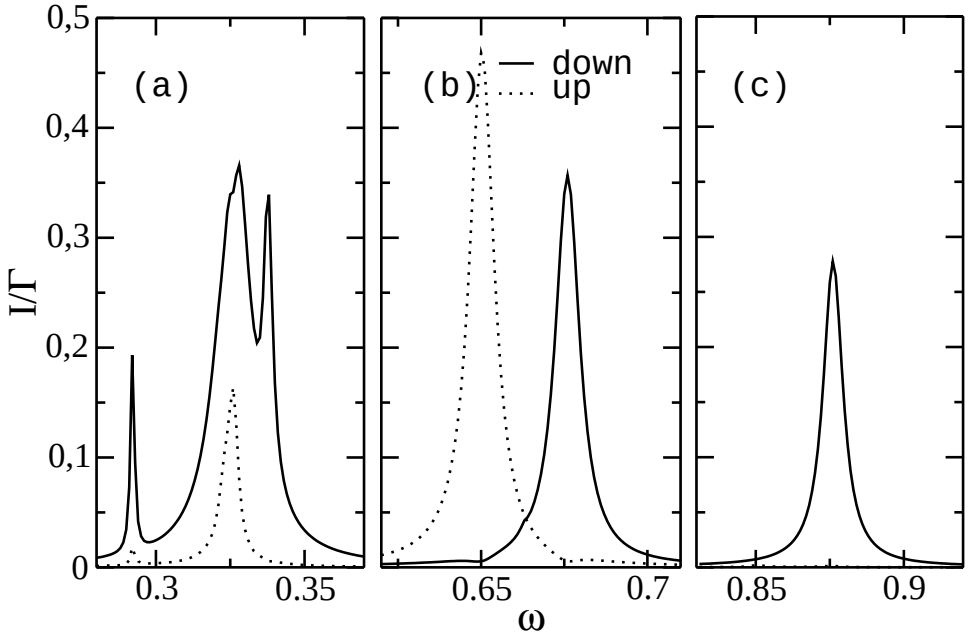

Fig. 4.2: Pumped current as a function of the ac frequency ($\Delta_L \neq \Delta_R$), for the resonances (a) $\omega_{T_0\uparrow} = \omega_{T_+\uparrow} \approx 0.65$ and $\omega_{T_0\downarrow} = \omega_{T_-\downarrow} \approx 0.676$ and (b) $\omega_{S_0\downarrow} \approx 0.326$. The current at the resonance $\omega = \omega_{S_0\downarrow}$ is partially spin down polarized due to the overlapping satellite peaks (at $\omega = \omega_{T_0\downarrow}/2 \approx 0.338$, $\omega = \omega_{T_+\uparrow}/2 \approx 0.325$, $\omega = \omega_{S_1\downarrow}/3 \approx 0.292$). Parameters: $t_{LR} = 0.005$, $\Gamma = 0.001$, $U_L = 1.0$, $U_R = 1.3$, $\Delta_L = 0.026$, $\Delta_R = 2\Delta_L$, $\Delta\varepsilon = 0.4$, $J = -0.2$, $V_{ac} = \omega_{T_+\uparrow}$[89].

each dot, or quantum dots with different g factors. Also, hyperfine interaction between the electronic spins in the quantum dots and the nuclei underneath hs demonstrated to cause an additional Zeeman splitting which may be different in each QD depending on the number of nuclei[87, 88]. On the other hand, hyperfine interaction is the responsible for spin relaxation and decoherence which will be analyzed below.

This introduces a separation $\Delta\omega \approx \frac{\Delta_R - \Delta_L}{n}$ (where n is the number of photons involved in the resonant transition) between peaks with different spin polarization, as can be seen for example by comparing figures 4.1 and 4.2. The resonances $\omega_{T_0\downarrow} (= \omega_{T_-\downarrow})$ are shifted by an amount $\Delta_R - \Delta_L$ with respect to the resonance at $\omega_{T_+\uparrow} (= \omega_{T_0\uparrow})$ which is independent of Zeeman splitting (see Fig.4.2b). So fully spin-up polarized current at $\omega_{T_+\uparrow} \approx 0.65$ and fully spin-down polarized current at $\omega_{T_0\downarrow} \approx 0.676$ are obtained.

That is not the case of the resonances involvig the state $|S_1\rangle$, which is connected to the initial state $|\uparrow\downarrow,\uparrow\rangle$ only by the tunneling of the spin-down electron. Then, fully spin-down polarized current appears at $\omega_{S_1\downarrow}$ but, at $\omega_{S_1\uparrow}$, the system remains unaffected by the AC field, cf. Fig. 4.2c.

In Fig.4.2a, the resonance $\omega = \omega_{S_0\downarrow} \approx 0.326$ is not well resolved because there are overlapping satellite peaks (at $\omega = \omega_{T_0\downarrow}/2 \approx 0.338$, $\omega = \omega_{T_+\uparrow}/2 \approx 0.325$, $\omega = \omega_{S_1\downarrow}/3 \approx 0.292$). In concrete, one finds different processes that contribute to opposite spin polarization currents and depend on the absorption of a different number of photons (therefore, their Rabi frequencies are renormalized with Bessel functions of different orders, Eq. (4.12)). It has been shown that for certain AC parameters and sample

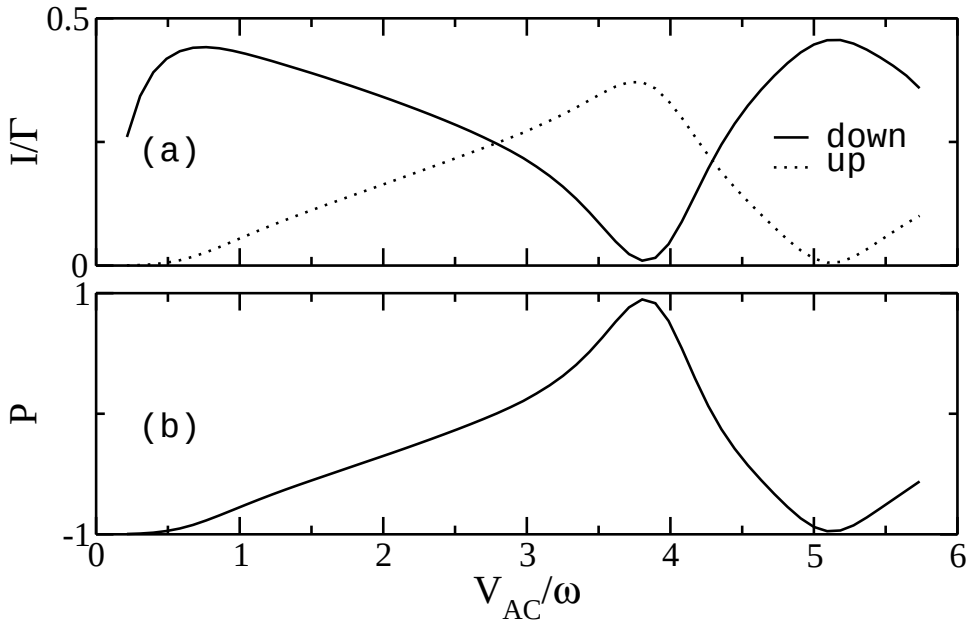

Fig. 4.3: (a) Current and (b) current polarization (defined as $P = (I_\uparrow - I_\downarrow)/(I_\uparrow + I_\downarrow)$) dependence on the AC field intensity, for $\omega_{S_0\downarrow} = 0.326$. There is fully spin-up polarization for intensities such that $J_1(\alpha) = 0$ and fully spin-down-polarization when $J_2(\alpha) = 0$. The sample parameters are the same as in Fig. 4.2.

configurations[48] the height of the current peaks depend on Ω_R, which is a non linear function on the AC intensity (see Eq. (4.12)). Thus, one can take chance of the coincidence of different processes at the same frequency to manipulate the spin polarization by tuning the intensity of the AC field. In Fig. 4.3 the current and current polarization are shown as a function of AC-field intensity at ω=$\omega_{S_0\downarrow}$. Here, the spin-up contribution comes from a two-photon resonance ($\omega = \omega_{T_+\uparrow}/2 \approx 0.325$) and, thus, is expected to vanish when $J_2(\alpha) = 0$ due to the dynamical localization phenomena[68]discussed in the previous chapter. Furthermore, for AC intensities such that $J_1(\alpha) = 0$, the one-photon resonance $\omega_{S_0\downarrow}$ is quenched and fully spin-up polarized current is obtained at this frequency. Thus, if one tunes the AC intensity to the value where the first(second)-order Bessel function vanishes, we obtain fully spin-up(down) current. Fig.4.3(a) shows that at low AC intensities, the contribution of multi-photon processes is small and the $\omega_{S_0\downarrow} \approx 0.326$ resonance corresponding to practically fully spin-down current is clearly resolved. However, this property needs high intensities where photon-assisted tunneling through the contacts may contribute, leading to the reduction of the polarization. The effect of these processes will be treated below.

4.3 Spin relaxation effects

It is important to note also that, contrary to the case for spin-down pumping, the pumping of spin up electrons leaves the double dot in the excited state $|\downarrow,\uparrow\rangle$. This makes the spin-up current sensitive to spin relaxation processes. If the spin $\downarrow$ decays before the next electron enters into the left dot, a spin-down current appears through the cycle

$$|\downarrow\uparrow,\uparrow\rangle \overset{\text{AC}}{\leftrightsquigarrow} |\downarrow,T_+\rangle \overset{\Gamma_R}{\rightarrow} |\downarrow,\uparrow\rangle \overset{W_{\uparrow\downarrow}}{\rightarrow} |\uparrow,\uparrow\rangle \overset{\Gamma_L}{\rightarrow} |\uparrow\downarrow,\uparrow\rangle \tag{4.19}$$

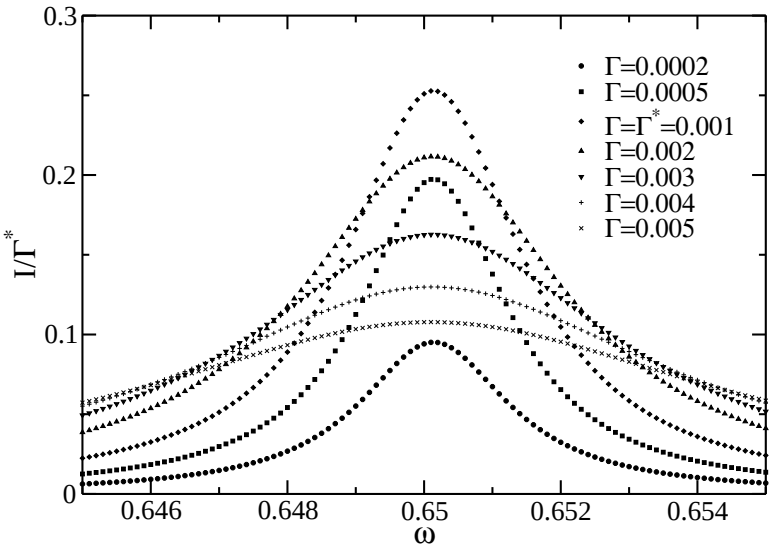

Fig. 4.4: Pumped current near resonance $\omega = 0.65$ for different symmetric couplings to the leads. $\Delta_{\rm R} = \Delta_{\rm L}/0.3$, $W_{\uparrow\downarrow} = 5 \times 10^{-6}$, $V_{\rm AC} = 0.14$ and ${T_2}^* = 0.1T_1$. When increasing the coupling to the leads, the current decreases which may be an artefact due to the formulation basis that is not the eigenbasis of the DQD, as discussed in chapter 2.

and the pumping cycle is no longer 100% spin-up polarized leading to a reduction of the spin-up current at this frequency. Note that spin-flip processes lift the conservation of spin currents through the device.

In Fig. 4.4, the current due to the $\omega_{T_+\uparrow} = 0.65$ resonance is plotted for different values of the coupling with the contacts, Γ, at $V_{\rm AC} = 0.14$ meV when including a finite spin-flip relaxation probability, $W_{\uparrow\downarrow} = 1/T_1 = 5 \times 10^{-6}$meV and ${T_2}^*$=$0.1T_1$. The full widths (FWHM) of the current peaks are plotted as a function of Γ in Fig. 4.5(a) for weak (circles) and strong (squares) AC-field intensity, V_{AC}. In order to minimize nonlinear effects, in Fig. 4.5(b) the low intensity regime ($V_{\rm AC} = 0.14$) is investigated where one expects a FWHM dominated by decoherence, for two different values of the spin dephasing time: ${T_2}^* = 0.1T_1$ and ${T_2}^* = .001T_1$. In every case, one finds that for large Γ, the behaviour of the FWHM is linear with a slope which approaches 2, i.e., FWHM $\sim 2\Gamma$, which can be directly related to the decoherence time T_2 as shown below. Thus, experiments along these lines would complement the information about decoherence extracted from other setups [97]. As an illustration we present below an analytical treatment which allows us to relate the current peak widths with the spin decoherence time.

4.3.1 Analytical treatment

In the following we present an analytical treatment in the stationary regime of the case discussed above where the influence of spin-flip processes on the spin up current peak coming from the ac-induced resonance between $|1\rangle = |\uparrow\downarrow,\uparrow\rangle$ and $|2\rangle = |\downarrow,\uparrow\uparrow^*\rangle$ was numerically obtained.

As discussed in the previous section, at $\omega = \omega_{T_+\uparrow}$, these states are brought into resonance and the current, for $\Delta_R \approx \Delta_L/0.3$, is fully spin-up polarized. Intermediate states are $|3\rangle = |\downarrow,\uparrow\rangle$, $|4\rangle = |\uparrow\downarrow,\uparrow\uparrow^*\rangle$, $|5\rangle = |\uparrow,\uparrow\uparrow^*\rangle$ and $|6\rangle = |\uparrow,\uparrow\rangle$. From [48, 77] it is known that the dynamics of the system at large time scales is obtained by a time-dependent basis transformation on the density matrix (rotating

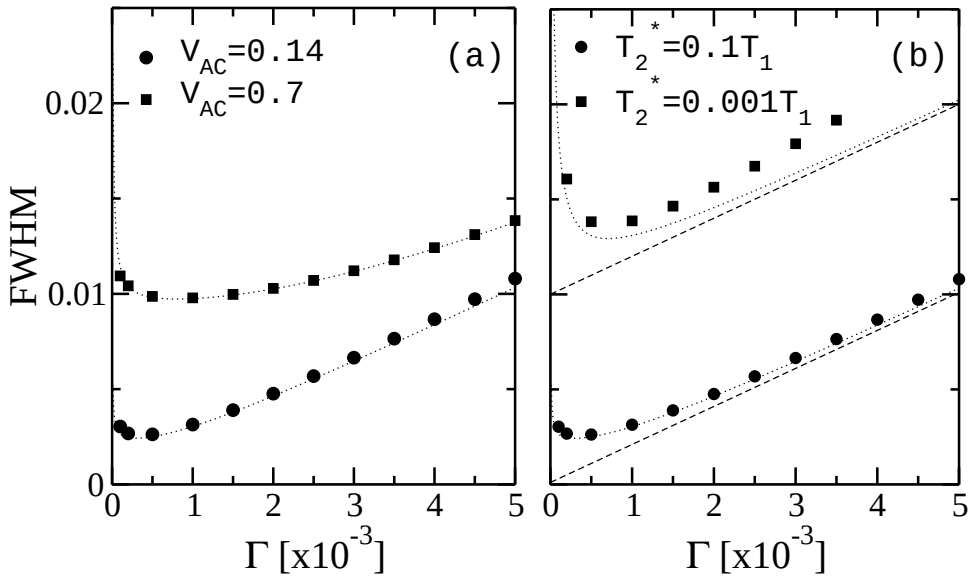

Fig. 4.5: Full width at half maximum of the total current in Fig. 4.4 as a function of coupling to the leads, Γ, at frequency $\omega = 0.65$ (a) for strong (squares) and weak (circles) field intensities and $T_2{}^* = 0.1T_1$ and (b) for different spin dephasing times $T_2{}^* = 0.1T_1$ (circles) and $T_2{}^* = 0.001T_1$ (squares), for the weak field intensity case. In both cases, the numerical results are compared to the analytic prediction (dotted lines) given by (4.27). (a) In the weak field case, $V_{\rm AC} = 0.14$, $\Omega_{\rm R} \approx 0.001$ (circles), for $\Gamma \gg \Omega_{\rm R}$, the curve follows a linear behaviour: FWHM $\approx 2\gamma = 2(W_{\uparrow\downarrow}/2 + 1/T_2{}^* + \Gamma)$. For the high field intensity case $V_{\rm AC} = 0.7$, $\Omega_{\rm R} \approx 0.004$ and the same behaviour is expected at larger Γ. In (b), for $T_2{}^* = 0.001T_1$ (squares), we see that the width of the peak is larger than the expected asymptotic behavior for large Γ. This is due to overlapping with the peak at $\omega_{T_0\downarrow}$. As discussed in the text, the extrapolation of the asymptotic curves at $\Gamma = 0$ gives the value of $2(1/2T_1 + 1/T_2{}^*)$. Thus, for the case where $T_2{}^* \ll T_1$, would allow to estimate the value of the spin dephasing time. In both graphics, $\Delta_{\rm R} = \Delta_{\rm L}/0.3$, $W_{\uparrow\downarrow} = 1/T_1 = 5 \times 10^{-6}$.

wave approximation, RWA) such that $\epsilon(t) \to \epsilon_0 - n\omega$ and $t_{\rm LR} \to \tilde{t}_{\rm LR} = (-1)^n J_n(V_{AC}/\omega) t_{\rm LR}$, see also the previous discussion in chapter 3. The equations of motion for the corresponding reduced density matrix elements in the RWA are:

$$\begin{aligned} \dot{\rho}_1 &= -2\tilde{t}_{\rm LR}\Im\rho_{2,1} + \Gamma_{\rm L}\rho_3 + \Gamma_{\rm R}\rho_4 + \Gamma_{\rm L}\rho_6 \\ \dot{\rho}_2 &= 2\tilde{t}_{\rm LR}\Im\rho_{2,1} - (\Gamma_{\rm R} + \Gamma_{\rm L} + W_{\uparrow\downarrow})\rho_2 \end{aligned} \tag{4.20}$$

while for the intermediate states,

$$\begin{aligned} \dot{\rho}_3 &= \Gamma_{\rm R}\rho_2 - (\Gamma_{\rm L} + W_{\uparrow\downarrow})\rho_3 \\ \dot{\rho}_4 &= \Gamma_{\rm L}\rho_2 - \Gamma_{\rm R}\rho_4 + \Gamma_{\rm L}\rho_5 \\ \dot{\rho}_5 &= W_{\uparrow\downarrow}\rho_2 - (\Gamma_{\rm L} + \Gamma_{\rm R})\rho_5 \\ \dot{\rho}_6 &= -\Gamma_{\rm L}\rho_6 + \Gamma_{\rm R}\rho_5 + W_{\uparrow\downarrow}\rho_3 \end{aligned} \tag{4.21}$$

The equation for the off-diagonal density matrix element is

$$\dot{\rho}_{2,1} = [i(\epsilon_0 - n\omega) + \gamma]\rho_{2,1} + i\tilde{t}_{\rm LR}(\rho_2 - \rho_1) \tag{4.22}$$

where $\gamma = T_2^{-1}$ is the decoherence rate:

$$\gamma = \frac{1}{2}(\Gamma_{\rm L} + \Gamma_{\rm R} + W_{\uparrow\downarrow}) + \frac{1}{T_2{}^*} \tag{4.23}$$

This, together with the condition of conservation of probability $\Sigma_i \rho_i = 1$ gives for the total current (at this frequency), in the stationary regime, an expression which we can write[77] as:

$$I = I_0 \frac{W^2}{W^2 + (\epsilon_0 - n\omega)^2} \tag{4.24}$$

where $I_0 = 2\gamma \tilde{t}_{\rm LR}^2 / W^2$ is the current maximum and W is the half width at half maximum:

$$W^2 = \frac{2\gamma \tilde{t}_{\rm LR}^2}{\Gamma_{\rm L} + \Gamma_{\rm R} + W_{\uparrow\downarrow}} \left(\tilde{\Gamma} + \frac{W_{\uparrow\downarrow}}{\Gamma_{\rm L} + \Gamma_{\rm R}} \left(\tilde{\Gamma} - 1 \right) \right) + \gamma^2 \tag{4.25}$$

Here, $\tilde{\Gamma} = (\Gamma_{\rm L} + \Gamma_{\rm R})^2 / \Gamma_{\rm L}\Gamma_{\rm R}$. For the symmetric case, $\Gamma_{\rm L} = \Gamma_{\rm R} = \Gamma$ ($\tilde{\Gamma} = 4$) one can rewrite this in terms of the Rabi frequency $\Omega_R = 2\tilde{t}_{\rm LR}$ as :

$$W^2 = \frac{2\gamma \Omega_{\rm R}^2}{2\Gamma + W_{\uparrow\downarrow}} \left(1 + \frac{3W_{\uparrow\downarrow}}{8\Gamma} \right) + \gamma^2 \tag{4.26}$$

In these calculations, $W_{\uparrow\downarrow} = 5 \times 10^{-6} \ll \Omega_{\rm R}, \Gamma$ throughout the range of values considered. Then, Eq. (4.26) simplifies to

$$W^2 = \frac{\gamma \Omega_{\rm R}^2}{\Gamma} + \gamma^2. \tag{4.27}$$

In the limit $W_{\uparrow\downarrow}, 1/T_2^* \ll \Gamma$, then $\gamma \approx \Gamma$, and we get $W^2 = \Omega_R^2 + \Gamma^2$ in agreement with previous analytical results[48, 77].

From (4.27), one obtains the following asymptotic behaviors:

1. $\Gamma \ll \Omega_{\rm R}$ (strong inter-dot tunneling)$\Rightarrow W^2 \approx \Omega_{\rm R}^2 \gamma / \Gamma$
2. $\Gamma \gg \Omega_{\rm R}$ (weak inter-dot tunneling) $\Rightarrow W \approx \gamma$
3. $\Gamma \approx \Omega_{\rm R} \Rightarrow W^2 \approx \gamma_{\rm R}(\Omega_{\rm R} + \gamma_{\rm R})$, where $\gamma_{\rm R} = \Omega_{\rm R} + 1/T_2{}^*$.

In Fig. 4.5(a) the full width at half maximum (FWHM) of the spin-up current peak is represented as a function of Γ for the case $T_2{}^* = 0.1 T_1$ together with the analytical curve (4.26). For the weak field case $V_{\rm AC} = 0.14$ (full circles) with $\Omega_{\rm R} \approx 0.001$, we see that the predictions of the theory are indeed fulfilled. In particular, in the range $\Gamma \gg \Omega_{\rm R}$, the FWHM as a function of Γ is a straight line with slope 2 as expected (FWHM $\approx 2\gamma = 2/T_2{}^* + 1/T_1 + 2\Gamma$). This means that a direct measure of the decoherence time for the isolated system T_2^{iso}:

$$\frac{1}{T_2^{iso}} = \frac{1}{T_2{}^*} + \frac{1}{2T_1} \tag{4.28}$$

can be obtained from this linear behavior. In this limit, however, the effects of the chosen basis (on the eigenstates one) may affect the results, as seen in chapter 2. From Fig. 4.5a it can be verified that the cases (i) ($W^2 \approx a + b/(\Gamma T_2^{iso})$) and (iii) are also reproduced. Besides, it is interesting to mention that from these cases one can get information on the Rabi frequency. The same analysis also holds for the strong field case $V_{\rm AC} = 0.7$ (full squares), where $\Omega_{\rm R} \approx 0.004$.

Recently, it has been measured that the spin dephasing time $T_2{}^*$ induced by hyperfine interaction is tens of nanoseconds[81, 82]. This, together with experimental values for T_1 as long as miliseconds[74]

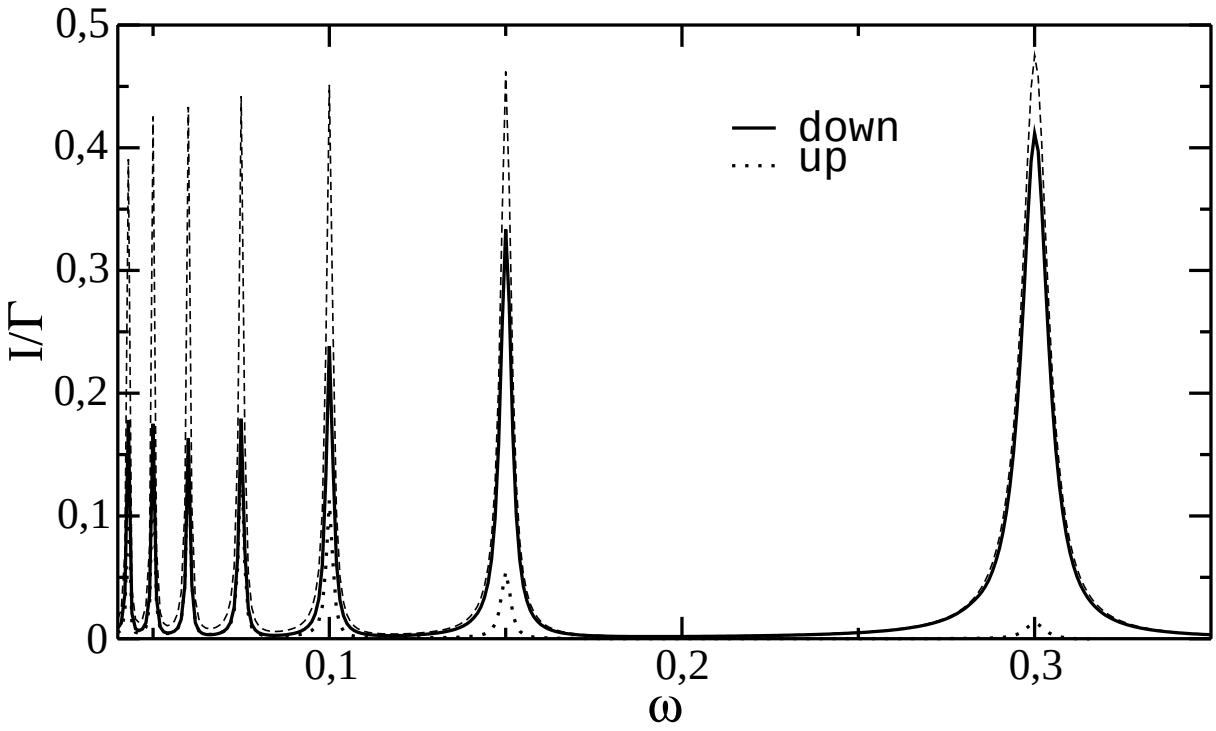

Fig. 4.6: Pumped current as a function of the AC frequency compared to the fully spin-down polarized current (dashed line) obtained by neglecting photon-assisted tunneling in the contact barriers. The subharmonic resonant peaks are shown up to the one involving seven photons in the intradot transitions. The height of the polarized currents depends non-linerarly in the relation between the AC intensity and frequency. Parameters: $t_{\rm LR} = 0.005$, $\Gamma = 0.001$, $U_{\rm L} = 1.0$, $U_{\rm R} = 1.3$, $\Delta_{\rm L} = \Delta_{\rm R} = 0.026$, $V_{\rm AC} = \omega_{S_1\downarrow}$.

in GaAs quantum dots, such that $1/T_1 \ll 1/{T_2}^*$, would allow to estimate the spin dephasing time ${T_2}^*$ directly from the intersection of the large Γ asymptote with the vertical axis (Fig. 4.5b, dotted line).

Note, from Fig. 4.5b, that the numerical results differ from the expected analytical curves for the case ${T_2}^* = 10^{-3}T_1$ for large Γ. This is because the parameters that contribute to FWHM (Γ or $1/{T_2}^*$) are large enough to make the current peak overlap with its neighboring spin-down current peak at $\omega_{T_0\downarrow}$. Then, it loses its lorenztian shape, mixes its spin polarization and gets wider than what it is analytically expected. This problem should hold in the experimental measurements unless the energy difference between both peaks were large enough so they do not overlap and they can be fitted to a lorenztian curve. This is the case when $\Delta_{\rm R} - \Delta_{\rm L} \gg 2\gamma$.

4.4 Photon-assisted tunneling effects

4.4.1 Limitation of the spin filter

As discussed in chapter 3, even if the AC gate voltage is applied to the dots, photon-assisted tunneling also affects the tunneling through the contact barriers. Then, processes that were considered

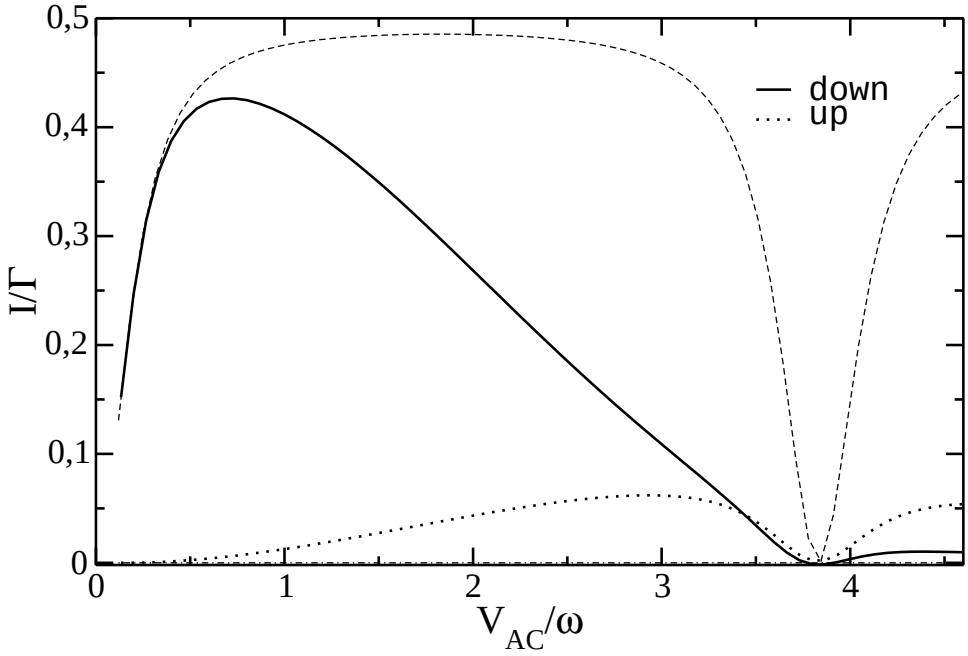

Fig. 4.7: Dependence of the pumped currents on the AC field intensity compared to the fully spin-down polarized current obtained when neglecting PAT in the contact barriers (dashed line), for fixed ac frequency $\omega_{S_1\downarrow} = 0.3$.

energetically forbiden can now occur by the absorption or emission of photons with rates

$$\Gamma_{mn} = 2\pi \sum_{l} \sum_{\nu=-\infty}^{\infty} J_\nu^2 \left(\frac{V_{\rm AC}}{2\omega}\right) |\gamma_{mn}|^2 (f(\omega_{mn} + \nu\omega - \mu_l)\delta_{N_m,N_n+1} + (1 - f(\omega_{nm} + \nu\omega - \mu_l))\delta_{N_m,N_n-1}). \tag{4.29}$$

so new tunneling channels appear[90, 91]. Also, the probability of processes considered in the previous section are reduced. Now, there is a finite probability (via the absorption or emission of photons) for transitions that previously were not available due to the concrete energy configuration. Specifically, there will be processes which extract spin-up electrons from the right dot doubly occupied singlet state by photon absorption through the right contact, that is: $|\uparrow\downarrow\rangle_{\rm R} \rightarrow |\downarrow\rangle_{\rm R}$. In order to give an stimation of the effect of these processes, let consider the resonance between the singlet states with lower energy of each QD, $\omega_{S_0\downarrow}$, so the higher level of the right QD can be extracted form the integration–it would only contribute with satellite peaks, as seen in the previous section. There, the device was operated as a spin-down filter following the cycle

$$|\uparrow\downarrow,\uparrow\rangle \leftrightsquigarrow |\uparrow,\uparrow\downarrow\rangle \rightarrow \{|\uparrow,\uparrow\rangle \quad \text{or} \quad |\uparrow\downarrow,\uparrow\downarrow\rangle\} \rightarrow |\uparrow\downarrow,\uparrow\rangle. \tag{4.30}$$

Considering the same Zeeman splitting in both dots, both resonances $|\uparrow\downarrow,\uparrow\rangle \leftrightsquigarrow |\uparrow,\uparrow\downarrow\rangle$ and $|\uparrow\downarrow,\downarrow\rangle \leftrightsquigarrow |\downarrow,\uparrow\downarrow\rangle$ occur at the same frequency $\omega_{S_1\downarrow}$. So, through the sequence

$$|\uparrow\downarrow,\uparrow\downarrow\rangle \rightarrow |\uparrow\downarrow,\downarrow\rangle \leftrightsquigarrow |\downarrow,\uparrow\downarrow\rangle \rightarrow |\uparrow\downarrow,\uparrow\downarrow\rangle, \tag{4.31}$$

a net spin-up polarized current appears (see Fig. 4.6). This sequence is much less efficient than (4.30) since processes that do not depend on the absorption of photons through the contacts are more probable,

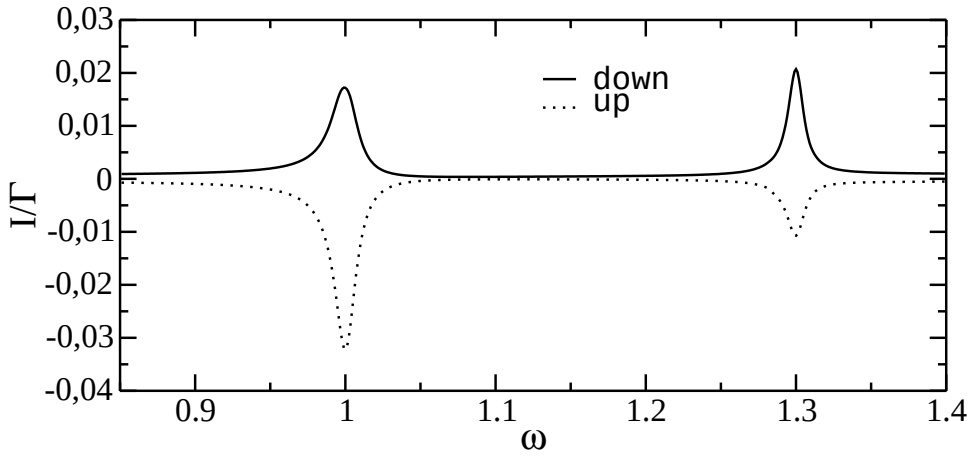

Fig. 4.8: Pumped current as a function of the AC frequency. Parameters (in meV): $t_{\rm LR} = 0.005$, $\Gamma = 0.001$, $U_{\rm L} = 1.6$, $U_{\rm R} = 1.3$, $\Delta_{\rm L} = \Delta_{\rm R} = 0.026$ (corresponding to a magnetic field $B \approx 1T$), $\varepsilon_{\rm L} = \varepsilon_{\rm R} = 0.5$, $\mu = 1.81$, $V_{\rm AC} = 1.0$ and $k_{\rm B}T = 0.001$. As discussed in the text, when the frequency of the driving field matches the intradot Coulomb repulsion of each dot, some photon-assisted resonances that show up.

as shown in chapter 3. Also, the transitions $|\uparrow\downarrow,\downarrow\rangle \rightarrow |\uparrow\downarrow,\uparrow\downarrow\rangle \rightarrow |\uparrow\downarrow,\uparrow\rangle$ and $|\downarrow,\uparrow\downarrow\rangle \rightarrow |\downarrow,\uparrow\rangle \rightarrow |\uparrow\downarrow,\uparrow\rangle$ take the system *back* to the states involved in the spin-down cycle (4.30).

However, the generated spin-up current produced under PAT through the contacts, being small, can be mostly removed as the AC-field intensity becomes small (see Fig. 4.7). In this case (low AC intensity), neglecting PAT through the contacts is a good approximation[48], and we recover the spin-down filter behaviour. On the other hand, the contribution of the new processes increases with the AC intensity, so the spin-up current becomes more important, while the spin-down one is reduced when including photon-assisted tunneling effects n the contact barriers. This behaviour was also predicted for the two electrons case discussed in section 3.4.3. As expected, the current vanishes as the renormalized Rabi frequency does, due to dynamical charge localization when $J_1\left(\frac{V_{\rm AC}}{\omega}\right) = 0$.

This dependence of the photon-assisted spin-up current with $V_{\rm AC}$ is manifested also in the height of the two-photons satellite peak (Fig. 4.6) at $\omega_{S_0\downarrow}/2$. The new PAT processes through the contacts increase their rate with the AC intensity (via the Bessel function $J_n\left(\frac{V_{\rm AC}}{2\omega}\right)$, being $n > 0$, see Eq.(4.29)), so they increase their relative contribution to the current, as can be seen in the higher spin-up peak and the lower spin-down one (Fig. 4.7).

4.4.2 Hidden resonances

Photon-assisted tunneling in the contacts may also give rise to new features that cannot be predicted when neglecting it. The frequency of the AC field may be in resonance with the energy required by the internal electrons to perform transitions to states from where they do not have enough energy to tunnel to the reservoir–unless they absorbed one or more photons[91].

In the same configuration, with one level in each QD, when introducing the AC field, the electrons of the state $|\uparrow\downarrow,\uparrow\rangle$ are able, by the absorption of a certain number of photons, to leave the DQD, giving a finite occupation probability to states that otherwise would never be populated as, for instance, $|\downarrow,\uparrow\rangle$, once the spin-up electron of the left dot tunnels out towards the left contact. If the

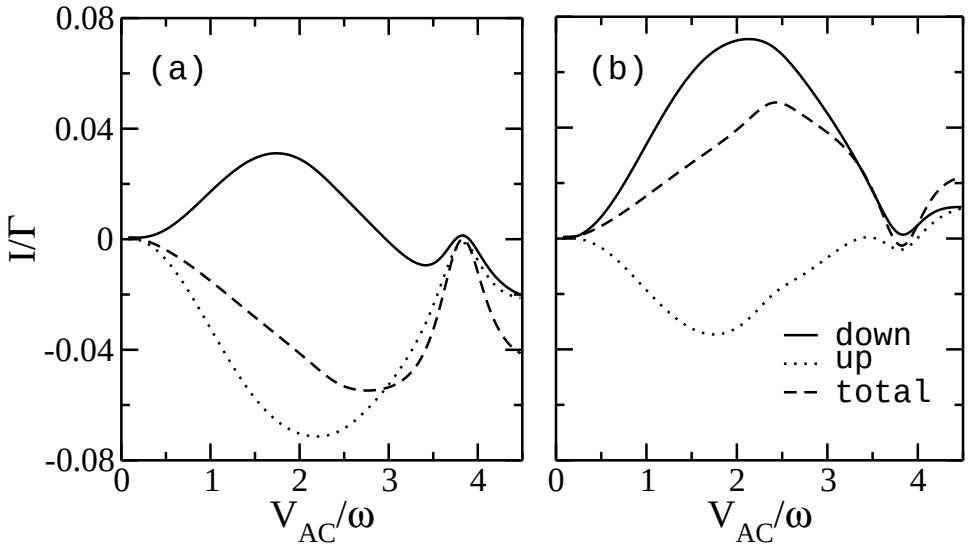

Fig. 4.9: Pumped spin up (dotted line) and spin down (solid line) current and total (dashed line) current as a function of the intensity of the AC field for the fixed frequencies (a) $\omega = U_L = 1.0$ and (b) $\omega = U_R = 1.3$. The rest of parameters are the same as in Fig. 4.8.

frequency of the AC field is tuned to be enough to compensate the Coulomb repulsion of the left dot (that is, $\omega = \omega_{\rm L} \approx U_{\rm L}$), the spin-up electron in the right dot is delocalized between both dots so that another electron can enter from the right contact. Then, net spin-up current is created from the right to the left contact through the sequence

$$|\uparrow\downarrow,\uparrow\rangle \rightarrow |\downarrow,\uparrow\rangle \leftrightsquigarrow |\uparrow\downarrow,0\rangle \rightarrow |\uparrow\downarrow,\uparrow\rangle. \tag{4.32}$$

On the other hand, at this frequency, the state $|\uparrow\downarrow,0\rangle$ is also resonant with $|\uparrow,\downarrow\rangle$, which contributes to spin down current to the right lead (and to spin up current to the left as well) by the sequence $|\uparrow,\downarrow\rangle \rightarrow |\uparrow,\uparrow\downarrow\rangle \rightarrow |\uparrow,\uparrow\rangle$. In this way, different spin polarized currents can flow in different directions, as can be seen in figure 4.8.

Increasing the frequency of the AC field, the higher Coulomb repulsion of the right dot can now be compensated if $\omega = \omega_{\rm R} \approx U_{\rm R}$. Then, the spin-down electron is delocalized between the states $|\downarrow,\uparrow\rangle$ and $|0,\uparrow\downarrow\rangle$, so spin-down current flows to the right contact through the cycle

$$|\uparrow\downarrow,\uparrow\rangle \rightarrow |\downarrow,\uparrow\rangle \leftrightsquigarrow |0,\uparrow\downarrow\rangle \rightarrow |0,\uparrow\rangle \tag{4.33}$$

(in this point, a spin down electron can enter the left dot, restoring the resonant state, $|\downarrow,\uparrow\rangle$, or two electrons can form the initial singlet state, $|\uparrow\downarrow,\uparrow\rangle$). The resonance between $|0,\uparrow\downarrow\rangle$ and $|\uparrow,\downarrow\rangle$ at the same frequency allows the flow of spin up electrons from the right to the left lead through a sequence

$$|0,\uparrow\downarrow\rangle \Leftrightarrow |\uparrow,\downarrow\rangle \rightarrow |\uparrow,\uparrow\downarrow\rangle \rightarrow |\uparrow,\uparrow\rangle \rightarrow |\uparrow\downarrow,\uparrow\rangle, \tag{4.34}$$

that also contributes to spin-down current from the left to right lead.

In figures 4.8 and 4.9, the pumped current is plotted as a function of the AC frequency and intensity respectively. Spin up and spin down current contributions flow in opposite directions, giving

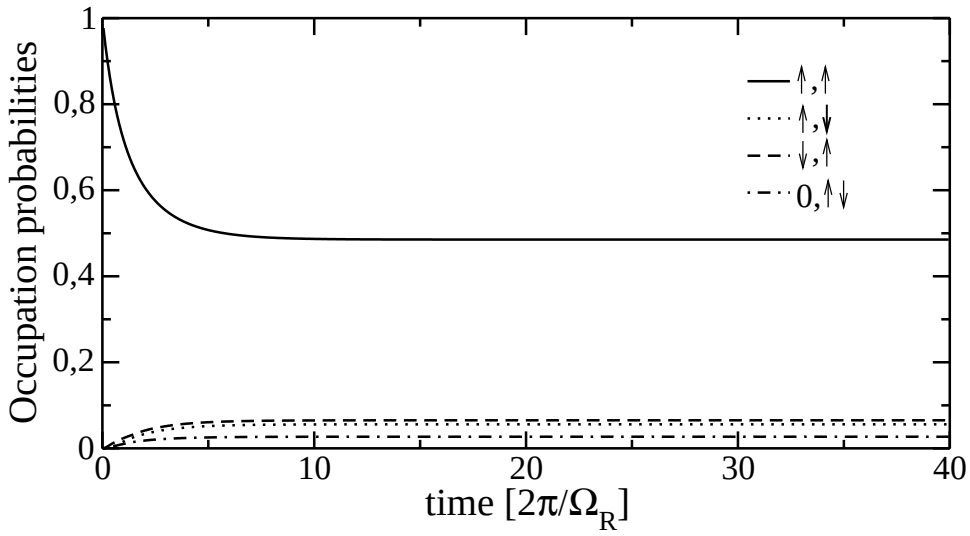

Fig. 4.10: Time evolution (normalized to $\tau = 2\pi/\Omega_{\rm R}$, being $\Omega_{\rm R} = 2J_1(\alpha)t_{\rm LR}$ the Rabi frequency of the delocalization processes) of the diagonal density matrix elements which describe the occupation probability of the states relevant for transport. Photon assisted tunneling through the contacts is manifested in the de-population of state $|\uparrow,\uparrow\rangle$[**?**]. Parameters (in meV): $t_{\rm LR} = 0.005$, $\Gamma = 0.001$, $U_{\rm L} = 1.6$, $U_{\rm R} = 1.3$, $\Delta_{\rm L} = \Delta_{\rm R} = 0.2$ (corresponding to a magnetic field $B \approx 8T$), $\varepsilon_{\rm L} = \varepsilon_{\rm R} = 0.5$, $\mu = 1.9$, $\omega = U_{\rm R} = V_{\rm AC}/2$.

rise to a finite spin current and a very small charge current. Then, tuning the AC parameters one would expect a situation where the net charge current is very small and $I_\uparrow \approx -I_\downarrow$. However, to reach a configuration where charge current is zero whereas spin current is finite by tuning the AC parameters and sample configuration is not trivial due to the large number of tunneling processes involved.

4.4.3 Spin blockade lifting

As discussed at the begining of this chapter, if the gate voltages of the quantum dots are tuned so, in the absence of driving, each quantum dot allows only one electron, pumping is limited by spin blockade[63]. Pauli exlusion principle avoids interdot tunneling when both spins have the same polarization[92, 93]. This effect has been exploited for current rectification[94] and coherent spin operations by means of AC fields[95].

Then, the introduction of an AC electric field in resonance between states with one electron in each dot and the doubly occupied singlet state of one of them (the one in the right, in this case) would not have any effect in the absence of photon-assited tunneling[96]. This effect has to be taken into account when coherently manipulating single spins by oscillating external fields[95].

This would be the case when trying to pump spin-down currents when $\mu < U_l + \varepsilon_l + \Delta_l$ and $\mu > U_R + \varepsilon_R$, so the non-driven DQD would be in a stable state with one electron in the left dot and a spin-up electron *trapped* in the right QD– the state $|\downarrow\rangle_{\rm R}$ decais through the sequence $|\downarrow\rangle_{\rm R} \rightarrow |\uparrow\downarrow\rangle_{\rm R} \rightarrow |\uparrow\rangle_{\rm R}$.

Introducing an AC field in resonance with the states $|\downarrow,\uparrow\rangle$ and $|0,\uparrow\downarrow\rangle$ (and, since $\Delta_{\rm L} = \Delta_{\rm R}$, also with $|0,\uparrow\downarrow\rangle$ and $|\uparrow,\downarrow\rangle$), the spin-down electron will be delocalized between both quatum dots and there will be a finite probability for it to leave the DQD to the right lead. Then, one should expect a net

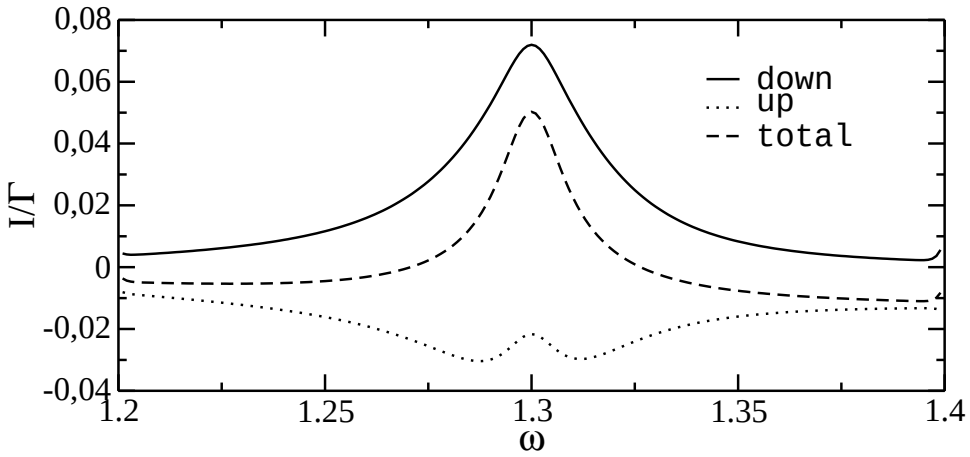

Fig. 4.11: Pumped current (normalized to the tunneling probability, Γ) as a function of the frequency of the AC field (in meV). Considering the *blocking state*, $|\uparrow,\uparrow\rangle$, if the electron in the left QD absorbs a photon and tunnels to the left lead, net spin down current to the right lead is created due to the sequence: $|\uparrow,\uparrow\rangle \rightarrow |0,\uparrow\rangle \rightarrow |\downarrow,\uparrow\rangle \leftrightsquigarrow |0,\uparrow\downarrow\rangle \rightarrow \{|0,\uparrow\rangle \quad \text{or} \quad |\uparrow,\uparrow\downarrow\rangle\} \rightarrow |\uparrow,\uparrow\rangle$, while spin up current flows in the opposite direction (from right to left) by the sequence: $|\uparrow,\uparrow\rangle \rightarrow |0,\uparrow\rangle \rightarrow |\downarrow,\uparrow\rangle \leftrightsquigarrow |0,\uparrow\downarrow\rangle \leftrightsquigarrow |\uparrow,\downarrow\rangle \rightarrow |\uparrow,\uparrow\downarrow\rangle \rightarrow |\uparrow,\uparrow\rangle$ (in this cycle, spin down current through the right contact is also produced). On the other hand, if the spin up in the right QD is extracted from $|\uparrow,\uparrow\rangle$, there is a positive contribution to spin up current through the sequence: $|\uparrow,\uparrow\rangle \rightarrow |\uparrow,0\rangle \rightarrow |\uparrow,\downarrow\rangle \leftrightsquigarrow |0,\uparrow\downarrow\rangle \rightarrow \{|\uparrow,\uparrow\downarrow\rangle \quad \text{or} \quad |0,\uparrow\rangle\} \rightarrow |\uparrow,\uparrow\rangle$. The contribution of this sequence is smaller (since it compites with the sequence $|\uparrow,\uparrow\rangle \rightarrow |\uparrow,0\rangle \rightarrow |\uparrow,\downarrow\rangle \rightarrow |\uparrow,\downarrow\rangle \rightarrow |\uparrow,\uparrow\downarrow\rangle \rightarrow |\uparrow,\uparrow\rangle$ that recovers rapidly the state $|\uparrow,\uparrow\rangle$ without contributing to the current) and is only apreciable at high enough field intensities. However, it may be the responsible of the supression of negative spin up current near resonance, giving a small bump. Note also that, since so many states are contributing to the dynamics of the system, the behaviour of the resonance peaks differs from the typical Lorentzian shape. The parameters are the same as in Fig. 4.10.

spin down current through the system through the *pumping cycle*

$$|\downarrow,\uparrow\rangle \Leftrightarrow |0,\uparrow\downarrow\rangle \rightarrow \{|0,\uparrow\rangle \quad \text{or} \quad |\downarrow,\uparrow\downarrow\rangle\} \rightarrow |\downarrow,\uparrow\rangle. \tag{4.35}$$

However, since the empty left QD can be also filled with a spin up electron, in the absence of photon-assisted tunneling in the contacts, the system asymptotically evolves to the state $|\uparrow,\uparrow\rangle$ (i.e., $\rho_{\uparrow\uparrow,\uparrow\uparrow}(t \rightarrow \infty) = 1$ and $\rho_{i,j}(t \rightarrow \infty) = 0$, otherwise) that leads to SB[63].

However, the rates (4.29) allow the *trapped* spins in the DQD to absorb a certain number of photons and tunnel out to the leads giving a finite ocuppation probability through the sequences

$$|\uparrow,\uparrow\rangle \rightarrow |0,\uparrow\rangle \rightarrow |\downarrow,\uparrow\rangle \tag{4.36}$$

$$|\uparrow,\uparrow\rangle \rightarrow |\uparrow,0\rangle \rightarrow |\uparrow,\downarrow\rangle \tag{4.37}$$

to the states $|\downarrow,\uparrow\rangle$ and $|\uparrow,\downarrow\rangle$. These states are in resonance with the $|0,\uparrow\downarrow\rangle$ that allows electronic tunneling to the right lead (cf. Fig. 4.10). Then, PAT through the contacts creates a finite current through the system (Fig. 4.11), removing the SB.

4.5 Conclusions

A new scheme of realizing *both* spin filtering and spin pumping by using AC-driven double quantum dots coupled to unpolarized leads has been proposed and analyzed. The results demonstrate that the spin polarization of the current can be manipulated (including fully reversing) by tuning the parameters of the AC field. For homogeneous magnetic field, $\Delta_{\mathrm{L}} = \Delta_{\mathrm{R}}$, one obtains spin down polarized current involving singlet states in both dots. In order to obtain spin up polarized current, an inhomogeneous magnetic field is required to break the degeneracy in transitions involving triplet states in the right dot. These results also show, both analytically and numerically, that the width in frequency of the spin-up pumped current gives information about the *spin decoherence time* T_2 and also about the *spin dephasing time* T_2^* of the isolated double quantum dot system. Experiments along these lines would allow to get information, from transport measurements, on the different mechanisms producing spin decoherence in quantum dots.

It has been also shown how photon-assisted tunneling through the contact barriers in AC driven DQD's gives additional contributions to the pumped current and the limits where this effect can be neglected. In particular, it modifies the spin filtering behaviour of a DQD device working as a spin pump. However, this contribution is effective only for high AC-intensities.

Additionally, photon-assisted transport is manifested in resonances through states that otherwise would not participate in the current. Different spin polarization contributions to the current. Interestigly, currents involving the different spin polarizations flow in opposite direction, leading to the possibility of manipulating spin currents even when the net charge transport is quenched.

These photon-assisted channel opening implies effects as spin blockade removal that are to be taken into account when manipulating electrons in quantum dot systems by external AC potentials.

Chapter 5

Coherent spin rotations in double quantum dots

The accurate tunability of time dependent fields has allowed the access and manipulation of quantum systems by the resonant illumination of atoms, finding interesting effects such as the possibility of trapping the atom in a non-absorbing coherent superposition (*dark state*) which is known as Coherent Population Trapping [99, 100, 101, 102]. This effect has been applied to non-conducting states in quantum dots (QD) – also known as *artificial atoms*– for spinless electrons [103, 105], having revealed several advantages for practical issues such as electronic current switching[103, 104] or de-coherence probing[106].

Great interest is recently focussed in the coherent control of electron spin states in the search of candidates for qubits. Within this scope, optical trapping of localized spins has been treated in self-assembled quantum dots[107] and achieved in diamond deffects[108]. Electron spin states in QD's have been proposed as qubits because of their long spin de-coherence and relaxation times[109, 110, 111]. The controlled rotation of a single electron spin is one of the challenges for quantum computation purposes. In combination with the recently measured controlled exchange gate between two neighboring spins[79], driven coherent spin rotations would permit universal quantum operations. Recently, experimental and theoretical efforts have been devoted to describe Electron Spin Resonance (ESR) in single[97, 98] and double quantum dots (DQDs)[**?**, 113, 114, 115]. There, an AC magnetic field, B_{AC}, with a frequency resonant with the Zeeman splitting Δ induced by a DC magnetic field, B_{DC}, drives electrons to perform spin coherent rotations which can be perturbed by electron spin flip induced by scattering processes such as spin orbit or hyperfine interactions. These are manifested as a damping of the oscillations. In particular, hyperfine interaction between electron and nuclei spins induces flip-flop transitions and an effective Zeeman splitting which adds to the one induced by $B_{\rm DC}$[87, 93, 95]. ESR mechanism also allows to access spin-orbit physics in the presence of AC electric fields[116, 117] or vibrational degrees of freedom in nano-mechanical resonators[118].

In the experiments of Ref. [95], fast electric field switching was required in order to reach the Coulomb blockade regime and to manipulate the spin electron system. In this chapter, a simpler configuration is analyzed which is easier to perform experimentally than the one proposed in [95], which does not require to bring the double occupied electronic state in the right dot to the Coulomb blockade configuration and which consists on conventional tunnel spectroscopy in a DQD under crossed DC and AC magnetic fields, *without additional electric pulses*.

The main purpose is to analyze the spin dynamics and the tunneling current and to propose

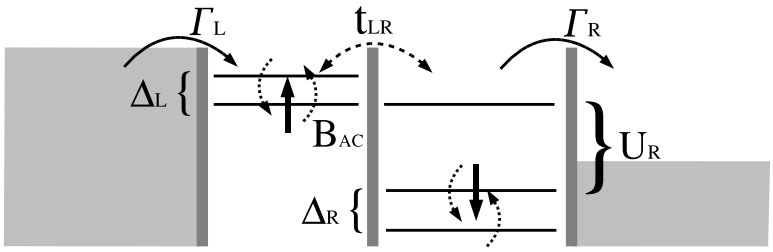

Fig. 5.1: Schematic diagram of the DQD in the presence of crossed DC and AC magnetic fields.

for the first time how to trap electrons in a DQD performing coherent spin rotations by a resonant AC magnetic field which can be unambiguously detected by conventional tunnelling spectroscopy measurements. It is also shown how to trap electrons in a concrete state by means of resonant bi-chromatic magnetic fields in the case where the Zeeman splitting is different in both QD's (as it usually happens in the presence of hyperfine interaction).

Let consider a DQD in the *spin blockade* regime[92], i.e., inter-dot tunnelling is suppressed due to Pauli exclusion principle[94] as the electrons in the DQD have parallel spins. This effect may be lifted by the rotation of the electrons spin, under certain conditions, by the introduction of crossed $B_{\rm DC}$ and $B_{\rm AC}$. Then, when $B_{\rm AC}$ is resonant with the Zeeman splitted level, the electrons both rotate their spins within each QD and tunnel, performing spatial oscillations between the left and right QD. The electronic current through such a system performs coherent oscillations which depend non trivially on both the AC intensity and the inter-dot coupling. As will be shown, when the effective $B_{\rm DC}$ is homogeneous through the sample, the current is quenched since the system is coherently trapped in the triplet subspace (*dark subspace*) in spite of the driving field. However, a finite current may flow as a consequence of spin relaxation processes. In this case, measuring the current would give information about the spin relaxation time by identifying its effect and separating it from leakage currents due to higher order tunneling processes[86]. If Δ is different within eachQD (it can be due to an inhomogeneous $B_{\rm DC}$, different g factors or the presence of hyperfine interaction[87, 88] with different intensity within each quantum dot), $B_{\rm AC}$ is resonant only in one of them and the trapping is lifted. Then, off-resonance dynamics of the other electron should in principle affect the total dynamics of the system and it should be included in a theoretical description not restricted to the rotating wave approximation[**?**] which is valid just at resonance. Finally it will be shown that it is possible to trap the electrons also in this configuration, where Δ is different within each quantum dot, by applying a bichromatic $B_{\rm AC}$, such that each frequency matches the Zeeman splitting of the electron in each quantum dot.

5.1 Electron spin resonance in an open double quantum dot

The two weakly coupled quantum dot system connected to two fermionic leads, is described by the model Hamiltonian:

$$\hat{H} = \hat{H}_0 + \hat{H}_{\rm LR} + \hat{H}_{\rm T} + \hat{H}_{\rm leads}, \tag{5.1}$$

where $\hat{H}_0 = \sum_{i\sigma} \varepsilon_i \hat{c}^\dagger_{i\sigma}\hat{c}_{i\sigma} + \sum_i U_i \hat{n}_{i\uparrow}\hat{n}_{i\downarrow} + U_{\rm LR}\hat{n}_{\rm L}\hat{n}_{\rm R}$ describes the uncoupled double quantum dot, $\hat{H}_{\rm LR} = -\sum_\sigma (t_{\rm LR}\hat{c}^\dagger_{{\rm L}\sigma}\hat{c}_{{\rm R}\sigma} + {\rm H.c.})$ is the inter-dot coupling and $\hat{H}_{\rm T} = \sum_{l\epsilon\{{\rm L,R}\}{\rm k}\sigma}(\gamma_l \hat{d}^\dagger_{lk\sigma}\hat{c}_{l\sigma} + {\rm H.c.})$ gives the

tunnelling between the DQD and the leads, described by: $\hat{H}_{\text{leads}} = \sum_{lk\sigma} \varepsilon_{lk} \hat{d}^{\dagger}_{lk\sigma} \hat{d}_{lk\sigma}$, where ε_i is the energy of an electron located in dot i and U_i (U_{LR}) is the intra-dot (inter-dot) Coulomb repulsion. For simplicity, the Heisenberg exchange interaction[93, 94] is disregarded. Finite exchange, would slightly split the inter-dot singlet-triplet energy separation without modifying qualitatively the results presented here. The chemical potentials of the leads, μ_i, are such that only two electrons (one in each dot) are allowed in the system: $\varepsilon_i < \mu_i - U_{\text{LR}} < \varepsilon_i + U_i$ and $\mu_i < \varepsilon_i + 2U_{\text{LR}}$. In this configuration, the spin blockade is manifested when a bias voltage is applied such that the state with two electrons in the right dot (the one which contributes to the current) is in resonance with those with one electron in each dot. The current is then quenched when the electrons in each QD have the same spin polarization and Pauli exclusion principle avoids the inter-dot tunneling[94]. Now, a magnetic field is introduced with a DC component along the Z axis (which breaks the spin degeneracy by a Zeeman splitting $\Delta_i = g_i B_{z,i}$) and a circularly polarized AC component in the perpendicular plane XY that rotates the Z component of the electron spin when its frequency satisfies the resonance condition, $\omega = \Delta_i$[98]:

$$\hat{H}_{\text{B}}(t) = \sum_i [\Delta_i S^i_z + B_{\text{AC}} \left(\cos\omega t S^i_x + \sin\omega t S^i_y\right)], \tag{5.2}$$

where $\mathbf{S}_i = \frac{1}{2} \sum_{\sigma\sigma'} c^{\dagger}_{i\sigma} \sigma_{\sigma\sigma'} c_{i\sigma'}$ are the spin operators of each dot (see Fig. 7.1).

The dynamics of the system is given by the time evolution of the reduced density matrix elements, whose equation of motion, within the Born-Markov approximation[119], see chapter 2, reads:

$$\dot{\rho}_{ln}(t) = -i\langle l|[H_0 + H_{\text{LR}} + H_{\text{B}}(t), \rho]|n\rangle + \sum_{k\neq n} \left(\Gamma_{nk}\rho_{kk} - \Gamma_{kn}\rho_{nn}\right)\delta_{ln} - \Lambda_{ln}\rho_{ln}(1-\delta_{ln}). \tag{5.3}$$

where Γ_{ln} are the transition rates induced by the coupling to the leads, $\Gamma_i = 2\pi|\gamma_i|^2$, and the eventual spin scattering processes (introduced phenomenologically by the spin relaxation and de-coherence times, T_1 and $T_2^* = 0.1T_1$, respectively [**?**]). At low temperatures, the incoherent spin flip excitation is negligible: $\Gamma_{\downarrow\leftarrow\uparrow} = e^{-\beta\Delta_z}\frac{1}{T_1}$. The decoherence term is $\Lambda_{ln} = \frac{1}{2}\sum_k(\Gamma_{kl} + \Gamma_{kn}) + {T_2}^{-1}$, where ${T_2}^{-1} = \frac{1}{2}{T_1}^{-1} + {T_2^*}^{-1}$. The evolution of the occupation probabilities is given by the diagonal elements of the density matrix. In our configuration, the states relevant to the dynamics are: $|0,\uparrow\rangle$, $|0,\downarrow\rangle$, $|T_+\rangle = |\uparrow,\uparrow\rangle$, $|T_-\rangle = |\downarrow,\downarrow\rangle$, $|\uparrow,\downarrow\rangle$, $|\downarrow,\uparrow\rangle$, $|S_R\rangle = |0,\uparrow\downarrow\rangle$. This latest states is the only tha contributes to tunneling to the right lead, so the current is given by

$$I(t) = 2e\Gamma_{\text{R}}\rho_{S_{\text{R}},S_{\text{R}}}(t). \tag{5.4}$$

5.2 Closed system. Coherent dynamics

The purely coherent dynamics is present only in the closed system (for $\Gamma = 0$) and infinite T_1 and T_2. The properties of such a system will prevail–at least transiently–in the transport configuration and it is interesting to consider them with some detail[122].

5.2.1 One electron spin resonance

The single electron case is formally equivalent to the photon-assisted delocalization in a double quantum dot studied in chapter 3 and the Rabi problem for a particle with angular momentum one half[120, 121]. Considering a Zeeman splitting Δ_z, the Hamiltonian can be written as

$$H(t) = \frac{\Delta_z}{2}\sigma_z + \frac{B_{\text{AC}}}{2}\left(\cos\omega t\sigma_x + \sin\omega t\sigma_y\right) \tag{5.5}$$

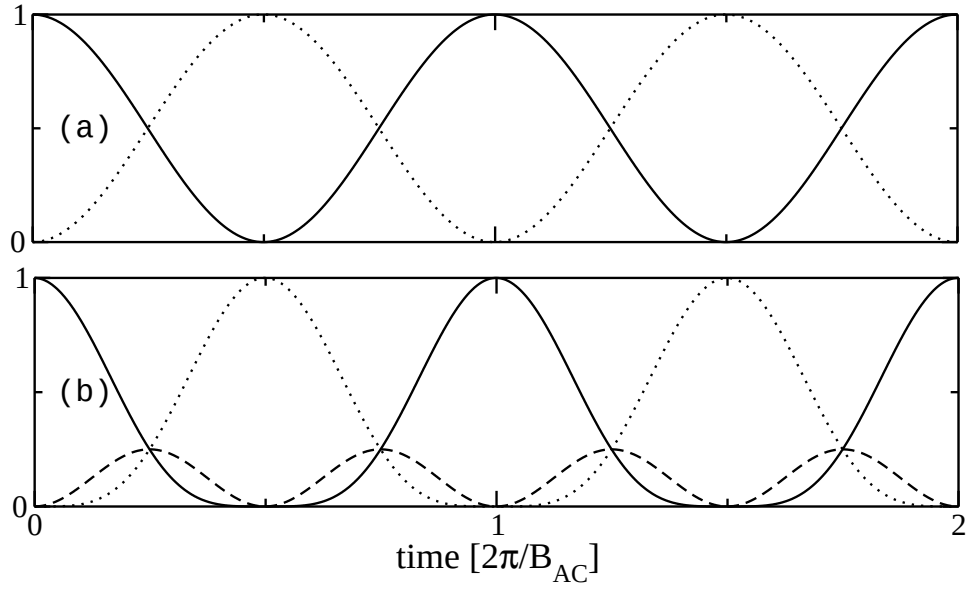

Fig. 5.2: Time dependence of the occupation probabilities for (a) the states $|\uparrow\rangle$ (solid) and $|\downarrow\rangle$ (dotted) of an isolated electron and (b) $|\uparrow,\uparrow\rangle$ (solid), $|\downarrow,\downarrow\rangle$ (dotted) and $|\uparrow,\downarrow\rangle$ and $|\downarrow,\uparrow\rangle$ (dashed) of two isolated electrons. As discussed in the text, the probability of flipping a single spin oscillates with double frequency in the presence of a second electron.

and, in matricial form, in the basis $\uparrow\rangle$ and $|\downarrow\rangle$

$$H_{\rm ESR} = \begin{pmatrix} \varepsilon + \Delta_z & \frac{B_{\rm AC}}{2} e^{-i\omega t} \\ \frac{B_{\rm AC}}{2} e^{i\omega t} & \varepsilon \end{pmatrix}, \quad |\downarrow\rangle == \begin{pmatrix} 1 \\ 0 \end{pmatrix}, \quad |\uparrow\rangle == \begin{pmatrix} 0 \\ 1 \end{pmatrix}, \tag{5.6}$$

with the Pauli matrices

$$\sigma_x = \begin{pmatrix} 0 & 1 \\ 1 & 0 \end{pmatrix}, \quad \sigma_y = \begin{pmatrix} 0 & -i \\ i & 0 \end{pmatrix}, \quad \sigma_z = \begin{pmatrix} 1 & 0 \\ 0 & -1 \end{pmatrix}. \tag{5.7}$$

Then, the Liouville equation is

$$\begin{aligned} \dot\rho_\uparrow(t) &= -i\frac{B_{\rm AC}}{2}\left(e^{i\omega t}\rho_{\downarrow\uparrow}(t) - e^{-i\omega t}\rho_{\uparrow\downarrow}(t)\right) \\ \dot\rho_{\uparrow\downarrow}(t) &= i(\Delta_z - \omega)\rho_{\uparrow\downarrow}(t) - i\frac{B_{\rm AC}}{2}\left(e^{i\omega t}\rho_\downarrow(t) - e^{-i\omega t}\rho_\uparrow(t)\right) \\ \dot\rho_\downarrow(t) &= i\frac{B_{\rm AC}}{2}\left(e^{i\omega t}\rho_{\downarrow\uparrow}(t) - e^{-i\omega t}\rho_{\uparrow\downarrow}(t)\right). \end{aligned} \tag{5.8}$$

By the transformation $\rho'_{\uparrow\downarrow}(t) = e^{-i\omega t}\rho_{\uparrow\downarrow}(t)$, the explicit time dependence disapears and one can write these equation in matricial form $\dot\rho = \mathcal{M}\rho$ by the inverse Laplace transform

$$\begin{pmatrix} \dot\rho_\uparrow \\ \dot\rho'_{\uparrow\downarrow} \\ \dot\rho'_{\uparrow\downarrow} \\ \dot\rho_\downarrow \end{pmatrix} = \begin{pmatrix} 0 & i\frac{B_{\rm AC}}{2} & -i\frac{B_{\rm AC}}{2} & 0 \\ i\frac{B_{\rm AC}}{2} & \Delta - \omega & 0 & -i\frac{B_{\rm AC}}{2} \\ -i\frac{B_{\rm AC}}{2} & 0 & \Delta - \omega & i\frac{B_{\rm AC}}{2} \\ 0 & -i\frac{B_{\rm AC}}{2} & i\frac{B_{\rm AC}}{2} & 0 \end{pmatrix} \begin{pmatrix} \rho_\uparrow \\ \rho'_{\uparrow\downarrow} \\ \rho'_{\uparrow\downarrow} \\ \rho_\downarrow \end{pmatrix}. \tag{5.9}$$

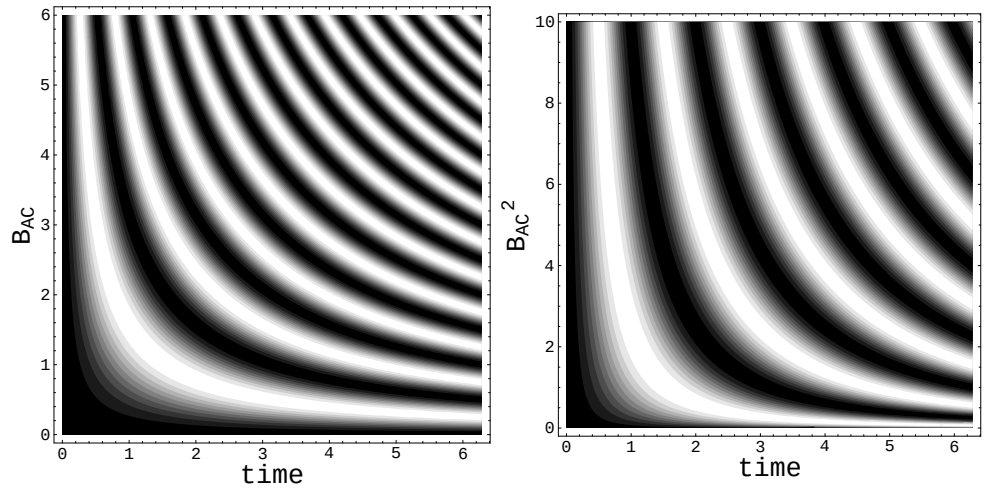

Fig. 5.3: Probability of flipping any of the two isolated spins, P_f, as a function of time and (left) $B_{\rm AC}$ and (right) $B_{\rm AC}^2$ (proportional to the RF power[95]) for $\Delta_L = \Delta_R = \Delta$ in resonance ($\omega = \Delta$).

This set of equations can be solved analytically by taking the Laplace transform, so $\rho(z) = (z - \mathcal{M})^{-1}\rho(0)$. If the initial condition is $\rho(0) = \rho_\uparrow(0)$, the occupation probabilities are

$$\rho_\downarrow = 1 - \rho_\uparrow = \frac{B_{\rm AC}^2/2}{B_{\rm AC}^2 + (\Delta_z - \omega)^2} \sin^2\left(\frac{1}{2}\sqrt{B_{\rm AC}^2 + (\Delta - \omega)^2}t\right), \tag{5.10}$$

revealing coherent spin rotations which, if the AC field is resonant with the Zeeman splitting, show a *Rabi* frequency $\Omega_{\rm ESR} = B_{\rm AC}$[32], cf. Fig. 5.2a. It is interesting to compare (5.10) with (2.99), describing the delocalization of an electron between two tunneling-coupled quantum dots. This two processes–spin rotation and spatial charge delocalization–will be the responsible of the dynamics showed in this chapter.

5.2.2 Two electrons spin resonance

However, the presence of an additional particle modifies the dynamics, even if both of them are isolated in different quantum dots. In general, each of them is affected by a different Zeeman splitting, so only one of them would be in resonance with the AC field. Then, the system is described by the Hamiltonian $\hat{H}(t) = \hat{H}_0 + \hat{H}_{\rm B}(t)$ and the basis $|1\rangle = |\uparrow,\uparrow\rangle$, $|2\rangle = |\downarrow,\uparrow\rangle$, $|3\rangle = |\uparrow,\downarrow\rangle$ and $|4\rangle = |\downarrow,\downarrow\rangle$. Again, after a similar variable transformation to the one performed in the one electron case, $\rho'_{12,24,34} = e^{-i\omega t}\rho_{12,24,34}$ and $\rho_{14} = e^{-i2\omega t}\rho_{14}$, the Liouville equation $\dot{\rho}(t) = -i[H(t), \rho(t)]$ has the form

$$\begin{aligned}
\dot{\rho}_1 &= -i\frac{B_{\rm AC}}{2}(\rho'_{21} - \rho'_{12} + \rho'_{31} - \rho'_{13}) \\
\dot{\rho}_2 &= -i\frac{B_{\rm AC}}{2}(\rho'_{12} - \rho'_{21} + \rho'_{42} - \rho'_{24}) \\
\dot{\rho}_3 &= -i\frac{B_{\rm AC}}{2}(\rho'_{43} - \rho'_{34} + \rho'_{13} - \rho'_{31}) \\
\dot{\rho}_4 &= -i\frac{B_{\rm AC}}{2}(\rho'_{34} - \rho'_{43} + \rho'_{24} - \rho'_{42}),
\end{aligned} \tag{5.11}$$

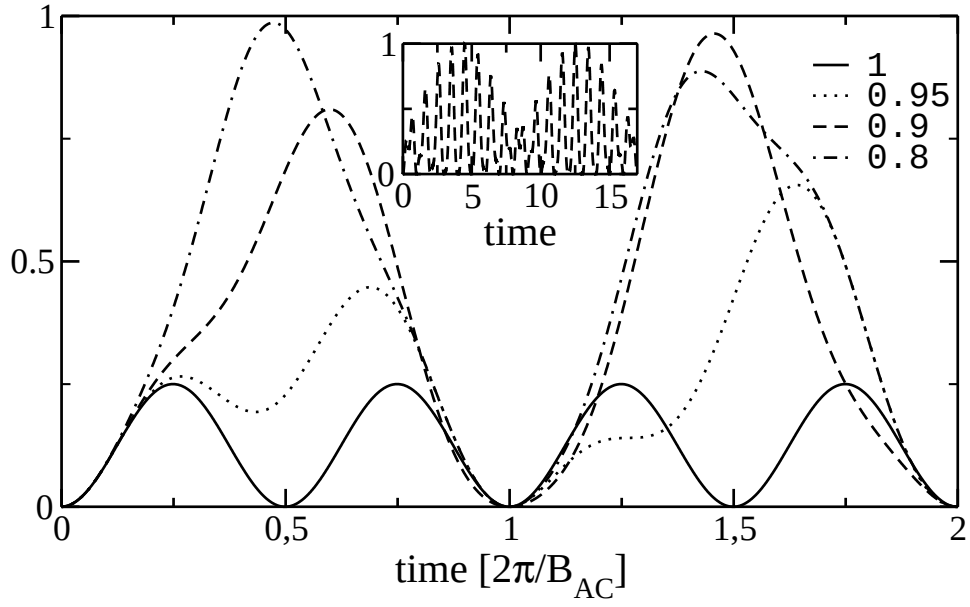

Fig. 5.4: Probability of finding the system in $\uparrow\downarrow\rangle$ (for the closed system case) when the left electron is out of resonance, for different ratios $\Delta_{\rm L}/\Delta_{\rm R}$. The crossover from the oscillations of two electrons to the single resonant electron can be appreciated. Inset: the case $\Delta_{\rm L}/\Delta_{\rm R} = 0.9$ for longer times.

for the diagonal terms, and

$$\begin{aligned}
\dot{\rho}'_{12} &= -i\frac{B_{\rm AC}}{2}((\rho_2 - \rho_1 + \rho_{32}) - \rho'_{14}) + i(\omega_{21} - \omega)\rho'_{12} \\
\dot{\rho}'_{13} &= -i\frac{B_{\rm AC}}{2}((\rho_3 - \rho_1 + \rho_{23}) - \rho'_{14}) + i(\omega_{31} - \omega)\rho'_{13} \\
\dot{\rho}'_{14} &= -i\frac{B_{\rm AC}}{2}(\rho'_{24} + \rho'_{34} - \rho'_{12} - \rho'_{13}) + i(\omega_{41} - 2\omega)\rho'_{14} \\
\dot{\rho}_{23} &= -i\frac{B_{\rm AC}}{2}((\rho'_{43} - \rho'_{21}) + \rho'_{13} - \rho'_{24} - i\omega_{23}\rho_{23} \\
\dot{\rho}'_{24} &= -i\frac{B_{\rm AC}}{2}(\rho_4 - \rho_2 - \rho_{23} + \rho'_{14}) + i(\omega_{42} - \omega)\rho'_{24} \\
\dot{\rho}'_{34} &= -i\frac{B_{\rm AC}}{2}(\rho_4 - \rho_3 - \rho_{32} + \rho'_{14}) + i(\omega_{43} - \omega)\rho'_{34},
\end{aligned} \tag{5.12}$$

for the coherences, where $\omega_{21} = \omega_{43} = \Delta_{\rm L}$, $\omega_{31} = \omega_{42} = \Delta_{\rm R}$, $\omega_{41} = \Delta_{\rm L} + \Delta_{\rm R}$ and $\omega_{23} = \Delta_{\rm L} - \Delta_{\rm R}$.

If the effect of the magnetic field is the same in both electrons, that is, they suffer the same Zeeman splitting, $\Delta_L = \Delta_R = \Delta$, the probability of flipping a spin is equal in both dots, so $\rho_3 = \rho_4 = \rho_S/2$. The equations can be solved by doing the Laplace transform, $\mathcal{L}\dot{\rho} = z\rho - \rho_0$. The probability of finding one of the electrons flipped, $P_f = \rho_2 + \rho_3$ is:

$$P_f = \frac{2B_{\rm AC}^2}{(B_{\rm AC}^2 + (\Delta-\omega)^2)^2}\left(\frac{B_{\rm AC}^2}{4}\sin^2\sqrt{B_{\rm AC}^2 + (\Delta-\omega)^2}t + (\Delta-\omega)^2\sin^2\frac{\sqrt{B_{\rm AC}^2 + (\Delta-\omega)^2}}{2}t\right), \tag{5.13}$$

and, in the resonant case $\omega = \Delta$:

$$P_f = \frac{1}{2}\sin^2 B_{\rm AC}t. \tag{5.14}$$

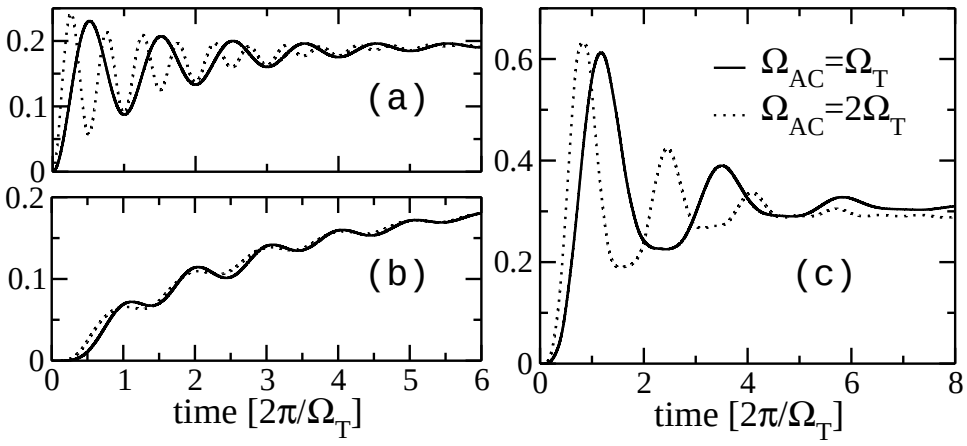

Fig. 5.5: Occupation probabilities (for the closed system) for the states (a) $|\downarrow,\uparrow\rangle$ and (b) $|0,\uparrow\downarrow\rangle$ for $\Delta_L = \Delta_R$ and (c) $|0,\uparrow\downarrow\rangle$ for $\Delta_L \neq \Delta_R$, for different ratios B_{AC}/t_{LR}. When $\Delta_L = \Delta_R$, $\rho_{\downarrow,\uparrow} = \rho_{\uparrow,\downarrow}$ oscillates with a frequency Ω_{AC} while $\rho_{0,\uparrow\downarrow}$, with Ω_T, while in (c) both the spin rotation and the tunnelling dynamics contribute to the time evolution of $\rho_{0,\uparrow\downarrow}$. Finite relaxation and de-coherence rates have been included: $\frac{1}{T_1} = 0.04\tau_{LR}$ and $T_2^* = 0.1T_1$.

Therefore, the Rabi frequency for this configuration is:

$$\Omega_{AC} = 2B_{AC}, \tag{5.15}$$

twice the one found for the single electron case, cf. Fig. 5.2.

On the other hand, if $\Delta_L \neq \Delta_R$, the resonance condition holds only for one of them. Then, in first approximation one could consider that the dynamics of one electron and one obtains for the probability of flipping the spin of the resonant electron: $P_f = sin^2 B_{AC}t$. However, we will see that the off-resonance electron plays also a role in the dynamics and modifies it in a non trivial way. If, for example, $\omega = \Delta_L$, one obtains:

$$P_f = \frac{B_{AC}^2}{4\Lambda^2}\Big(2 - cos\sqrt{2B_{AC}^2 + \delta^2 + 2B_{AC}\Lambda}t - cos\sqrt{2B_{AC}^2 + \delta^2 - 2B_{AC}\Lambda}t + \frac{4\delta^2}{B_{AC}^2} sin^2 \frac{B_{AC}}{2}t\Big)$$

where $\Lambda^2 = B_{AC}^2 + \delta^2$ and $\delta = \Delta_L - \Delta_R$. As can be seen in Fig. 5.4, there is a superposition of different oscillations which results in a complicated dynamics as δ increases. Then, it is not true in general that even in the case where the two QD's are decoupled, and just one of the two electrons is on resonance with B_{AC}, one could consider the electron dynamics for a single electron. However, the probability of finding the resonant electron rotated is the same as having only one electron: $\rho_2 + \rho_4 = \sin^2 \frac{1}{2}B_{AC}t$, while for the off-resonance one: $\rho_3 + \rho_4 = \frac{B_{AC}^2}{\Lambda^2}\sin^2 \frac{1}{2}\Lambda t$.

5.2.3 Electron delocalization

The interdot coupling term, H_{LR}, induces electron tunneling between both dots. In the present configuration, it involves the states $|1\rangle = |\uparrow,\downarrow\rangle$, $|2\rangle = |\downarrow,\uparrow\rangle$ and $|3\rangle = |0,\uparrow\downarrow\rangle$ so, in the absence of

magnetic field, the Liouville equation $\dot{\rho} = -i[H_0 + H_{\rm LR}, \rho]$ gives:

$$\begin{aligned}
\dot{\rho}_1 &= it_{\rm LR}(\rho_{31} - \rho_{13}) \\
\dot{\rho}_2 &= -it_{\rm LR}(\rho_{32} - \rho_{23}) \\
\dot{\rho}_3 &= -it_{\rm LR}(\rho_{31} - \rho_{13} + \rho_{23} - \rho_{32}) \\
\dot{\rho}_{12} &= it_{\rm LR}(\rho_{32} + \rho_{13}) - i(\Delta_{\rm R} - \Delta_{\rm L})\rho_{12} \\
\dot{\rho}_{13} &= it_{\rm LR}(\rho_3 - \rho_1 + \rho_{12}) - i\left(\varepsilon_{\rm L} - \varepsilon_{\rm R} - U_{\rm R}\right)\rho_{13} \\
\dot{\rho}_{23} &= -it_{\rm LR}(\rho_3 - \rho_2 + \rho_{21}) - i\left(\varepsilon_{\rm L} - \varepsilon_{\rm R} + \Delta_{\rm L} - \Delta_{\rm R} - U_{\rm R}\right)\rho_{13}
\end{aligned} \tag{5.16}$$

In resonance, the occupation of the state $|0, \uparrow\downarrow\rangle$ is:

$$\rho_3 = \frac{1}{2}\sin^2\sqrt{2}t_{\rm LR}t, \tag{5.17}$$

so the Rabi frequency is modified respect to the single electron case ($\Omega_{1e} = 2t_{\rm LR}$, see section 2.6):

$$\Omega_{\rm T} = 2\sqrt{2}t_{\rm LR}. \tag{5.18}$$

5.2.4 Mixing of spatial delocalization and spin rotation

For $\Delta_{\rm L} = \Delta_{\rm R}$, the spin rotation and tunnelling dynamics do not mix and can be parametrized by the frequencies $\Omega_{\rm AC} = 2B_{\rm AC}$ and $\Omega_{\rm T} = 2\sqrt{2}t_{\rm LR}$, respectively, cf. Fig. 5.5a,b. On the other hand, if $\Delta_{\rm L} \neq \Delta_{\rm R}$, one finds a coherent oscillation that depends in both magnetic field and interdot hopping magnitudes. This dependence should be manifested in the current (proportional to $\rho_{0,\uparrow\downarrow}$) for the open system, that will be analyzed in the next section.

The most simple case showing both tunneling and ESR is when the Zeeman splitting is very different in the two QD's. In this case, if the field is resonant with the left QD, the equations are, considering the basis $|1\rangle = |\uparrow,\uparrow\rangle$, $|2\rangle = |\downarrow,\uparrow\rangle$ and $|3\rangle = |0,\uparrow\downarrow\rangle$:

$$\begin{aligned}
\dot{\rho}_1 &= -i\frac{B_{\rm AC}}{2}(\rho_{21} - \rho_{12}) \\
\dot{\rho}_2 &= -i\frac{B_{\rm AC}}{2}(\rho_{12} - \rho_{21}) - it_{\rm LR}(\rho_{32} - \rho_{23}) \\
\dot{\rho}_3 &= -it_{\rm LR}(\rho_{23} - \rho_{32}) \\
\dot{\rho}_{12} &= -i\frac{B_{\rm AC}}{2}(\rho_2 - \rho_1) + it_{\rm LR}\rho_{13} + i(\Delta_{\rm L} - \omega)\rho_{12} \\
\dot{\rho}_{13} &= -i\frac{B_{\rm AC}}{2}\rho_{23} + it_{LR}\rho_{12} - i\left(\varepsilon_{\rm L} - \varepsilon_{\rm R} - U_{\rm R} - \Delta_{\rm R} + \omega\right)\rho_{13} \\
\dot{\rho}_{23} &= -i\frac{B_{\rm AC}}{2}\rho_{13} - it_{\rm LR}(\rho_3 - \rho_2) - i\left(\varepsilon_{\rm L} - \varepsilon_{\rm R} - U_{\rm R} + \Delta_{\rm L} - \Delta_{\rm R} + \omega\right)\rho_{23}.
\end{aligned} \tag{5.19}$$

If the gate voltages are tuned in a way that the left electron can tunnel to the doubly occupied singlet state in the right dot (having both electrons opposite spin polarization), one finds that the frequency of the oscillations depends on both the tunneling coupling and the field intensity, cf. Fig. 5.5:

$$\rho_1 = \frac{1}{(\frac{1}{4}B_{\rm AC}^2 + t_{\rm LR}^2)^2}\left(t_{\rm LR}^2 + \frac{1}{4}B_{\rm AC}^2\cos\frac{1}{2}\sqrt{B_{\rm AC}^2 + 4t_{\rm LR}^2}t\right)^2 \tag{5.20}$$

$$\rho_2 = \frac{B_{\rm AC}^2}{B_{\rm AC}^2 + 4t_{\rm LR}^2}\sin^2\frac{1}{2}\sqrt{B_{\rm AC}^2 + 4t_{\rm LR}^2}t \tag{5.21}$$

$$\rho_3 = \frac{B_{\rm AC}^2 T_{\rm LR}^2}{(\frac{1}{4}B_{\rm AC}^2 + t_{\rm LR}^2)^2}\sin^4\frac{1}{4}\sqrt{B_{\rm AC}^2 + 4t_{\rm LR}^2}t \tag{5.22}$$

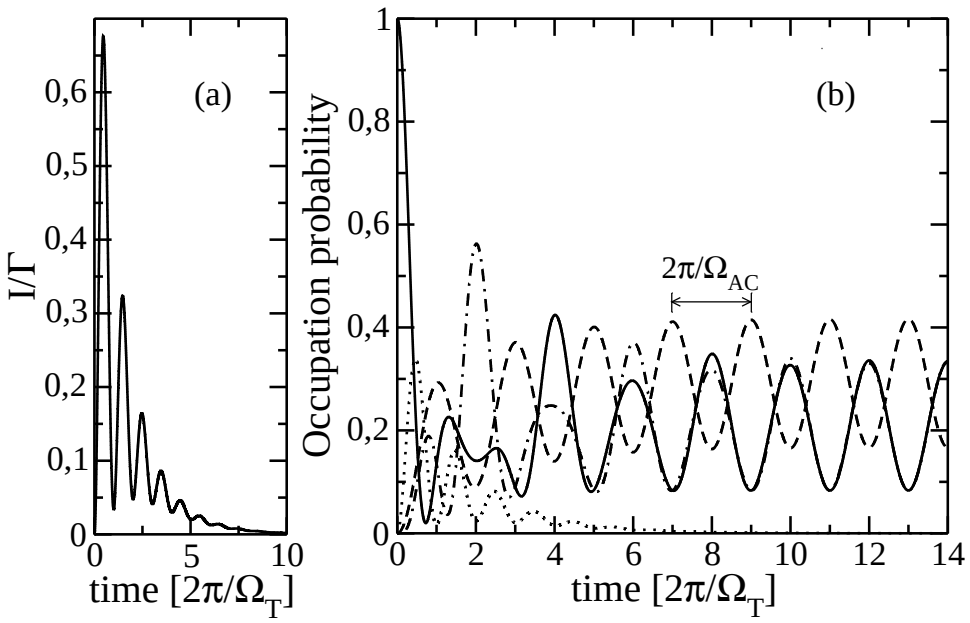

Fig. 5.6: (a) I(t) for initial state $|\uparrow,\downarrow\rangle$ in the absence of spin relaxation for $\Delta_{\rm L}=\Delta_{\rm R}=\Delta$ and $\Omega_{\rm AC}=\Omega_{\rm T}/2$. (b) The corresponding occupation probabilities: $|\uparrow,\downarrow\rangle$ (solid), $|\downarrow,\uparrow\rangle$ (dash-dotted), $|0,\uparrow\downarrow\rangle$ (dotted) and $|\uparrow,\uparrow\rangle$ and $|\downarrow,\downarrow\rangle$ (dashed). Parameters ($e=\hbar=1$): $\Gamma_L=\Gamma_R=\Gamma=10^{-3}$meV, $T_{1(2)}^{-1}=0$, $\Omega_{\rm T}=11.2$GHz and holding for the rest of the plots (in meV): $\varepsilon_{\rm L}=1.5$, $\varepsilon_{\rm R}=0.45$, $\Delta=0.026$ ($B_{\rm DC}\sim 1T$), $U_{\rm L}=1$, $U_{\rm R}=1.45125$, $V=0.4$, $\mu_{\rm L}=2$ and $\mu_{\rm R}=1.1$.

5.3 Transport regime

Each coherent process can be parametrized in terms of a *Rabi-like* frequency, as described in the previous section. For instance, in the case of two *isolated* spins, one in each QD, which are in resonance with $B_{\rm AC}$ ($\Delta_L=\Delta_R$), the oscillation frequency is: $\Omega_{\rm AC}=2B_{\rm AC}$, see (5.15). On the other hand, the inter-dot tunnelling events can be described by the resonance transitions between the states $|\uparrow,\downarrow\rangle$, $|\downarrow,\uparrow\rangle$ and $|S_{\rm R}\rangle$, whose populations oscillate with a frequency $\Omega_{\rm T}=2\sqrt{2}t_{\rm LR}$, see (5.18).

Let consider initially the ideal case where there is not spin relaxation or de-coherence in the system and $B_{\rm DC}$ is homogeneous, so that $\Delta_{\rm R}=\Delta_{\rm L}$ and both spins rotate simultaneously. Then, the dynamics of the system is properly described in terms of the dynamics of the total spin of the DQD. $B_{\rm AC}$ acts only on the states with a finite total magnetic moment: $|T_\pm\rangle$ and $|T_0\rangle=\frac{1}{\sqrt{2}}(|\uparrow,\downarrow\rangle+|\downarrow,\uparrow\rangle)$, while the inter-dot tunnelling, that does not change the spin, is only possible between $|S_{\rm R}\rangle$ and $|S_0\rangle=\frac{1}{\sqrt{2}}(|\uparrow,\downarrow\rangle-|\downarrow,\uparrow\rangle)$. Therefore, in the absence of spin relaxation, spin rotation and inter-dot hopping (essential for transport) are independent processes so any eventual singlet component will decay by tunnelling to the contacts. This produces a transient current that rapidly drops to zero for longer times. This process is independent of $B_{\rm AC}$, which is manifested in the frequency of the current oscillations, $\Omega_{\rm T}$, cf. Fig. 5.6a. Thus, for large enough times ($t\gg\Gamma_i^{-1}$), transport is cancelled and one electron will be confined in each QD. The electrons will be coherently trapped in the inter-dot triplet subspace, $T_\pm$, T_0 (dark subspace) and behave as an isolated single particle of angular momentum $S=1$ performing coherent spin rotations with a frequency $\Omega_{\rm AC}$ (Fig. 5.6b).

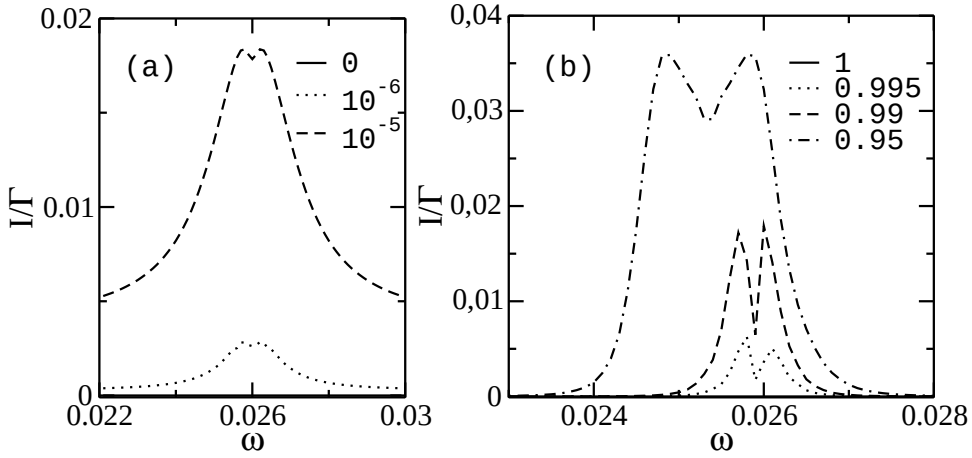

Fig. 5.7: Effect of (a) finite spin relaxation rates, T_1^{-1} and (b) the Zeeman inhomogenity, Δ_L/Δ_R, on the stationary current when tuning the frequency of the magnetic field. In (a), Δ_L/Δ_R; in (b), $T_1 = 0$. (Same parameters as in Fig. 5.6 but $\Gamma = 10^{-2}$meV).

A finite spin relaxation time mixes the dynamics of the singlet and the triplet subspaces[123], so that inter-dot tunnelling is allowed and finite current appears, cf. Fig. 5.7a. The shorter the spin relaxation time, the larger is the singlet-triplet mixing and therefore, the higher is the current, cf. Fig. 5.8a, up to relaxation times fast enough to dominate the electron dynamics ($T_1^{-1} \gg \Omega_{AC}$). In this case, ESR is not effective in order to rotate the spins and spin blockade is recovered, cf. Fig. 5.8b. Since both, spin rotations and spatial delocalization are resonant processes, this singlet-triplet mixing produces complicated dynamics in the current that shows oscillations with a frequency that depends both on the inter-dot coupling and the AC field intensity, cf. Fig. 5.8c. When B_{AC} increases, the frequency of the current oscillations increases but not linearly due to the interplay with the hopping. This effect is small for long spin relaxation times.

However, if one introduces an inhomogeneous B_{DC}, so that only one of the electrons is in resonance with B_{AC} (for instance, $\omega = \Delta_R \neq \Delta_L$), the total spin symmetry is broken and then the electron in each QD behaves differently. In fact, the states $|\downarrow,\uparrow\rangle$ and $|\uparrow,\downarrow\rangle$ have different occupation probabilities and inter-dot hopping induces the delocalization of the individual spins. This populates the state $|S_R\rangle$ and a finite current appears showing a double peak, cf. Fig. 5.7b, which can be the origing of the under-resolved structure measured in Ref. [95]. By tuning the Zeeman splittings difference, the current presents an anti-resonance of depth ~ 0.1nA near $\Delta_L = \Delta_R$, cf. Fig. 5.9a, pretty similar to the coherently trapped atom spectrum[102]. As expected, taking one electron slightly out of resonance, the frequency of the current oscillation is modified in comparison with the double resonance situation. If one electron is far enough from resonance, the frequency of the current oscillation becomes roughly half of the value as it would be the case for the rotation of one electron spin, cf. Fig. 5.9b. Otherwise, the off-resonant electron modifies the Rabi frequency for spin rotations in a more complicated way depending on B_{AC}, t_{LR} and how much both dynamics are mixed (which is related to $\Delta_L - \Delta_R$), cf. Fig. 5.9c. In the limiting case when Δ_L and Δ_R are very different and only the electron in the right QD is affected effectively by B_{AC}, the system performs coherent oscillations with a frequency $\Omega = \sqrt{B_{AC}^2 + 4t_{LR}^2}$ between the states $|T_+\rangle$, $|\uparrow,\downarrow\rangle$ and $|S_R\rangle$.

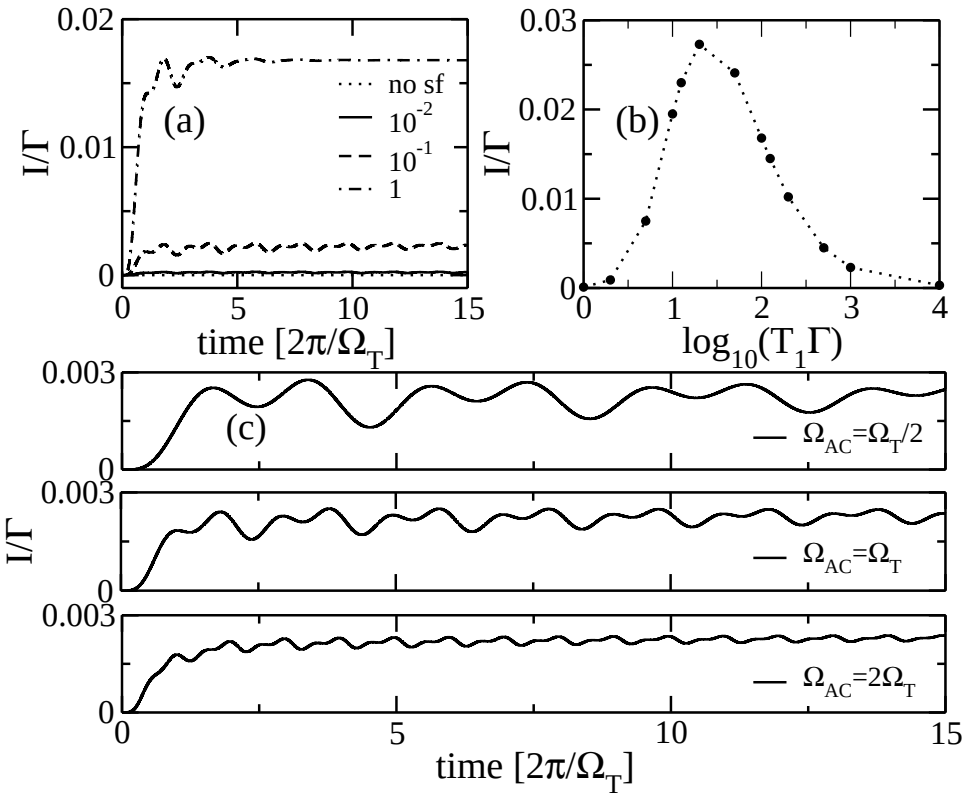

Fig. 5.8: (a) I(t) for different spin-flip times (in μs), with $\Omega_{\rm AC} = \Omega_{\rm T} = 11.2$GHz and $\Delta_{\rm L} = \Delta_{\rm R} = \Delta$). The initial state here is $|\uparrow,\uparrow\rangle$, then, for $T_1^{-1} = 0$, there is no mixing of the triplet and singlet subspaces and therefore, no current flows through the system. Spin relaxation processes contribute to populate the singlet, producing a finite current. (b) Stationary current as a function of spin relaxation time. For long T_1, electrons remain in the dark space. As T_1 decreases, I begins to flow, being again suppressed for short enough T_1, as discussed in the text. (c) I(t) for different ratios between the AC field intensity and the inter-dot hopping, i.e., between $\Omega_{\rm AC}$ and $\Omega_{\rm T}$, with $T_1 \sim 0.1\mu$s. (Same parameters as in Fig. 5.7).

5.3.1 Bichromatic magnetic field

There is a way for trapping the system in a dark state even for different Zeeman splittings by introducing a bichromatic $B_{\rm AC}$ with a different frequency that also brings into resonance the electron in the left QD:

$$\hat{H}_{\rm B}^{(2)}(t) = \sum_{i,j} [\Delta_i S_z^i + B_{\rm AC} \left(\cos\omega_j t S_x^i + \sin\omega_j t S_y^i\right)] \tag{5.23}$$

($i = \{{\rm L}, {\rm R}\}$, $j = \{1, 2\}$), with $\omega_1 = \Delta_{\rm L}$ and $\omega_2 = \Delta_{\rm R}$. Then, each electron is resonant with one of the field frequencies. In this case, as Δ_i is different in both QD's, $|T_0\rangle$ mixes with $|S_0\rangle$ and a finite current flows until the electrons fall in the superposition: $\frac{1}{\sqrt{2}}(|\uparrow,\uparrow\rangle - |\downarrow,\downarrow\rangle)$ which is not affected by $\hat{H}_{\rm B}^{(2)}$ but for off-resonant oscillations that can be averaged out. Then the population of the states $|\uparrow,\downarrow\rangle$, $|\downarrow,\uparrow\rangle$ and $|S_{\rm R}\rangle$ and, therefore, the current drop to zero, see Fig. 5.10a. This transport quenching also allows to operate the system as a *current switch* by tuning the frequencies of the AC fields (Fig. 5.10b) and the inicialization of the system in a concrete superposition to be manipulated.

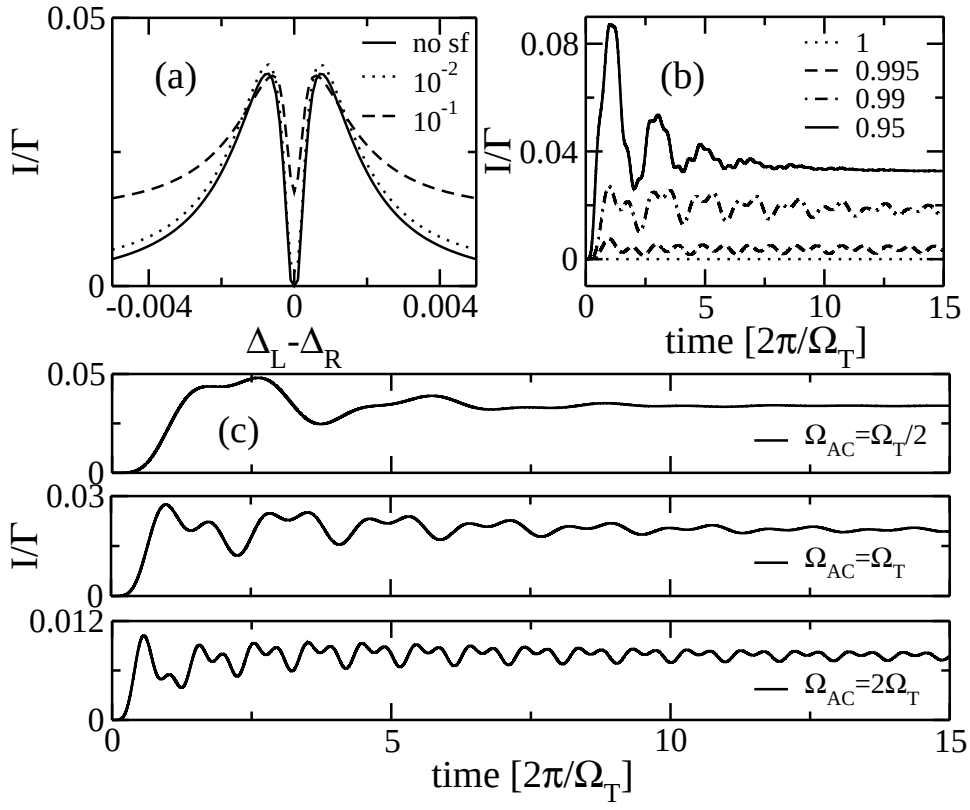

Fig. 5.9: (a) Dependence of the time averaged current on the DC field inhomogeneity $\Delta_L - \Delta_R$ for different relaxation times (in μs). The quenching of the current for $\Delta_L = \Delta_R$ is lifted by spin relaxation. (b) I(t) for different values of Δ_L/Δ_R when the electron in the right QD is kept in resonance, in the absence of relaxation. A crossover to the one electron spin resonance is observed by increasing the difference between Δ_L and $\Delta_R = \Delta$. (c) Dependence of the current oscillations on B_{AC} for $\Delta_L = 0.99\Delta_R$ and $T_1^{-1} \sim 0.1\mu$s. Same parameters as in Fig. 5.8.

The application of a bichromatic magnetic field provides a direct measurement of the Zeeman splittings of the dots by tuning the frequencies untill the current is brought to a minimum as in Fig. 5.10b. Then, by *switching* one of the frequencies off and tuning the Zeeman splitting by an additional B_{DC} in one of the dots, the antiresonance configuration of Fig. 5.9a could be achieved. In this case, electrons in both QD's perform coherent spin rotations, as shown in Fig. 5.6b.

5.4 Conclusions

In summary, the coherent electron spin dynamics in a DQD has been described, in the spin blockade regime, with up to two extra electrons, where crossed DC and AC magnetic fields are applied. The time dependent magnetic field produces coherent spin rotations between spin up and down states while resonant inter-dot hopping allows the spatial delocalization of the electrons.

The interplay between coherent oscillations coming from inter-dot tunnel and those due to B_{AC} gives rise to a non trivial electron dynamics which strongly depends on the ratio between the different

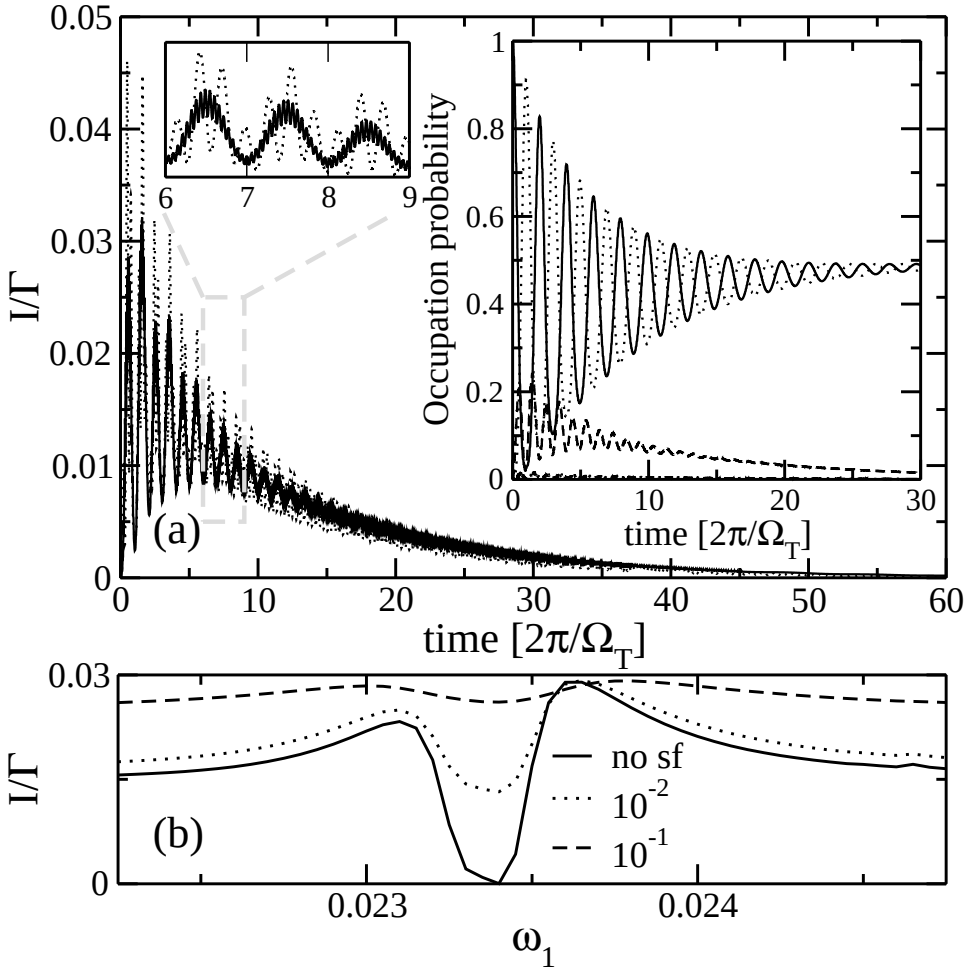

Fig. 5.10: (a) Transient current in the presence of a bichromatic B, when $\omega_{1(2)} = \Delta_{\mathrm{L(R)}}$ for: $\Delta_{\mathrm{L}} = \Delta_{\mathrm{R}}/2$ (solid) and $\Delta_{\mathrm{L}} = 0.9\Delta_{\mathrm{R}}$ (dotted) and T_1^{-1}=0. Left inset: detail of the current oscillation. In the case where $\Delta_{\mathrm{L}} = \Delta_{\mathrm{R}}/2$, I oscillates with Ω_{T} and it presents faster oscillations over-imposed (more important for $\Delta_{\mathrm{L}} = 0.9\Delta_{\mathrm{R}}$) coming from the effect of each frequency on its off-resonance electron. Right Inset: occupation probabilities for $\Delta_{\mathrm{L}} = \Delta_{\mathrm{R}}/2$: $|\uparrow,\uparrow\rangle$ (solid), $|\downarrow,\downarrow\rangle$ (dotted), $|\uparrow,\downarrow\rangle \sim |\downarrow,\uparrow\rangle$ (dashed) and $|0,\uparrow\downarrow\rangle$ (dash-dotted, remaining very close to zero). The occupation of $|0,\uparrow\downarrow\rangle$ drops to zero, and therefore, I drops as well. At long times the electrons fall in a coherent superposition of $|\uparrow,\uparrow\rangle$ and $|\downarrow,\downarrow\rangle$. b) Time-averaged current as a function of ω_1 when $\omega_2 = \Delta_{\mathrm{R}}$, for different relaxation rates, T_1^{-1}. I drops at $\omega_1 = \Delta_{\mathrm{L}}$. ($\Delta_{\mathrm{R}} = \Delta$, $\Gamma = 10^{-3}$meV, $\Omega_{\mathrm{T}} = 1.12$GHz).

Rabi frequencies involved. If the Zeeman splitting is the same for the left and the right QD, electrons remain performing coherent spin rotations in the $S = 1$ dark subspace and the current is quenched. This electron trapping is removed by spin relaxation or inhomogeneous B_{DC} and finite current flows.

Measuring the current will allow to control coherent spin rotations and also to extract information on the spin relaxation time. However, electron trapping is possible even when the Zeeman splittings are different by applying a bi-chromatic magnetic field such that each frequency matches the Zeeman splitting within one QD. Then, tunnelling spectroscopy experiments in DQD's under tunable mono- and

bi-chromatic magnetic fields allow to drive the electrons to perform coherent spin rotations which *can be unambiguously detected* by measuring the tunnelling current.

Chapter 6

Shot noise

All the results presented above concerned the electronic current through quantum dot systems, that is, the averaged time derivative of the number of electrons accumulated in the collector

$$I = -e\langle\dot{\hat{\mathcal{N}}}_{\mathrm{R}}\rangle = -e\langle[\hat{H},\hat{\mathcal{N}}_{\mathrm{R}}]\rangle = -tr\left(e[\hat{H},\hat{\mathcal{N}}_{\mathrm{R}}]\hat{\rho}\right), \tag{6.1}$$

as seen in chapter 2. However, there is a lot of information of the transport characteristics that is not contained in the average current but is provided by the study of its fluctuations $\Delta I(t) = I(t) - \langle I(t)\rangle$. In concrete, their correlation function

$$S(t,t') = \frac{1}{2}\langle\Delta I(t)\Delta I(t') + \Delta I(t')\Delta I(t)\rangle \tag{6.2}$$

defines the noise of the transport signal[25, 26]. Measurement of the noise allows to get information on the effective transferred charge[124, 33], its particle or wave nature[125] or entanglement[126].

Schottky predicted that the electronic current being ejected from a cathode in a vacuum tube showed some unavoidable fluctuations originated in the discreteness of the electronic charge–shot noise[127]. This seminal work states the referencial quantity for classical charge fluctuations

$$S_{Schottky} = 2e\langle I\rangle \tag{6.3}$$

typical for uncorrelated processes ocurring in time intervals that obey the Poisson distribution function $P(\Delta t) = \frac{1}{\tau}e^{-\frac{\Delta t}{\tau}}$, where τ is the mean time interval between two events[25]. Therefore, classical shot noise as the one studied by Schottky or, for intance, electrons tunneling incoherently through a biased quantum point contact is referred as *Poissonian*. In contrast, systems where correlations play a role as chaotic cavities[128] or quantum dots[174, 175] deviate from this value and their fluctuations are then said to have sub- or super-Poissonian character depending on whether their shot noise is higher or lower than $S_{Schottky}$, respectively.

These correaltions are strongly influenced by Pauli exclusion principle. Thus, in the absence of further interaction, one expects different fluctuations being the transferred particles fermions or bosons. For particles obeying the Fermi-Einstein statistics, the time interval between two events tends to be enhanced thus showing sub-Poissonian values[129]. On the other hand, bosonic bunching usually involves super-Poissonian fluctuations[130].

However, as will be discussed below, this is not always the case and one can find systems where bosonic fluctuations are sub-Poissonian, as a resonant fluorescent two level system[154], see chapter 8,

or fermions are transferred in bunches, as an entanglement interferometer[126] or capacitively coupled several channel conductors[161].

In this chapter, the current and noise charateristics of quantum dot system will be analyzed, with a particular attention to AC driven double quantum dots.

6.1 Master equation

As seen in chapter 2, the non-equilibrium dynamics of a quantum dot system can be described by means of the equation of motion for the reduced density matrix elements., ρ, which can be written in Liouville space[131, 132] as

$$\dot{\rho} = -\frac{i}{\hbar}[H, \rho] = \mathcal{L}\rho, \tag{6.4}$$

where $\mathcal{L}$ is the Liouvillian superoperator acting on the density operator, ρ. When evaluating this equation on the eigenbasis of the system, one recovers the master equation (2.55) and (2.56) in matricial form: $\dot{\rho}_i = \mathcal{M}_{ij}\rho_j$, where the vector ρ_j contains all the diagonal and non-diagonal elements of the density matrix.

In the same way, one can define the current superoperators, $\mathcal{J}_\pm$, that acting on the reduced density operator give the positive and negative contributions of the current. Thus, (2.81) can be formuled as the trace of the current operator[133, 134]

$$I = tr(\mathcal{J}\rho) = tr((\mathcal{J}_+ - \mathcal{J}_-)\rho). \tag{6.5}$$

Note that the trace over the system states can be considered as a vector $v_0^\dagger$ in Liouvillian space with properties

$$v_0^\dagger \rho = 1, \tag{6.6}$$

from the normalization condition of the density matrix, and

$$v_0^\dagger \mathcal{L} = 0 \tag{6.7}$$

from the derivative $0 = tr\dot{\rho} = v_0^\dagger \mathcal{L}\rho$. In matricial form, it is expressed as (10...010...01), where the the elements corresponding to populations in ρ_i are 1, while the ones corresponding to the coherences are 0. Then, the current can be written as $I = v_0^\dagger \mathcal{J}\rho$.

It is convenient to include explicitely the current operators in the master equation, which is easily done by separating those terms that do not change the number of particles in the collector

$$\dot{\rho}(t) = \mathcal{L}\rho(t) = (\mathcal{L}_0 + J_+ + J_-)\,\rho(t). \tag{6.8}$$

In a quantum dot system, the superoperator $\mathcal{L}_0$ is responsible for the internal dynamics and the tunneling through the emitter barrier.

The shot noise can be written in terms of the accumulated charge in the collector $\mathcal{R}$, $Q_{\mathrm{R}}(t) = e\,(N_{\mathrm{R}}(t) - N_{\mathrm{R}}(t_0)) = \int dt' I(t')$

$$\frac{d}{dt}\left(\langle Q_{\mathrm{R}}^2(t)\rangle - \langle Q_{\mathrm{R}}(t)\rangle^2\right) = S(t) \tag{6.9}$$

directly related with the MacDonnald formula[170] that describes shot noise by the correlations $\langle N_{\mathrm{R}}\rangle$ and $\langle N_{\mathrm{R}}^2\rangle$. Based on this, one can obtain the higher order moments of the fluctuations by evaluating the moments $\langle N_{\mathrm{R}}^\alpha\rangle$ that define the statistics of the electronic transference–*full counting statistics*. This

technique was originally developed for the detection of photons emitted from an atomic source[145, 148, 166] and recently adapted to electronic transport through mesoscopic conductors[150, 151].

One can define the operator

$$G(z,t) = tr_{\mathrm{R}}\left(z^{N_{\mathrm{R}}}\chi(t)\right) \tag{6.10}$$

that generalizes the density operator, which is recovered when evaluating $G(1,t) = tr_{\mathrm{R}}\chi(t) = \rho(t)$, and satisfies the derivatives

$$g^{(\alpha)}(t) = \left(z\frac{\partial}{\partial z}\right)^{\alpha}_{z=1} G(z,t) = tr_{\mathrm{R}}\left(N_{\mathrm{R}}^{\alpha}\chi(t)\right). \tag{6.11}$$

Note that $g^{(0)}(t) = g(t) = \rho(t)$.

The equations of motion for $G(z,t)$ are easily obtained from the N-particles resolved master equation, as done in section 2.4 (for a derivation of the master equation in this formalism, see Ref. [21])

$$\dot{\rho}(t) = tr_{\mathrm{R}}\dot{\chi}(t) = \sum_{N}\left(\mathcal{L}_0\chi_N + \mathcal{J}_+\chi_{N-1} + \mathcal{J}_-\chi_{N+1}\right) \tag{6.12}$$

and therefore

$$\begin{aligned}\dot{G}(z,t) &= tr_{\mathrm{R}}\left(z^N\dot{\chi}\right) = tr_{\mathrm{R}}\left(z^N\left(\mathcal{L}_0\chi_N + \mathcal{J}_+\chi_{N-1} + \mathcal{J}_-\chi_{N+1}\right)\right) \\ &= tr_{\mathrm{R}}\left(\mathcal{L}_0\chi_N z^N + z\mathcal{J}_+\chi_{N-1}z^{N-1} + \mathcal{J}_-\chi_{N+1}z^{N+1}\right).\end{aligned} \tag{6.13}$$

By adding $\mathcal{J}_+\chi_{N-1}z^{N-1} - \mathcal{J}_+\chi_{N-1}z^{N-1}$ and a corresponding one for $\mathcal{J}_-$, one gets

$$\dot{G}(z,t) = \left(\mathcal{L} + (z-1)\mathcal{J}_+ + \left(z^{-1}-1\right)\mathcal{J}_-\right)G(z,t) \tag{6.14}$$

which together with

$$\langle N^{\alpha}\rangle = v_0^{\dagger}\left(z\frac{\partial}{\partial z}\right)^{\alpha}_{z=1} G(z,t) \tag{6.15}$$

up to second order will provide the current and shot noise by:

$$\frac{d}{dt}\langle N\rangle = v_0^{\dagger}\left(z\frac{\partial}{\partial z}\right)_{z=1}\left(\mathcal{L} + (z-1)\mathcal{J}_+ + \left(z^{-1}-1\right)\mathcal{J}_-\right)G(z,t) = v_0^{\dagger}\left(\mathcal{J}_+ - \mathcal{J}_-\right)\rho(t) \tag{6.16}$$

and

$$\begin{aligned}\frac{d}{dt}\langle N^2\rangle &= v_0^{\dagger}\left(z\frac{\partial}{\partial z}\right)^2_{z=1}\left(\mathcal{L} + (z-1)\mathcal{J}_+ + \left(z^{-1}-1\right)\mathcal{J}_-\right)G(z,t) \\ &= v_0^{\dagger}\left(\left(\mathcal{J}_+ + \mathcal{J}_-\right)\rho(t) + 2\left(\mathcal{J}_+ - \mathcal{J}_-\right)g^{(1)}(t)\right),\end{aligned} \tag{6.17}$$

where (6.14), (6.15) and (6.7) were used.

The equations of motion for the different moment generators, $g^{(\alpha)}$, can be derived from (6.14). The zeroth order one coincides with the master equation when evaluated in $z = 1$:

$$\dot{g}(t) = \dot{\rho}(t) = \mathcal{L}\rho(t). \tag{6.18}$$

At first order, one gets

$$\dot{g}'(t) = \left(z\frac{\partial}{\partial z}\right)_{z=1}\dot{G}(z,t) = \mathcal{L}g'(t) + (\mathcal{J}_+ - \mathcal{J}_-)\rho(t), \tag{6.19}$$

and similarly for higher orders[134].

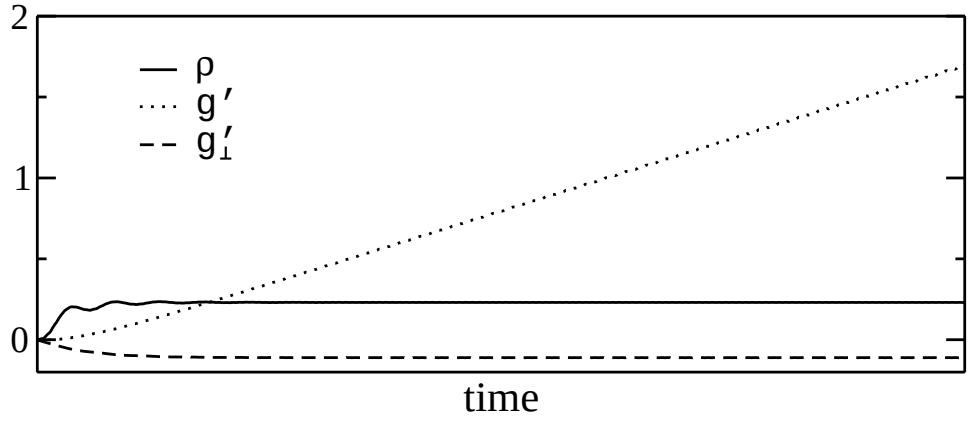

Fig. 6.1: Time dependence of one element of the density matrix, ρ, the moment generator, g' and its proyection out of the Liouvillian null space, $g'_\perp = (1 - \rho_\infty v_0^\dagger) g'$.

6.1.1 Stationary solution

For long times, the system evolves to a stationary state given by

$$\mathcal{L}\rho_\infty = 0. \tag{6.20}$$

The stationary solution is related with the zero eigenvalue of the Liouvillian superoperator. Therefore, the normalization condition $v_0^\dagger \rho_\infty = 1$ is required. By introducing it in (6.21) one obtains

$$\dot{g}'(t) = \mathcal{L}g'(t) + (\mathcal{J}_+ - \mathcal{J}_-)\rho_\infty. \tag{6.21}$$

The null eigenvalue of $\mathcal{L}$ involves a solution with a component linear in time that can be separated by the projector to the nullspace, $\rho_\infty v_0^\dagger$:

$$g'(t) = \rho_\infty v_0^\dagger (\mathcal{J}_+ - \mathcal{J}_-)\rho_\infty t + g'_\perp(t), \tag{6.22}$$

cf. Fig. 6.1. The orthogonal component, $g'_\perp(t)$, converges for long times and, as will be shown, is the only that will contribute to the noise. Introducing (6.22) into (6.21), one has

$$\rho_\infty v_0^\dagger (\mathcal{J}_+ - \mathcal{J}_-)\rho_\infty = \mathcal{L}g'_\perp(\infty) + (\mathcal{J}_+ - \mathcal{J}_-)\rho_\infty. \tag{6.23}$$

Therefore,

$$\mathcal{L}g'_\perp(\infty) = \left(\rho_\infty v_0^\dagger - 1\right)(\mathcal{J}_+ - \mathcal{J}_-)\rho_\infty, \tag{6.24}$$

with the orthogonality condition $v_0^\dagger g'_\perp(\infty) = 0$.

Known ρ_∞ and $g'_\perp(\infty)$, one obtains the stationary current

$$I = -e\frac{d}{dt}\langle N\rangle = -etr(\mathcal{J}_+ - \mathcal{J}_-)\rho_\infty \tag{6.25}$$

and the zero frequency shot noise

$$S = e^2\left(\frac{d}{dt}\langle N^2\rangle - 2\langle N\rangle\frac{d}{dt}\langle N\rangle\right) = e^2 tr\left((\mathcal{J}_+ - \mathcal{J}_-)g'_\perp(\infty) + (\mathcal{J}_+ + \mathcal{J}_-)\rho_\infty\right). \tag{6.26}$$

The ratio between them defines the Fano factor

$$F = \frac{S}{e|I|} \tag{6.27}$$

and the sub- or super-Poissonian character of the noise if $F < 1$ or $F > 1$, respectively. For instance, one finds that Poissonian processes satisfy $tr\mathcal{J}_+ g'(\infty) = tr\mathcal{J}_- g'(\infty)$.

Alternatively, one can solve the problem numerically by integrating simultaneously (6.18) and (6.21) until $g'_\perp(t)$ converges, see Fig. 6.1.

This method is valid for AC driven systems provided that one considered the averaged $\bar{I}$ and $\bar{S}$ over one period of the field[135].

6.2 Single resonant level in a quantum dot–Sub-Poissonian shot noise

The most simple case one can consider is a single quantum dot with one level in the high bias and Coulomb blockade regime, i.e. electrons are transferred one by one due to high Coulomb repulsion inside the quantum dot. The master equation then is reduced to

$$\begin{pmatrix} \dot{\rho}_{00} \\ \dot{\rho}_{11} \end{pmatrix} = \begin{pmatrix} -\Gamma_{10} & \Gamma_{01} \\ \Gamma_{10} & -\Gamma_{01} \end{pmatrix} \begin{pmatrix} \rho_{00} \\ \rho_{11} \end{pmatrix}, \tag{6.28}$$

where $|0\rangle$ and $|1\rangle$ are the states without and with one extra electron in the system. The current operators are

$$\mathcal{J}_+ = \begin{pmatrix} 0 & \Gamma_{01} \\ 0 & 0 \end{pmatrix} \tag{6.29}$$

and $\mathcal{J}_- = 0$, since no electron can tunnel from the collector to the system. Then, one can easily calculate the stationary current

$$I = \frac{\Gamma_{01}\Gamma_{10}}{\Gamma_{01} + \Gamma_{10}} \tag{6.30}$$

and the shot noise[175]

$$S = \frac{\Gamma_{01}\Gamma_{10}\left(\Gamma_{01}^2 + \Gamma_{10}^2\right)}{(\Gamma_{01} + \Gamma_{10})^3}. \tag{6.31}$$

This gives a reduction of the shot noise

$$F = 1 - \frac{2\Gamma_{01}\Gamma_{10}}{(\Gamma_{01} + \Gamma_{10})^2} \tag{6.32}$$

compared to the single barrier case. For intance, if both barriers ar equal, $\Gamma_{01} = \Gamma_{10} = \Gamma$, the Fano factor becomes exactly $F = \frac{1}{2}$. Coulomb repulsion is the responsible for the introduction of a time scale of the order $\Gamma^{-}1$ between two tunneling events, thus reducing the fluctuations in the time separation between them.

6.3 Shot noise in double quantum dots

Let consider a two level system consisting on a double quantum dot quantum dot (DQD) connected in series to two electron reservoirs which can be described by the Hamiltonian:

$$\hat{H} = \hat{H}_0 + \hat{H}_{\mathrm{LR}} + \hat{H}_{\mathrm{T}}, \tag{6.33}$$

where $\hat{H}_0 = \varepsilon_{\rm L}\hat{c}_{\rm L}^\dagger\hat{c}_{\rm L} + \varepsilon_{\rm R}\hat{c}_{\rm R}^\dagger\hat{c}_{\rm R} + U\hat{n}_{\rm L}\hat{n}_{\rm R}$ describes the uncoupled DQD plus leads system. The inter-dot coupling is: $\hat{H}_{\rm LR} = t_{\rm LR}\hat{c}_{\rm L}^\dagger\hat{c}_{\rm R} + \text{H.c.}$ while the coupling to the leads, $\hat{H}_{\rm T} = \sum_{l\epsilon\{\rm L,R\}k}(\gamma_l\hat{d}_{lk}^\dagger\hat{c}_l + \text{H.c.})$, is considered weak and treated perturbatively, similarly to what was done in section 2.6. Considering infinite *on site* Coulomb repulsion, so double occupancy is avoided in a single quantum dot, spin does not play any role and one can consider spinless electrons.

The stationary current through such systems was already studied in chapter 2.

6.3.1 Up to one electron: $U \to \infty$.

The high Coulomb repulsion does not allow a second electron to enter the DQD when it already contains one. The basis is then reduced to: $|0\rangle$, $|L\rangle$ and $|R\rangle$. In the high bias regime[142], the master equation can be written in matricial form, $\dot{\rho}_i = \mathcal{M}_{ij}\rho_j$ as:

$$\begin{pmatrix} \dot{\rho}_{00} \\ \dot{\rho}_{\rm LL} \\ \dot{\rho}_{\rm LR} \\ \dot{\rho}_{\rm RL} \\ \dot{\rho}_{\rm RR} \end{pmatrix} = \begin{pmatrix} -\Gamma_{\rm L0} & 0 & 0 & 0 & \Gamma_{0\rm R} \\ \Gamma_{\rm L0} & 0 & it_{\rm LR} & -it_{\rm LR} & 0 \\ 0 & it_{\rm LR} & i\varepsilon - \frac{\Gamma_{0\rm R}}{2} & 0 & -it_{\rm LR} \\ 0 & -it_{\rm LR} & -i\varepsilon - \frac{\Gamma_{0\rm R}}{2} & 0 & it_{\rm LR} \\ 0 & 0 & -it_{\rm LR} & it_{\rm LR} & -\Gamma_{0\rm R} \end{pmatrix} \begin{pmatrix} \rho_{00} \\ \rho_{\rm LL} \\ \rho_{\rm LR} \\ \rho_{\rm RL} \\ \rho_{\rm RR} \end{pmatrix}. \tag{6.34}$$

A similar one can be written for (6.21) by wrtting the current operators as

$$\mathcal{J}_+ = \begin{pmatrix} 0 & 0 & 0 & 0 & \Gamma_{0\rm R} \\ 0 & 0 & 0 & 0 & 0 \\ 0 & 0 & 0 & 0 & 0 \\ 0 & 0 & 0 & 0 & 0 \\ 0 & 0 & 0 & 0 & 0 \end{pmatrix} \tag{6.35}$$

and $\mathcal{J}_- = 0$.

Thus, from the stationary solution, $\mathcal{L}\rho_\infty = 0$, the current and shot noise are given by

$$I = \frac{4t_{\rm LR}^2\Gamma_{\rm L}\Gamma_{\rm R}}{4\Gamma_{\rm R}t_{\rm LR}^2 + \Gamma_{\rm L}\left(4\varepsilon^2 + 8t_{\rm LR}^2 + \Gamma_{\rm R}^2\right)} \tag{6.36}$$

$$S = \frac{4t_{\rm LR}^2\Gamma_{\rm L}\Gamma_{\rm R}\left(16\Gamma_{\rm R}^2t_{\rm LR}^4 + \Gamma_{\rm L}^2\left(\Gamma_{\rm R}^4 + 8(\varepsilon^2 - t_{\rm LR}^2)\Gamma_{\rm R}^2 + 16\left(\varepsilon^4 + 6t_{\rm LR}^2\varepsilon^2 + 4t_{\rm LR}^4\right)\right)\right)}{\left(4\Gamma_{\rm R}t_{\rm LR}^2 + \Gamma_{\rm L}\left(4\varepsilon^2 + 8t_{\rm LR}^2 + \Gamma_{\rm R}^2\right)\right)^3}, \tag{6.37}$$

resulting in a sub-Poissonian Fano factor at resonance[33]

$$F = 1 - \frac{8t_{\rm LR}^2\Gamma_{\rm L}\left(\Gamma_{\rm R}\left(8t_{\rm LR}^2 + \Gamma_{\rm R}^2\right) + 3\Gamma_{\rm L}\Gamma_{\rm R}^2 + 4\varepsilon^2\left(\Gamma_{\rm R} - \Gamma_{\rm L}\right)\right)}{\left(4t_{\rm LR}^2(2\Gamma_{\rm L} + \Gamma_{\rm R}) + \Gamma_{\rm L}\left(4\varepsilon^2 + \Gamma_{\rm R}^2\right)\right)^2}, \tag{6.38}$$

cf. Fig. 6.2. Note that the shot noise shows a small deep at the resonance condition. It can be interpreted in terms of the scattering theory that describes current by a transmition coefficient, T, and shot noise by $T(1-T)$[25]. At resonance, the transmition is maximal, so $1-T$ is minimal.

Also, as will be the studied below, the noise may be super-Poissonian out of resonance in an asymmetrically coupled DQD if $\Gamma_{\rm L} > \Gamma_{\rm R}$[136, 138] for $\varepsilon^2 > \frac{\Gamma_{\rm R}\left(8t_{\rm LR}^2+\Gamma_{\rm R}^2\right)+3\Gamma_{\rm L}\Gamma_{\rm R}^2}{4(\Gamma_{\rm L}-\Gamma_{\rm R})}$.

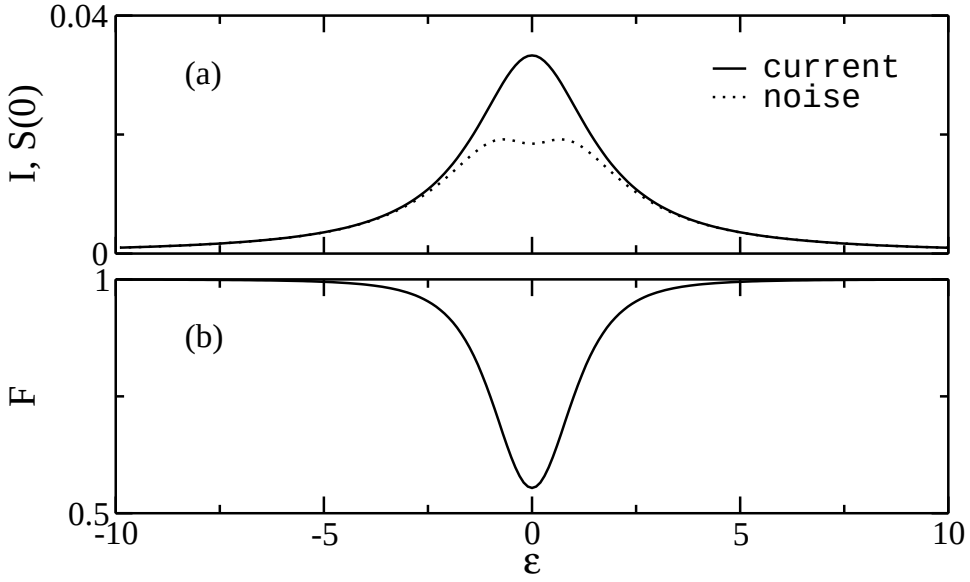

Fig. 6.2: (a) Current, shot noise and (b) Fano factor as a function of the difference of the level energies: $\varepsilon = \varepsilon_L - \varepsilon_R$ for $U \to \infty$, $\Delta = 1$, $\Gamma = 0.1$ and $k_B T = 10^{-3}$.

6.3.2 Up to two electrons: $U = 0$.

In the limiting case when the Coulomb repulsion is negligible between electrons in different dots, the system can be populated by two electrons simultaneously and thus described by the basis: $|0\rangle$, $|L\rangle$, $|R\rangle$ and $|2\rangle$. In the high bias and low temperature regime, the master equation is:

$$\begin{pmatrix} \dot{\rho}_{00} \\ \dot{\rho}_{\mathrm{LL}} \\ \dot{\rho}_{\mathrm{LR}} \\ \dot{\rho}_{\mathrm{RL}} \\ \dot{\rho}_{\mathrm{RR}} \\ \dot{\rho}_{22} \end{pmatrix} = \begin{pmatrix} -\Gamma_{\mathrm{L0}} & 0 & 0 & 0 & \Gamma_{\mathrm{0R}} & 0 \\ \Gamma_{\mathrm{L0}} & 0 & it_{\mathrm{LR}} & -it_{\mathrm{LR}} & 0 & \Gamma_{\mathrm{L2}} \\ 0 & it_{\mathrm{LR}} & i\varepsilon - \frac{\Gamma_{\mathrm{0R}}+\Gamma_{\mathrm{2R}}}{2} & 0 & -it_{\mathrm{LR}} & 0 \\ 0 & -it_{\mathrm{LR}} & -i\varepsilon - \frac{\Gamma_{\mathrm{0R}}+\Gamma_{\mathrm{2R}}}{2} & 0 & it_{\mathrm{LR}} & 0 \\ 0 & 0 & -it_{\mathrm{LR}} & it_{\mathrm{LR}} & -(\Gamma_{\mathrm{0R}}+\Gamma_{\mathrm{2R}}) & 0 \\ 0 & 0 & 0 & 0 & \Gamma_{\mathrm{2R}} & -\Gamma_{\mathrm{L2}} \end{pmatrix} \begin{pmatrix} \rho_{00} \\ \rho_{\mathrm{LL}} \\ \rho_{\mathrm{LR}} \\ \rho_{\mathrm{RL}} \\ \rho_{\mathrm{RR}} \end{pmatrix}. \quad (6.39)$$

Again, transport is unidirectional, so $\mathcal{J}_- = 0$ and

$$\mathcal{J}_+ = \begin{pmatrix} 0 & 0 & 0 & 0 & \Gamma_{\mathrm{0R}} & 0 \\ 0 & 0 & 0 & 0 & 0 & \Gamma_{\mathrm{L2}} \\ 0 & 0 & 0 & 0 & 0 & 0 \\ 0 & 0 & 0 & 0 & 0 & 0 \\ 0 & 0 & 0 & 0 & 0 & 0 \\ 0 & 0 & 0 & 0 & 0 & 0 \end{pmatrix} \quad (6.40)$$

In the same way as in the previous case, one obtains the current

$$I = \frac{8t_{\mathrm{LR}}^2 \Gamma_R}{16t_{\mathrm{LR}}^2 + (\Gamma_{\mathrm{L}} + \Gamma_{\mathrm{R}})^2 + 4\varepsilon^2} \quad (6.41)$$

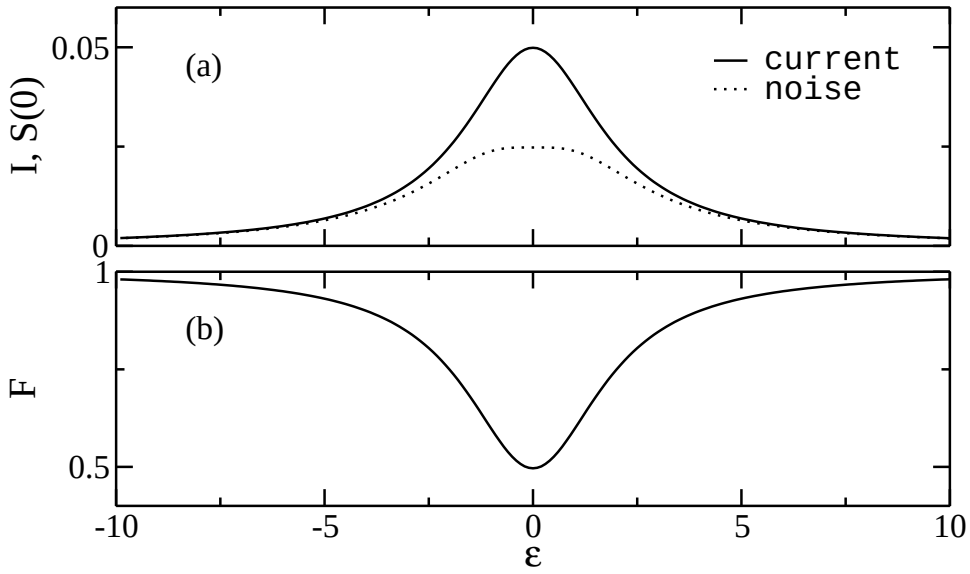

Fig. 6.3: (a) Current, shot noise and (b) Fano factor as a function of the difference of the level energies: $\varepsilon = \varepsilon_L - \varepsilon_R$ for $U = 0$, $\Delta = 1$, $\Gamma = 0.1$ and $k_B T = 10^{-3}$.

and the shot noise in resonance ($\varepsilon = 0$)

$$S = \frac{8t_{\mathrm{LR}}^2\Gamma_{\mathrm{R}}\left(64\left(3\Gamma_{\mathrm{L}}-\Gamma_{\mathrm{R}}\right)t_{\mathrm{LR}}^4+8\left(\Gamma_{\mathrm{L}}+\Gamma_{\mathrm{R}}\right)\left(3\Gamma_{\mathrm{L}}^2-4\Gamma_{\mathrm{R}}\Gamma_{\mathrm{L}}-\Gamma_{\mathrm{R}}^2\right)t_{\mathrm{LR}}^2+\Gamma_{\mathrm{L}}\left(\Gamma_{\mathrm{L}}+\Gamma_{\mathrm{R}}\right)^4\right)}{\Gamma_{\mathrm{L}}\left(16t_{\mathrm{LR}}^2+\left(\Gamma_{\mathrm{L}}+\Gamma_{\mathrm{R}}\right)^2\right)^3}, \tag{6.42}$$

giving a Fano factor

$$F = 1 - \frac{8t_{\mathrm{LR}}^2\left(\Gamma_{\mathrm{L}}+\Gamma_{\mathrm{R}}\right)\left(8t_{\mathrm{LR}}^2+\Gamma_{\mathrm{L}}^2+\Gamma_{\mathrm{R}}^2+8\Gamma_{\mathrm{L}}\Gamma_{\mathrm{R}}\right)}{\Gamma_{\mathrm{L}}\left(16t_{\mathrm{LR}}^2+\left(\Gamma_{\mathrm{L}}+\Gamma_{\mathrm{R}}\right)^2\right)^2}, \tag{6.43}$$

see Fig. 6.3. As a difference to the upt to one electron case seen previously, the Fano factor when two electrons can occupy simultaneously the DQD is always sub-Poissonian. This may be due to coherence destroying when the second electron enters the system[136].

6.4 Double quantum dot pumps

One can consider driven systems and numerically integrate (6.18) and (6.21) until the stationary solution is reached, as described in section 6.1.1. However, it is also possible to obtain analytical results for simple systems as the charge pump studied in chapter 3. If the levels of the double quantum dot considered in the previous section are coupled to unbiased leads, with chemical potential, μ, and $\varepsilon_{\mathrm{L}} < \mu < \varepsilon_{\mathrm{R}}$, finite current flows if an AC potential is applied shuch that its frequency, ω, matches the energy difference $\varepsilon_{\mathrm{R}} - \varepsilon_{\mathrm{L}}$, cf. section 3.4. Also, it has been shown that the noise of such a system reaches a minimum at resonance (where the current shows a peak)[137]. In the rotating wave approximation one disregards the contribution of all the off-resonance harmonics of the field, being possible to write the master equation

as

$$\begin{pmatrix} \dot{\rho}_{00} \\ \dot{\rho}_{\rm LL} \\ \dot{\rho}_{\rm LR} \\ \dot{\rho}_{\rm RL} \\ \dot{\rho}_{\rm RR} \end{pmatrix} = \begin{pmatrix} -\left(\Gamma_{\rm L0}+\Gamma_{\rm R0}\right) & \Gamma_{\rm 0L} & 0 & 0 & \Gamma_{\rm 0R} \\ \Gamma_{\rm L0} & -\Gamma_{\rm 0L} & i\frac{\Omega_1}{2} & -i\frac{\Omega_1}{2} & 0 \\ 0 & i\frac{\Omega_1}{2} & i(\varepsilon-\omega)-\frac{\Gamma_{\rm 0R}}{2} & 0 & -i\frac{\Omega_1}{2} \\ 0 & -i\frac{\Omega_1}{2} & -i(\varepsilon-\omega)-\frac{\Gamma_{\rm 0R}}{2} & 0 & i\frac{\Omega_1}{2} \\ \Gamma_{\rm R0} & 0 & -i\frac{\Omega_1}{2} & i\frac{\Omega_1}{2} & -\Gamma_{\rm 0R} \end{pmatrix} \begin{pmatrix} \rho_{00} \\ \rho_{\rm LL} \\ \rho_{\rm LR} \\ \rho_{\rm RL} \\ \rho_{\rm RR} \end{pmatrix}, \tag{6.44}$$

where $\Omega_1 = 2J_1\left(\frac{V_{\rm AC}}{\omega}\right)t_{\rm LR}$ is the Rabi frequency (3.49) of the delocalization of an electron within the DQD by the absoption of one photon from the field. The tunneling rates are modified by the action of the AC field

$$\Gamma_{\rm 0L} = \frac{\pi}{\hbar}\left(1+J_0^2\left(\frac{V_{\rm AC}}{2\hbar\omega}\right)\right)|\gamma_{\rm L}|^2 \tag{6.45}$$

$$\Gamma_{\rm L0} = \frac{\pi}{\hbar}\left(1-J_0^2\left(\frac{V_{\rm AC}}{2\hbar\omega}\right)\right)|\gamma_{\rm L}|^2 \tag{6.46}$$

$$\Gamma_{\rm 0R} = \frac{\pi}{\hbar}\left(1-J_0^2\left(\frac{V_{\rm AC}}{2\hbar\omega}\right)\right)|\gamma_{\rm R}|^2 \tag{6.47}$$

$$\Gamma_{\rm R0} = \frac{\pi}{\hbar}\left(1+J_0^2\left(\frac{V_{\rm AC}}{2\hbar\omega}\right)\right)|\gamma_{\rm R}|^2, \tag{6.48}$$

Photon-assited tunneling allows electrons tunneling *backwards* from the right dot, so the current operators are

$$\mathcal{J}_+ = \begin{pmatrix} 0 & 0 & 0 & 0 & \Gamma_{\rm 0R} \\ 0 & 0 & 0 & 0 & 0 \\ 0 & 0 & 0 & 0 & 0 \\ 0 & 0 & 0 & 0 & 0 \\ 0 & 0 & 0 & 0 & 0 \end{pmatrix} \quad \text{and} \quad \mathcal{J}_- = \begin{pmatrix} 0 & 0 & 0 & 0 & 0 \\ 0 & 0 & 0 & 0 & 0 \\ 0 & 0 & 0 & 0 & 0 \\ 0 & 0 & 0 & 0 & 0 \\ \Gamma_{\rm R0} & 0 & 0 & 0 & 0 \end{pmatrix}. \tag{6.49}$$

In the simpler case, where the strength of both couplings to the leads are the same, $\Gamma_{\rm L0} = \Gamma_{\rm 0R} = \Gamma_+$ and $\Gamma_{\rm 0L} = \Gamma_{\rm R0} = \Gamma_-$, one can parametrize the system by the tunneling rate, Γ, $\alpha = J_0^2\left(\frac{V_{\rm AC}}{2\hbar\omega}\right)$ and $\beta = J_1\left(\frac{V_{\rm AC}}{\hbar\omega}\right)$ such that $\frac{\Gamma}{2} = \frac{\Gamma_+}{1-\alpha} = \frac{\Gamma_-}{1+\alpha}$. Then the stationary current results

$$I = \frac{4\alpha^2\beta^2\Gamma t_{\rm LR}^2}{\left(\alpha^4+3\right)\Gamma^2 + 12\beta^2 t_{\rm LR}^2} \tag{6.50}$$

and the shot noise

$$S = \frac{2\beta^2\Gamma t_{\rm LR}^2\left(\left(\alpha^4+1\right)\left(\alpha^4+3\right)^2\Gamma^4 - 8\left(\alpha^8+16\alpha^4-9\right)\beta^2 t_{\rm LR}^2\Gamma^2 + 16\left(\alpha^4+9\right)\beta^4 t_{\rm LR}^4\right)}{\left(\left(\alpha^4+3\right)\Gamma^2 + 12\beta^2 t_{\rm LR}^2\right)^3}. \tag{6.51}$$

As can be seen in Fig. 6.5, Fano factor

$$F = \frac{\left(\alpha^4+1\right)\left(\alpha^4+3\right)^2\Gamma^4 - 8\left(\alpha^8+16\alpha^4-9\right)\beta^2 t_{\rm LR}^2\Gamma^2 + 16\left(\alpha^4+9\right)\beta^4 t_{\rm LR}^4}{2\left(\alpha\left(\alpha^4+3\right)\Gamma^2 + 12\alpha\beta^2 t_{\rm LR}^2\right)^2} \tag{6.52}$$

can be tuned from sub- to super-Poissonian values when increasing the AC intensity. As discussed in chapter 3, when the Bessel function of first order (that modulates interdot tunneling) vanishes, $\beta = 0$, the

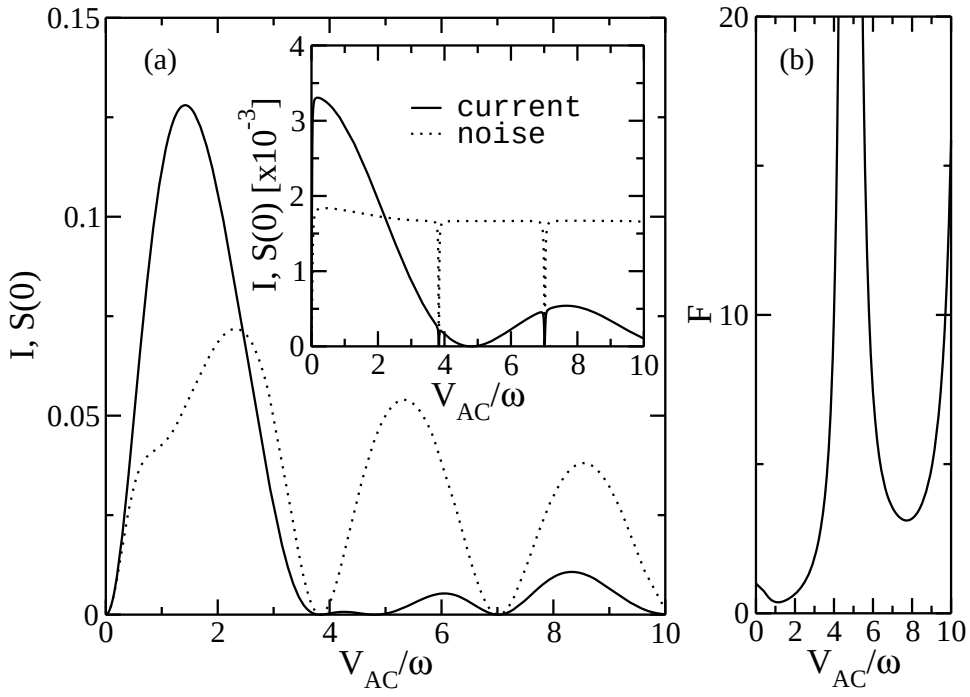

Fig. 6.4: (a) Current, shot noise and (b) Fano factor as a function of AC intensity for a double quantum dot pump: $\omega = \varepsilon_L - \varepsilon_R$ for $U \to \infty$, $t_{\rm LR} = 1$ and $\Gamma = 1$. Inset of panel (a): current and shot noise in the same configuration but $\Gamma = 0.01$.

current is cancelled by dynamical charge localization, but the noise is not, since photon-assisted tunneling induce charge fluctuations without contributng to the net current. Then, at those points, within this approximation[1], the Fano factor diverges.

Additionaly, since $J_0(x)$ goes to zero when $x \to \infty$, the currents flowing in opposite directions are asymptotically cancelled, though tunneling is not supressed. Thus, the net current vanishes but shot noise is kept finite. Therefore, the Fano factor increases asymptotically with $V_{\rm AC}$.

Interestingly, when the coupling to the leads is small compared to the interdot barrier, $\Gamma \ll t_{\rm LR}$, the dependence of the current on the AC intensity is given exclusively by the Bessel function of zeroth order, $I \sim \frac{1}{3}\alpha^3\Gamma$, except for those intensities that satisfy the dynamical charge localization condition, $\beta = 0$, where it is rapidly supressed, cf. instet in Fig. 6.5. Additionally, the shot noise is roughly constant at high AC intensities, $S \sim \frac{\alpha^4+9}{54}\Gamma$, when $\beta \neq 0$. Then, the Fabno factor increases with the intensity of tha AC field as $F \sim \frac{1}{2\alpha^2} + \frac{\alpha^2}{18}$

6.5 Shot noise in spin pumps

The spin pump device discussed in chapter 4 presents similar characteristics to the single electron pump seen in the previous section. In the absence of photon-assisted tunneling inthe contact barriers, the

[1]The current will not vanish completely at dynamical charge localization due to the contribution of out of resonance subharmonics, disregarded in the rotating wave approximation.

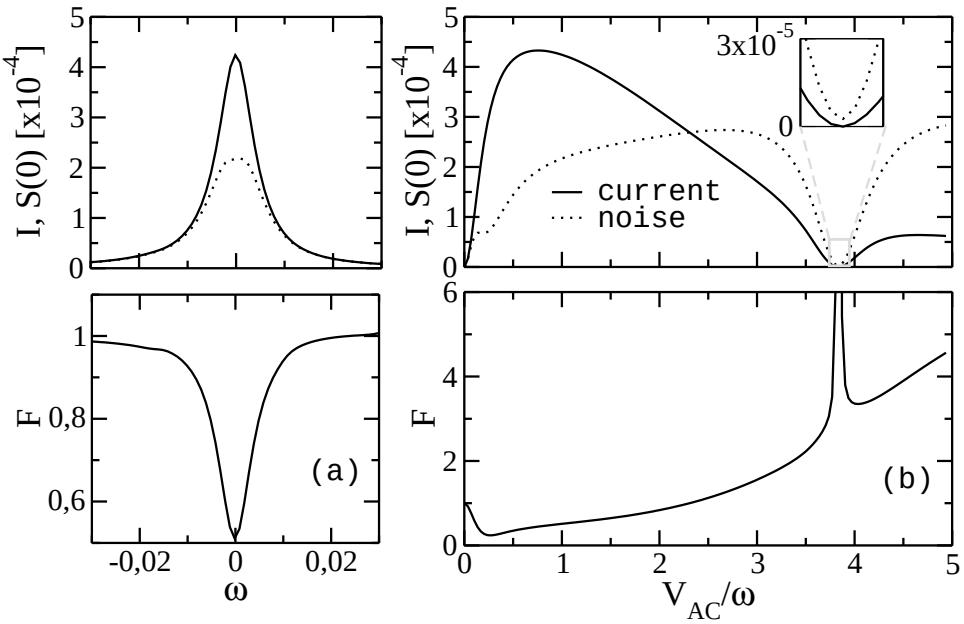

Fig. 6.5: Current, shot noise and Fano factor dependence on (a) the frequency and (b) the intensity of the AC field in the spin pumping configuration (see chapter 4). Parameters (in meV): $\varepsilon_L = \varepsilon_R = 0.5$, $\Delta_z = 0.026$ (corresponding to a magnetic field $B_z \sim 1T$), $U_L = 1$, $U_R = 1.3$, $\mu = 1.81$, $t_{\rm LR} = 0.005$, $\Gamma = 0.001$. For these parameters, the current is mostly spin-down polarized[90].

electrons with spin up remain in ther sites and only the spin-down electrons are transferred from the left lead to the right one[63] through the singlet states of each dot, thus producing fully spin-down polarized current. It was shown how photon absorption modified the tunneling across the leads reducing the spin polarization of the current[90].

The system is modeled by the Hamiltonian $\hat{H} = \hat{H}_{\rm L} + \hat{H}_{\rm R} + \hat{H}_{\rm LR} + \hat{H}_{\rm leads} + \hat{H}_{\rm T} + \hat{H}_{\rm AC}(t)$, where each dot is represented by $\hat{H}_{j=\{L,R\}} = \sum_\sigma \varepsilon_{j\sigma}\hat{n}_{j\sigma} + U_j\hat{n}_{j\uparrow}\hat{n}_{j\downarrow}$ and the reservoirs: $\hat{H}_{\rm leads} = \sum_{l\epsilon\{\rm L,R\}k\sigma} \varepsilon_{lk}\hat{d}^\dagger_{lk\sigma}\hat{d}_{lk\sigma}$. The energies $\varepsilon_{j\sigma}$ include the Zeeman splitting Δ_j stemming from the interaction with a magnetic fiel which breaks the spin degeneracy, such that the spin-up state becomes the ground state. Thus, $\varepsilon_{j\downarrow} = \varepsilon_{j\uparrow} + \Delta_j$. The QDs are weakly connected between them and to the leads through tunneling barriers: $\hat{H}_{\rm LR} = -t_{\rm LR}\sum_\sigma \hat{c}^\dagger_{{\rm L}\sigma}\hat{c}_{{\rm R}\sigma} + h.c.$ and $\hat{H}_{\rm T} = \sum_{l\epsilon\{\rm L,R\}k\sigma}(\gamma\hat{d}^\dagger_{lk\sigma}\hat{c}_{l\sigma} + h.c.)$. As in previous sections, the external AC field is introduced as an oscillation with different phase in the gate voltages of the dots ($\hbar = e = 1$): $\hat{H}_{\rm AC}(t) = \frac{1}{2}V_{\rm AC}\sum_\sigma(\hat{n}_{L\sigma} - \hat{n}_{R\sigma})\cos\omega t$. For instance, when the frequency of the AC field matches the energy difference between the states $|\uparrow\downarrow,\uparrow\rangle$ and $|\uparrow,\uparrow\downarrow\rangle$, the spin down electron is delocalized by the interaction with *one* photon and the interdot hopping strongly depends on the Bessel function of *first* order.

One can derivate the master equation for the densty matrix

$$\dot{\rho}(t) = \mathcal{L}(t)\rho(t), \tag{6.53}$$

as done for (4.9) in chapter 4 and, similarly write the equations of motion for the moment generator

$$\dot{g}'(t) = \mathcal{L}(t)g'(t) + \mathcal{J}_+ - \mathcal{J}_-\rho(t), \tag{6.54}$$

where the current superoperators can b defined as

$$\mathcal{J}_{\pm}\rho = \sum_{m'm} \Gamma_{m'm}\rho_{mm}\delta_{N^{\rm R}_m, N^{\rm R}_{m'}\pm 1}|m'\rangle\langle m'|, \tag{6.55}$$

with the tunneling rates (4.29).

Then, one integrates numerically the equations of motion (4.9) and (7.6) extracting the convergent component of $g'(t)$ until the stationary solution is reached. As expected, the current shows a resonance peak when the frequency of the AC field matches the frequency $\omega = \omega_0 = (\omega^2_{\rm RL} + 4t^2_{RL})^{1/2}$, where $\omega_{\rm RL}$ is the energy difference between the states $|\uparrow,\uparrow\downarrow\rangle$ and $|\uparrow\downarrow,\uparrow\rangle$, while the shot noise is reduced with respect to the Poissonian statistics (for which $S = I$) typical for resonant tunneling processes[25], cf. Fig. 6.5a, following roughly the same behaviour shown in the previous section for a single electron being pumped through an empty double quantum dot.

Most interesting is the dependence of the current and shot noise on the AC amplitude, because the photon absorption rate strongly depends on the field intensity and, eventually, one no longer finds an ideal spin pump behaviour [90]. Moreover, the dependence of the renormalized interdot tunneling on the Bessel function of first order, leads to dynamical localization [49, 26] in the DQD that supresses the current, as shown in Fig. 6.5b. On the other hand, photon-assisted tunneling through the right contact is not supressed. This enhances the fluctuations of the electron number in the right lead with the consequence that the shot noise becomes larger while the net pump current remains low. Consequently, the Fano factor reaches huge values.

Additionally, as the AC intensity increases, the contribution of electrons tunneling from right to left reduces the net current–until it asymptotically vanishes– while the shot noise remains roughly unaffected–tunneling events still hold. Thus, one observes super-Possonain noise characterized by $S > I$[139] and an increasing Fano factor.

6.6 Spin blockade in AC driven double quantum dots

In section 4.4.3, it was discussed how Pauli exclusion principle blocks the current through double quantum dots with up to two electrons (one in each dot) when they have the same spin polarization and how this effect is removed by photon-assisted tunneling in AC driven system when one of the electrons is extracted to the collector and another one with opposite polarization occupies its site.

Then, current only flows in the short (compared to the time that the system remains blocked) periods of time when the two electrons have the same polarization. This means that electrons are transferred in bunches separated by lapses of time when no current is detected and the shot noise is super-Poissonian. This kind of dynamics are similar to dynamical channel blockade, which will be discussed in chapters 7 and 8, where tunneling through a conducting channel is supressed by the occupation of a trapped that is capacitively coupled to it. Here, two channels are not needed and Coulomb repulsion is replaced by spin interaction.

Let consider a double quantum dot in a slightly different configuration as that treated in section 4.4.3, though still in the pumping regime, $\mu_{\rm L} = \mu_{\rm R} = \mu$[2]. The single occupation states of both dots are below the chemical potential of the leads: $\mu > \varepsilon_l$ but the doubly occupied singlets $|\uparrow\downarrow\rangle_l$ are well above it, $U_l + \varepsilon_l > \mu$, so any of the two electrons can be extracted, independently of their spin.

[2]In the high bias regime, where photon-assisted tunneling is minimized in the leads, no essential differences with the undriven case would appear–except for dynamical charge localization– and the system would be asymptotically trapped in a superposition of the states $|\uparrow,\uparrow\rangle$ and $|\downarrow,\downarrow\rangle$.

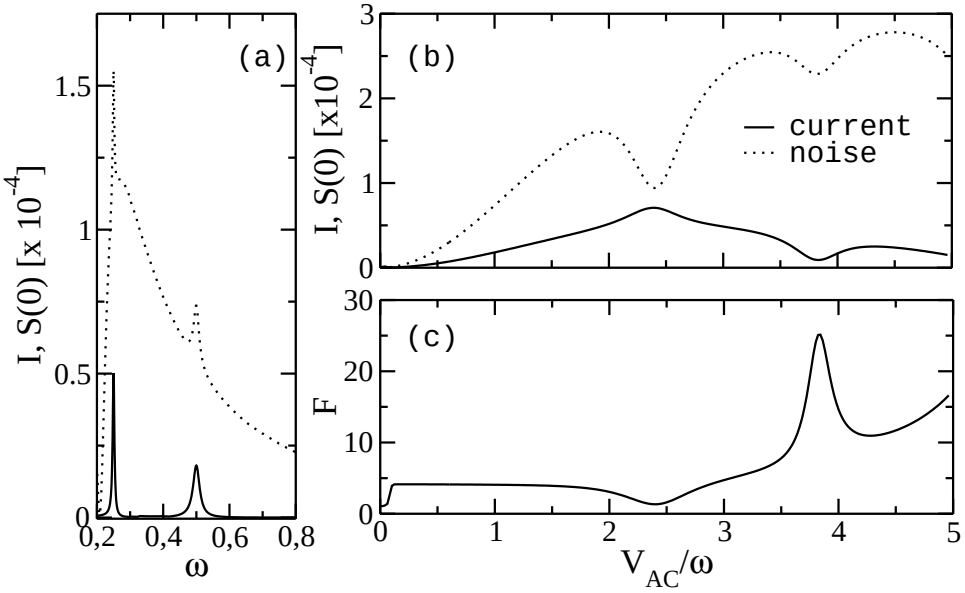

Fig. 6.6: (a) Current, shot noise and (b) Fano factor dependence on the intensity of the AC field in the spin blockade configuration. Parameters (in meV): $\varepsilon_L = \varepsilon_R = 0.5$, $\Delta_z = 0.026$ (corresponding to a magnetic field $B_z \sim 1T$), $U_L = 3$, $U_R = 1$, $V = 0.5$, $\mu = 1.2$, $t_{\rm LR} = 0.005$, $\Gamma = 0.001$.

An AC field is applied with a frequency tuned to match the energy separation between the states $|0, \uparrow\downarrow\rangle = |0, S_{\rm R}\rangle$ and $|\uparrow, \downarrow\rangle$, i.e., $\omega = \varepsilon_{\rm R} - \varepsilon_{\rm L} + U_{\rm R} - U_{\rm LR}$, where ε_l is the energy of the single occupied states and $U_{\rm R}$ $U_{\rm LR}$ are the Coulomb repulsion between electrons in the right dot and in different dots, respectively. A magnetic field is applied as in the spin pump device, so the electrons with spin down polarization are shifted by an energy Δ_l. In such a configuration, the spin up electron is delocalized within the DQD until one of the electrons tunnels out to the right lead. If the Zeeman splitting is the same in both dots, the spin down electron can also be delocalized at the same frequency between $|0, S_{\rm R}\rangle$ and $|\downarrow, \uparrow\rangle$. Then, current will flow until an electron enters the DQD being occupied by an electron of the same polarization, so the system is in one of the states $|\uparrow, \uparrow\rangle$ or $|\downarrow, \downarrow\rangle$ and interdot hopping is forbidden by Pauli exclusion principle[94, 93]. If the chemical potentials related to the extraction of any electron from these states, $\mu - \varepsilon_l - U_{\rm LR} > 0$, the system is trapped until one of them is extracted by photon-assisted tunneling.

As can be seen in Fig. 6.6a, current peaks appear when the frequency of the AC field is resonant with the energies $\omega = (\varepsilon_{\rm R} - \varepsilon_{\rm L} + U_{\rm R} - U_{\rm LR})/n$. As expected, the noise is super-Poissonian.

The dependence of the transport characteristics on the AC intensity is however more interesting, cf. Fig. 6.6b and c. The initial absence of transport at $V_{\rm AC} = 0$ is lifted when increasing the intensity so both current and noise grow roughly linearly. Then, the Fano factor rapidly reaches a *plateau* near $F = 4$. This situation changes when the AC intensity approches the value that makes $J_1\left(\frac{V_{\rm AC}}{\omega}\right)$ reach a maximum. Then, interdot hopping is most effective, so current is maximal and shot noise is reduced showing a pronunced deep. As discussed above for the spin pump configuration, further increasing of the AC intensity reduces the net current by making the tunneling rates of processes contributing to the current from right to left approach asymptotically those corresponding to electrons going from left to right. This does not affect the shot noise, so the Fano factor begins to increase. Particularly, when

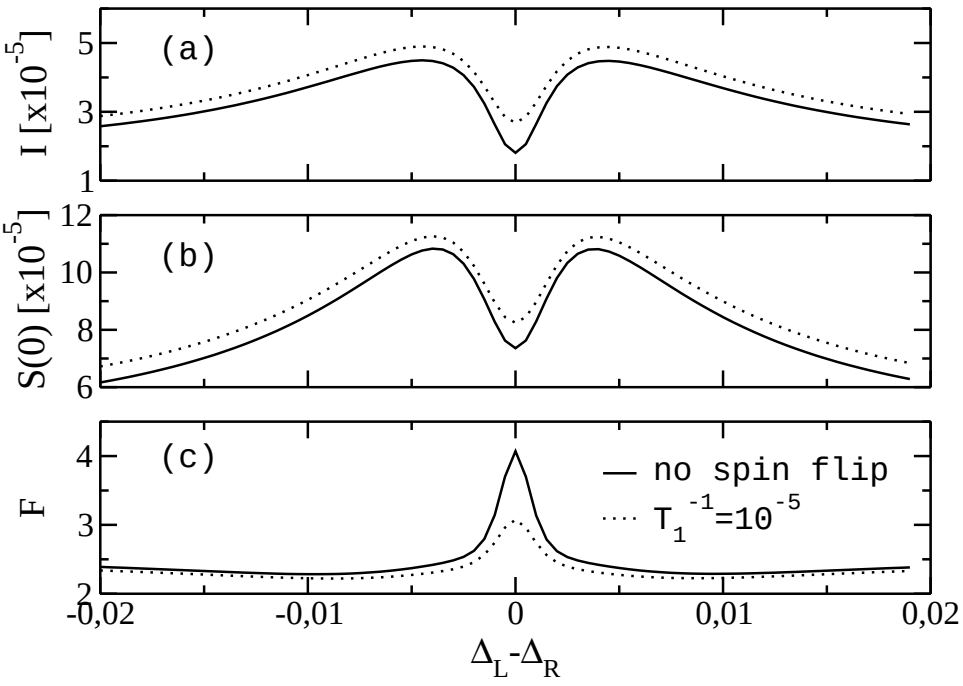

Fig. 6.7: (a) Current, (b) shot noise and (c) Fano factor dependence on the magnetic field inhomogenity in the spin blockade configuration, with and without the consideration of spin flip processes. The frequency of the AC field matches the energy difference between the states $|0,\uparrow\downarrow\rangle$ and $|\uparrow,\downarrow\rangle$. Parameters (in meV): $\varepsilon_L = \varepsilon_R = 0.5$, $\Delta_{\rm R} = 0.026$ (corresponding to a magnetic field $B_z \sim 1T$), $U_L = 3$, $U_R = 1$, $V = 0.5$, $\mu = 1.2$, $t_{\rm LR} = 0.005$, $\Gamma = 0.001$, $V_{\rm AC} = \omega$, $T_2^{-1} = 10T_1^{-1}$.

$J_1\left(\frac{V_{\rm AC}}{\omega}\right) = 0$, the interdot tunneling processes that are assited by one photon are supressed, the current is minimal as well as the shot noise. At this intensity, the Fano factor reaches a peak of around $F = 25$.

Another factor important for spin blockade is the difference between the Zeeman splittings, as also discused in chapter 5. It can be due to an inhomogeneous magnetic field, different g factors in each dot or the presence of hyperfine interaction[87, 88] which may also induce spin relaxation processes. If $\Delta_{\rm L} = \Delta_{\rm R}$, the states $|\uparrow,\downarrow\rangle$ and $|\downarrow,\uparrow\rangle$ are indistinguible, so interdot singlet $|S_0\rangle = \frac{1}{\sqrt{2}}(|\uparrow,\downarrow\rangle - |\downarrow,\uparrow\rangle)$ and triplet $|T_0\rangle = \frac{1}{\sqrt{2}}(|\uparrow,\downarrow\rangle + |\downarrow,\uparrow\rangle)$ states appear in the dynamics. Interdot tunneling does not change the total spin, so it can only occur between the singlet states $|S_0\rangle$ and $|0,S_{\rm R}\rangle$. Then, not only $|\uparrow,\uparrow\rangle$ and $|\downarrow,\downarrow\rangle$ contribute to the transport blocking, but also $|T_0\rangle$.

On the other hand, if $\Delta_{\rm L} \neq \Delta_{\rm R}$, $|T_0\rangle$ and $|S_0\rangle$ are mixed, so the current increases, cf. Fig. 6.7. If the difference between Zeeman splittings is high enough, only the electrons of one of the spin polarizations (in this case the spin-up ones) can tunnel resonantly, so current decreases again.

Also spin flip processes and decoherence contribute to the current enhancement by increasing the lifetime of the trapped states. The decreasing of the ratio between the trapped and conducting lapses of time is reflected in a reduction of the Fano factor, cf. Fig. 6.7.

6.7 Conclusions

A method for computing the zero frequency shot noise of AC driven systems is presented, allowing the analytical evaluation of the stationary properties of transport and an easy method for numerical calculations.

The shot noise characteristics has been studied for several double quantum dot configurations, complementing the ones presented in previous chapters. They include the undriven case in the Coulomb blockade regime, allowing one and two electrons in the system. Sub-Poissonian shot noise is found for this cases except for asymmetric contacts in the vicinity of resonance.

The effect of photon-assisted tunneling has been studied by introducing a resonant AC field in the unbiased configuration–*pumping* regime. The shot noise can be manipulated by means of the AC intensity, being possible to tune it back and forth between sub- and super-Poissonian values. For high AC intensities, the net current is asymptoticaly cancelled while tunneling events still hold, resulting in finite shot noise and a increasing Fano factor. Additionally, huge Fano factors are predicted at dynamical charge localization. The same behaviour appears in the spin pump device studied in chapter 4.

Spin dependent super-Poissonian shot noise has been studied in the spin blockade regime, where current is limited to the short lapses of time when the incoming electrons form an interdot singlet. All the triplet superpositions block the system. The effect of different parameters as the inhomogeneous Zeeman field or finite spin-flip times have been analyzed.

Chapter 7

Electron Bunching in Stacks of Coupled Quantum Dots

The aim of controlling and manipulating nanoscale devices requires good knowledge of the processes involved in the electronic transport through open quantum systems. The increasing success in accessing single electron states in semiconductor quantum dots and the unavoidable presence of lattice vibrations in such devices obliges one to consider dissipation caused by electron-phonon interaction [184, 185, 164]. The study of the electronic current fluctuations provides further information about the system [25, 26]. E.g., from the investigation of shot noise—a consequence of the charge discreteness—we know about deviations from Poissonian statistics indicating correlations between tunneling events.

A particular example for Poissonian statistics is the electron transport through a point contact, for which all tunneling events are statistically independent. For resonant tunneling through single quantum dots, this is no longer the case: As long as an electron populates the quantum dot, no further electron can enter and, consequently, tunneling events are anti-bunched[175], see section 6.2. However, when several of such transport channels conduct in parallel and are coupled capacitively, the current noise becomes super-Poissonian, as has been demonstrated experimentally [161, 162, 187]. This means that electrons tend to be transferred in bunches, which at first sight is counter-intuitive if one thinks in terms of the Pauli exclusion principle. The phenomenon can be understood in terms of Coulomb interactions between electrons in different channels, so that an electron in one channel suppresses the transport through the other [182, 183, 186, 140], and one observes *dynamical channel blockade*. Consequently the electron transport through one dot occurs in bunches during lapses of time when the other dots are empty.

In a recent experiment [188] with transport channels that consist of double quantum dots (see Fig. 7.1), intriguing noise properties have been observed: By slightly modifying the source-drain voltage, the levels of a double quantum dot can be tuned across a resonance which yields a current peak at whose center, the noise is sub-Poissonian. In the vicinity of such resonances, by contrast, the noise is super-Poissonian such that the Fano factor assumes values up to 1.5. This structure becomes washed out with increasing temperature, indicating the suspension of DCB by the interaction with substrate phonons. In this chapter, it is shown that a model with a single transport channel qualitatively reproduces this behavior. For a quantitative agreement with the experimentally observed Fano factor and temperature dependence, however, the capacitive coupling to a second, almost identical channel is found to be essential.

Let start out by modelling a single transport channel of the setup sketched in Fig. 7.1, which was analyzed (in the absence of phonons) in section 6.3. The double quantum dot coupled to fermionic

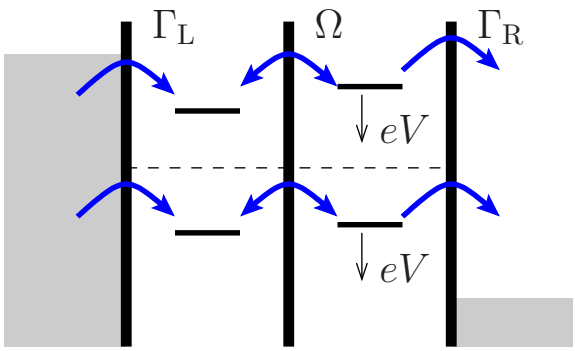

Fig. 7.1: Sketch of the transport through two parallel double quantum dots measured in Ref. [188]. Both transport channels are capacitively coupled. The source-drain voltage shifts the relative position of the levels by eV, albeit it is so large that all levels lie within the voltage window.

leads and substrate phonons is described by the Hamiltonian [141, 136]

$$H = H_0 + H_\mathrm{leads} + H_T + H_\mathrm{e-ph} + H_\mathrm{ph}, \tag{7.1}$$

where $H_0 = \sum_{l=\mathrm{L,R}} \varepsilon_l n_l + U n_\mathrm{L} n_\mathrm{R} - \Omega(c_\mathrm{L}^\dagger c_\mathrm{R} + c_\mathrm{R}^\dagger c_\mathrm{L})/2$ describes the coherent dynamics inside the double dot and n_l denotes the population of dot $l = \mathrm{L,R}$. Henceforth it will be assumed that the Coulomb repulsion U is so strong that only the zero-electron state $|0\rangle$ and the states with one electron in the left or the right dot, $|\mathrm{L}\rangle$ and $|\mathrm{R}\rangle$, play a role. The leads and the phonons are described by $H_\mathrm{leads} = \sum_{l,k} \varepsilon_{lk} n_{lk}$ and $H_\mathrm{ph} = \sum_\nu \hbar\omega_\nu a_\nu^\dagger a_\nu$, respectively, where n_{lk} is the electron number in state k in lead l and a_ν is the annihilation operator of the νth phonon mode. The interaction with the double dot is given by the tunneling Hamiltonian $H_T = \sum_{l,k} (\gamma_l d_{lk}^\dagger c_l + \mathrm{h.c.})$ and the electron-phonon coupling $H_\mathrm{e-ph} = \sum_\nu (n_L - n_R)\lambda_\nu (a_\nu^\dagger + a_\nu)$[185]. By tracing out the leads and the bath within a Born-Markov approximation, one obtains for the reduced density matrix the equation of motion

$$\dot\rho = \mathcal{L}\rho = (\mathcal{L}_0 + \mathcal{L}_T + \mathcal{L}_\mathrm{e-ph})\,\rho. \tag{7.2}$$

Introducing for the density matrix the vector notation $\rho = (\rho_{00}, \rho_\mathrm{LL}, \rho_\mathrm{LR}, \rho_\mathrm{RL}, \rho_\mathrm{RR})^T$, the Liouvillian reads

$$\mathcal{L} = \frac{1}{\hbar}\begin{pmatrix} -\Gamma_\mathrm{L} & 0 & 0 & 0 & \Gamma_\mathrm{R} \\ \Gamma_\mathrm{L} & 0 & -\frac{i}{2}\Omega & \frac{i}{2}\Omega & 0 \\ 0 & -\frac{i}{2}\Omega + A_+ & i\delta - B & 0 & \frac{i}{2}\Omega - A_- \\ 0 & \frac{i}{2}\Omega + A_+ & 0 & -i\delta - B & -\frac{i}{2}\Omega - A_- \\ 0 & 0 & \frac{i}{2}\Omega & -\frac{i}{2}\Omega & -\Gamma_\mathrm{R} \end{pmatrix}, \tag{7.3}$$

where the detuning $\delta = \varepsilon_\mathrm{R} - \varepsilon_\mathrm{L} - eV$ depends on the source-drain voltage (or on the gate voltages in lateral quantum dots) and $E^2 = \delta^2 + \Omega^2$. For the phonons, one can assume an Ohmic spectral density $J(\omega) = \pi \sum_\nu \lambda_\nu^2 \delta(\omega - \omega_\nu) = 2\pi\alpha\omega$ [184], so that their influence is determined by the coefficients

$$A_\pm = 2\pi\alpha\Omega \pm 2\pi\alpha\delta\Omega\Big(\frac{2k_BT}{E^2} - \frac{1}{E}\coth\frac{E}{2k_BT}\Big), \tag{7.4}$$

$$B = 4\pi\alpha\Big(\frac{2\delta^2 k_BT}{E^2} + \frac{\Omega^2}{E}\coth\frac{E}{2k_BT}\Big) + \gamma, \tag{7.5}$$

where $\gamma = \Gamma_R/2$ stems from the additional decoherence associated with the tunneling to the leads. In consistency with the experiment of Ref. [188], the voltage is asumed to be so large that the Fermi level of the left (right) lead is well above (below) the energy of the left (right) dot level. Therefore it is sufficient to consider only unidirectional transport from the left lead to the right lead described by the effective tunneling rates Γ_l which are proportional to $|\gamma_l|^2$ [142].

Within the same approximation, one can derive for the current, defined as the time derivative of the charge in the right lead, the expression $I = e\mathrm{tr}_{\mathrm{sys}}[(\mathcal{J}_+ - \mathcal{J}_-)\rho_0]$, where ρ_0 denotes the stationary solution of the master equation (7.2) and $\mathcal{J}_\pm$ are the superoperators describing the tunneling of an electron from the right dot to the right lead and back, respectively. For unidirectional transport, they read $\mathcal{J}_- = 0$ and $\mathcal{J}_+\rho = (\Gamma_R/\hbar)\rho_{RR}|0\rangle\langle 0|$.

The noise will be characterized by the variance of the transported net charge which at long times grows linear in time, $\langle \Delta Q_R^2 \rangle = St$. For its computation, one introduces the operator $\mathrm{tr}_{\mathrm{leads+ph}}(N_R\rho_{\mathrm{total}})$ [143, 134], see chapter 6, which resembles the reduced density operator and obeys

$$\dot{g}'(t) = \mathcal{L}g'(t) + (\mathcal{J}_+ - \mathcal{J}_-)\,\rho(t). \tag{7.6}$$

As discussed in the previous chapter, g' has a divergent component which is proportional to ρ_∞ and does not contribute to the zero-frequency noise S. Thus, S is fully determined by the traceless part $g'_\perp = g'_0 - \rho_\infty \mathrm{tr}g'$. In terms of ρ_∞ and $g'_\perp$, the zero-frequency noise reads [134]

$$S = e^2\mathrm{tr}_{\mathrm{sys}}[2(\mathcal{J}_+ - \mathcal{J}_-)g'_\perp + (\mathcal{J}_+ + \mathcal{J}_-)\rho_\infty]. \tag{7.7}$$

A proper dimensionless measure for the noise is the Fano factor $F = S/eI$ which equals unity for a Poisson process, while a larger value reflects electron bunching.

7.1 Transport through a single channel

Let first consider the simplest case, consisting in a double quantum dot, similar to that studied in section 6.3.2 in the absence of dissipation. Figure 7.2a shows the differential conductance and the current for various temperatures as a function of the internal bias. In contrast to the dissipationless case ($\alpha = 0$) [142, 41], the shape of the curve is no longer Lorentzian but exhibits an asymmetry. At higher temperatures, the peak becomes broader and more symmetric. This behavior is also reflected by the noise. In the absence of dissipation, the Fano factor deviates from the Poissonian value $F = 1$: For $\Gamma_L > \Gamma_R$ (as in the experiment) and $\alpha = 0$, we observe an anti-resonant behavior with a dip ($F \approx 0.5$), which is accompanied by two maxima with values slightly above 1. This double peak structure does not appear if $\Gamma_L \leq \Gamma_R$. With increasing dissipation strength α and increasing temperature, the maxima vanish and the Fano factor eventually tends to the Poissonian value $F = 1$.

Although this behavior resembles the experimental findings reported in Ref. [188], there are significant quantitative differences. For the maximal peak value of the Fano factor, which is assumed in the dissipationless limit $\alpha \to 0$ for $\delta = \Omega/\sqrt{2}$, we find the analytic expression

$$F_p(\alpha = 0) = 1 + \frac{\Omega^2\,(\Gamma_L - \Gamma_R)^2}{2\Omega^2(\Gamma_L\Gamma_R + 2\Gamma_L^2 - \Gamma_R^2) + 8\Gamma_L^2\Gamma_R^2}. \tag{7.8}$$

It implies $F_p \leq 5/4$, with the maximum assumed for $\Gamma_R \ll \Gamma_L, \Omega$. This means that for a single channel, the theoretical prediction for the maximal Fano factor is clearly smaller than the value observed in the experiment even at finite temperature and in the presence of dissipation [188]; cf. inset in Fig. 7.2b. Therefore one must conclude that the one-channel model does not fully capture the experimentally observed shot noise enhancement.

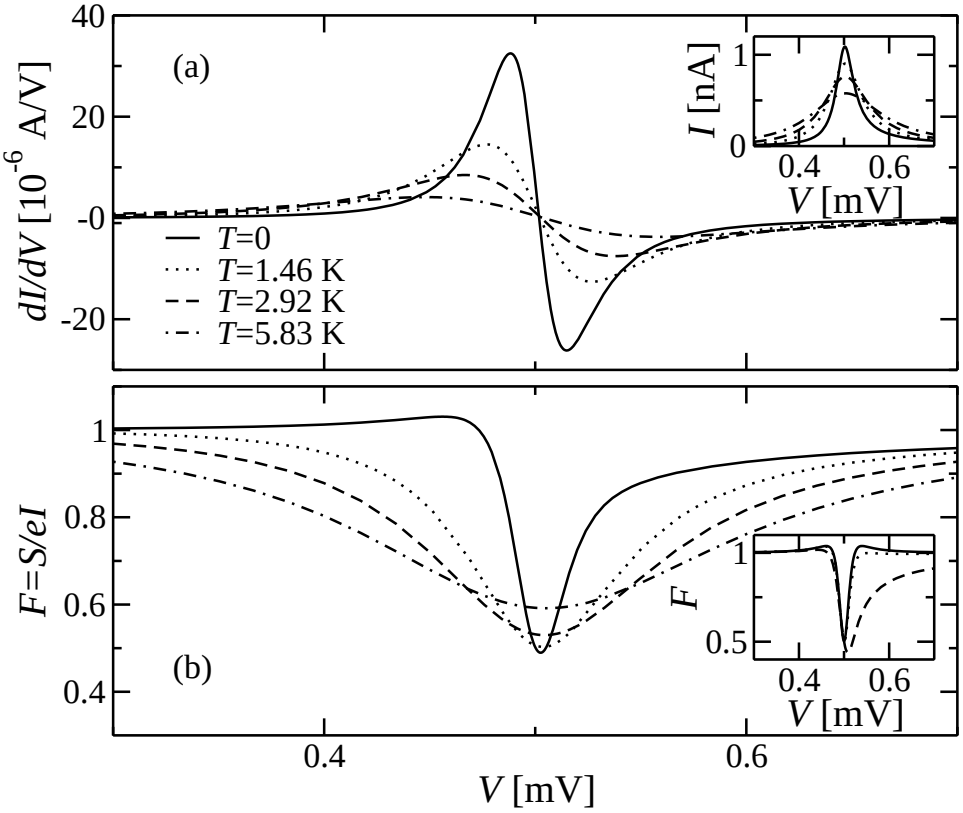

Fig. 7.2: (color online) (a) Differential conductance, current (inset), and (b) Fano factor through a single channel for various temperatures and $\Gamma_{\rm L} = 0.025$, $\Gamma_{\rm R} = 0.0125$, $\Omega = 0.025$, $\varepsilon = 0.5$, $\alpha = 0.005$ (in meV). The inset of panel (b) shows the Fano factor for dissipation strength $\alpha = 0$ (solid), 10^{-3} (dashed), and 10^{-2} (dotted) at zero temperature.

7.2 Transport through two coupled channels

The natural assumption is now that the shot noise must be influenced also by the interaction with a second transport channel; cf. Fig. 7.1 and Ref. [188]. Thus, we now consider two capacitively coupled channels, so that the system Hamiltonian reads $H_0 = \sum_{i,l}(\varepsilon_{il} n_{il} + \frac{1}{2}\sum_{i',l'} U_{ii'll'} n_{il} n_{i'l'})$, where $i = 1, 2$ labels the different transport channels. Note that without inter-channel interaction ($U_{ii'll'} = 0$ for $i \neq i'$), both channels are statistically independent. Thus, the behavior observed in the one-channel case is repeated at a different voltage (see dotted lines in Fig. 7.3), but still the Fano factor cannot exceed the value 5/4.

In order to simplify the model, we assume that the interaction $U_{ii'll'}$ is huge whenever $i = i'$ or $l = l'$. Then, the system will accept up to two extra electrons provided that they are placed in different stacks and different layers [186, 144]. This means that we have to consider the following 7 states (the ith letter refers to channel i): the empty state $|00\rangle$, the one-electron states $|\mathrm{L}0\rangle$, $|\mathrm{R}0\rangle$, $|0\mathrm{L}\rangle$, $|0\mathrm{R}\rangle$, and the two-electron states $|\mathrm{RL}\rangle$, $|\mathrm{LR}\rangle$. It is assumed that both dots on the right-hand side couple to the same lead, while each channel couples to an individual phonon bath. Then we derive for the coupled channels

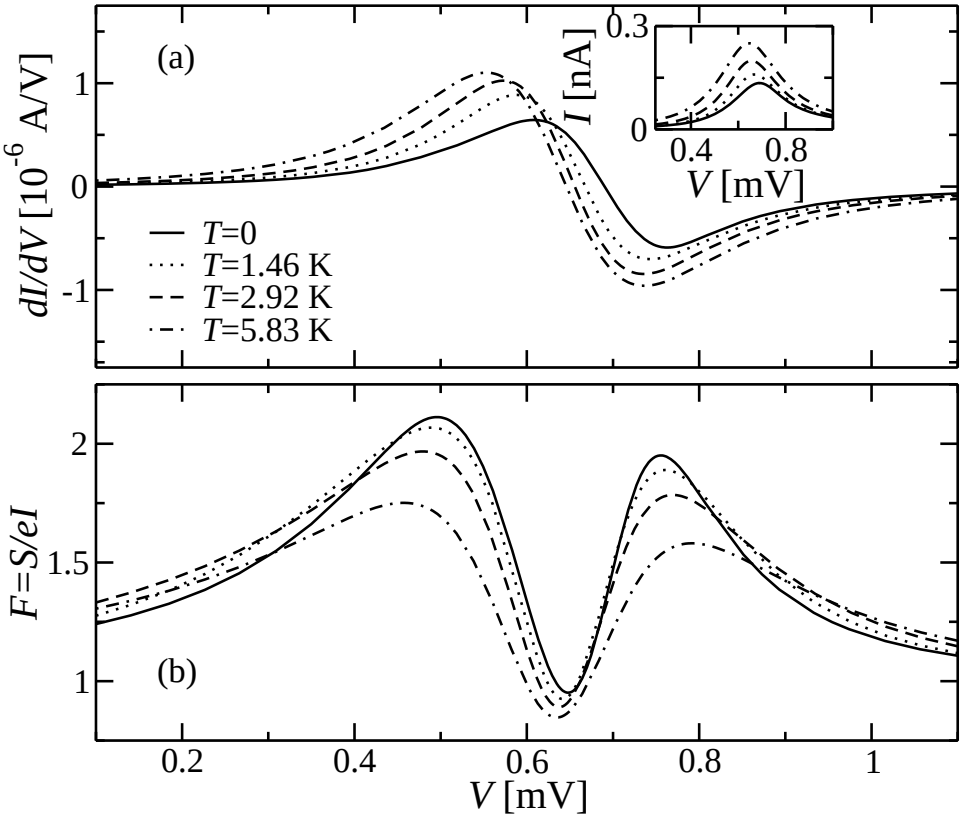

Fig. 7.3: (color online) (a) Differential conductance and (b) Fano factor for two coupled channels for various temperatures and the parameters $\Gamma_{\rm L} = 0.025$, $\Gamma_{\rm R} = 0.0125$, $\Omega = 0.025$, $\alpha = 0.005$, $\varepsilon_1 = 0.5$, $\varepsilon_2 = 0.75$ (in meV). Dotted lines: corresponding results for two uncoupled channels. The inset shows the temperature broadening of the current peak.

a master equation of the form (4.9) with a Liouvillian given by an 11×11 matrix. A closer inspection of this Liouvillian reveals that—formally—it can be obtained also in the following way: One writes the reduced density operator of the double channel as a direct product of each channel, $\rho = \rho^{(1)} \otimes \rho^{(2)}$, and the Liouvillian accordingly as $\mathcal{L} = \mathcal{L}^{(1)} + \mathcal{L}^{(2)}$, where $\mathcal{L}^{(i)}$ is the Liouvillian (7.3) with the parameters replaced by those of channel i. In this case, $\gamma_i = (\Gamma_{j\rm L} + \Gamma_{i\rm R})/2$, $j \neq i$. Finally, one removes all lines and columns that contain one of the "forbidden" states $|{\rm LL}\rangle$, $|{\rm RR}\rangle$.

For self-assembled quantum dots, a realistic assumption is that all barriers are almost identical, so that $\Gamma_{\rm L/R}$ and Ω do not depend on the channel index i. By contrast, for the internal bias $\varepsilon_i = \varepsilon_{i\rm R} - \varepsilon_{i\rm L}$, it will be shown that already small differences play a role, so that we have to maintain the channel index i in the effective detunings $\delta_i = \varepsilon_i - eV$. For unidirectional transport, the current operators now read $\mathcal{J}_- = 0$, while $\mathcal{J}_+ = \mathcal{J}_+^{(1)} + \mathcal{J}_+^{(2)}$ acts on the reduced density operator as $\mathcal{J}_+\rho = (\Gamma_{\rm R}/\hbar)[(\rho_{\rm R0} + \rho_{0\rm R})|00\rangle\langle 00| + \rho_{\rm RL}|0{\rm L}\rangle\langle 0{\rm L}| + \rho_{\rm LR}|{\rm L}0\rangle\langle {\rm L}0|]$.

In the absence of the phonons, one finds the scenario discussed already in Ref. [186]: The Fano factor exhibits two peaks, but their origin is now different than in the one-channel case. If both double quantum dots become resonant at different source-drain voltages, an electron in the double dot that

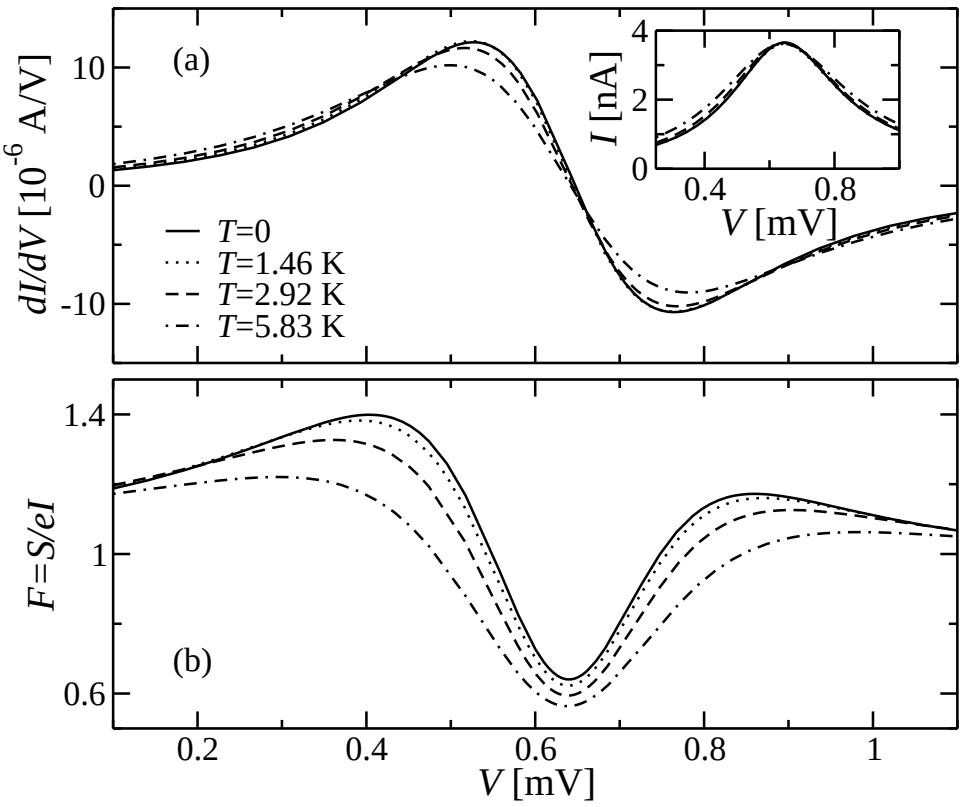

Fig. 7.4: (a) Differential conductance and (b) Fano factor for two coupled channels for various temperatures and the parameters $\Gamma_{\rm L} = 0.11$, $\Gamma_{\rm R} = 0.055$, $\Omega = 0.11$, $\alpha = 0.005$, $\varepsilon_1 = 0.5$, $\varepsilon_2 = 0.75$ (in meV). The inset shows the temperature broadening of the current peak.

is out of resonance has only a small probability to tunnel through the central barrier. Therefore, the non-resonant double dot will mostly be occupied with one electron and thereby block the other channel, so that the current peaks becomes smaller than in the one-channel case; cf. insets of Figs. 7.2a and 7.3a. Whenever the non-resonant channel is empty, however, the resonant channel will transmit a bunch of electrons, so that eventually the noise is super-Poissonian.

Figures 7.3 and 7.4 show the corresponding current and the Fano factor in the presence of dissipation for two different configurations. We observe two striking features which are in accordance with the experimental results of Ref. [188]: First, dynamical channel blocking is less pronounced at higher temperatures and, second, the structure of the Fano factor exhibits a clear asymmetry.

This behavior can be explained within the following picture: Let us consider, for instance, the situation sketched in Fig. 7.5 where $\varepsilon_1 < \varepsilon_2$. When the source-drain voltage puts the first double quantum dot in resonance, i.e. $\delta_1 = 0$, the second double dot is still *above resonance* ($\delta_2 > 0$), thus, blocking the resonant channel. If now the electron in channel 2 absorbs a phonon, the blockade is lifted. On the other hand, when $\delta_2 = 0$, double dot 1 one is already *below resonance* ($\delta_1 < 0$) and phonon emission can resolve the blockade. Both processes are more frequent the higher the temperature, so that dynamical channel blockade is eventually resolved. The fact that emission is more likely than absorption, explains

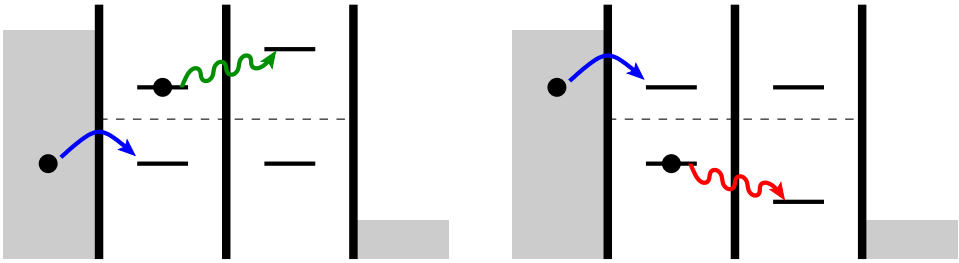

Fig. 7.5: Phonon-assisted channel opening: The blocking electron in the off-resonant channel can tunnel through the interdot barrier after phonon absorption (left) or emission (right) and thereby open the resonant channel.

the observed asymmetry and its reduction with increasing temperature. We emphasize that this does not rely on differences in the inter-dot hoppings Ω_i, in contrast to the mechanism of Ref. [186].

This *phonon-induced channel opening* is also manifested in the enhancement of the current shown in the inset of Fig. 7.3a. The current peak becomes larger with increasing temperature and experiences a slight shift away in its location. At low temperatures it tends to be around the larger resonance voltage (ε_2) which is driven by phonon relaxation. As phonon emission becomes important with temperature, the current peak becomes larger and shifts towards $eV_0 = (\varepsilon_1 + \varepsilon_2)/2$ coinciding with the maximal current voltage in the absence of dissipation.

This effect is weaker when considering stronger tunneling couplings: the Fano factor is reduced by DCB lifting and the current peak remains centered at eV_0 when increasing temperature, which only affects to its boadening, cf. Fig. 7.4.

7.2.1 Leakage currents

The observed behavior reproduces rather well the measurements reported in Ref. [188], but there is still one difference: In the experiment, the Fano factor far from resonance is clearly smaller than 1, while for the two-channel model, it tends to be Poissonian. This can be explained by leakage currents I_k that inevitably flow through the whole sample, but have been ignored so far. We assume that the leakage currents are statistically independent of each other and of the coupled double dots considered. Then we can write both the current and the noise of the complete sample as a sum of the independent channels:

$$I_{\text{sample}} = I_{\text{sys}} + \sum_k I_k \tag{7.9}$$

and

$$S_{\text{sample}} = S_{\text{sys}} + \sum_k F_k I_k, \tag{7.10}$$

where F_k is the Fano factor associated to I_k. If the leakage currents stem from resonant tunneling through single quantum dots or double dots far from resonance, $F_i < 1$ [175] and, thus, the total Fano factor is decreased: $F_{\text{sample}} = S_{\text{sample}}/I_{\text{sample}} < F_{\text{sys}}$. However, since there are about 10^6 leakage channels [188], it is not possible to estimate their effect more precisely.

7.3 Conclusions

To summarize, the effect of electron-phonon interaction in the transport through double quantum dots systems has been studied, predicting super-Poissonian shot noise whenever the source-drain voltage tunes a double dot close to resonance. The corresponding Fano factor exhibits an asymmetric double-peak structure which becomes less pronounced with increasing temperature. In order to obtain the experimentally observed values [188] for the Fano factor, one can assume that two transport channels are so close that they can block each other. The temperature dependence of the double peaks have been explained by the suspension of dynamical channel blocking via phonon emission or absorption. The sub-Poissonian noise observed far from resonance is attributed to the appearance of independent leakage currents. So experiments with devices where these systems were isolated from these additional noise sources are highly desirable.

Chapter 8

Electron and Phonon Counting Statistics.

The complete knowledge of the statistics and, in concrete, the properties of the fluctuations of the number of particles emitted from a quantum system has been a topic of intense studies in quantum optics [145, 146, 147, 148, 166, 149] and, in more recent years, in quantum transport[150, 151, 25, 26, 152, 153]. In particular, interesting features like an anti-bunching of photons emitted from a closed two-level atom under a resonant field[154], or a bunching of electrons tunneling through interacting two-levels quantum dots (QD) connected to fermionic reservoirs [155, 156, 157, 158, 159, 160] have been reported. The electronic case appears to be specially important since measurements of higher order electron noise correlations have been recently realized[161, 162, 163].

In this paper, it is show how the *combined* statistics of Fermions and Bosons is a very sensitive tool for extracting information from time-dependent, driven systems. In particular, phonon emission has been measured by its influence on the electronic current in two-levels systems[164]. We analyze the electron and phonon noises and find that they can be tuned back and forth between sub- and super-Poissonian character by using the strength of an ac driving field or the bias voltage.

For this purpose, we develop a general method to simultaneously extract the full counting statistics of single electron tunnelling and (phonon mediated) relaxation events.

Our system consists of a two level quantum dot (QD) connected to two fermionic leads by tunnel barriers. The Coulomb repulsion inside the QD is assumed to be so large that only single occupation is allowed (*Coulomb blockade* regime). The lattice vibrations induce, at low temperatures, inelastic transitions from the upper to the lower state. In analogy to Resonance Fluorescence in quantum optics, a time-dependent ac field with a frequency ω drives the transition between the two levels ε_1, ε_2 close to resonance, $\Delta_\omega = \varepsilon_2 - \varepsilon_1 - \omega \approx 0$, which allows us to assume the rotating wave approximation. Thus, the electron in the QD is coherently delocalized between both levels performing *photon-assisted Rabi oscillations*[68]. For simplicity, we consider spinless electrons.

This system is modelled by the Hamiltonian:

$$\begin{aligned}\hat{H}(t) &= \sum_i \varepsilon_i \hat{d}_i^\dagger \hat{d}_i + \frac{\Omega}{2}\left(e^{-i\omega t}\hat{d}_2^\dagger \hat{d}_1 + hc.\right) + \sum_Q \omega_Q \hat{a}_Q^\dagger \hat{a}_Q + \sum_{k\sigma} \varepsilon_{k\alpha} \hat{c}_{k\alpha}^\dagger \hat{c}_{k\alpha} \\ &\quad + \sum_{k\alpha i} V_{\alpha i}\left(c_{k\alpha}^\dagger \hat{d}_i + hc.\right) + \sum_Q \lambda_Q \left(\hat{d}_2^\dagger \hat{d}_1 \hat{a}_Q + hc.\right), \end{aligned} \tag{8.1}$$

where $\hat{a}_Q$, $\hat{c}_{k\alpha}$ and $\hat{d}_i$ are annihilation operators of phonons and electrons in the leads and in the QD, respectively and Ω is the Rabi frequency of the intra-dot oscillations, which is proportional to the intensity of the ac field.

The last two terms in Eq. (8.1) give the coupling of the electrons in the QD to the fermionic leads and to the phonon field, respectively. These terms are responsible for the incoherent dynamics and they can be considered apart in the derivation of the master equation for the reduced density matrix. Applying the quantum-jump approach[165, 21] to electronic transport and phonic emission events, it can be written:

$$\dot{\rho}(t) = \mathcal{L}_0(t)\rho(t) + \mathcal{L}_e(t)\rho(t) + \mathcal{L}_p(t)\rho(t), \tag{8.2}$$

where $\mathcal{L}_e$ and $\mathcal{L}_p$ are the Liouvillian superoperator responsible for the incoherent events: electron tunneling from the system to the collector and relaxation by spontaneous phonon emission. Thus, the density matrix can be integrated iteratively:

$$\begin{aligned}
\rho(t) &= e^{-\mathcal{L}_0 t}\rho(0) + \int_0^t dt' e^{-\mathcal{L}_0(t-t')}\left(\mathcal{L}_p(t') + \mathcal{L}_e(t')\right) e^{-\mathcal{L}_0 t'}\rho(0) \\
&\quad + \int_0^t dt' \int_0^{t'} dt'' e^{-\mathcal{L}_0(t-t')}\left(\mathcal{L}_p(t') + \mathcal{L}_e(t')\right) e^{-\mathcal{L}_0(t'-t'')}\left(\mathcal{L}_p(t'') + \mathcal{L}_e(t'')\right) e^{-\mathcal{L}_0 t''}\rho(0) + ... \\
&= \sum_{n_e,n_p} \rho^{(n_e,n_p)},
\end{aligned} \tag{8.3}$$

where $\rho^{(n_e,n_p)}(t)$ gives the probability that, during a certain time interval t, n_e electrons have tunneled out of a given electron-phonon system and n_p phonons have been emitted:

$$\begin{aligned}
\rho^{(0,0)} &= e^{-\mathcal{L}_0 t}\rho(0) \\
\rho^{(1,0)} &= \int_0^t dt' e^{-\mathcal{L}_0(t-t')}\mathcal{L}_e(t')e^{-\mathcal{L}_0 t'}\rho(0) \\
\rho^{(0,1)} &= \int_0^t dt' e^{-\mathcal{L}_0(t-t')}\mathcal{L}_p(t')e^{-\mathcal{L}_0 t'}\rho(0) \\
\rho^{(2,0)} &= \int_0^t dt' \int_0^{t'} dt'' e^{-\mathcal{L}_0(t-t')}\mathcal{L}_e(t')e^{-\mathcal{L}_0(t'-t'')}\mathcal{L}_e(t'')e^{-\mathcal{L}_0 t''}\rho(0) \\
\rho^{(0,2)} &= \int_0^t dt' \int_0^{t'} dt'' e^{-\mathcal{L}_0(t-t')}\mathcal{L}_p(t')e^{-\mathcal{L}_0(t'-t'')}\mathcal{L}_p(t'')e^{-\mathcal{L}_0 t''}\rho(0) \\
\rho^{(1,1)} &= \int_0^t dt' \int_0^{t'} dt'' e^{-\mathcal{L}_0(t-t')}\left(\mathcal{L}_p(t')e^{-\mathcal{L}_0(t'-t'')}\mathcal{L}_e(t'') + \mathcal{L}_e(t')e^{-\mathcal{L}_0(t'-t'')}\mathcal{L}_p(t'')\right) e^{-\mathcal{L}_0 t''} \\
&\vdots
\end{aligned} \tag{8.4}$$

By introducing the electron (phonon) counting variables, $s_{e(ph)}$, one can define the generating function [1] [166, 168]

$$G(t, s_e, s_p) = \sum_{n_e,n_p} s_e^{n_e} s_p^{n_p} \rho^{(n_e,n_p)}(t), \tag{8.7}$$

[1] The generating function was introduced by R. Ellickson as a method for calculating the fluctuations in disintegration problems described by rate equations[169] and later applied by D.K.C. MacDonald to describe Poissonian processes[170] like emission of electrons from a cathode, an analogy to tunnel through a single barrier. The probability of n tunnelling events wit a rate Γ in a time t, $P_n(t)$, obeys

$$\dot{P}_n(t) = -\Gamma(P_n(t) - P_{n-1}(t)). \tag{8.5}$$

whose derivatives give the correlations:

$$\frac{\partial^{\ell+m} trG(t,1,1)}{\partial s_e^{\ell} \partial s_p^{m}} = \left\langle \prod_{i=1}^{\ell} \prod_{j=1}^{m} (n_e - i + 1)(n_p - j + 1) \right\rangle . \tag{8.8}$$

One can derive the equations of motion for the generating function as previously done for the density matrix:

$$\dot{G}(t, s_e, s_p) = M(s_e, s_p) G(t, s_e, s_p), \tag{8.9}$$

that generalizes the master equation, $\dot{\rho}(t) = M(1,1)\rho(t)$, by introducing the counting variables in those terms corresponding to the tunneling of an electron to the collector lead and the emission of a phonon. Writing the density matrix as a vector, $\rho = (\rho_{00}, \rho_{11}, \rho_{12}, \rho_{21}, \rho_{22})^T$, the equation of motion of the GF (8.9) is described, in the Born-Markov approximation, by the matrix[119, 172]:

$$M(s_e, s_p) = \begin{pmatrix} -2\Gamma_{\rm L} - (f_1 + f_2)\Gamma_{\rm R} & s_e \bar{f}_1 \Gamma_{\rm R} & 0 & 0 & s_e \bar{f}_2 \Gamma_{\rm R} \\ \Gamma_{\rm L} + s_e^{-1} f_1 \Gamma_{\rm R} & -\bar{f}_1 \Gamma_{\rm R} & i\frac{\Omega}{2} & -i\frac{\Omega}{2} & s_p \gamma \\ 0 & i\frac{\Omega}{2} & \Lambda_{12} + i\Delta_\omega & 0 & -i\frac{\Omega}{2} \\ 0 & -i\frac{\Omega}{2} & 0 & \Lambda_{12} - i\Delta_\omega & i\frac{\Omega}{2} \\ \Gamma_{\rm L} + s_e^{-1} f_2 \Gamma_{\rm R} & 0 & -i\frac{\Omega}{2} & i\frac{\Omega}{2} & -\gamma - \bar{f}_2 \Gamma_{\rm R} \end{pmatrix}, \tag{8.10}$$

where ρ_{00} gives the occupation of the empty state, ρ_{11} and ρ_{22} correspond to the ground and excited electronic states, respectively, and ρ_{12} and ρ_{21} are the coherences, $\gamma = 2\pi|\lambda_{\varepsilon_2 - \varepsilon_1}|^2$ is the spontaneous emission rate due to the coupling with the phonon bath, $\Gamma_{\rm L(R)} = 2\pi|V_{\rm L(R)}|^2$ is the tunneling rate through the left(right) contact (considering $V_{\alpha 1} = V_{\alpha 2}$) and $f_i = f(\varepsilon_i - \mu) = \left(1 + e^{(\varepsilon_i - \mu)\beta}\right)^{-1}$ and $\bar{f}_i = 1 - f_i$ are the Fermi distribution functions that weight the tunneling of electrons between the right lead (with a chemical potential μ) and the state i in the QD. The decoherence is given by $\Lambda_{12} = -\frac{1}{2}\left((\bar{f}_1 + \bar{f}_2)\Gamma_{\rm R} + \gamma\right)$. The Fermi energy of the left lead is considered high enough that no electrons can tunnel from the QD to the left lead. All the parameters in these equations, except the sample-depending coupling to the phonon bath, can be externally manipulated.

Taking the Laplace transform of the generating function, $\tilde{G}(z, s_e, s_p) = (z - M)^{-1}\rho(0)$, where $\rho(0)$ is the initial state, the long-time behaviour is given by the residue for the pole near $z = 0$. From the Taylor expansion of the pole $z_0 = \sum_{m,n>0} c_{mn}(s_e - 1)^m (s_p - 1)^n$, one can write $trG(t, s_e, s_p) \sim g(s_e, s_p) e^{z_0 t}$ and obtain, from (8.8), the cumulants, $\kappa_{e(p)}^{(i)} = \left\langle \left(n_{e(p)} - \langle n_{e(p)} \rangle\right)^i \right\rangle$:

$$\kappa_{e(p)}^{(1)} = \langle n_{e(p)} \rangle = \frac{\partial g(1,1)}{\partial s_{e(p)}} + c_{10(01)} t \tag{8.11a}$$

$$\kappa_{e(p)}^{(2)} = \sigma_{e(p)}^2 = \frac{\partial^2 g(1,1)}{\partial s_{e(p)}^2} - \left(\frac{\partial g(1,1)}{\partial s_{e(p)}}\right)^2 + (c_{10(01)} + 2c_{20(02)})t \tag{8.11b}$$

where

$$\sigma_{ij}^2 = \langle n_i n_j \rangle - \langle n_i \rangle \langle n_j \rangle \tag{8.11c}$$

Defining the generating function, $Q(x,t) = \sum_{n=0}^{\infty} x^n P_n(t)$, it is easy to derive the differential equation

$$\dot{Q}(x,t) = \Gamma(x-1)Q(x,t), \tag{8.6}$$

with the initial condition $Q(x,0) = 1$. Then, by the Taylor expansion of the solution, $Q(x,t) = e^{\Gamma(x-1)t}$, one obtains the Poisson distribution, $P_n(t) = e^{-\Gamma t}\frac{(\Gamma t)^n}{n!}$, for which $\kappa_1 = \kappa_2 = \kappa_3 = \Gamma t$.

and the noise for the emitted electronic and phononic signals becomes: $S_{e(p)} = \sigma^2_{e(p)}$.

$$\kappa^{(3)}_{e(p)} = \frac{\partial^3 g(1,1)}{\partial s^3_{e(p)}} - 3\frac{\partial g(1,1)}{\partial s_{e(p)}}\frac{\partial^2 g(1,1)}{\partial s^2_{e(p)}} + 2\left(\frac{\partial g(1,1)}{\partial s_{e(p)}}\right)^3 + \frac{\partial g(1,1)}{\partial s_{e(p)}} + (c_{10(01)} + 6c_{20(02)} + 6c_{30(03)})t, \quad (8.11d)$$

which give the mean, variance and skewness, respectively. In the large time asymptotic limit, all the information is included in the coefficients c_{mn}. Thus, the mean $\langle n_{e(p)}\rangle \sim c_{10(01)}t$ and the variance $\sigma^2_{e(p)} \sim (c_{10(01)} + 2c_{20(02)})t$ from where one gets the current $I_{e(p)} = \frac{d}{dt}\langle n_{e(p)}\rangle \sim c_{10(01)}$ and the low frequency noise $S(0) = \frac{d}{dt}\sigma^2_{e(p)} \sim (c_{10(01)} + 2c_{20(02)})$. Then, the Fano factor is $F_{e(ph)} = 1 + 2c_{20(02)}/c_{10(01)}$ so that, the sign of the second term in the right hand side defines the sub- ($F < 1$) or super-($F > 1$) Poissonian character of the noise.

In the limit $\Gamma_{L(R)} \to 0$ we obtain the pure Resonance Fluorescence case for the noise of the emitted phonons, formally equivalent to the expression for emitted photons in quantum optics[166],

$$F_p(\Gamma_i = 0) = 1 - \frac{2\Omega^2(3\gamma^2 - 4\Delta^2_\omega)}{(\gamma^2 + 2\Omega^2 + 4\Delta^2_\omega)^2}, \quad (8.12)$$

yielding the famous sub-Poissonian noise result at resonance ($\Delta_\omega = 0$). In the following, only the resonant case will be considered unless the opposite were indicated.

Electron-phonon correlations are obtained from:

$$\langle n_e n_p\rangle = \frac{\partial g(1,1)}{\partial s_e}c_{01}t + \frac{\partial g(1,1)}{\partial s_p}c_{10}t + c_{11}t + c_{10}c_{01}t^2 \quad (8.13)$$

Then,

$$\sigma^2_{ep} = \frac{\partial^2 g(1,1)}{\partial s_e \partial s_p} + c_{11}t. \quad (8.14)$$

The long time behaviour is given by $\sigma^2_{ep} \sim c_{11}t$. The correlation coefficient is then defined as[167]:

$$r = \frac{\sigma_{ep}}{\sqrt{\sigma^2_e \sigma^2_p}} = \frac{c_{11}}{\sqrt{(c_{10} + 2c_{20})(c_{01} + 2c_{02})}}. \quad (8.15)$$

Similarly to the electronic(phononic) correlations, where the sign of the second order cummulant, $c_{20(02)}$, defined the sub- or super-Poissonian character of the noise, the sign of c_{11} gives the character of the electron-phonon correlations. If $c_{11} > 0$, the detection of a transmitted electron would involve the detection of a phonon in a short lapse of time, while $c_{11} < 0$ involves distant events.

The electron-phonon correlation coefficient is limited to $|r| < 1$, having $r = 1$ for the case where the number of detected electrons is proportional to the number of detected phonons: $n_e \propto n_p$. $r = 0$ means uncorrelated events. Note that independent events give $r = 0$, but the opposite is not necessary true, all will be shown below. Analogously to the Fano factor for the second order cumulants, the deviation of the third cumulants from the Poissonian statistics can be parametrized by the coefficient:

$$\eta_{e(p)} = \frac{\kappa^{(3)}_{e(p)}}{\kappa^{(1)}_{e(p)}} = \frac{\langle n^3_{e(p)}\rangle - 3\langle n_{e(p)}\rangle\langle n^2_{e(p)}\rangle + 2\langle n_{e(p)}\rangle^3}{\langle n_{e(p)}\rangle} = 1 + 6\frac{c_{20(02)} + c_{30(03)}}{c_{10(01)}}. \quad (8.16)$$

In what follows, we will discuss different configurations concerning the relative positions of the energy levels with respect to the chemical potentials of the contacts. As we will see, electron and phonon fluctuations and their correlations are strongly sensitive to the levels and to the chemical potentials of the contacts configuration.

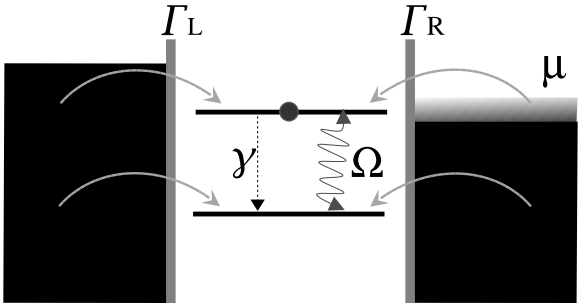

Fig. 8.1: In the low bias regime, the electron remains in the QD, in analogy to resonance fluorescent atoms.

8.1 Low bias regime. Resonance Fluorescent Phonon Emission

If the chemical potential of the left and right lead is above the energies of both levels, $\mu > \varepsilon_{1(2)}$, the QD is always populated by one electron and transport is cancelled. Then, this case is completely analogue to the resonance fluorescence problem, where spontaneously emitted phonons play the role of fluorescent photons: the trapped electron is coherently delocalized by the driving field between the two levels performing photo-assisted Rabi oscillations until the emission of a phonon, then the electron is relaxed to the lower level, cf. Fig. 8.1.

In the case shown in Fig. 1, where ϵ_2 is below but very close to μ, the electron in the upper level has a small probability, $x\Gamma_{\rm R}$, to be extracted to the right lead due to the thermal broadening of the Fermi level: $f_1 = 1$, $f_2 = 1 - x$, where $x \approx e^{\beta(\varepsilon_2 - \mu)}$ and $\beta = k_B T$. Then, the phonons deviate from the resonance fluorescence like statistics because the QD may be empty during short lapses of time. It would be the case if the resonance fluorescent atom could be eventually ionized.

The phononic resonance fluorescence behaviour as well as electronic transport quenching is recovered for $x = 0$. From the expressions shown in Appendix A.1, one can obtain the following Fano factors for electrons and phonons :

$$F_e = 1 + \Gamma_{\rm L}\Gamma_{\rm R}\left(\frac{\gamma(\gamma^2 - 2\Omega^2)}{\left(\gamma^2 + 2\Omega^2\right)^2\left(\Gamma_{\rm L} + \Gamma_{\rm R}\right)} - \frac{\Omega^2}{\left(\Gamma_{\rm L} + \Gamma_{\rm R}\right)^2}\right)x + O\left(x^2\right) \tag{8.17}$$

$$\begin{aligned} F_p = {} & 1 - \frac{6\gamma^2\Omega^2}{\left(\gamma^2 + 2\Omega^2\right)^2} \\ & - \frac{\gamma\Omega^2\Gamma_{\rm R}}{2\left(\gamma^2 + 2\Omega^2\right)^2}\left(\frac{\gamma^3 - 10\Omega^2\gamma}{\left(\gamma^2 + 2\Omega^2\right)\left(\Gamma_{\rm L} + \Gamma_{\rm R}\right)} - \frac{4\left(7\gamma^2 - 4\Omega^2\right)}{\gamma^2 + 2\Omega^2} - \frac{\Omega^2}{\left(\Gamma_{\rm L} + \Gamma_{\rm R}\right)^2}\right)x + O\left(x^2\right). \end{aligned} \tag{8.18}$$

The driving field induces sub-Poissonian phononic noise which (in the limit $x = 0$) reaches a minimum $F_{p,m} = \frac{1}{4}$ for $\Omega_{\rm m} = \gamma/\sqrt{2}$ before the Rabi oscillations dominate the dynamics over relaxation processes, cf. Fig. 8.2. The electron-phonon correlation coefficient becomes (see Appendix A.1):

$$r = \left(\gamma\left(\Gamma_{\rm L} + \Gamma_{\rm R}\right)\left(\gamma^2 - 10\Omega^2\right) - \Omega^2\left(\gamma^2 + 2\Omega^2\right)\right)\sqrt{\frac{\gamma\Gamma_{\rm L}\Gamma_{\rm R}x}{2\left(\Gamma_{\rm L} + \Gamma_{\rm R}\right)^3\left(\gamma^4 - 2\Omega^2\gamma^2 + 4\Omega^4\right)}} + O\left(x^{3/2}\right). \tag{8.19}$$

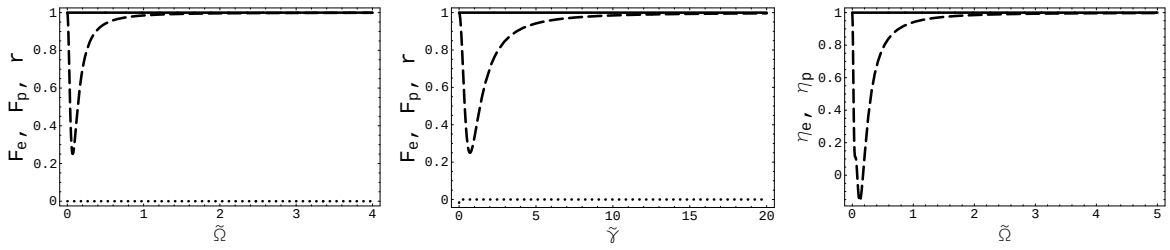

Fig. 8.2: **Low bias:** Dependence of F_e (solid), F_p (dashed) and r (dotted) with (a) the field intensity, $\tilde{\Omega}$, for $\tilde{\gamma} = 0.1$, (b) the phonon emission rate, $\tilde{\gamma} = \gamma/\Gamma$ for $\Omega = \Gamma/2$ in the low bias regime: $\varepsilon_{1,2} < \mu$. $\Gamma_{\rm L} = \Gamma_{\rm R} = \Gamma$, $\tilde{\Omega} = \Omega/\Gamma$, $\tilde{\gamma} = \gamma/\Gamma$, $x \approx 0$. c) Dependence of η_e (solid), η_p (dashed) with the field intensity, $\tilde{\Omega}$, for $\tilde{\gamma} = 0.1$ in the low bias regime: $\varepsilon_{1,2} < \mu$. $\Gamma_{\rm L} = \Gamma_{\rm R} = \Gamma$, $\tilde{\Omega} = \Omega/\Gamma$, $\tilde{\gamma} = \gamma/\Gamma$, $x \approx 0$.

The third cumulants become:

$$\eta_e = 1 + \frac{3\Gamma_{\rm L}\Gamma_{\rm R}\left(\gamma(\gamma^2 - 4\Omega^2)\left(\Gamma_{\rm L} + \Gamma_{\rm R}\right) - \Omega^2\left(\gamma^2 + 2\Omega^2\right)\right)x}{\left(\gamma^2 + 2\Omega^2\right)^2\left(\Gamma_{\rm L} + \Gamma_{\rm R}\right)^2} + O\left(x^2\right) \tag{8.20}$$

$$\eta_p = 1 - \frac{6\left(3\Omega^2\gamma^6 - 4\Omega^4\gamma^4 + 16\Omega^6\gamma^2\right)}{\left(\gamma^2 + 2\Omega^2\right)^4} + O\left(x\right) \tag{8.21}$$

We will analyze now two asymptotic limits of the results presented above:

8.1.1 Undriven case.

Without driving, there is no process that removes the electron from the lower level, so the stationary state of the system coincides with $\rho_2 = 1$. Then, both phonon emission and electron tunneling are cancelled:

$$c_{ij} = 0 \quad \forall i, j. \tag{8.22}$$

However, the electronic Fano factor and the electron-phonon correlation coefficient deviate from one and zero, respectively:

$$F_e = 1 + \frac{2x\Gamma_{\rm L}\Gamma_{\rm R}}{\left(\Gamma_{\rm L} + \Gamma_{\rm R}\right)\left(2\gamma + x\Gamma_{\rm R}\right) - x\gamma\Gamma_{\rm R}} \overset{\Gamma_{\rm L}=\Gamma_{\rm R}}{\longrightarrow} 1 + \frac{2\Gamma x}{4\gamma + x\Gamma} \tag{8.23}$$

$$F_p = 1 \tag{8.24}$$

$$r = \sqrt{\frac{x\gamma\Gamma_{\rm L}\Gamma_{\rm R}\left(2\Gamma_{\rm L} + (2-x)\Gamma_{\rm R}\right)}{2\left(\Gamma_{\rm L}\left(2\gamma + x\Gamma_{\rm R}\right) + \Gamma_{\rm R}\left(x\Gamma_{\rm R} + (2-x)\gamma\right)\right)\left(\Gamma_{\rm R}\left(x\Gamma_{\rm R} + (2-x)\gamma\right) + \Gamma_{\rm L}\left(2\gamma + 3x\Gamma_{\rm R}\right)\right)}}$$
$$\overset{\Gamma_{\rm L}=\Gamma_{\rm R}}{\longrightarrow} \sqrt{\frac{(4-x)\gamma x}{2(2x\Gamma + (4-x)\gamma)(4x\Gamma + (4-x)\gamma)}} \tag{8.25}$$

$$\eta_e = 1 + \frac{6x\Gamma_{\rm L}\Gamma_{\rm R}\left(2\Gamma_{\rm L}\left(\gamma + x\Gamma_{\rm R}\right) + \Gamma_{\rm R}\left(x\Gamma_{\rm R} - (x-2)\gamma\right)\right)}{\left(\Gamma_{\rm L}\left(2\gamma + x\Gamma_{\rm R}\right) + \Gamma_{\rm R}\left(x\Gamma_{\rm R} - (x-2)\gamma\right)\right)^2} \tag{8.26}$$

$$\eta_p = 1. \tag{8.27}$$

8.1.2 High intensity limit: $\Omega \to \infty$

Increasing the intensity of the ac field, the electron tends to occupy the upper level with a probability: $\rho_2 = \frac{2\Gamma_{\rm L} + (2-x)\Gamma_{\rm R}}{4\Gamma_{\rm L} + (4-x)\Gamma_{\rm R}} \sim \frac{1}{2}$. Then, it can tunnel to the right contact with a probability $x\Gamma_{\rm R}$,

producing a finite current:

$$c_{10} \xrightarrow{x\to 0} \frac{x\Omega^2\Gamma_{\rm L}\Gamma_{\rm R}}{(\gamma^2+2\Omega^2)(\Gamma_{\rm L}+\Gamma_{\rm R})} \tag{8.28}$$

and the electronic statistics becomes sub-Poissonian:

$$F_e = 1 - \frac{8x\Gamma_{\rm L}\Gamma_{\rm R}}{\left(4\Gamma_{\rm L}+(4-x)\Gamma_{\rm R}\right)^2} \xrightarrow{\Gamma_{\rm L}=\Gamma_{\rm R}} 1 - \frac{8x}{(8-x)^2} \sim 1 - \frac{x}{8}. \tag{8.29}$$

This result should be compared with the single level case, where it is known that $F_e = 1 - \frac{x}{2}$ and the probability of finding an electron in the QD is $\rho = \frac{2-x}{2} \sim 1$, see Appendix B.

Since the occupation probability of the upper level at high intensity field is maximum, so it is the probability of finding the QD unoccupied, $\rho_0 = \frac{x\Gamma_{\rm R}}{4\Gamma_{\rm L}+(4-x)\Gamma_{\rm R}}$. This introduces lapses of time when phonon emission is suppressed, affecting the phononic statistics by turning it super-Poissonian:

$$F_p = 1 + \frac{2x\gamma\Gamma_{\rm R}}{\left(4\Gamma_{\rm L}+(4-x)\Gamma_{\rm R}\right)^2} \xrightarrow{\Gamma_{\rm L}=\Gamma_{\rm R}} 1 + \frac{2\gamma x}{(8-x)^2\Gamma} \tag{8.30}$$

On contrary, the electron-phonon correlation is negative since the detection of an electron (phonon) reduces the probability of detecting a phonon (electron): when an electron has tunnelled out of the system, this is left empty and phonon emission is suppressed and when a phonon has been emitted, the upper level is unoccupied and no electron can be extracted from the QD:

$$r = -\frac{\sqrt{2x\gamma\Gamma_{\rm L}\Gamma_{\rm R}}}{\sqrt{32\Gamma_{\rm L}^3+48(2-x)\Gamma_{\rm R}\Gamma_{\rm L}^2+2\left(9x^2-40x+48\right)\Gamma_{\rm R}^2\Gamma_{\rm L}+(4-x)^2(2-x)\Gamma_{\rm R}^3}} \tag{8.31}$$

$$\times\frac{4\Gamma_{\rm L}+(4-3x)\Gamma_{\rm R}}{\sqrt{16\Gamma_{\rm L}^2+8(4-x)\Gamma_{\rm R}\Gamma_{\rm L}+\Gamma_{\rm R}\left(\Gamma_{\rm R}(4-x)^2+2x\gamma\right)}} \tag{8.32}$$

For the higher moments, one obtains:

$$\eta_e = 1 - \frac{24x\Gamma_{\rm L}\Gamma_{\rm R}\left(16\Gamma_{\rm L}^2+16(2-x)\Gamma_{\rm R}\Gamma_{\rm L}+(4-x)^2\Gamma_{\rm R}^2\right)}{\left(4\Gamma_{\rm L}+(4-x)\Gamma_{\rm R}\right)^4} \tag{8.33}$$

$$\eta_p = 1 + \frac{6x\gamma\Gamma_{\rm R}\left(16\Gamma_{\rm L}^2+4\left(2(4-x)\Gamma_{\rm R}-\gamma\right)\Gamma_{\rm L}+\Gamma_{\rm R}\left(\Gamma_{\rm R}(4-x)^2-(4-3x)\gamma\right)\right)}{\left(4\Gamma_{\rm L}+(4-x)\Gamma_{\rm R}\right)^4} \tag{8.34}$$

8.2 Dynamical Channel Blockade regime.

If the chemical potential of the right lead lies between the energy levels of the QD, $\varepsilon_1 < \mu < \varepsilon_2$ and therefore, $f_1 = 1-x$, $f_2 = 0$, where $x \approx e^{\beta(\varepsilon_1-\mu)}$ and $\beta = k_BT$, electronic transport is strongly suppressed through the lower level, cf. Fig. 8.3. Then, since only one electron is allowed in the system, the occupation of the lower level avoids the tunneling of electrons from the left lead and the current is blocked. This mechanism, which is known as *dynamical channel blockade*, predicts electronic super-Poissonian shot noise in multichannel systems like, for instance, two-level quantum dots[155] or capacitively coupled double quantum dots[186] as well as positive cross-correlations in three terminal devices[181, 182, 183]. It has been proposed as the responsible of noise enhancement measured experimentally in multilevel quantum dots[187] and double quantum dots (DQDs)[188].

The blocking of the current is not forever since the electron in the lower level has a finite but small probability of tunneling to the collector, $x\Gamma_{\rm R}$, due to the thermal smearing of the Fermi level.

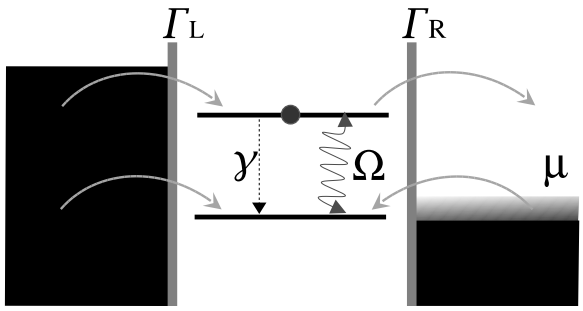

Fig. 8.3: Dynamical channel blockade configuration, where the electronic transport is strongly suppressed through the lower level.

Then, the trapped electron eventually escapes to the right lead allowing electrons to tunnel through the upper level before the lower one is again occupied. Thus, the current is restricted to short lapses of time while for long periods $t \sim (x\Gamma_{\rm R})^{-1}$ transport is quenched. This *bunching* of electrons is reflected in super-Poissonian shot noise.

Phonon-mediated relaxation introduces an additional way to occupy the lower level when current is flowing through the upper one, shortening the lapse of time when transport is allowed. Thus, the electrons are transferred in smaller bunches and the super-Poissonian character of the electronic noise is reduced. The detection of a phonon is always at the end of a bunch of electrons and implies the cancelation of the current, leading to a positive electron-phonon correlation.

The introduction of the AC field pumps the electron in the lower state to the upper one, giving the electron a finite probability to tunnel to the right lead or to be relaxed by the emission of one phonon. This reduces the electronic shot noise by reducing the duration of the lapses of time when transport is blocked (opposite to the effect of phonons). Thus, when $x = 0$, the electronic current and the phononic emission are proportional to the driving intensity and channel blockade is removed. Considering, for simplicity, the case $\Gamma_{\rm L} = \Gamma_{\rm R} = \Gamma$, the Fano factors become (see Appendix A.2):

$$F_e = 1 - \frac{8\Omega^4 + 2\left(2\gamma^2 + 15\Gamma\gamma + 9\Gamma^2\right)\Omega^2 - 2\Gamma(\gamma+\Gamma)^2(3\gamma+2\Gamma)}{\left(7\Omega^2 + (\gamma+\Gamma)(3\gamma+2\Gamma)\right)^2} \tag{8.35}$$

$$F_p = 1 - \frac{2\gamma\Omega^2\left(22\Gamma^2 + 28\gamma\Gamma - \Omega^2\right)}{\Gamma\left(7\Omega^2 + (\gamma+\Gamma)(3\gamma+2\Gamma)\right)^2}. \tag{8.36}$$

The electron-phonon correlation coefficient will be considered in the asymptotic non-driven and high intensity cases. As expected, the driving contributes to make the electronic noise sub-Poissonian and the phononic one super-Poissonian. However, it has to compete with the phonon emission that contributes to bring the electron to the lower state and to block the current, cf. Fig. 8.4. The positive electron-phonon correlation is decreased by the ac field since the emission of a phonon does not imply transport blocking anymore, cf. Fig. 8.4.

8.2.1 Undriven case.

The most interesting features appear in the absence of the AC field, where the consequences of the dynamical channel blockade are maximal and there is a strong dependence of the statistics on the

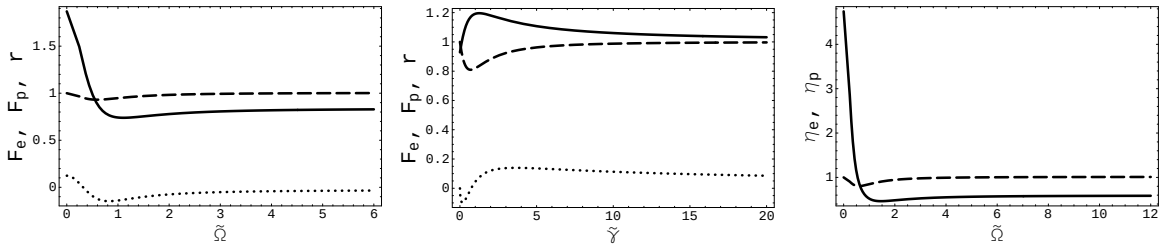

Fig. 8.4: **Dynamical Channel Blockade:** Dependence of F_e (solid), F_p (dashed) and r (dotted) with (a) the field intensity, $\tilde{\Omega}$, for $\tilde{\gamma} = 0.1$, (b) the phonon emission rate, $\tilde{\gamma} = \gamma/\Gamma$ for $\Omega = \Gamma/2$ in the dynamical channel blockade regime: $\varepsilon_1 < \mu < \varepsilon_2$. $\mu < \varepsilon_{1,2}$. $\Gamma_{\rm L} = \Gamma_{\rm R} = \Gamma$, $\tilde{\Omega} = \Omega/\Gamma$, $\tilde{\gamma} = \gamma/\Gamma$, $x \approx 0$. c) Dependence of η_e (solid), η_p (dashed) with the field intensity, $\tilde{\Omega}$, for $\tilde{\gamma} = 0.1$ in the dynamical channel blockade regime: $\varepsilon_1 < \mu < \varepsilon_2$. $\Gamma_{\rm L} = \Gamma_{\rm R} = \Gamma$, $\tilde{\Omega} = \Omega/\Gamma$, $\tilde{\gamma} = \gamma/\Gamma$, $x \approx 0$.

thermal smearing factor, x. In the absence of phonons, the electronic current and Fano factor are:

$$c_{10} = \frac{2x\Gamma_{\rm L}\Gamma_{\rm R}}{(x+1)\Gamma_{\rm L}+\Gamma_{\rm R}} \approx \frac{2x\Gamma_{\rm L}\Gamma_{\rm R}}{\Gamma_{\rm L}+\Gamma_{\rm R}} \tag{8.37}$$

$$F_e = 1 + \frac{2\Gamma_{\rm L}\left((1-x)^2\Gamma_{\rm L} + (1-3x)\Gamma_{\rm R}\right)}{((x+1)\Gamma_{\rm L}+\Gamma_{\rm R})^2} \approx 1 + \frac{2\Gamma_{\rm L}}{\Gamma_{\rm L}+\Gamma_{\rm R}}. \tag{8.38}$$

It is interesting to see here how the Fano factor can be tuned by the asymmetric coupling to the leads: $F_e = 3$ (if $\Gamma_{\rm L} \gg \Gamma_{\rm R}$), $F_e = 2$ (if $\Gamma_{\rm L} = \Gamma_{\rm R}$) and $F_e = 1$ (if $\Gamma_{\rm L} \ll \Gamma_{\rm R}$). In the last case, the contribution of $x\Gamma_{\rm R}$ is diminished and the left barrier controls the transport (in this limit, the current is $c_{10} = 2x\Gamma_{\rm L}$). Then, the transferred electrons are uncorrelated one from the others resembling the behaviour of the single barrier problem briefly discussed above. The particular case $\Gamma_{\rm L} \ll \Gamma_{\rm R}$ was studied in Ref. [155] without considering the processes that introduce an electron from the collector to the lower level, with a rate $(1-x)\Gamma_{\rm R}$, giving a Fano factor $F_e = 2$.

Considering phonon emission and for small x, one can expand the first coefficients for the electronic and phononic statistics, as well as for the electron-phonon correlations.The Fano factors and the correlation coefficient r become:

$$F_e = 1 + \frac{2\Gamma_{\rm L}\Gamma_{\rm R}}{\Gamma_{\rm R}(\gamma+\Gamma_{\rm R})+\Gamma_{\rm L}(2\gamma+\Gamma_{\rm R})} - \frac{2\left(\Gamma_{\rm L}\Gamma_{\rm R}\left(2\gamma^2+5\Gamma_{\rm R}\gamma+3\Gamma_{\rm R}^2+2\Gamma_{\rm L}(\gamma+2\Gamma_{\rm R})\right)\right)x}{\left(\Gamma_{\rm R}(\gamma+\Gamma_{\rm R})+\Gamma_{\rm L}(2\gamma+\Gamma_{\rm R})\right)^2} + O\left(x^2\right)$$
$$\stackrel{\Gamma_{\rm L}=\Gamma_{\rm R}}{\longrightarrow} 1 + \frac{2\Gamma}{3\gamma+2\Gamma} + O(x) \tag{8.39}$$

$$F_p = 1 - \frac{2\gamma\Gamma_{\rm L}\Gamma_{\rm R}(\gamma+2\Gamma_{\rm L}+2\Gamma_{\rm R})x}{\left(\Gamma_{\rm R}(\gamma+\Gamma_{\rm R})+\Gamma_{\rm L}(2\gamma+\Gamma_{\rm R})\right)^2} + O\left(x^2\right) \stackrel{\Gamma_{\rm L}=\Gamma_{\rm R}}{\longrightarrow} 1 - \frac{2\gamma(\gamma+4\Gamma)x}{(3\gamma+2\Gamma)^2} + O(x^2) \tag{8.40}$$

$$r = (2\Gamma_{\rm L}+\Gamma_{\rm R})\sqrt{\frac{\gamma(\gamma+\Gamma_{\rm R})}{2\left(\Gamma_{\rm R}(\gamma+\Gamma_{\rm R})+\Gamma_{\rm L}(2\gamma+\Gamma_{\rm R})\right)\left(\Gamma_{\rm R}(\gamma+\Gamma_{\rm R})+\Gamma_{\rm L}(2\gamma+3\Gamma_{\rm R})\right)}} + O(x)$$
$$\stackrel{\Gamma_{\rm L}=\Gamma_{\rm R}}{\longrightarrow} 3\sqrt{\frac{\gamma(\gamma+\Gamma)}{(3\gamma+2\Gamma)(3\gamma+4\Gamma)}} + O(x). \tag{8.41}$$

The expected super-Poissonian electronic statistics and positive electron-phonon correlation are obtained. Interestingly, the presence of phonons reduces the electronic Fano factor (*noise reduction by noise*), but does not affect to its super-Poissonian character. On the other hand, the presence of electronic

transport affects the Poissonian phononic statistics by introducing a sub-Poissonian component: once a phonon has been emitted, the electron is relaxed to the lower level blocking the transport. A second phonon will not be detected until the electron tunnels to the collector and another one enters the upper level, so phononic events are well separated in time.

For the third cummulants, one obtains:

$$\eta_e = 1 + \frac{6\Gamma_L\Gamma_R\left(\gamma+\Gamma_R\right)\left(2\Gamma_L+\Gamma_R\right)}{\left(\Gamma_R\left(\gamma+\Gamma_R\right)+\Gamma_L\left(2\gamma+\Gamma_R\right)\right)^2} + O\left(x\right) \tag{8.42}$$

$$\eta_p = 1 - \frac{6\left(\gamma\Gamma_L\Gamma_R\left(\gamma+2\Gamma_L+2\Gamma_R\right)\right)x}{\left(\Gamma_R\left(\gamma+\Gamma_R\right)+\Gamma_L\left(2\gamma+\Gamma_R\right)\right)^2} + O\left(x^2\right). \tag{8.43}$$

8.2.2 High intensity limit: $\Omega \to \infty$

If the intensity of the driving field is large enough, the dynamical channel blockade is completely lifted, so sub-Poissonian electronic noise and super-Poissonian phononic noise are recovered:

$$F_e = 1 - \frac{8\Gamma_L\Gamma_R}{\left(4\Gamma_L+3\Gamma_R\right)^2} + O(x) \overset{\Gamma_L=\Gamma_R}{\longrightarrow} \frac{41}{49} + O(x) \tag{8.44}$$

$$F_p = 1 + \frac{2\gamma\Gamma_R}{\left(4\Gamma_L+3\Gamma_R\right)^2} + O(x) \overset{\Gamma_L=\Gamma_R}{\longrightarrow} 1 + \frac{2\gamma}{49\Gamma} + O(x). \tag{8.45}$$

Also, the ac field allows the extraction through the upper level of an electron that has been relaxed by the emission of one phonon. This means that the electron-phonon correlation becomes negative:

$$\begin{aligned} r &= -\frac{\sqrt{2\gamma\Gamma_L\Gamma_R}\left(4\Gamma_L+\Gamma_R\right)}{\sqrt{\left(32\Gamma_L^3+48\Gamma_R\Gamma_L^2+34\Gamma_R^2\Gamma_L+9\Gamma_R^3\right)\left(16\Gamma_L^2+24\Gamma_R\Gamma_L+\Gamma_R\left(2\gamma+9\Gamma_R\right)\right)}} + O\left(x\right) \\ &\overset{\Gamma_L=\Gamma_R}{\longrightarrow} -5\sqrt{\frac{2\gamma}{123(2\gamma+49\Gamma)}} + O(x). \end{aligned} \tag{8.46}$$

Then, by tuning the driving intensity, one can manipulate the character of the shot noise of electrons and phonons, turning the super(sub)-Poissonian statistics to sub(super)-Poissonian for electrons(phonons) when increasing Ω.

Higher moments are also obtained, giving

$$\eta_e = 1 - \frac{24(x+1)\Gamma_L\Gamma_R\left(16\Gamma_L^2-16(x-1)\Gamma_R\Gamma_L+(x-3)^2\Gamma_R^2\right)}{\left((x-3)\Gamma_R-4\Gamma_L\right)^4} \tag{8.47}$$

$$\eta_p = 1 + \frac{6(x+1)\gamma\Gamma_R\left(16\Gamma_L^2-4\left(\gamma+2(x-3)\Gamma_R\right)\Gamma_L+\Gamma_R\left(\Gamma_R(x-3)^2+(3x-1)\gamma\right)\right)}{\left((x-3)\Gamma_R-4\Gamma_L\right)^4}. \tag{8.48}$$

8.3 High Bias regime.

If the energy of both levels are above μ, $\varepsilon_1, \varepsilon_2 > \mu$ ($f_1 = f_2 = 0$), the two of them contribute to electronic transport, cf. Fig. 8.5. In this particular case, quantum interference effects may be important[178] depending on the concrete geometry of the system. However, in the weak coupling and high frequency limit case considered here, $\varepsilon_2 - \varepsilon_1 \gg \Gamma_{L,R}$, they can be disregarded.

Contrary to the previous regimes, the contribution of the empty state:

$$\rho_0 = \frac{\Gamma_R}{2\Gamma_L+\Gamma_R} \tag{8.49}$$

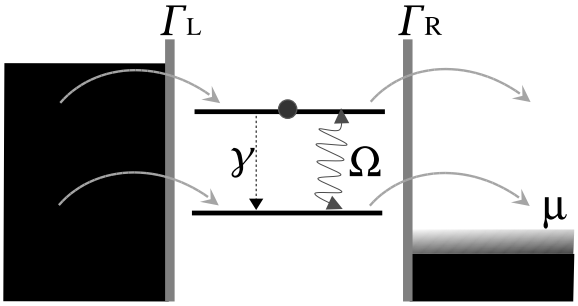

Fig. 8.5: Pure transport configuration.

plays an important role here. It strongly affects the sub-Poissonian character of the phononic noise.

Since the tunneling rates are considered independent on the energy, electronic transport does not depend on the level that the electron occupies when tunneling through the QD. Then, the transport characteristics (electronic current and noise) are independent of the field intensity, detunning and the spontaneous emission. Similarly to the single resonant level, the Fano factor is sub-Poissonian. However, the contribution of the two levels increases the noise (see Appendix A.3):

$$F_e = \frac{4\Gamma_{\rm L}^2 + \Gamma_{\rm R}^2}{(2\Gamma_{\rm L} + \Gamma_{\rm R})^2} \overset{\Gamma_{\rm L}=\Gamma_{\rm R}}{\longrightarrow} \frac{5}{9}. \tag{8.50}$$

The normalized third cumulant becomes:

$$\eta_e = 1 - \frac{12\Gamma_{\rm L}\Gamma_{\rm R}\left(4\Gamma_{\rm L}^2 + \Gamma_{\rm R}^2\right)}{\left(2\Gamma_{\rm L} + \Gamma_{\rm R}\right)^4} \overset{\Gamma_{\rm L}=\Gamma_{\rm R}}{\longrightarrow} \frac{7}{27}. \tag{8.51}$$

Interestingly, the two resonant levels statistics coincides with the single resonant one when writing $\Gamma_{\rm L}/2$ for $\Gamma_{\rm L}$. That is not the case for the phononic statistics that depends on the population of the upper level and, therefore, on the ac field parameters.

The expressions for the second order moments are quite lengthy, so considering the simpler case, $\Gamma_{\rm L} = \Gamma_{\rm R} = \Gamma$, one obtains a sub-Poissonian Fano factor:

$$F_p = 1 - 2\gamma \frac{\Gamma(\gamma + 2\Gamma)^2(\gamma + 4\Gamma) + \left(14\Gamma^2 + 17\Gamma\gamma - \gamma^2\right)\Omega^2 - 2\Omega^4}{9\Gamma\left(2\Omega^2 + (\gamma + \Gamma)(\gamma + 2\Gamma)\right)^2}. \tag{8.52}$$

which can be tuned to super-Poissonian for high enough intensities. The electron-phonon correlation:

$$c_{11} = -\gamma \frac{\Gamma(\Gamma - 5\gamma)(\gamma + 2\Gamma)^2 + 2\left(\gamma^2 + 16\Gamma\gamma + 4\Gamma^2\right)\Omega^2 + 4\Omega^4}{27\left(2\Omega^2 + (\gamma + \Gamma)(\gamma + 2\Gamma)\right)^2}. \tag{8.53}$$

may be positive or negative depending on the concrete parametrization of the system, as discussed below. In concrete, positive correlation is obtained when $\Gamma_{\rm L} \ll \Gamma_{\rm R}$ as well as, for low intensity driving, when the tunneling rates are small compared to the phonon emission rate, cf. Fig. 8.6.

8.3.1 Undriven case, $\Omega = 0$:

The emission of a phonon, in this case, depends on the tunneling of an electron from the left lead to the upper level. Then, it can tunnel to the collector directly or after being relaxed to the lower

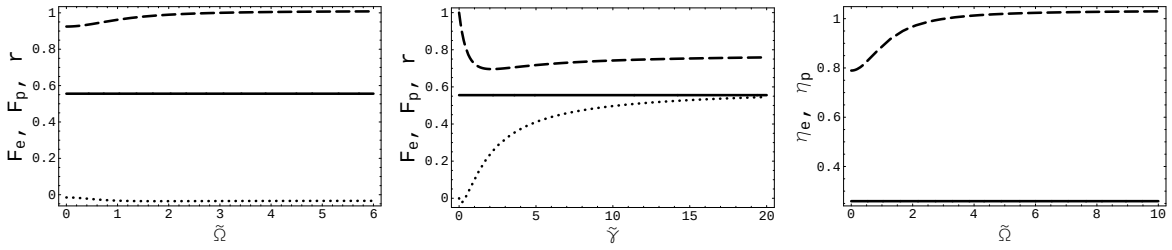

Fig. 8.6: **High Bias:** Dependence of F_e (solid), F_p (dashed) and r (dotted) with (a) the field intensity, $\tilde{\Omega}$, for $\tilde{\gamma} = 0.1$ and (b) the phonon emission rate, $\tilde{\gamma} = \gamma/\Gamma$ for $\Omega = \Gamma/2$ in the high bias regime: $\mu < \varepsilon_{1,2}$. $\Gamma_{\rm L} = \Gamma_{\rm R} = \Gamma$, $\tilde{\Omega} = \Omega/\Gamma$, $\tilde{\gamma} = \gamma/\Gamma$. c)Dependence of η_e (solid), η_p (dashed) with the field intensity, $\tilde{\Omega}$, for $\tilde{\gamma} = 0.1$ in the high bias regime: $\mu < \varepsilon_{1,2}$. $\Gamma_{\rm L} = \Gamma_{\rm R} = \Gamma$, $\tilde{\Omega} = \Omega/\Gamma$, $\tilde{\gamma} = \gamma/\Gamma$.

level by the emission of one phonon. Therefore, phonons *adopt* the electronic sub-Poissonian statistics. The first moments give a phononic Fano factor:

$$F_p = 1 - \frac{2\gamma\Gamma_{\rm L}\Gamma_{\rm R}\left(\gamma + 2\Gamma_{\rm L} + 2\Gamma_{\rm R}\right)}{\left(\gamma + \Gamma_{\rm R}\right)^2\left(2\Gamma_{\rm L} + \Gamma_{\rm R}\right)^2} \tag{8.54}$$

The electron-phonon correlation is given by:

$$r = \frac{\sqrt{\gamma}\left(4\gamma\Gamma_{\rm L}^2 - 2\Gamma_{\rm R}^2\Gamma_{\rm L} + \Gamma_{\rm R}^2\left(\gamma + \Gamma_{\rm R}\right)\right)}{\sqrt{2\left(\gamma + \Gamma_{\rm R}\right)\left(4\Gamma_{\rm L}^2 + \Gamma_{\rm R}^2\right)\left(4\left(\gamma^2 + \Gamma_{\rm R}\gamma + \Gamma_{\rm R}^2\right)\Gamma_{\rm L}^2 + 2\Gamma_{\rm R}\left(\gamma^2 + 2\Gamma_{\rm R}\gamma + 2\Gamma_{\rm R}^2\right)\Gamma_{\rm L} + \Gamma_{\rm R}^2\left(\gamma + \Gamma_{\rm R}\right)^2\right)}} \tag{8.55}$$

If the phonon emission rate is large enough compared to the tunneling rate, concretely: once an electron occupies the upper level, it will rather be relaxed to the lower level and tunnel to the collector than directly tunnel from the upper level. Then, the probability of detecting consequently one phonon and one electron increases, thus making the electron-phonon correlation positive if:

$$\gamma > \frac{\Gamma_{\rm R}^2(2\Gamma_{\rm L} + \Gamma_{\rm R})}{4\Gamma_{\rm L}^2 + \Gamma_{\rm R}^2}. \tag{8.56}$$

This is more clearly seen when considering $\Gamma_{\rm L} = \Gamma_{\rm R} = \Gamma$:

$$r = (5\gamma - \Gamma)\sqrt{\frac{\gamma}{10(\gamma + \Gamma)(7\gamma^2 + 10\gamma\Gamma + 9\Gamma^2)}}. \tag{8.57}$$

The coefficient

$$\eta_p = 1 - \frac{2\gamma\left(7\gamma^3 + 41\Gamma\gamma^2 + 52\Gamma^2\gamma + 36\Gamma^3\right)}{27(\gamma + \Gamma)^4} \tag{8.58}$$

also shows sub-Poissonian behaviour.

8.3.2 High intensity limit: $\Omega \to \infty$

For high ac field intensities, the contribution of the chemical potencial of the collector is only reflected in the occupation probabilities. Particularly important for the phononic dynamics is the probability of finding the QD in its empty and lower states, since they limits phonon emission. As seen in

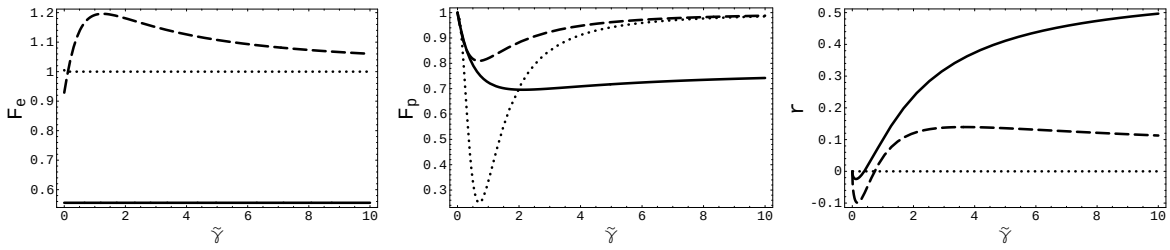

Fig. 8.7: Dependence on the relation between the relaxation and tunneling rates, $\tilde{\gamma} = \gamma/\Gamma$ for the different chemical potential configurations: $\mu < \varepsilon_{1,2}$ (solid), $\varepsilon_1 < \mu < \varepsilon_2$ (dashed), $\varepsilon_{1,2} < \mu$ (dotted) for $\Omega = 0.5$. Compare with Figs. **??** and **??**.

the previous regimes, the occupation of the empty state affects the sub-Poissonian statistics (expected for resonance fluorescence) by turning it to super-Poissonian values:

$$F_p = 1 + \frac{\gamma\Gamma_{\mathrm{R}}}{\left(2\Gamma_{\mathrm{L}} + \Gamma_{\mathrm{R}}\right)^2} \overset{\Gamma_{\mathrm{L}}=\Gamma_{\mathrm{R}}}{\longrightarrow} 1 + \frac{\gamma}{9\Gamma}. \tag{8.59}$$

Comparing to (8.30) and (8.45), the higher *unoccupation* of the QD involves a higher super-Poissonian character in the phononic statistics.

High intensities allow the emission of several phonons before the electron is extracted to the collector. Also, an electron tunneling from the emitter to the upper level, can be extracted to the collector from the lower level without the emission of a phonon. Then, the electron-phonon correlation tends to be negative. However, if Γ_{L} is small, $\rho_0 \approx 1 - 2\Gamma_{\mathrm{L}}/\Gamma_{\mathrm{R}} \gg \rho_1, \rho_2$, i. e., the probability of finding the QD empty is almost one. Then, the detection of phonons and electrons is restricted to short lapses of time, which makes the electron-phonon correlation positive:

$$r = \left(\Gamma_{\mathrm{R}} - 2\Gamma_{\mathrm{L}}\right)\sqrt{\frac{\gamma\Gamma_{\mathrm{R}}}{2\left(4\Gamma_{\mathrm{L}}^2 + \Gamma_{\mathrm{R}}^2\right)\left(4\Gamma_{\mathrm{L}}^2 + 4\Gamma_{\mathrm{R}}\Gamma_{\mathrm{L}} + \Gamma_{\mathrm{R}}\left(\gamma + \Gamma_{\mathrm{R}}\right)\right)}} \tag{8.60}$$

The third order coefficient

$$c_{03} = \frac{\gamma^3\Gamma_{\mathrm{L}}\Gamma_{\mathrm{R}}\left(\Gamma_{\mathrm{R}} - 2\Gamma_{\mathrm{L}}\right)}{4\left(2\Gamma_{\mathrm{L}} + \Gamma_{\mathrm{R}}\right)^5} \tag{8.61}$$

gives

$$\eta_p = 1 + \frac{3\gamma\Gamma_{\mathrm{R}}\left(8\Gamma_{\mathrm{L}}^2 - 2\left(\gamma - 4\Gamma_{\mathrm{R}}\right)\Gamma_{\mathrm{L}} + \Gamma_{\mathrm{R}}\left(\gamma + 2\Gamma_{\mathrm{R}}\right)\right)}{2\left(2\Gamma_{\mathrm{L}} + \Gamma_{\mathrm{R}}\right)^4}. \tag{8.62}$$

8.4 High Bias–Step Configuration.

A particularly interesting configuration in the high bias regime ($f_1 = f_2 = 0$) where the electron-phonon correlation is paradigmatic, needs *unusual* coupling to the leads: electrons can enter only to the upper level and tunnel out only from the lower one. That is: $\Gamma_{\mathrm{uL}} = \Gamma_{\mathrm{dR}} = \Gamma$, $\Gamma_{\mathrm{dL}} = \Gamma_{\mathrm{uR}} = 0$, cf. left diagram in Fig. 8.8. This selective coupling to the leads could be obtained by zero-dimensional contacts consisting in neighbour single-level QDs strongly coupled to the leads[179]. Then, if the level of the

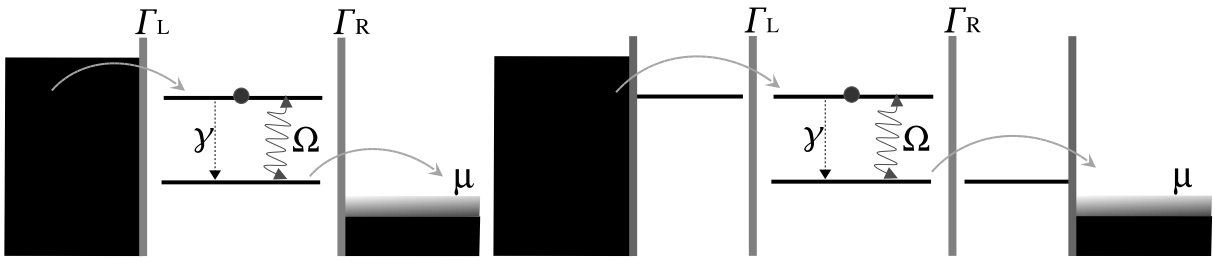

Fig. 8.8: Schematic diagrams of the *step* configuration.

left(right) dot is resonant with the upper(lower) level, the emitter(collector) will be uncoupled of the lower(upper) level, see right diagram in Fig. 8.8.

In the absence of driving field, an electron that enters the upper level can only be transferred to the collector after being relaxed by the emission of one phonon. This makes the electronic and phononic dynamics completely identical, giving sub-Poissonian Fano factors and maximal electron-phonon correlation (see Appendix A.4):

$$F_e = F_p = 1 - \frac{2\gamma\Gamma_{\rm L}\Gamma_{\rm R}(\gamma+\Gamma_{\rm L}+\Gamma_{\rm R})}{(\gamma\Gamma_{\rm R}+\Gamma_{\rm L}(\gamma+\Gamma_{\rm R}))^2} \tag{8.63}$$

$$r = 1. \tag{8.64}$$

The third cumulants give:

$$\eta_e = \eta_p = 1 - 6\gamma\Gamma_{\rm L}\Gamma_{\rm R}\frac{\left(\gamma^2+\Gamma_{\rm R}^2\right)\Gamma_{\rm L}^3+\left(\gamma+\Gamma_{\rm R}\right)\left(\gamma^2+\Gamma_{\rm R}\left(\gamma+\Gamma_{\rm R}\right)\right)\Gamma_{\rm L}^2+2\gamma^2\Gamma_{\rm R}^2\Gamma_{\rm L}+\gamma^2\Gamma_{\rm R}^2\left(\gamma+\Gamma_{\rm R}\right)}{\left(\gamma\Gamma_{\rm R}+\Gamma_{\rm L}\left(\gamma+\Gamma_{\rm R}\right)\right)^4} \tag{8.65}$$

The AC field allows the tunneling of an electron to the collector without having previously emitted a phonon as well as the emission of several phonons from the relaxation of the same electron. This un-correlates the electronic and phononic statistics.Considering $\Gamma_{\rm L} = \Gamma_{\rm R} = \Gamma$, for simplicity, we obtain for the Fano factors:

$$F_e = 1 - \frac{2\left(\gamma^4+4\Gamma\gamma^3+5\Gamma^2\gamma^2+3\Omega^2\gamma^2+2\Gamma^3\gamma+3\Gamma\Omega^2\gamma+2\Omega^4+4\Gamma^2\Omega^2\right)}{\left(2\gamma^2+3\Gamma\gamma+\Gamma^2+3\Omega^2\right)^2} \tag{8.66}$$

$$F_p = 1 - \frac{2\gamma\left(2\Gamma^4-\Omega^2\Gamma^2+\gamma^3\Gamma-\Omega^4+\gamma^2\left(4\Gamma^2-\Omega^2\right)+\gamma\left(5\Gamma^3+6\Omega^2\Gamma\right)\right)}{\Gamma\left(2\gamma^2+3\Gamma\gamma+\Gamma^2+3\Omega^2\right)^2} \tag{8.67}$$

From the Fano factor, it can be seen that the electrons obey sub-Poissonian statistics while the phonons become super-Poissonian for high enough field intensities. The driving field also contributes to make the electron-phonon correlation coefficient negative:

$$\begin{aligned} r = {} & \sqrt{\gamma}\left(\Gamma(\gamma+\Gamma)^3\left(2\gamma^2+\Gamma^2\right)-\gamma\Gamma(\gamma-11\Gamma)(\gamma+\Gamma)\Omega^2-\left(\gamma^2+\Gamma\gamma-4\Gamma^2\right)\Omega^4-\Omega^6\right) \\ & \times[\left((2\gamma+9\Gamma)\Omega^4+2\left(\gamma^3+10\Gamma^2\gamma+3\Gamma^3\right)\Omega^2+\Gamma(\gamma+\Gamma)^2\left(2\gamma^2+\Gamma^2\right)\right) \\ & \times\left(\Omega^2+\gamma(\gamma+\Gamma)\right)\left(\Omega^2+\Gamma(\gamma+\Gamma)\right)\left(5\Omega^4+2\left(3\gamma^2+6\Gamma\gamma-\Gamma^2\right)\Omega^2+(\gamma+\Gamma)^2\left(2\gamma^2+\Gamma^2\right)\right)]^{-1/2}. \end{aligned} \tag{8.68}$$

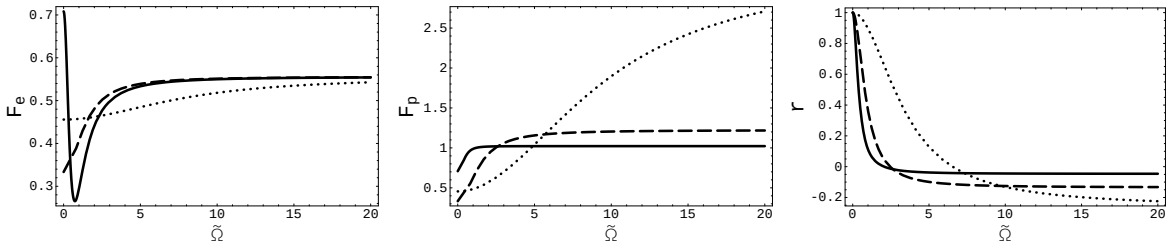

Fig. 8.9: **Step:** $\Gamma_{\rm L}=\Gamma_{\rm R}=\Gamma=1$, $\gamma=0.1$ (solid), $\gamma=1$ (dashed), $\gamma=10$ (dotted).

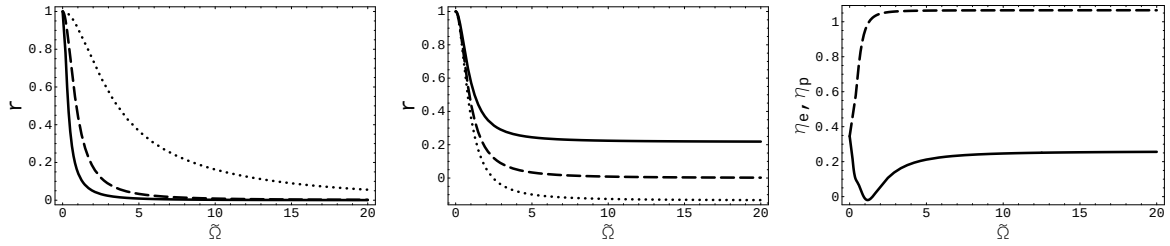

Fig. 8.10: **Step:** (a) For $\Gamma_{\rm R}=2\Gamma_{\rm R}$, the driving un-correlates the electronic and phononic statistics. $\Gamma_{\rm R}=1$, $\Gamma_{\rm L}=0.5$, $\gamma=0.1$ (solid), $\gamma=1$ (dashed), $\gamma=10$ (dotted). (b) The correlation can be tuned from negative to positive by the tunneling rate from the emitter: $\Gamma_{\rm L}=0.25$ (solid), $\Gamma_{\rm L}=0.5$ (dashed), $\Gamma_{\rm L}=1$ (dotted), with $\Gamma_{\rm R}=\gamma=1$. $\tilde{\Omega}=\Omega/\Gamma_{\rm R}$. η_e (solid) and η_p (dashed) as a function of the driving intensity for $\Gamma_{\rm L}=\Gamma_{\rm R}=\Gamma=1$ and $\gamma=0.1$. The ac field rapidly separates the electronic and phononic behaviours.

8.4.1 High intensity limit: $\Omega\to\infty$

An intense driving involves the delocalization of the electron between the upper and lower level, so it has the same probability of occupying each of them: $\rho_1=\rho_2=\Gamma_{\rm L}/(2\Gamma_{\rm L}+\Gamma_{\rm R})$. Then, the system resembles the single resonant level, for which one expects sub-Poissonian shot noise:

$$F_e=1-\frac{4\Gamma_{\rm L}\Gamma_{\rm R}}{(2\Gamma_{\rm L}+\Gamma_{\rm R})^2}. \tag{8.69}$$

The high probability of finding the QD empty, $\rho_0=\Gamma_{\rm R}/(2\Gamma_{\rm L}+\Gamma_{\rm R})$, kills the *resonance fluorescence like* phonon anti-bunching and the phononic statistics become super-Poissonian:

$$F_p=1+\frac{2\gamma\Gamma_{\rm R}}{(2\Gamma_{\rm L}+\Gamma_{\rm R})^2}. \tag{8.70}$$

As discussed in the previous section, the electron-phonon correlation is lost by the influence of the ac field. However, if the coupling to the leads is asymmetric and $\Gamma_{\rm R}>2\Gamma_{\rm L}$, the QD spends most of the time empty, so the detection of electrons and phonons is restricted to the short periods of time when the QD is occupied and r remains positive, cf. Fig. 8.10:

$$r=\frac{\sqrt{\gamma\Gamma_{\rm R}}\,(\Gamma_{\rm R}-2\Gamma_{\rm L})}{\sqrt{(4\Gamma_{\rm L}^2+\Gamma_{\rm R}^2)\,(4\Gamma_{\rm L}^2+4\Gamma_{\rm R}\Gamma_{\rm L}+\Gamma_{\rm R}\,(2\gamma+\Gamma_{\rm R}))}}. \tag{8.71}$$

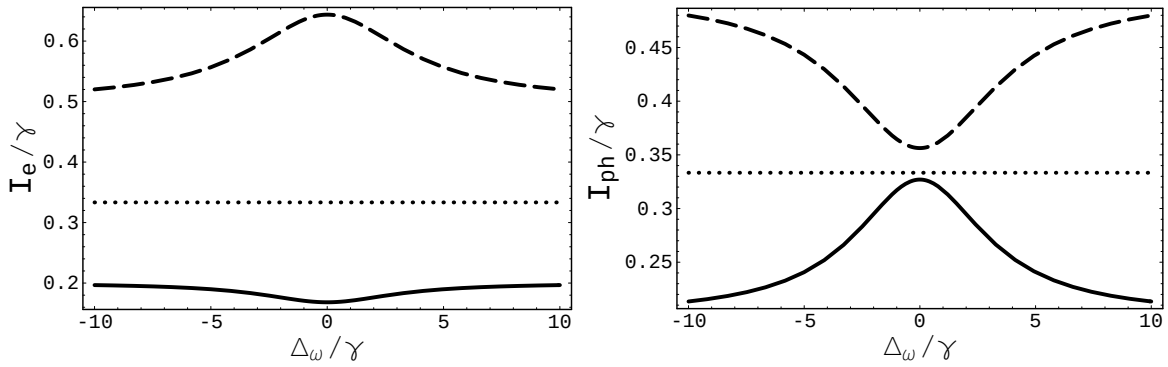

Fig. 8.11: **Step:** (a) Electronic and (b) phononic currents as a function of the detuning for $\Omega = 5\gamma$. The different curves correspond to different tunneling rates: $\Gamma = \gamma/2$ (solid), $\Gamma = \gamma$ (dotted) and $\Gamma = 2\gamma$ (dashed).

The third order cumulants:

$$c_{30} = \frac{8\Gamma_L^3\Gamma_R^3}{(2\Gamma_L+\Gamma_R)^5} \tag{8.72}$$

$$c_{03} = \frac{\gamma^3\Gamma_L\Gamma_R(\Gamma_R-2\Gamma_L)}{(2\Gamma_L+\Gamma_R)^5} \tag{8.73}$$

give

$$\eta_e = 1-\frac{12\Gamma_L\Gamma_R\left(4\Gamma_L^2+\Gamma_R^2\right)}{(2\Gamma_L+\Gamma_R)^4} \tag{8.74}$$

$$\eta_p = 1+\frac{6\gamma\Gamma_R\left(4\Gamma_L^2-2(\gamma-2\Gamma_R)\Gamma_L+\Gamma_R(\gamma+\Gamma_R)\right)}{(2\Gamma_L+\Gamma_R)^4} \tag{8.75}$$

8.4.2 Phonon relaxation rate probe

However, the special electron-phonon correlation properties are not the only interesting feature of this configuration. From a detailed study of the current, including a finite detuning:

$$c_{10} = \frac{\Gamma_L\Gamma_R\left(4\gamma\Delta_\omega^2+(\gamma+\Gamma_R)\left(\gamma^2+\Gamma_R\gamma+\Omega^2\right)\right)}{\Gamma_L(\gamma+\Gamma_R)(\gamma^2+2\Gamma_R\gamma+2\Omega^2+\Gamma_R^2+4\Delta_\omega^2)+\Gamma_R(4\gamma\Delta_\omega^2+(\gamma+\Gamma_R)(\gamma^2+\Gamma_R\gamma+\Omega^2))} \tag{8.76}$$

$$c_{01} = \frac{\gamma\Gamma_L\left(4\Gamma_R\Delta_\omega^2+(\gamma+\Gamma_R)\left(\Omega^2+\Gamma_R(\gamma+\Gamma_R)\right)\right)}{\Gamma_L(\gamma+\Gamma_R)(\gamma^2+2\Gamma_R\gamma+2\Omega^2+\Gamma_R^2+4\Delta_\omega^2)+\Gamma_R(4\gamma\Delta_\omega^2+(\gamma+\Gamma_R)(\gamma^2+\Gamma_R\gamma+\Omega^2))}, \tag{8.77}$$

it can be seen that their second derivative obey:

$$\frac{\partial^2 c_{10(01)}}{\partial\Delta_\omega^2} \propto \Gamma_R-\gamma, \tag{8.78}$$

which is reflected in a resonance to anti-resonance crossover, cf. Fig. 8.11. As a consequence, one can extract information on the sample-depending spontaneous phonon emission rate, γ, by externally modifying the tunneling couplings to the collector[180].

8.5 High Bias–Level-dependent tunneling

If the left and right barriers are equal, the tunneling events may differ on which level participates due to the concrete orbital distribution of each level. Then, one have $V_{\mathrm{L}i} = V_{\mathrm{R}i}$ for the couplings in (8.1) and electronic transport can be parametrized by the tunneling rates $\Gamma_{\mathrm{u}} = 2\pi|V_{\mathrm{L}2}|^2$ and $\Gamma_{\mathrm{d}} = 2\pi|V_{\mathrm{L}1}|^2$ when the electron tunnels to or from the upper or the lower level, respectively[171].

The equations of motion for the generating function and the density matrix (after setting $s_e = s_p = 1$) are then given by the matrix

$$M(s_e, s_p) = \begin{pmatrix} -\Gamma_{\mathrm{u}} - \Gamma_{\mathrm{d}} & s_e\Gamma_{\mathrm{d}} & 0 & 0 & s_e\Gamma_{\mathrm{u}} \\ \Gamma_{\mathrm{d}} & -\Gamma_{\mathrm{d}} & i\frac{\Omega}{2} & -i\frac{\Omega}{2} & s_p\gamma \\ 0 & i\frac{\Omega}{2} & -\frac{\Gamma_{\mathrm{u}}+\Gamma_{\mathrm{d}}+\gamma}{2} + i\Delta_\omega & 0 & -i\frac{\Omega}{2} \\ 0 & -i\frac{\Omega}{2} & 0 & -\frac{\Gamma_{\mathrm{u}}+\Gamma_{\mathrm{d}}+\gamma}{2} - i\Delta_\omega & i\frac{\Omega}{2} \\ \Gamma_{\mathrm{u}} & 0 & -i\frac{\Omega}{2} & i\frac{\Omega}{2} & -\gamma - \Gamma_{\mathrm{u}} \end{pmatrix} \tag{8.79}$$

in the same matrix form chosen to write (8.10).

The dependence on the level which is occupied introduces the effect of the driving field and phonon emission in the electronic current even in the high bias regime. If, for instance, the tunneling rate through the lower level is smaller than the one through the upper level, transport will be reduced by phonon emission. The electronic and phononic currents are, in the general case:

$$c_{10} = \frac{(\Gamma_{\mathrm{u}}+\Gamma_{\mathrm{d}})\left((\Gamma_{\mathrm{u}}+\Gamma_{\mathrm{d}})\left(\Gamma_{\mathrm{u}}\Gamma_{\mathrm{d}}+\Omega^2\right)+\gamma\Gamma_{\mathrm{d}}\left(\gamma+\Gamma_{\mathrm{d}}+2\Gamma_{\mathrm{u}}\right)\right)}{(\gamma+3\Gamma_{\mathrm{d}})\,\Gamma_{\mathrm{u}}^2+(\gamma^2+3\Omega^2+3\Gamma_{\mathrm{d}}\,(2\gamma+\Gamma_{\mathrm{d}}))\,\Gamma_{\mathrm{u}}+\Gamma_{\mathrm{d}}\,(2\gamma^2+2\Gamma_{\mathrm{d}}\gamma+3\Omega^2)} \tag{8.80}$$

$$c_{01} = \frac{\gamma\left((\Gamma_{\mathrm{u}}+\Gamma_{\mathrm{d}})\left(\Gamma_{\mathrm{u}}\Gamma_{\mathrm{d}}+\Omega^2\right)+\gamma\Gamma_{\mathrm{u}}\right)}{(\gamma+3\Gamma_{\mathrm{d}})\,\Gamma_{\mathrm{u}}^2+(\gamma^2+3\Omega^2+3\Gamma_{\mathrm{d}}\,(2\gamma+\Gamma_{\mathrm{d}}))\,\Gamma_{\mathrm{u}}+\Gamma_{\mathrm{d}}\,(2\gamma^2+2\Gamma_{\mathrm{d}}\gamma+3\Omega^2)}. \tag{8.81}$$

As expected, if $\Gamma_{\mathrm{d}} < \Gamma_{\mathrm{u}}$, the emission of phonons inhibits the transport of electrons. However, the oposite is not true: if $\Gamma_{\mathrm{u}} < \Gamma_{\mathrm{d}}$, electrons will rather tunnel through the lower level, thus avoiding phonon emission. These two limiting cases will be further analyzed bellow.

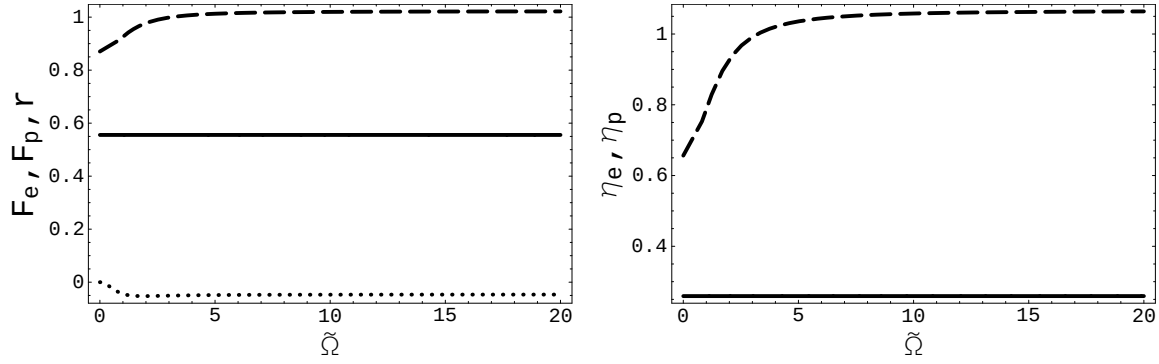

Fig. 8.12: **Level dependent tunneling:** (a) F_e (solid), F_p (dashed) and r (dotted) and (b) η_e (solid) and η_p (dashed) in resonance for $\Gamma_{\mathrm{d}} = \Gamma_{\mathrm{u}} = \Gamma = 5\gamma$. The field introduces negative correlation. $\tilde{\Omega} = \Omega/\Gamma$.

8.5.1 Undriven case.

In the absence of the driving field, the difference in the tunneling rates of each level is enough to define the sub- or super-Poissonian electronic statistics:

$$F_e = 1 + \frac{2\Gamma_u\left(\Gamma_d^3 + (\gamma+\Gamma_d)\Gamma_u^2\right) - 2\Gamma_d\left(\gamma^2 + (\gamma+\Gamma_u)(\gamma+4\Gamma_d)\Gamma_u\right)}{\left(2\gamma\Gamma_d + (\gamma+3\Gamma_d)\,\Gamma_u\right)^2}. \tag{8.82}$$

Interestingly, in the absence of phonon relaxation, the Fano factor diverges when one of the levels becomes uncoupled of the leads:

$$F_e(\gamma=0) = 1 + \frac{2}{9}\left(\frac{\Gamma_d}{\Gamma_u} + \frac{\Gamma_u}{\Gamma_d} - 4\right). \tag{8.83}$$

Phonon emission diminish this effect, contributing to recover the sub-Poissonian shot noise observed in the high bias regime, cf. Eq. (8.50):

$$F_e(\gamma\to\infty) = 1 - \frac{2\Gamma_d(\Gamma_d+\Gamma_u)}{\left(2\Gamma_d+\Gamma_u\right)^2}. \tag{8.84}$$

On the other hand, phononic statistics remain sub-Poissonian, independently of the configuration:

$$F_p = 1 - \frac{2\gamma\Gamma_d\Gamma_u\left(\gamma+2\Gamma_d+2\Gamma_u\right)}{\left(2\gamma\Gamma_d+(\gamma+3\Gamma_d)\,\Gamma_u\right)^2}. \tag{8.85}$$

The electron-phonon correlation coefficient

$$r = \frac{\sqrt{\gamma\Gamma_u}}{\sqrt{(\gamma+\Gamma_u)\left(\Gamma_d+\Gamma_u\right)\left((4\gamma^2+8\Gamma_u\gamma+9\Gamma_u^2)\,\Gamma_d^2+2\gamma\Gamma_u\left(\gamma+\Gamma_u\right)\Gamma_d+\gamma^2\Gamma_u^2\right)}} \tag{8.86}$$

$$\times\frac{\left((\gamma-\Gamma_d)\,\Gamma_u^3+(\gamma+\Gamma_d)^2\,\Gamma_u^2+\Gamma_d\left(2\gamma^2+3\Gamma_d\gamma-\Gamma_d^2\right)\Gamma_u+2\gamma\left(\gamma-\Gamma_d\right)\Gamma_d^2\right)}{\sqrt{2\left(\gamma+\Gamma_d\right)\Gamma_u^3+(\gamma^2+4\Gamma_d\gamma+\Gamma_d^2)\,\Gamma_u^2+2\Gamma_d\left(\gamma+\Gamma_d\right)^2\Gamma_u+2\gamma^2\Gamma_d^2}}. \tag{8.87}$$

shows how electrons and phonons can be uncorrelated by the manipulation of the tunneling rates. As a simple example, $r=0$ if $\Gamma_u=\Gamma_d=5\gamma$, cf. Fig. 8.12.

8.5.2 High intensity limit: $\Omega\to\infty$

As the driving field couples the two levels, it tends to annihilate the particular behaviour introduced by the different couplings to the leads. Thus, the high field intensity asymptotic electronic Fano factor and skewness recover the case where all tunneling rates are the same:

$$F_e = \frac{5}{9} \tag{8.88}$$

$$\eta_e = \frac{7}{27}. \tag{8.89}$$

Similarly, one can compare the phononic Fano factor

$$F_p = 1 + \frac{2\gamma}{9\left(\Gamma_d+\Gamma_u\right)} \tag{8.90}$$

with Eq. (8.59). As expected, electron-phonon correlation becomes negative:

$$r = -\sqrt{\frac{\gamma}{5\left(2\gamma+9\left(\Gamma_d+\Gamma_u\right)\right)}}. \tag{8.91}$$

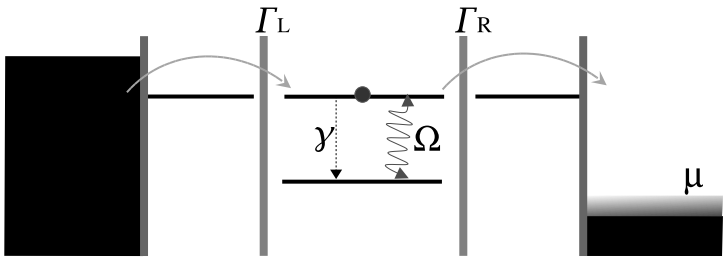

Fig. 8.13: Schematic diagram of the proposed setup for a level dependent tunneling configuration where $\Gamma_d \ll \Gamma_u$.

Finally, the third moment for the phononic statistics gives

$$\eta_p = 1 - \frac{2\gamma\left(\gamma - 9\Gamma_d - 9\Gamma_u\right)}{27\left(\Gamma_d + \Gamma_u\right)^2}. \tag{8.92}$$

8.5.3 $\Gamma_d \ll \Gamma_u$ limit:

The zero-dimentional contacts introduced in the previous section can also be employed to simulate energy-dependent tunneling. If both zero-dimentional contacts are aligned (by tuning the gate voltages of the left and right QDs) with the same level of the QD, transport through the other level will be strongly suppressed, cf. Fig. 8.13. Thus, the occupation of the off resonant level blocks the electronic current. This configuration can be analogue to double quantum dot systems where only one of them is coupled to the leads that have been proposed as qubits.

If the levels of the surrounding QDs are aligned with the upper level, in the absence of driving, as soon as the lower level is ocuppied (by the relaxation of an electron from the upper level), transport is canceled in a high bias version of dynamical channel blockade. Thus, electrons flow in bunches, while phononic transport is highly supressed.

Again, the driving field removes the blockade, producing finite electronic and phononic currents

$$\frac{c_e}{\Gamma_u} = \frac{c_p}{\gamma} = \frac{\Omega^2}{\gamma^2 + \gamma\Gamma_u + 3\Omega^2} \tag{8.93}$$

thus reducing the super-Poissonian electron noise

$$F_e = 1 + 2\frac{(\gamma + \Gamma_u)^2\left(\Gamma_u\gamma - \Omega^2\right) - 2\Omega^4}{(\gamma^2 + \gamma\Gamma_u + 3\Omega^2)^2}, \tag{8.94}$$

which becomes sub-Poissonian for high enough driving intensities. For low intensities, the phononic noise is sub-Poissonian, resembling the resonance fluorescence but, for $\Omega > \sqrt{2\Gamma_u(2\gamma + \Gamma_u)}$, the contribution of the empty state turns it super-Poissonian:

$$F_p = 1 - 2\gamma\Omega^2\frac{2\Gamma_u(2\gamma + \Gamma_u) - \Omega^2}{\Gamma_u\left(\gamma^2 + 3\Omega^2 + \gamma\Gamma_u\right)^2}. \tag{8.95}$$

It is interesting to note that, though the electronic and phononic mean counts are proportional, their variances are not, which is reflected in the electron-phonon correlation

$$c_{11} = \gamma\Omega^2\frac{\gamma\Gamma_u(\gamma + \Gamma_u)^2 - \Omega^2(\gamma^2 + \Gamma_u^2 + 6\gamma\Gamma_u) - \Omega^4}{(\gamma^2 + 3\Omega^2 + \gamma\Gamma_u)^3} \tag{8.96}$$

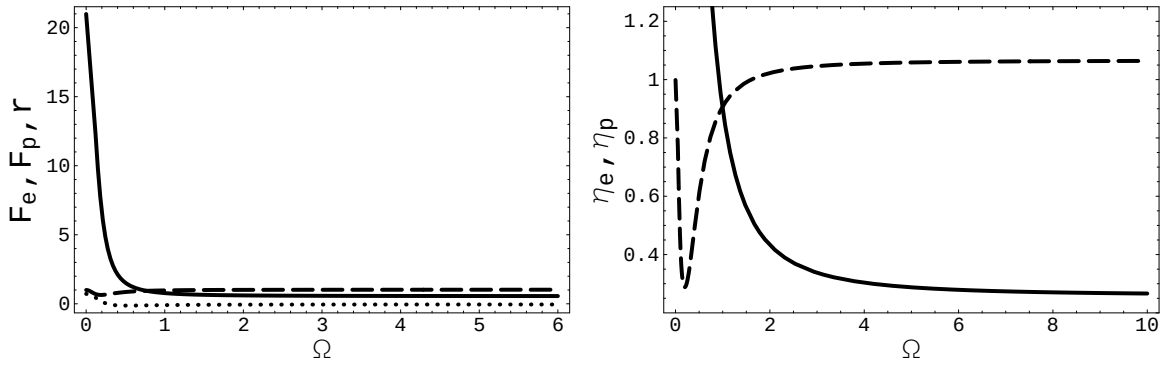

Fig. 8.14: **Level dependent tunneling** (a) F_e (solid), F_p (dashed) and r (dotted) and (b) η_e (solid) and η_p (dashed) as a function of the driving intensity in resonance for $\gamma = 0.1$, $\Gamma_{\rm d} = 10^{-5}$ and $\Gamma_{\rm u} = 1$.

that gives $r < 1$. The third cummulants give, for $\Omega = 0$:

$$\eta_e = \frac{\gamma^2 + 6\Gamma_{\rm u}^2(\gamma + \Gamma_{\rm u})}{\gamma^2} \tag{8.97}$$

$$\eta_p = 1. \tag{8.98}$$

8.5.4 $\Gamma_{\rm u} \ll \Gamma_{\rm d}$ limit:

This case is similar to the previous one with the difference that the contribution of phonon emission has the opposite effect: the upper level is very weakly coupled to the leads so its population quenches the electronic current, cf. Fig. 8.15. Therefore, relaxation by phonon emission opens the lower level channel.

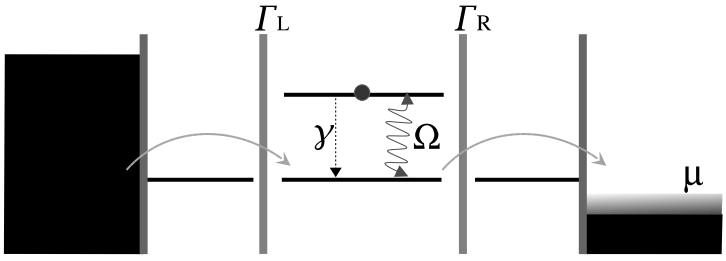

Fig. 8.15: Schematic diagram of the proposed setup for a level dependent tunneling configuration where $\Gamma_{\rm u} \ll \Gamma_{\rm d}$.

In the absence of driving, the electrons tend to be transferred through the lower level (and the system is reduced to the single resonant level), so there is no chance for phonon emission. The driving

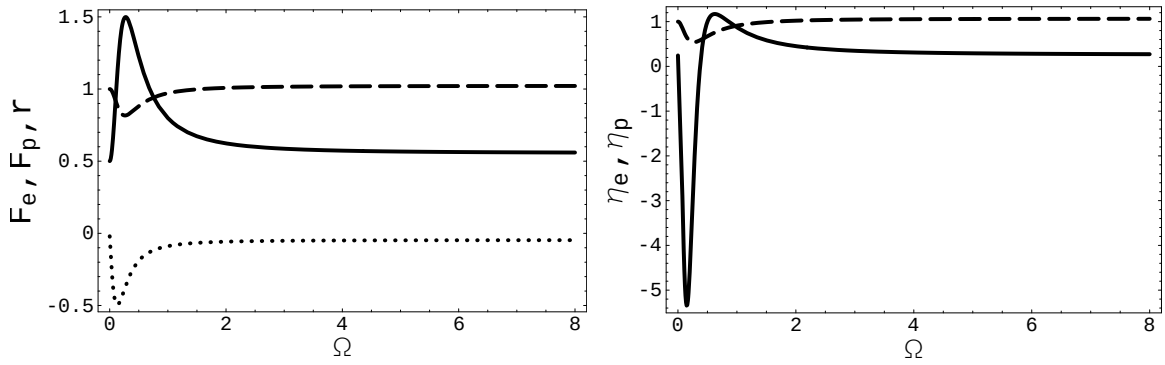

Fig. 8.16: **Level dependent tunneling** (a) F_e (solid), F_p (dashed) and r (dotted) and (b) η_e (solid) and η_p (dashed) as a function of the driving intensity in resonance for $\gamma = 0.1$, $\Gamma_{\rm u} = 10^{-5}$ and $\Gamma_{\rm d} = 1$.

populates the upper level giving a finite probaility to phonons to be emitted:

$$c_e = \frac{\Gamma_{\rm d}\left(\gamma^2 + \gamma\Gamma_{\rm d} + \Omega^2\right)}{2\gamma^2 + 2\Gamma_{\rm d}\gamma + 3\Omega^2} \tag{8.99}$$

$$c_p = \frac{\gamma\Omega^2}{2\gamma^2 + 2\Gamma_{\rm d}\gamma + 3\Omega^2}. \tag{8.100}$$

The ac field modifies the electronic Fano factor typical from the single resonant level, $F_e = 1/2$, without changing its sub-Poissonian character but for $\Gamma_{\rm d} > \sqrt{2}\Omega \gg \gamma$:

$$F_e = 1 - \frac{2\left(\gamma^2(\gamma+\Gamma_{\rm d})^2 + \Omega^2\left(3\gamma^2 - \Gamma_{\rm d}^2\right) + 2\Omega^4\right)}{\left(2\gamma^2 + 2\Gamma_{\rm d}\gamma + 3\Omega^2\right)^2}. \tag{8.101}$$

The phononic Fano factor

$$F_p = 1 + \frac{2\gamma\Omega^2\left(\gamma^2 - 5\Gamma_{\rm d}\gamma - 2\Gamma_{\rm d}^2 + \Omega^2\right)}{\Gamma_{\rm d}\left(2\gamma^2 + 2\Gamma_{\rm d}\gamma + 3\Omega^2\right)^2} \tag{8.102}$$

can be turned from sub-Poissonian to super-Poissonian by increasing the field intensity if $\Gamma_{\rm d} > \frac{1}{4}(\sqrt{33} - 5)\gamma$. The electron-phonon correlation is always negative:

$$c_{11} = -\frac{\gamma\Omega^2\left(2\gamma\Gamma_{\rm d}^3 + \left(8\gamma^2 + \Omega^2\right)\Gamma_{\rm d}^2 + \left(6\gamma^3 + 4\Omega^2\gamma\right)\Gamma_{\rm d} + \Omega^2\left(\gamma^2 + \Omega^2\right)\right)}{\left(2\gamma^2 + 2\Gamma_{\rm d}\gamma + 3\Omega^2\right)^3}. \tag{8.103}$$

The third electronic cumulant varies between $\eta_e = \frac{1}{4}$, for $\Omega = 0$, and $\eta_e = \frac{7}{27}$ for the high intensity limit, but it shows a deep minimum for low voltages where it is negative, cf. Fig. 8.16. The phononic one is removed by the ac field from $\eta_p = 1$ to the asymptotic limit:

$$\eta_p = 1 - \frac{2\gamma(\gamma - 9\Gamma_{\rm d})}{27\Gamma_{\rm d}^2}, \tag{8.104}$$

for $\Omega \to \infty$. Then, the skewness of the phononic statistics can be tuned by the strength of the tunneling couplings.

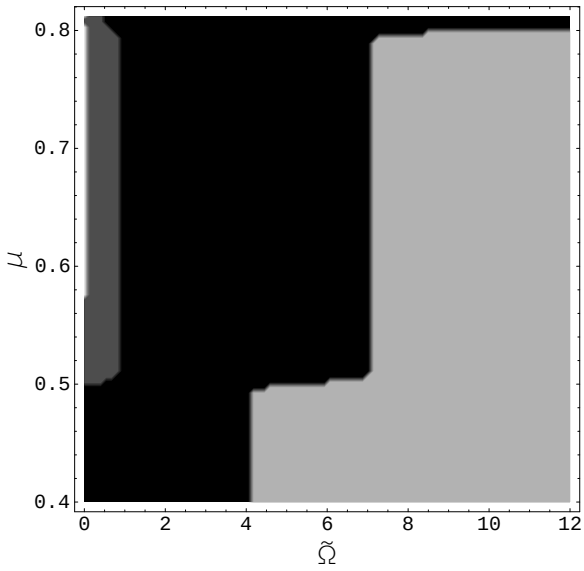

Fig. 8.17: Color plot showing the different regions where one can find $F_e, F_{ph} \geq 1$ (white, appearing only for $\tilde{\Omega} = 0$), $F_e < 1, F_{ph} \geq 1$ (light grey), $F_e \geq 1, F_{ph} < 1$ (dark grey) and $F_e, F_{ph} < 1$ (black) by tuning μ and $\tilde{\Omega} = \Omega/\Gamma$, for $\Gamma = \Gamma_{\rm L} = \Gamma_{\rm R} = \gamma$.

8.6 Conclusions

A method for extracting the simultaneous counting statistics for electrons tunneling through a two levels driven QD and phonons emitted in the intradot relaxation processes is presented. It allows to calculate all the electronic and phononic cumulants well as the correlation between fermionic and bosonic statistics, showing how they affect one to the other. For instance, phonon emission reduce the super-Poissonian electronic shot noise in the dynamical channel blockade regime, while the sub-Poissonian statistics for spontaneously emitted bosons form a driven two level system (resonance fluorescence) is turned to super-Poissonian (typical for thermal particles obeying Bose-Einstein statistics) by effect of electronic transport.

It is shown how the character of the electronic and phononic fluctuations can be manipulated by tuning the external parameters like the intensity of the ac field, the chemical potencial of the right lead or the tunneling barriers. By this kind of measurements, information about electron relaxation times can be obtained. As shown in Fig. 8.17, all the combinations of sub- and super-Poissonian noise can be selected this way.

The calculation of the electron-phonon correlations also helps to understand the dynamical behaviour of each concrete configuration and the importance of relaxation processes in transport properties. In this sense, a configuration with a maximal electron-phonon correlation is proposed. Additionally, this configuration can serve as a probe for the phononic emission rate.

Apendix A

Moments of the electron-phonon counting statistics

In this appendix, the moments c_{mn} calculated in chapter 8 are presented for completity and in order to give there a clearer explanation of the physical processes.

A.1 Low Bias Regime

The first coefficients from the Taylor expansion are, for electrons:

$$c_{10} = \frac{\Omega^2\Gamma_{\rm L}\Gamma_{\rm R}}{\left(\gamma^2+2\Omega^2\right)\left(\Gamma_{\rm L}+\Gamma_{\rm R}\right)}x+O\left(x^2\right) \tag{A.1}$$

$$c_{20} = -\frac{\Omega^2\Gamma_{\rm L}^2\Gamma_{\rm R}^2\left(\Omega^2\left(\gamma^2+2\Omega^2\right)-\gamma(\gamma-2\Omega)(\gamma+2\Omega)\left(\Gamma_{\rm L}+\Gamma_{\rm R}\right)\right)}{2\left(\left(\gamma^2+2\Omega^2\right)^3\left(\Gamma_{\rm L}+\Gamma_{\rm R}\right)^3\right)}x^2+O\left(x^3\right) \tag{A.2}$$

$$\begin{aligned} c_{30} = {} & \frac{\Omega^2\Gamma_{\rm L}^3\Gamma_{\rm R}^3x^3}{4\left(\gamma^2+2\Omega^2\right)^5\left(\Gamma_{\rm L}+\Gamma_{\rm R}\right)^5}\left(2\left(\gamma^2+2\Omega^2\right)^2\Omega^4\right. \\ & \left.+\gamma\left(\Gamma_{\rm L}+\Gamma_{\rm R}\right)\left(24\Omega^6+6\gamma^2\Omega^4-3\gamma^4\Omega^2+\gamma\left(\gamma^4-10\Omega^2\gamma^2+48\Omega^4\right)\left(\Gamma_{\rm L}+\Gamma_{\rm R}\right)\right)\right)+O\left(x^4\right) \end{aligned} \tag{A.3}$$

and, for phonons:

$$c_{01} = \frac{\gamma\Omega^2}{\gamma^2+2\Omega^2}-\frac{\gamma\Omega^2\Gamma_{\rm R}\left(\Omega^2+3\gamma\left(\Gamma_{\rm L}+\Gamma_{\rm R}\right)\right)}{2\left(\left(\gamma^2+2\Omega^2\right)^2\left(\Gamma_{\rm L}+\Gamma_{\rm R}\right)\right)}x+O\left(x^2\right) \tag{A.4}$$

$$\begin{aligned} c_{02} = {} & -\frac{3\gamma^3\Omega^4}{\left(\gamma^2+2\Omega^2\right)^3} \\ & -\frac{\gamma^2\Omega^4\Gamma_{\rm R}}{\left(\gamma^2+2\Omega^2\right)^3}\left(\frac{\gamma(\gamma^2-16\Omega^2)}{4\left(\gamma^2+2\Omega^2\right)\left(\Gamma_{\rm L}+\Gamma_{\rm R}\right)}-\frac{\Omega^2}{4(\Gamma_{\rm L}+\Gamma_{\rm R})^2}-\frac{23\gamma^2-8\Omega^2}{2(\gamma^2+2\Omega^2)}\right)x+O\left(x^2\right). \end{aligned} \tag{A.5}$$

$$c_{03} = \frac{4\gamma^3\Omega^6\left(4\gamma^2-\Omega^2\right)}{\left(\gamma^2+2\Omega^2\right)^5}+O\left(x\right). \tag{A.6}$$

The electron-phonon correlation is given by:

$$c_{11} = \frac{\gamma\Omega^2\Gamma_{\rm L}\Gamma_{\rm R}\left(\gamma\left(\gamma^2-10\Omega^2\right)\left(\Gamma_{\rm L}+\Gamma_{\rm R}\right)-\Omega^2\left(\gamma^2+2\Omega^2\right)\right)}{2\left(\gamma^2+2\Omega^2\right)^3\left(\Gamma_{\rm L}+\Gamma_{\rm R}\right)^2}x+O\left(x^2\right) \tag{A.7}$$

A.1.1 High Intensity Limit

$$c_{30} = \frac{64x^3\Gamma_L^3\Gamma_R^3}{(4\Gamma_L+(4-x)\Gamma_R)^5} \tag{A.8}$$

$$c_{03} = -\frac{x\gamma^3\Gamma_R\,(4\Gamma_L+(4-3x)\Gamma_R)\,(2\Gamma_L+(2-x)\Gamma_R)}{(4\Gamma_L+(4-x)\Gamma_R)^5} \tag{A.9}$$

A.2 Dynamical Channel Blockade regime.

$$c_{10} = \frac{2\Omega^2\Gamma_L\Gamma_R}{\Gamma_R\,(\gamma^2+2\Gamma_R\gamma+3\Omega^2+\Gamma_R^2)+\Gamma_L\,(2\gamma^2+3\Gamma_R\gamma+4\Omega^2+\Gamma_R^2)} \tag{A.10}$$

$$c_{01} = \frac{\gamma\Omega^2\,(2\Gamma_L+\Gamma_R)}{\Gamma_R\,(\gamma^2+2\Gamma_R\gamma+3\Omega^2+\Gamma_R^2)+\Gamma_L\,(2\gamma^2+3\Gamma_R\gamma+4\Omega^2+\Gamma_R^2)} \tag{A.11}$$

Considering, for simplicity, the case $\Gamma_L=\Gamma_R=\Gamma$, the following moments become:

$$c_{20} = -\frac{2\Gamma\Omega^2\left(4\Omega^4+\left(2\gamma^2+15\Gamma\gamma+9\Gamma^2\right)\Omega^2-\Gamma(\gamma+\Gamma)^2(3\gamma+2\Gamma)\right)}{(7\Omega^2+(\gamma+\Gamma)(3\gamma+2\Gamma))^3} \tag{A.12}$$

$$c_{02} = -\frac{3\gamma^2\Omega^4\left(22\Gamma^2+28\gamma\Gamma-\Omega^2\right)}{\Gamma\,(7\Omega^2+(\gamma+\Gamma)(3\gamma+2\Gamma))^3} \tag{A.13}$$

$$c_{11} = -\frac{\gamma\Omega^2\left(10\Omega^4+\left(6\gamma^2+101\Gamma\gamma+71\Gamma^2\right)\Omega^2-3\Gamma(\gamma+\Gamma)^2(3\gamma+2\Gamma)\right)}{(7\Omega^2+(\gamma+\Gamma)(3\gamma+2\Gamma))^3} \tag{A.14}$$

and

$$\begin{aligned} c_{30} = {} & \frac{2\Gamma\Omega^2}{(7\Omega^2+(\gamma+\Gamma)(3\gamma+2\Gamma))^5}\left(\Gamma^2(\gamma+\Gamma)^4(3\gamma+2\Gamma)^2\right. \\ & -2\Gamma(\gamma+\Gamma)^2(3\gamma+2\Gamma)\left(3\gamma^2+20\Gamma\gamma+13\Gamma^2\right)\Omega^2 \\ & \left.+\left(8\gamma^4+62\Gamma\gamma^3+545\Gamma^2\gamma^2+700\Gamma^3\gamma+241\Gamma^4\right)\Omega^4+4\left(8\gamma^2+46\Gamma\gamma+29\Gamma^2\right)\Omega^6+32\Omega^8\right) \end{aligned} \tag{A.15}$$

$$c_{03} = \frac{3\gamma^3\Omega^6\left(-5\Omega^4-\left(3\gamma^2+110\Gamma\gamma+503\Gamma^2\right)\Omega^2+\Gamma\left(3\gamma^3+1396\Gamma\gamma^2+2171\Gamma^2\gamma+850\Gamma^3\right)\right)}{\Gamma^2\,(7\Omega^2+(\gamma+\Gamma)(3\gamma+2\Gamma))^5} \tag{A.16}$$

A.2.1 Undriven case.

Considering phonon emission and for small x, one can expand the first coefficients for the electronic statistics:

$$c_{10} = \frac{2\Gamma_L\Gamma_R\,(\gamma+\Gamma_R)\,x}{\Gamma_R\,(\gamma+\Gamma_R)+\Gamma_L\,(2\gamma+\Gamma_R)}+O\left(x^2\right) \tag{A.17}$$

$$c_{20} = \frac{2\Gamma_L^2\Gamma_R^2\,(\gamma+\Gamma_R)\,x}{(\Gamma_R\,(\gamma+\Gamma_R)+\Gamma_L\,(2\gamma+\Gamma_R))^2}+O\left(x^2\right) \tag{A.18}$$

$$c_{30} = \frac{2\Gamma_L^3\Gamma_R^3\,(\gamma+\Gamma_R)\,x}{(\Gamma_R\,(\gamma+\Gamma_R)+\Gamma_L\,(2\gamma+\Gamma_R))^3}+O\left(x^2\right), \tag{A.19}$$

phononic statistics:

$$c_{01} = \frac{\gamma\Gamma_L\Gamma_R x}{\Gamma_R(\gamma+\Gamma_R)+\Gamma_L(2\gamma+\Gamma_R)} + O\left(x^2\right) \tag{A.20}$$

$$c_{02} = -\frac{\gamma^2\Gamma_L^2\Gamma_R^2(\gamma+2\Gamma_L+2\Gamma_R)x^2}{(\Gamma_R(\gamma+\Gamma_R)+\Gamma_L(2\gamma+\Gamma_R))^3} + O\left(x^3\right) \tag{A.21}$$

$$c_{03} = -\frac{\gamma^2\Gamma_L^2\Gamma_R^2(\gamma+2\Gamma_L+2\Gamma_R)x^2}{(\Gamma_R(\gamma+\Gamma_R)+\Gamma_L(2\gamma+\Gamma_R))^3} + O\left(x^3\right). \tag{A.22}$$

and for electron-phonon correlations:

$$c_{11} = \frac{\gamma\Gamma_L\Gamma_R(\gamma+\Gamma_R)(2\Gamma_L+\Gamma_R)x}{(\Gamma_R(\gamma+\Gamma_R)+\Gamma_L(2\gamma+\Gamma_R))^2} + O\left(x^2\right) \tag{A.23}$$

A.2.2 High intensity limit

$$c_{30} = \frac{64(x+1)^3\Gamma_L^3\Gamma_R^3}{(4\Gamma_L+(3-x)\Gamma_R)^5} \tag{A.24}$$

$$c_{03} = -\frac{(x+1)\gamma^3\Gamma_R\left(8\Gamma_L^2+2(3-5x)\Gamma_R\Gamma_L+\left(3x^2-4x+1\right)\Gamma_R^2\right)}{(4\Gamma_L-(x-3)\Gamma_R)^5}. \tag{A.25}$$

A.3 High Bias regime.

Electron statistics:

$$c_{10} = \frac{2\Gamma_L\Gamma_R}{2\Gamma_L+\Gamma_R} \tag{A.26}$$

$$c_{20} = -\frac{4\Gamma_L^2\Gamma_R^2}{(2\Gamma_L+\Gamma_R)^3} \tag{A.27}$$

$$c_{30} = \frac{16\Gamma_L^3\Gamma_R^3}{(2\Gamma_L+\Gamma_R)^5}. \tag{A.28}$$

Phonon statistics:

$$c_{01} = \frac{\gamma\Gamma_L\left(2\Omega^2+\Gamma_R(\gamma+2\Gamma_R)\right)}{(2\Gamma_L+\Gamma_R)(\gamma^2+2\Omega^2+3\gamma\Gamma_R+2\Gamma_R^2)}. \tag{A.29}$$

The expressions for the second order moments are quite lengthy, so considering the simpler case, $\Gamma_L = \Gamma_R = \Gamma$:

$$c_{01} = \frac{\gamma\Gamma(\gamma+2\Gamma)+2\gamma\Omega^2}{3(\gamma+\Gamma)(\gamma+2\Gamma)+6\Omega^2} \tag{A.30}$$

$$c_{02} = -\frac{\gamma^2\left(-2\Omega^4+\left(-\gamma^2+17\Gamma\gamma+14\Gamma^2\right)\Omega^2+\Gamma(\gamma+2\Gamma)^2(\gamma+4\Gamma)\right)\left(\gamma\Gamma+2\left(\Gamma^2+\Omega^2\right)\right)}{27\Gamma\left(2\Omega^2+(\gamma+\Gamma)(\gamma+2\Gamma)\right)^3}, \tag{A.31}$$

A.3.1 Undriven Case

Statistics for phonons:

$$c_{01} = \frac{\gamma\Gamma_L\Gamma_R}{(\gamma+\Gamma_R)(2\Gamma_L+\Gamma_R)} \overset{\Gamma_L=\Gamma_R}{\longrightarrow} \frac{\gamma\Gamma}{3(\gamma+\Gamma)} \tag{A.32}$$

$$c_{02} = -\frac{\gamma^2\Gamma_L^2\Gamma_R^2(\gamma+2\Gamma_L+2\Gamma_R)}{(\gamma+\Gamma_R)^3(2\Gamma_L+\Gamma_R)^3} \overset{\Gamma_L=\Gamma_R}{\longrightarrow} -\frac{\gamma^2\Gamma(\gamma+4\Gamma)}{27\Gamma(\gamma+\Gamma)^3} \tag{A.33}$$

$$c_{03} = \frac{\gamma^3\Gamma_L^3\Gamma_R^3\left(2\gamma^2+8\Gamma_L^2+7\Gamma_R(\gamma+\Gamma_R)+2\Gamma_L(3\gamma+7\Gamma_R)\right)}{(\gamma+\Gamma_R)^5(2\Gamma_L+\Gamma_R)^5}, \tag{A.34}$$

A.4 High Bias-Step Configuration

In the absence of driving field, an electron that enters the upper level can only be transferred to the collector after being relaxed by the emission of one phonon. This makes the electronic and phononic dynamics completely identical:

$$c_{10} = c_{01} = \frac{\gamma\Gamma_L\Gamma_R}{\gamma\Gamma_L+\gamma\Gamma_R+\Gamma_L\Gamma_R} \tag{A.35}$$

$$c_{20} = c_{02} = -\frac{\gamma^2\Gamma_L^2\Gamma_R^2(\gamma+\Gamma_L+\Gamma_R)}{(\gamma\Gamma_L+\gamma\Gamma_R+\Gamma_L\Gamma_R)^3} \tag{A.36}$$

$$c_{11} = \gamma\Gamma_L\Gamma_R\frac{\gamma^2\Gamma_L^2+\gamma^2\Gamma_R^2+\Gamma_L^2\Gamma_R^2}{(\gamma\Gamma_L+\gamma\Gamma_R+\Gamma_L\Gamma_R)^3} \tag{A.37}$$

$$c_{30} = c_{03} = \gamma^3\Gamma_L^3\Gamma_R^3\frac{2\left(\gamma^2+\Gamma_L^2+\Gamma_R^2\right)+3(\gamma\Gamma_L+\gamma\Gamma_R+\Gamma_L\Gamma_R)}{(\gamma\Gamma_L+\gamma\Gamma_R+\Gamma_L\Gamma_R)^5} \tag{A.38}$$

In the presence of an ac field the first moments are:

$$c_{10} = \frac{\Gamma_L\Gamma_R\left(\gamma^2+\Gamma_R\gamma+\Omega^2\right)}{\Gamma_R(\gamma^2+\Gamma_R\gamma+\Omega^2)+\Gamma_L(\gamma^2+2\Gamma_R\gamma+2\Omega^2+\Gamma_R^2)} \tag{A.39}$$

$$c_{01} = \frac{\gamma\Gamma_L\left(\Omega^2+\Gamma_R(\gamma+\Gamma_R)\right)}{\Gamma_R(\gamma^2+\Gamma_R\gamma+\Omega^2)+\Gamma_L(\gamma^2+2\Gamma_R\gamma+2\Omega^2+\Gamma_R^2)} \tag{A.40}$$

$$\begin{aligned} c_{20} = {} & \frac{c_{10}2\Gamma_L\Gamma_R\left(2\gamma^2+2\Gamma_R\gamma+\Omega^2\right)}{(\gamma+\Gamma_R)\left(\Gamma_R(\gamma^2+\Gamma_R\gamma+\Omega^2)+\Gamma_L(\gamma^2+2\Gamma_R\gamma+2\Omega^2+\Gamma_R^2)\right)} \\ & -c_{10}^2\frac{\gamma^3+2\Omega^2\gamma+\Gamma_R\left(7\gamma^2+7\Gamma_R\gamma+4\Omega^2+\Gamma_R^2\right)+\Gamma_L\left(5\gamma^2+4\Omega^2+5\Gamma_R(2\gamma+\Gamma_R)\right)}{(\gamma+\Gamma_R)\left(\Gamma_R(\gamma^2+\Gamma_R\gamma+\Omega^2)+\Gamma_L(\gamma^2+2\Gamma_R\gamma+2\Omega^2+\Gamma_R^2)\right)} \end{aligned} \tag{A.41}$$

$$\begin{aligned} c_{02} = {} & \frac{c_{01}\gamma\left((\gamma+\Gamma_R)\Omega^2+2\Gamma_L\left(\Omega^2+2\Gamma_R(\gamma+\Gamma_R)\right)\right)}{(\gamma+\Gamma_R)\left(\Gamma_R(\gamma^2+\Gamma_R\gamma+\Omega^2)+\Gamma_L(\gamma^2+2\Gamma_R\gamma+2\Omega^2+\Gamma_R^2)\right)} \\ & -c_{01}^2\frac{\gamma^3+2\Omega^2\gamma+\Gamma_R\left(7\gamma^2+7\Gamma_R\gamma+4\Omega^2+\Gamma_R^2\right)+\Gamma_L\left(5\gamma^2+4\Omega^2+5\Gamma_R(2\gamma+\Gamma_R)\right)}{(\gamma+\Gamma_R)\left(\Gamma_R(\gamma^2+\Gamma_R\gamma+\Omega^2)+\Gamma_L(\gamma^2+2\Gamma_R\gamma+2\Omega^2+\Gamma_R^2)\right)} \end{aligned} \tag{A.42}$$

and, considering $\Gamma_L=\Gamma_R=\Gamma$, for simplicity:

$$c_{11} = \frac{\gamma\left(\Gamma(\gamma+\Gamma)^3\left(2\gamma^2+\Gamma^2\right)-\gamma(\gamma-11\Gamma)\Gamma(\gamma+\Gamma)\Omega^2-\left(\gamma^2+\Gamma\gamma-4\Gamma^2\right)\Omega^4-\Omega^6\right)}{\left(3\Omega^2+(\gamma+\Gamma)(2\gamma+\Gamma)\right)^3}. \tag{A.43}$$

Apendix B

Single resonant level shot noise

Let consider a one level quantum dot connected to the left lead (with infinite chemical potential) by a tunneling rate $\Gamma_{\rm L}$ and to the right one with $f\Gamma_{\rm R}$, where f is the Fermi function describing the right lead. Written in matricial form, the density matrix is represented by $(\rho_{00}, \rho_{11})^T$, where $|0\rangle$ and $|1\rangle$ denote the empty and one electron states. The density matrix is then

$$\begin{pmatrix} \dot{\rho}_{00} \\ \dot{\rho}_{11} \end{pmatrix} = \begin{pmatrix} -\Gamma_{\rm L} - (1-f)\Gamma_{\rm R} & f\Gamma_{\rm R} \\ \Gamma_{\rm L} + (1-f)\Gamma_{\rm R} & -f\Gamma_{\rm R} \end{pmatrix} \begin{pmatrix} \rho_{00} \\ \rho_{11} \end{pmatrix}, \tag{B.1}$$

with the stationary solution

$$\rho_{00} = \frac{f\Gamma_{\rm R}}{\Gamma_{\rm L}+\Gamma_{\rm R}} \tag{B.2}$$

$$\rho_{11} = \frac{\Gamma_{\rm L} + (1-f)\Gamma_{\rm R}}{\Gamma_{\rm L}+\Gamma_{\rm R}}. \tag{B.3}$$

The generating function satisfies the equation of motion, $\dot{G}(t, s_e) = \mathcal{M}(s_e)G(t, s_e)$, where:

$$M(s_e) = \begin{pmatrix} -\Gamma_{\rm L} - (1-f)\Gamma_{\rm R} & f\Gamma_{\rm R}s_e \\ \Gamma_{\rm L} + \frac{1}{s_e}(1-f)\Gamma_{\rm R} & -f\Gamma_{\rm R} \end{pmatrix}.$$

Following the proccedure shown in chapter 8, one can obtain the moments of the distribution function. The first ones, that allow to calculate the mean current and shot noise, are the first moments are:

$$c_1 = \frac{f\Gamma_L\Gamma_R}{\Gamma_L+\Gamma_R} \tag{B.4}$$

$$c_2 = -\frac{c_1^2}{\Gamma_L+\Gamma_R}. \tag{B.5}$$

Thus, the Fano factor is[176]:

$$F = 1 - \frac{2f\Gamma_{\rm L}\Gamma_{\rm R}}{(\Gamma_{\rm L}+\Gamma_{\rm R})^2} \tag{B.6}$$

with the limiting cases[151]:

$$F(f=1) = \frac{\Gamma_{\rm L}^2+\Gamma_{\rm R}^2}{(\Gamma_{\rm L}+\Gamma_{\rm R})^2} \overset{\Gamma_{\rm L}=\Gamma_{\rm R}}{\longrightarrow} \frac{1}{2} \tag{B.7}$$

$$F(f=0) = 1. \tag{B.8}$$

Apendix C

Bessel functions

Here, some properties of the Bessel functions of the first kind that are useful for the analytical treatment of photon-assisted processes are presented, considering real aguments, α.

Limit for $\alpha \to 0$:

$$J_\nu(\alpha) \sim \frac{1}{\nu!}\left(\frac{\alpha}{2}\right)^\nu \quad \text{when} \tag{C.1}$$

Ascending series:

$$J_\nu(\alpha) = \left(\frac{\alpha}{2}\right)^\nu \sum_{k=0}^{\infty} \left(-\frac{1}{4}\right)^k \frac{1}{k!\nu!} \tag{C.2}$$

Recurrence relation:

$$J_0'(\alpha) = -J_1(\alpha) \tag{C.3}$$

Generating function:

$$e^{\frac{1}{2}\alpha(t-1)/t} = \sum_{k=-\infty}^{\infty} t^k J_k(\alpha) \tag{C.4}$$

Upper bounds:

$$|J_\nu(\alpha)| \leq 1 \quad (\nu \geq 0), \quad |J_\nu(\alpha)| \leq \frac{1}{\sqrt{2}} \quad (\nu \geq 1) \tag{C.5}$$

Normalization:

$$1 = J_0^2(\alpha) + 2\sum_{k=1}^{\infty} J_k^2(\alpha) \tag{C.6}$$

Asymptotic limits for $|\alpha| \to \infty$:

$$J_\nu(\alpha) = \sqrt{\frac{2}{\pi\alpha}}\cos(\alpha - \frac{\nu\pi}{2} - \frac{\pi}{4}) + O(\alpha^{-1}) \quad \text{when} \tag{C.7}$$

Asymptotic limits for $\nu \to \infty$:

$$J_\nu(\alpha) \sim \frac{1}{\sqrt{2\pi\alpha}}\left(\frac{e\alpha}{2\nu}\right)^\nu \quad \text{when} \quad \alpha \to \infty \tag{C.8}$$

Zeros:

$J_0(\alpha)$	2.4048	5.5201
$J_1(\alpha)$	3.8317	
$J_2(\alpha)$	5.1356	

Publications

1. R. Sánchez, E. Cota, R. Aguado and G. Platero, *Spin filter effect in an AC-driven double quantum dot*, Physica E, **34** , 405 (2006).

2. R. Sánchez, G. Platero, R. Aguado and E. Cota, *Photon-assisted tunneling in ac driven quantum dot spin pumps*, phys. stat. sol. (a), **203**, 1154 (2006).

3. R. Sánchez, E. Cota, R. Aguado and G. Platero, *Spin-filtering through excited states in double-quantum-dot pumps*, Phys. Rev. B **74**, 35326 (2006).

4. R. Sánchez, G. Platero, R. Aguado and E. Cota, *Removing spin blockade by photon-assisted tunneling in double quantum dots*, phys. stat. sol. (b) **243**, 3932 (2006).

5. R. Sánchez, G. Platero, R. Aguado and E. Cota, *Spin currents in AC-driven double quantum dots*, phys. stat. sol. (c), **4**, 497 (2007).

6. R. Sánchez and G. Platero, *Rabi dynamics in driven tunneling devices*, , Progress in industrial mathematics at ECMI 2006. Mathematics in industry **12**, L.L. Bonilla, M.A. Boscoso, G. Platero and J.M. Vega (eds.), Springer Verlag, 444 (2007).

7. R. Sánchez, G. Platero and T. Brandes, *Resonance fluorescence in transport through driven quantum dots*, Phys. Rev. Lett. **98**, 146805 (2007).

8. R. Sánchez, S. Kohler, P. Hänggi and G. Platero, *Electron Bunching in Stacks of Coupled Quantum Dots*, Phys. Rev. B, in press.

9. R. Sánchez, C. López Monís, J. Iñarrea and G. Platero, *Electron Spin Resonance in Double Quantum Dots*, Phys. E, in press.

10. R. Sánchez, G. Platero and T. Brandes, *Phonon Emission in Two Levels Quantum Dots*, Phys. E, in press.

11. R. Sánchez, F.J. Kaiser, S. Kohler, P. Hänggi and G. Platero, *Shot Noise in Spin Pumps*, Phys. E, in press.

12. R. Sánchez, C. López-Monís and G. Platero, *Coherent Spin Dynamics in Open Driven Double Quantum Dots*, submitted for publication.

13. J. Villavicencio, I. Maldonado, R. Sánchez, E. Cota and G. Platero, *Tunneling spectroscopy in ac-driven quantum dot nanoresonators*, submitted for publication.

Bibliography

[1] K. von Klitzing, G. Dorda and M. Pepper, *New method for high-accuracy deermination of the fine-structure constant based on quantized Hall resistance*, Phys. Rev. Lett. **45**, 494 (1980).

[2] M.A. Kastner, *Artificial atoms*, Physics Today, January 1993.

[3] R.C. Ashoori, *Electrons in artificial atoms*, Nature **379**, 413 (1996).

[4] P.L. McEuen, *Artificial atoms: new boxes for electrons*, Science **278**, 1729 (1997).

[5] L.P. Kouwenhoven and C. Marcus, *Quantum dots*, Physicsa Today, June 1998, 35 (1998).

[6] L.P. Kouwenhoven, T.H. Oosterkamp, M.W.S. Danoesastro, M. Eto, D.G. Austing, T. Honda and S. Tarucha, *Excitation spectra of circular, few-electron quantum dots*, Science **278**, 1788 (1997).

[7] D.R. Stewart, D. Sprinzak, C.M. Marcus, C.I. Duruöz and J.S. Harris, Jr., *Correlations between ground and excited state spectra of a quantum dot*, Scienc **278**, 1784 (1997).

[8] L.P. Kouwenhoven, C.M. Marcus, P.L. McEuen, S. Tarucha, R.M. Westervelt and N.S. Wingreen, *Electron transport in quantum dots* in L.L. Sohn, L.P. Kouwenhoven and G. Schön (eds.), *Mesoscopic electron transport* (Kluwer, 1997).

[9] R. Hanson, L.P. Kouwenhoven, J.R. Petta, S. Tarucha and L.M.K. Vandersypen, *Spins in few-electron quantum dots*, Rev. Mod. Phys. **79**, 1217 (2007).

[10] T. Brandes, *Coherent and collective quantum optical effects in mesoscopic systems*, Phys. Rep. **408**, 315 (2005).

[11] W.G. van der Wiel, S. De Franceschi, J.M. Elzerman, T. Fujisawa, S. Tarucha and L.P. Kouwenhoven, *Electron transport through double quantum dots*, Rev. Mod. Phys. **75**, 1 (2003).

[12] I.O. Kulik and R.I. Shekhter, *Kinetic phenomena and charge discreteness effects in granulated media*, Sov. Phys.-JETP **41**, 308 (1975) [Zh. Eksp. Teor. Fiz. **68**, 623 (1975)].

[13] C.W.J. Beenakker, *Theory of Coulomb-blockade oscillations in the conductance of a quantum dot*, Phys. Rev. B **44**, 1646 (1991).

[14] D.V. Averin, A.N. Korotkov and K.K. Likharev, *Theory of single-electron charging of quantum wells and dots*, Phys. Rev. B **44**, 6199 (1991).

[15] S.A. Gurvitz, H.J. Lipkin and Ya.S. Prager, *The Pauli principle and quantum transport*, Mod. Phys. Lett. B **8**, 1377 (1994).

[16] C.V. Averin and Yu.V. Nazarov, *Virtual electron diffusion during quantum tunneling of the electric charge*, Phys. Rev. Lett. **65**,2446 (1990).

[17] D.V. Averin, *Periodic conductance oscillations in the single-electron tunneling transistor*, Physica B **194-196**, 979 (1994).

[18] K. Kang and B.I. Min, *Effect of quantum confinement on electron tunneling through a quantum dot*, Phys. Rev. B **55**, 15412 (1997).

[19] A.W. Holleitner, R.H. Blick, A.K. Hüttel, K. Eberl and J.P. Kotthaus, *Probing and controlling the bonds of an artificial molecule*, Science **297**, 70 (2002).

[20] Yu.V. Nazarov, *Quantum interference, tunnel junctions and resonant tunneling interferometer*, Physica B **189**, 57 (1993).

[21] S. A. Gurvitz and Ya. S. Prager, *Microscopic derivation of rate equations for quantum transport*, Phys. Rev. B, **53**, 15932 (1996).

[22] S.A. Gurvitz, *Rate equations for quantum transport in multidot systems*, Phys. Rev. B **57**, 6602 (1998).

[23] R. Ziegler, C. Bruder and H. Schoeller, *Transport through double quantum dots*, Phys. Rev. B **62**, 1961 (2000).

[24] S. A. Wolf, D. D. Awschalom, R. A. Buhrman, J. M. Daughton, S. von Molnar, M. L. Roukes, A. Y. Chtchelkanova, and D. M. Treger, *Spintronics: a spin-based electronics vision of the future*, Science **294**, 1488 (2001).

[25] Ya.M. Blanter and M. Büttiker, *Shot noise in mesoscopic conductors*, Phys. Rep. **336**, 1 (2000).

[26] S. Kohler, J. Lehmann and P. Hänggi, *Driven quantum transport on the nanoscale*, Phys. Rep. **406**, 379 (2005).

[27] L.D. Landau and E.M. Lifshitz, *Mecánica cuántica (teoría no relativista)* (Reverté, Barcelona, 1983).

[28] R.K. Wangsness and F. Bloch, *Dynamical theory of nuclear induction*, Phys. Rev. **89**, 728 (1953).

[29] F. Bloch, *Dynamical theory of nuclear induction. II*, Phys. Rev. **102**, 104 (1957).

[30] U. Fano, *Note on the quantum theory of irreversible processes*, Phys. Rev. **96**, 869 (1954).

[31] A.G. Redfield, *On the theory of relaxation processes*, IBM J. Res. Dev. **1**, 19 (1957).

[32] C. Cohen–Tannoudji, B. Diu and F. Lalöe, *Quantum Mechanics* (John Wiley & Sons, New York, 1977).

[33] B. Elattari and S. A. Gurvitz, *Shot noise in coupled dots and the 'fractional charges'*, Phys. Lett. A **292**, 289 (2002).

[34] T. Novotnỳ, *Investigation of apparent violation of the second law of thermodynamics in quantum transport studies*, Europhys. Lett. **59**, 648 (2002).

[35] M. Abramowitz and I. Stegun, *Handbook of mathematical functions with formulas, graphs and mathematical tables* (Dover, New York, 1965).

[36] P.K. Tien and J.P. Gordon, *Multiphoton process observed in the interaction of microwave fields with the tunneling between superconductor films*, Phys. Rev. **129**, 647 (1963).

[37] L.P. Kouwenhoven, S. Jauhar, K. McCormick, D. Dixon, P.L McEuen, Yu.V. Nazarov, N.C. vander Vaart, C.T. Foxon, *Photon-assisted tunneling through a quantum dot*, Phys. Rev. B **50**, 2019 (1994).

[38] T.H. Oosterkamp, L.P.Kouwenhoven, A.E.A. Koolen, N.C. van der Vaart and C.J.P.M. Harmans, *Photon-assisted tunneling through a quantum dot*, Semicond. Sci. Technol. **11**, 1512 (1996).

[39] T.H. Oosterkamp, L.P. Kouwenhoven, A.E.A. Koolen, N.C. vander Vaart and C.J.P.M. Harmans, *Photon sidebands of the ground state and first excited state of a quantum dot*, Phys. Rev. Lett. **78**, 1536 (1997).

[40] R. Aguado, J. Inãrrea and G. Platero, *Coherent resonant tunneling in ac fields*, Phys. Rev. B **53**, 10030 (1996).

[41] T.H. Stoof and Yu.V. Nazarov, *Time-dependent resonant tunneling via two discrete states*, Phys. Rev. B **53**, 1050 (1996).

[42] R. Sánchez and G. Platero, *Rabi dynamics in driven tunneling devices*, Progress in industrial mathematics at ECMI 2006. Mathematics in industry **12**, L.L. Bonilla, M.A. Boscoso, G. Platero and J.M. Vega (eds.), Springer Verlag, 444 (2007).

[43] F. Bloch and A. Siegert, Phys. Rev., **57**, 522 (1940).

[44] G.S. Agarwal, Phys. Rev. A, **4**, 1778 (1971).

[45] G.S. Agarwal, Phys. Rev. A, **7**, 1195 (1973).

[46] P.L. Knight and L. Allen, Phys. Rev. A, **7**, 368 (1973).

[47] I.I. Rabi, N.F. Ramsey and J. Schwinger, *Use of rotating coordinates in magnetic resonance problems*, Rev. Mod. Phys. **26**, 167 (1954).

[48] C.A. Stafford and N.S. Wingreen, *Resonant photon-assisted tunneling through a double-quantum dot: an electron pump from spatial Rabi oscillations*, Phys. Rev. Lett. **76**, 1916 (1996).

[49] F. Großman, T. Dittrich, P. Jung and P. Hänggi, *Coherent destruction of tunneling*, Phys. Rev. Lett. **67**, 516 (1991).

[50] F. Großman and P. Hänggi, *Localization in a driven two-level dynamics*, Europhys. Lett. **18**, 571 (1992).

[51] M. Grifoni and P. Hänggi, *Driven quantum tunneling*, Phys. Rep. **304**, 229 (1998).

[52] C.E. Creffield and G. Platero, *ac-driven localization in a two-electron quantum dot molecule*, Phys. Rev. B, **65** 113304 (2002).

[53] C.E. Creffield and G. Platero, *Localization of two interacting electrons in quantum dot arrays driven by an ac field*, Phys. Rev. B, **69** 165312 (2004).

[54] G. Della Valle, M. Ornigotti, E. Cianci, V. Foglietti, P. Laporta and S. Longhi, *Visualization of coherent destruction of tunneling in an optical double well system*, Phys. Rev. Lett. **98**, 263601 (2007).

[55] M. Johnson and R. H. Silsbee, *Interfacial charge-spin coupling: injection and detection of spin magnetization in metals*, Phys. Rev. Lett. **55**, 1790 (1985).

[56] F. J. Jedema, A. T. Filip and B. J. van Wees, *Electrical spin injection and accumulation at room temperature in an all-metal mesoscopic spin valve*, Nature(London) **410**, 345 (2001).

[57] R. Fiederling, M. Keim, G. Reuscher, W. Ossau, G. Schmidt, A. Waag, and L. W. Molenkamp, *Injection and detection of a spin-polarized current in a light-emitting diode*, Nature (London) **402**, 787 (1999).

[58] Y. Ohno, D. K. Young, B. Beschoten, F.Matsukura, H. Ohno, and D. D. Awschalom, *Electrical spin injection in a ferromagnetic semiconductor heterostructure*, Nature (London) **402**, 790 (1999).

[59] E. R. Mucciolo, C. Chamon, and C. Marcus, *Adiabatic quantum pump of spin-polarized current*, Phys. Rev. Lett. **89**, 146802 (2002).

[60] S.K. Watson, R. M. Potok, C. M. Marcus, and V. Umansky, *Experimental realization of a spim pump*, Phys. Rev. Lett. **91**, 258301 (2003).

[61] M. G. Vavilov, L. DiCarlo and C.M. Marcus, *Photovoltaic and rectification currents in quantum dots*, Phys. Rev. B **71**, 241309(R) (2005).

[62] T. Aono, *Adiabatic spin pumping through a quantum dot with a single orbital level*, Phys. Rev. B **67**, 155303 (2003).

[63] E. Cota, R. Aguado, C.E. Creffield and G. Platero, *Spin-polarized pumping in a double quantum dot*, Nanotechnology **14**, 152 (2003)

[64] R. Hanson, L.M.K. Vandersypen, L.H. Willems van Beveren, J.M. Elzerman, I.T. Vink and L.P. Kouwenhoven, Phys. Rev. B **70**, 241304 (2004).

[65] P. Recher, E. V. Sukhorukov and D. Loss, *Quantum dot as a spin filter and spin memory*, Phys. Rev. Lett. **85**, 1962 (2000).

[66] M. Blaauboer and C.M.L. Fricot, *Spin pump turnstile: parametric pumping of a spin-polarized current through a nearly closed quantum dot*, Phys. Rev. B **71**, 041303(R) (2005).

[67] M. Switkes, C.M. Marcus, K. Campman and A.C. Gossard, *An adiabatic quantum electron pump*, Science **283**, 1905 (1999).

[68] G. Platero and R. Aguado, *Photon-assisted transport in semiconductor nanostructures*, Phys. Rep. **395**, 1 (2004).

[69] W.G. van der Wiel, T.H. Oosterkamp, S. De Franceschi, C.J.P.M. Harmans and L.P. Kouwenhoven, *Photon assisted tunneling in quantum dots*, in: I.V. Lerner, B.L. Althsuler, V.I. Fal'ko, T. Giamarchi (Eds.), *Strongly correlated fermions and bosons in low-dimensional disordered systems*, Kluwer Academic Publishers, pp. 43-68 (2002).

[70] Qing-feng Sun, Hong Guo, and Jian Wang, Phys. Rev. Lett. **90**, 258301 (2003)

[71] R. López, R. Aguado, G. Platero and C. Tejedor, Phys. Rev. B **64**, 075319 (2001)

[72] J.M. Elzerman, S. de Franceschi, D. Goldhaber-Gordon, W.G. van der Wiel and L.P. Kouwenhoven, J. Low Temp. Phys. **118**, 375 (2000)

[73] J.M. Elzerman, R. Hanson, L.H. Willems van Beveren, B. Witkamp, L.M.K. Vandersypen and L.P. Kouwenhoven, Nature **430**, 431 (2004)

[74] R. Hanson,L.H. Willems van Beveren, I.T. Vink, J.M. Elzerman, W.J.M. Naber, F.H.L. Koppens, L.P. Kouwenhoven and L.M.K. Vandersypen, Phys. Rev. Lett. **94**, 196802 (2005)

[75] E. Cota, R. Aguado and G. Platero, *ac-driven double quantum dots as spin pumps and spin filters*, Phys. Rev. Lett. **94**, 107202 (2005)

[76] R. Sánchez, E. Cota, R. Aguado and G. Platero, *Spin-filtering through excited states in double-quantum-dot pumps*, Phys. Rev. B **74**, 035326 (2006).

[77] B. L. Hazelzet, M. R. Wegewijs, T. H. Stoof, and Yu. V. Nazarov, *Coherent and incoherent pumping of electrons in double quantum dots*, Phys. Rev. B **63**, 165313 (2001).

[78] T. H. Oosterkamp, T. Fujisawa, W.G. van der Wiel, K. Ishibashi, R.V. Hijman, S. Tarucha and L.P. Kouwenhoven, *Microwave spectroscopy of a quantum-dot molecule*, Nature (London) **395**, 873 (1998).

[79] J. R. Petta *et al.*, Phys. Rev. Lett. **93**, 186802 (2004).

[80] K. Ono and S. Tarucha, Phys Rev. Lett. **92**, 256803 (2004)

[81] F.H.L. Koppens, J.A. Folk, J.M. Elzerman, R. Hanson, L.H. Willems van Beveren, I.T. Vink, H.P. Tranitz, W. Wegscheider, L.P. Kouwenhoven and L.M.K. Vandersypen, Science **309**, 1346 (2005)

[82] J.R. Petta, A.C. Johnson, J.M. Taylor, E.A. Laird, A. Yacobi, M.D. Lukin, C.M. Marcus, M.P. Hanson and A.C. Gossard, *Coherent manipulation if coupled electron spins in semiconductor quantum dots*, Science **309**, 2180 (2005)

[83] K. Blum, Density Matrix Theory and Applications (Plenum Press, NY, 1996).

[84] Toshimasa Fujisawa, Yasuhiro Tokura and Yoshiro Hirayama, Phys. Rev. B **63**, 081304(R) (2001)

[85] V.N. Golovach, A. Khaetskii, and D. Loss, Phys. Rev. Lett. **93**, 016601 (2004).

[86] K. Saito, S. Okubo and M. Eto, *Analytical expression of leakage current through double quantum dots in Pauli spin blockade*, to appear in Phys. E (2007).

[87] O.N. Jouravlev *et al.*, Phys. Rev. Lett. **96**, 176804 (2006).

[88] J. Iñarrea *et al.*, Phys Rev. B **76**, 085329 (2007).

[89] R. Sánchez, E. Cota, R. Aguado and G. Platero, *Spin filter effect in an AC-driven double quantum dot* , Physica E **34**, 405 (2006).

[90] R. Sánchez, G. Platero, R. Aguado and E. Cota, *Photon-assisted tunneling in ac driven double quantum dot spin pumps*, phys. stat. sol. (a) **203**, 1154 (2006).

[91] R. Sánchez, G. Platero, R. Aguado and E. Cota, *Spin currents in AC-driven double quantum dots*, phys. stat. sol. (c) **4**, 497 (2007).

[92] D. Weinmann, W. Häusler and B. Kramer, *Spin blockades in linear and nonlinear transport through quantum dots*, Phys. Rev. Lett. **74**, 984 (1995).

[93] J. Fransson and M. Råsander, *Pauli spin blockade in weakly coupled quantum dots*, Phys. Rev. B **73**, 205333 (2006).

[94] K. Ono, D.G. Austing, Y. Tokura and S. Tarucha, *Current rectification by Pauli exclusion in a weakly coupled double quantum dot system*, Science, **297**, 1313 (2002).

[95] F.H.L. Koppens, C. Buizert, K.J. Tielrooij, I.T. Vink, K.C. Nowack, T. Meunier, L.P. Kouwenhoven and L.M.K. Vandersypen, *Driven coherent oscillations of a single electron spin in a quantum dot*, Nature **442**, 766 (2006).

[96] R. Sánchez, G. Platero, R. Aguado and E. Cota, *Removing spin blockade by photon-assisted tunneling in double quantum dots*, phys. stat. sol. (b) **243**, 3932 (2006).

[97] H.-A. Engel and D. Loss, *Detection of single spin decoherence in a quantum dot via charge currents*, Phys. Rev. Lett. **86**, 4648 (2001).

[98] H.A. Engel and D. Loss *Single-spin dynamics and decoherence in a quantum dot via charge transport*, Phys. Rev. B, **65**, 195321 (2002).

[99] E. Arimondo et al., Lett. Nuovo Cim. **17**, 333 (1976).

[100] G. Alzetta, A. Gozzini, L. Moi and G. Orriols, *An experimental method for the observation of R.F. transitions and laser beat resonances in oriented Na vapour*, Nuovo Cim. B **36**, 5 (1976).

[101] R.M. Whitley and C.R. Stroud, Jr., *Double optical resonance*, Phys. Rev. A **14**, 1498 (1976).

[102] H.R. Gray, R. M. Whitley and C.R. Stroud, Jr., *Coherent trapping of atomic populations*, Opt. Lett. **3**, 218 (1978).

[103] T. Brandes and F. Renzoni, *Current switch by coherent trapping of electrons in quantum dots*, Phys. Rev. Lett. **85**, 4148 (2000).

[104] C. Emary, *Dark states in the magnetotransport through triple quantum dots*, cond-mat/0705.2934 (2007).

[105] W. Chu, S. Duan and J.-L. Zhu, *Three-level structure design and optically controlled current in coupled quantum dots*, Appl. Phys. Lett. **90**, 222102 (2007).

[106] B. Michaelis, C. Emary and C.W.J. Beenakker, *All-electronic coherent population trapping in quantum dots*, Europhys. Lett. **73**, 677 (2006).

[107] S. E. Economou *et al.*, cond-mat/0703098.

[108] C. Santori *et al.*, Phys. Rev. Lett. **97** 247401 (2006).

[109] D. Loss *et al.*, Phys. Rev. A **57**, 120 (1998).

[110] D.Klauser *et al.*, Phys. Rev. B **73**, 205302 (2006).

[111] R. Hanson and. G. Burkard, *Universal set of quantum gates for double-dot spin qubits with fixed interdot coupling*, Phys. Rev. Lett. **98**, 050502 (2007).

[112] J.R. Petta, A.C. Johnson, J.M. Taylor, E.A. Laird, A. Yacobi, M.D. Lukin, C.M. Marcus, M.P. Hanson and A.C. Gossard, *Coherent manipulation of coupled electron spins in semiconductor quantum dots*, Science **309**, 2180 (2005).

[113] F.H.L. Koppens, C. Buizert, I.T. Vink, K.C. Nowack, T. Meunier, L.P. Kouwenhoven and L.M.K. Vandersypen, *Detection of single electron spin resonance in a double quantum dot*, J. Appl. Phys. **101**, 081706 (2007).

[114] F.H.L. Koppens, D. Klauser, W.A.Coish, K.C. Nowack, L.P. Kouwenhoven, D. Loss and L.M.K. Vandersypen *Universal phase shift and nonexponential decay of driven single-spin oscillations*, Phys. Rev. Lett. **99**, 106803 (2007).

[115] E.A. Laird, C. Barthel, E.I. Rashba, C.M. Marcus, M.P. Hanson and A.C. Gossard, *Hyperfine-mediated gate-driven electron spin resonance*, arXiv:0707.0557 (2007).

[116] L. Meier *et al.*, Nature Phys. **3**, 650 (2007).

[117] K.C. Nowack *et al.*, arXiv:0707.3080 (2007).

[118] N. Lambert, I. Mahboob, M. Pioro-Ladrière, Y. Tokura, S. Tarucha and H. Yamaguchi, *Electron spin manipulation and resonator readout in a double quantum dot nano-electromechanical system*, arXiv:0709.0593 (2007).

[119] K. Blum, Density Matrix Theory and Applications (Plenum Press, NY, 1996).

[120] I.I. Rabi, *On the process of space quantization*, Phys. Rev. **49**, 324 (1936).

[121] I.I. Rabi, *Space quantization in a magnetic gyrating field*, Phys. Rev. **51**, 652 (1937).

[122] R. Sánchez, C. López-Monís, J. Iñarrea and G. Platero, *Electron spin resonance in double quantum dots*, Phys. E, in press (2007).

[123] A. Pfund, I. Shorubalko, K. Ensslin and R. Leturcq, *Spin-state mixing in InAs double quantum dots*, Phys. Rev. B **76**, 161308(R) (2007).

[124] R. de-Picciotto, M. Reznikov, M. Heiblum, V. Umansky, G. Bunin and D. Mahalu, *Direct observation of a fractional charge*, Nature **389**, 162 (1997).

[125] C.W.J. Beenakker and C. Schönenberger, *Quantum shot noise*, Phys. Today, May 2003, 37.

[126] G. Burkard, D. Loss ans E.V. Sukhorukov, *Noise of entangled electrons: bunching and antibunching*, Phys. Rev. B **61**, 16303 (2000).

[127] W. Schottky, *Über spontane Stromschwankungen in verschiedenen Elecktrizitätsleitern*, Ann. Phys. (Leipzig) **57**, 541 (1918).

[128] S. Overholzer, E.V. Sukhorukov and C. Schönenberger, *Crossover between classical and quantum shot noise in chaotic cavities*, Nature **415**, 765 (2002).

[129] M. Büttiker, *Scattering theory of current and intensity noise correlations in conductors and wave guides*, Phys. Rev. B **46**, 12485 (1992).

[130] R. Hanbury Brown and R.Q. Twiss, *Correlation between photons in two coherent beams of light*, Nature **177**, 27 (1956).

[131] B.J. Dalton, *Liouville space theory of sequential quantum processes: I. General theory*, J. Phys. A: Math. Gen. **15**, 2157 (1982).

[132] B.J. Dalton, *Liouville space theory of sequential quantum processes: II. Application to a system with an internal reservoir*, J. Phys. A: Math. Gen. **15**, 2177 (1982).

[133] C. Flindt, T. Novotnỳ and A.-P- Jauho, *Current noise in a vibrating quantum dot array*, Phys. Rev. B **70**, 205334 (2004).

[134] F.J. Kaiser and S. Kohler, *Shot noise in non-adiabatically driven nanoscale conductors*, Ann. Phys. (Leipzig) **16**, 702 (2007).

[135] S. Camalet, S. Kohler and P. Hänggi, *Shot noise in ac-driven nanoscale conductors*, Phys. Rev. B **70**, 155326 (2004).

[136] G. Kießlich, E. Schöll, T. Brandes, F. Hohls and R.J. Haug, *Noise enhancement due to quantum coherence in coupled quantum dots*, arXiv:0706.1737 (2007).

[137] M. Strass, P. Hänggi and S. Kohler, *Nonadiabatic electron pumping: maximal current with minimal noise*, Phys. Rev. Lett. **95**, 130601 (2005).

[138] R. Sánchez, S. Kohler, P. Hänggi and G. Platero, *Electron bunching in stacks of coupled quantum dots*, Phys. Rev. B (to be published); arXiv:0706.2950 (2007).

[139] R. Sánchez, F.J. Kaiser, S. Kohler, P. Hänggi and G. Platero, *Shot noise in spin pumps*, Phys. E, to be published (2007).

[140] R. Sánchez, G. Platero, and T. Brandes, *Resonance fluorescence in transport through quantum dots: noise properties* , Phys. Rev. Lett. **98**, 146805 (2007).

[141] R. Aguado and T. Brandes, Phys. Rev. Lett. **92**, 206601 (2004).

[142] B. Elattari and S.A. Gurvitz, Phys. Lett. A **292**, 289 (2002).

[143] T. Novotnỳ, A. Donarini, C. Flindt, and A.-P. Jauho, Phys. Rev. Lett. **92**, 248302 (2004).

[144] N. Lambert, R. Aguado, and T. Brandes, Phys. Rev. B **75**, 045340 (2007).

[145] R.J. Glauber, *Photon correlations*, Phys. Rev. Lett. **10**, 84 (1963);

[146] P.L. Kelley and W.H. Kleiner, Phys. Rev. **136**, 316 (1964);

[147] M.O. Scully and W. E. Lamb, Jr., *ibid.* **179**, 368 (1969);

[148] R.J. Cook, *Photon number statistics in resonance fluorescence*, Phys. Rev. A **23** 1243 (1981);

[149] R.J. Cook, Opt. Commun. **35** 347 (1980).

[150] L.S. Levitov and G.B. Lesovik, Pis'ma Zh. Eksp. Teor. Fiz. **58**, 225 (1993)[JETP Lett. **58**, 230 (1993)];

[151] D. A. Bagrets and Yu.V. Nazarov, *Full counting statistics of charge transfer in Coulomb blockade systems*, Phys. Rev. B **67**, 85316 (2003).

[152] R. Aguado and T. Brandes, Phys. Rev. Lett. **92**, 206601 (2004).

[153] I. Djuric and C.P. Search, Phys. Rev. Lett. **74**, 115327 (2006).

[154] L. Mandel, *Sub-Poissonian photon statistics in resonance fluorescence*, Opt. Lett. **4** 205 (1979).

[155] W. Belzig, *Full counting statistics of super-Poissonian shot noise in multilevel quantum dots*, Phys. Rev. B **71**, 161301(R) (2005).

[156] I. Djuric *et al.*, Appl. Phys. Lett. **87**, 32105 (2005);

[157] G. Kießlich *et al.*, Phys. Rev. B **68**, 125320 (2003);

[158] G. Kießlich *et al.*, Phys. Rev. B **73**, 33312 (2006);

[159] A. Thielmann *et al.*, Phys. Rev. B **71**, 45341 (2005);

[160] C.W. Groth *et al.*, Phys. Rev. B **74**, 125315 (2006).

[161] S. Gustavsson, R. Leturcq, B. Simovič, R. Schleser, T. Ihn, P. Studerus, K. Ensslin, D.C. Driscoll and A.C. Gossard, *Counting statistics of single electron transport in a quantum dot*, Phys. Rev. Lett. **96**, 076605 (2006).

[162] S. Gustavsson, R. Leturcq, B. Simovič, R. Schleser, P. Studerus, T. Ihn, K. Ensslin, D.C. Driscoll and A.C. Gossard, *Counting statistics and super-Poissonian noise in a quantum dot: Time resolved measurements of electron transport*, Phys. Rev. B **74**, 195305 (2006).

[163] S. Gustavsson, R. Leturcq, T. Ihn, K. Ensslin, M. Reinwald and W. Wegscheider, *Measurements of higher-order noise correlations in a quantum dot with a finite bandwidth detector*, Phys. Rev. B **75**, 075314 (2007).

[164] T. Fujisawa, T.H. Oosterkamp, W.G. van der Wiel, B.W. Broer, R. Aguado, S. Tarucha and L.P. Kouwenhoven *Spontaneous emission spectrum in double quantum dot devices*, Science **282**, 932 (1998).

[165] M.B. Plenio and P. L. Knight, *The quantum-jump approach to dissipative dynamics in quantum optics*, Rev. Mod. Phys. **70**, 101 (1998).

[166] D. Lenstra, *Photon-number statistics in resonance fluorescence*, Phys. Rev. A **26** 3369 (1982).

[167] V.K. Zajárov, B.A. Sevastiánov and V.P. Christiakov, *Teoría de las peobabilidades*, (Mir, Moscú, 1985).

[168] B. Dong *et al.*, Phys. Rev. Lett. **94**, 66601 (2005).

[169] R. Ellickson, *A method of calculating fluctuations*, Phys. Rev. **54**, 572 (1938).

[170] D.K.C. MacDonald, *Spontaneous fluctuations*, Rep. Prog. Phys. **12**, 56 (1948).

[171] N. Lambert, PhD. thesis, University of Manchester (2005).

[172] H. Carmichael, *An Open Systems Approach to Quantum Optics* (Springer-Verlag, Berlin, 1993).

[173] I. Djuric *et al.*, J. Appl. Phys. **99**, 63710 (2006).

[174] J.H. Davies, P. Hyldgaard, S, Hersfield and J.W. Wilkins, *Classical theory of shot noise in resonant tunneling*, Phys. Rev. B **46**, 9620 (1992).

[175] S. Hershfield, J.H. Davies, P. Hyldgaard, C.J. Stanton and J.W. Wilkins, *Zero-frequency current noise for the double-tunnel-junction Coulomb blockade*, Phys. Rev. B **47**, 1967 (1993).

[176] G. Iannaccone, M. Macucci and B. Pellegrini, Phys. Rev. B **55**, 4539 (1997).

[177] T. Brandes *et al.*, Phys. Rev. B **69**, 205326 (2004).

[178] S.A. Gurvitz, *Quantum interference in resonant tunneling and single spin measurements*, IEEE Transactions on Nanotechnology **4**, 45 (2005).

[179] T. Bryllert, M. Borgstrom, T. Sass, B. Gustafson, L. Landin, l.-E. Wernersson, W. Seifert and L. Samuelson, *Designed emitter states in resonant tunneling through quantum dots*, Appl. Phys. Lett. **80**, 2681 (2002).

[180] R. Sánchez, G. Platero and T. Brandes, *Phonon emission in two levels quantum dots*, Physica E ... (2007).

[181] A. Cottet, W. Belzig and C. Bruder, Phys. Rev. B **70**, 115315 (2004).

[182] A. Cottet and W. Belzig, Europhys. Lett. **66**, 405 (2004).

[183] A. Cottet, W. Belzig, and C. Bruder, Phys. Rev. Lett. **92**, 206801 (2004).

[184] A. J. Leggett, S. Chakravarty, A.T. Dorsey, M.P.A. Fisher, A. Garg, and W. Zwerger, *Dynamics of the dissipative two-state system*, Rev. Mod. Phys. **59**, 1 (1987).

[185] T. Brandes and B. Kramer, Phys. Rev. Lett. **83**, 3021 (1999).

[186] M. Gattobigio, G. Iannaccone, and M. Macucci, *Enahancement and suppression of shot noise in capacitively coupled metallic double dots*, Phys. Rev. B **65**, 115337 (2002).

[187] Y. Zhang *et al.*, Phys. Rev. Lett. **99**, 036603 (2007).

[188] P. Barthold, F. Hohls, N. Maire, K. Pierz, and R. J. Haug, *Enhanced shot noise in tunneling through a stack of coupled quantum dots*, Phys. Rev. Lett. **96**, 246804 (2006).